Catalysis Under Transient Conditions

In Catalysis Under Transient Conditions; Bell, A., et al.;
ACS Symposium Series; American Chemical Society: Washington, DC, 1982.

Catalysis Under Transient Conditions

Alexis T. Bell, EDITOR
University of California—Berkeley

L. Louis Hegedus, EDITOR
W. R. Grace & Company

Based on a symposium sponsored by the Division of Colloid and Surface Chemistry at the Second Chemical Congress of the North American Continent (180th ACS National Meeting), Las Vegas, Nevada, August 27–28, 1980.

ACS SYMPOSIUM SERIES **178**

AMERICAN CHEMICAL SOCIETY
WASHINGTON, D. C. 1982

Library of Congress CIP Data

Catalysis under transient conditions.
(ACS symposium series, ISSN 0097-6156; 178)

Includes bibliographies and index.

1. Catalysis—Congresses.
I. Bell, Alexis T., 1942- . II. Hegedus, L. Louis, 1941- . III. American Chemical Society. Division of Colloid and Surface Chemistry. IV. Chemical Congress of rhe North American Continent (2nd: 1980: Las Vegas, Nevada). V. Series.

QD505.C385 541.3'95 81-20639
ISBN 0-8412-0688-0 AACR2 ACSMC8 178 1-308
1982

Copyright © 1982

American Chemical Society

All Righrs Reserved. The appearance of the code at the bottom of the first page of each article in this volume indicates the copyright owner's consent that reprographic copies of the article may be made for personal or internal use or for the personal or internal use of specific clients. This consent is given on the condition, however, that the copier pay the stated per copy fee through the Copyright Clearance Center, Inc. for copying beyond that permitted by Sections 107 or 108 of the U.S. Copyright Law. This consent does not extend to copying or transmission by any means—graphic or electronic—for any other purpose, such as for general distribution, for advertising or promotional purposes, for creating new collective work, for resale, or for information storage and retrieval systems.

The citation of trade names and/or names of manufacturers in this publication is not to be construed as an endorsement or as approval by ACS of the commercial products or services referenced herein; nor should the mere reference herein to any drawing, specification, chemical process, or other data be regarded as a license or as a conveyance of any right or permission, to the holder, reader, or any other person or corporation, to manufacture, reproduce, use, or sell any patented invention or copyrighted work that may in any way be related thereto.

PRINTED IN THE UNITED STATES OF AMERICA

American Chemical
Society Library
1155 16th St. N. W.
Washington, D. C. 20036

ACS Symposium Series

M. Joan Comstock, *Series Editor*

Advisory Board

David L. Allara
Robert Baker
Donald D. Dollberg
Robert E. Feeney
Brian M. Harney
W. Jeffrey Howe
James D. Idol, Jr.
Herbert D. Kaesz
Marvin Margoshes
Robert Ory
Leon Petrakis
Theodore Provder
Charles N. Satterfield
Dennis Schuetzle
Davis L. Temple, Jr.
Gunter Zweig

FOREWORD

The ACS SYMPOSIUM SERIES was founded in 1974 to provide a medium for publishing symposia quickly in book form. The format of the Series parallels that of the continuing ADVANCES IN CHEMISTRY SERIES except that in order to save time the papers are not typeset but are reproduced as they are submitted by the authors in camera-ready form. Papers are reviewed under the supervision of the Editors with the assistance of the Series Advisory Board and are selected to maintain the integrity of the symposia; however, verbatim reproductions of previously published papers are not accepted. Both reviews and reports of research are acceptable since symposia may embrace both types of presentation.

PREFACE

The interest in the dynamic operation of heterogeneous catalytic systems is experiencing a renaissance. Attention to this area has been motivated by several factors: the availability of experimental techniques for monitoring species concentrations both in the gas phase and at the catalyst surface with a temporal resolution and sensitivity not previously possible, the development of efficient numerical methods for predicting the dynamics of complex reaction systems, and the recognition that in selected instances operation of a catalytic reactor under dynamic conditions can yield a better performance than operation under steady-state conditions.

The papers in this book were selected so that both the chemical and the engineering aspects of catalyst dynamics are represented; in addition, an attempt was made to draw a balance between theory and experiment.

The editors thank all the contributors to this volume and express their hope that the material will stimulate further interest in the dynamic operation of catalysts, both for its diagnostic powers and for its potential in improving reactor performance.

ALEXIS T. BELL
University of California
Berkeley, California

L. LOUIS HEGEDUS
W. R. Grace & Company
Columbia, Maryland

July 27, 1981

Understanding Heterogeneous Catalysis Through the Transient Method

C. O. BENNETT

University of Connecticut, Department of Chemical Engineering, Storrs, CT 06268

Although catalysis can be understood through steady-state experiments, it seems clear that transient experiments will usually furnish much additional information. Often steady-state data can be explained by a number of different models, but the results of transient experiments are usually so rich that only a detailed, complex model will come close to explaining the results. These ideas have long been applied in other fields, but in heterogeneous catalysis they have come into acceptance only during the last 15 years or so. Pioneering experiments were done by Wagner (1) in 1938, and Tamaru (2) became an advocate of the method in 1963, emphasizing the measurement of adsorption during catalysis, the essence of the transient method. A quantitative framework was laid out in 1967 (3), and its implementation was carried out a few years later by Kobayashi and Kobayashi (4) and by Yang et al. (5).

Effects due to transport resistances must be carefully avoided in work at atmospheric pressure, so that chemical effects having response times less than about a second cannot be followed. These limitations are avoided at low pressure, and some of the first transient results under vacuum conditions have been reported by Bonzel and Ku (6) and by Jones et al. (7). Progress in transient studies up until about 1975 has been reviewed (8, 9).

The transient processes under discussion here must be described in terms of elementary steps, and the relative rates of the steps will change as conditions change during transients. This point of view has been advocated by Temkin (10), and it is central to a recent discussion by Krylov (11). The adsorptive capacity of the catalyst influences the transients--one has adsorption during reaction. Although modeling in terms of elementary steps is central to understanding catalysis and to modeling reactors during transients, chemical engineers did not take this idea into account until recently. From the first cycling studies of Dorawala and Douglas (12) through the time of the review of Schmitz in 1975 (13), reactor models were based on the use of a steady-state rate expression in the component balances. This state of affairs has now changed, and the importance of elementary step models is generally acknowledged (14).

0097-6156/82/0178-0001$08.00/0
© 1982 American Chemical Society

The bulk of this review concerns transient experiments on heterogeneous catalysis at atmospheric pressure. After some comments on current methods for doing the experiments, the application of the method will be illustrated by two examples: the oxidation of CO over Pt, and the hydrogenation of CO over Fe.

Some Experimental Methods

Gas-phase Kinetics. A better appreciation of the experiments to be discussed later will be obtained after a review of some experimental aspects of the transient method. Here we deal with experiments at atmospheric pressure. A flow sheet for kinetic measurements is given in Fig. 1, a descendant of that first given by Bennett et al. (15). Chemical analysis of the gases during transients is ideally done by a mass spectrometer, although Kobayashi and Kobayashi (4) used a number of gas chromatographs in order to get samples sufficiently frequently.

Step functions, pulses, and square waves can be generated with a low volume, chromatographic-type 4-way valve. We have found that the desired two gas mixtures are best made up and stored in cylinders rather than made continuously by blending two streams. At the time of the switch, there is a momentary stopping of the flow, and this usually results in a change in composition if the mixture is made by the continuous blending of two streams. By this method one or more spurious peaks are added to the desired step function. Naturally these are trivial for slow responses, but important for fast ones.

The needle valves of Fig. 1 are operated choked, so that there is a constant flow independent of downstream resistances. However, the valve shown upstream of the bubble meter is very important. It is adjusted so that the pressures at the switching valve and upstream are hardly perturbed by a switch. The flows of both mixtures are adjusted to be identical by the needle valves and the bubble meter. When all is properly regulated, the ball in each rotameter makes a short, quick (~1s) excursion at the moment of the switch, and identically for the return to the first position of the valve.

If the flow of each mixture to the switching valve is not identical, with minimal pressure disturbance at the switch, spurious peaks are also introduced. For instance in an experiment at steady state with H_2/CO (9/1) flowing to a differential reactor, a common transient experiment is a switch to H_2 alone, so that the hydrogen can react with a carbonaceous surface intermediate, produce methane, and effectively titrate the steady-state surface. If this experiment is not done by a switch from H_2/CO to H_2, but rather by suddenly closing the CO supply valve in a system using continuous gas blending, a peak of methane is formed which has nothing to do with titrating the surface. While H_2/CO is still in the line from the 4-way valve to the reactor (this

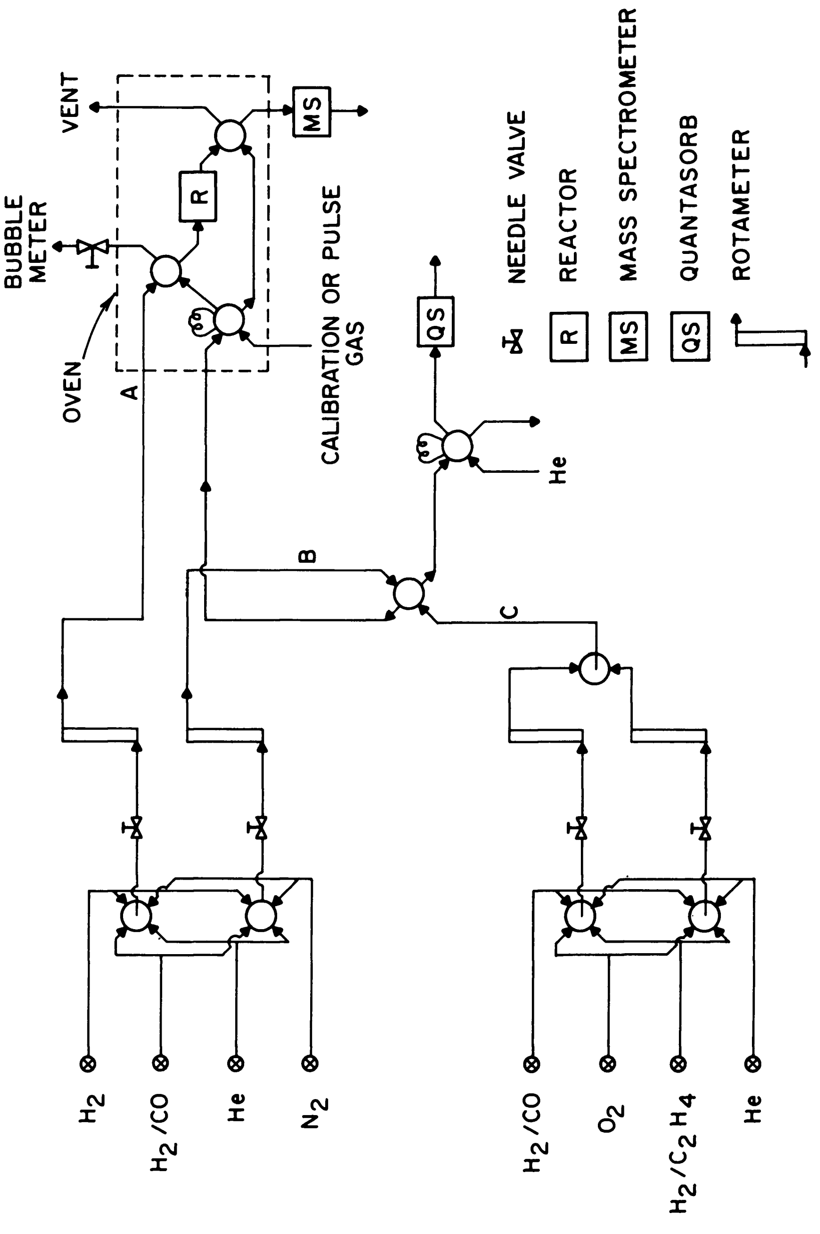

Figure 1. Flow sheet for transient experiments.

length should be minimized), its flow rate is reduced when the CO is cut off, conversion to CH_4 is increased, and there is a false peak at the beginning of the CH_4 transient caused by the reaction of H_2 with surface carbon.

The same effect is obtained by a switch from H_2/CO to helium flowing at a lower rate. There is a methane peak, leading to the erroneous idea that methane has been desorbed. With properly adjusted identical flows the CH_4 falls quickly to zero within the response time of the system - typically ~1s.

The four-way valve at the outlet of the reactor permits sending known gases to the mass spectrometer for calibration. The flow to the reactor need not be disturbed. This arrangement is particularly useful for measuring the water peak. It is well known that water adsorbs on the inside of the instrument. After a few days of pumping, preferably with bakeout, a stable water background peak can be obtained. A known water/helium mixture can be used to measure the peak caused by water entering through the continuous inlet. The response is slower than for other gases, but reproducible over several repititions a few minutes apart. However, if a reactor product stream containing water is sampled continuously, the background water peak gradually increases. Good analysis for water can be made by recording the 18-peak after a switch to dry helium via the reactor outlet 4-way valve. By thus keeping track of the varying background water peak we can make a good oxygen balance for the Fischer-Tropsch reaction at any instant; without the correct background correction this is not possible.

It is clear that the illustrated flowsheet is quite flexible. As shown, pulses can be produced by a 6-way valve. The valves are electrically actuated so a cycled feed can easily be produced. A separate mixture preparation apparatus has been built, so that preparing the various mixtures needed is quick and simple.

The 12" magnetic-sector mass spectrometer is computer-controlled. A typical arrangement is to jump the accelerating voltage over the desired mass numbers at a rate of about 5 numbers per second. The resulting voltages are appropriately converted to digital form, stored and used to give an output of mole fraction versus time for each component. Ordinarily hydrogen and helium cannot be obtained in such a moderately fast scan; for this the magnetic field would need to be changed. However, we have a separate side tube of small (4") radius, with a separate detector. With this arrangement a fast scan from 2 to about 100 is feasible. Either Faraday cup or electron multiplier detectors are used; the latter has the higher sensitivity but is subject to saturation effects.

A classical inlet system is used to obtain a fast response and to avoid mass fractionation. The gas to be sampled impinges on a capillary (150 μm I.D.) discharging into a small chamber (1mL) held at 10^2 Pa by an auxiliary pump. The viscous flow through the capillary is of the order of 5mL/mn. From the chamber a small sample of gas passes through *ca* 5-μm holes in a gold foil

in Knudsen flow and through a tube leading to the spectrometer source.

Infrared Measurements. Elementary-step models can be fit to transient gas-phase data (5) which are obtained by the methods described above. The models will then predict the surface intermediate concentration during transients and at steady state. It is clear that it is also important to observe these surface species experimentally, during transients as well as at steady state. Infrared spectroscopy can be used during catalysis in the presence of the gas phase, so it plays an important role in transient studies.

Some of the first transient infrared data on heterogeneous catalysis were gathered by Heyne and Tomkins in 1966 (16). The method has been advocated and used by Tamaru, who has recently reviewed his work since 1967 in this field (17). Dent and Kokes used the transient method in IR studies in 1970 (18). Since then the method has been applied to kinetic studies in particular by Ueno et al. (19, 20) and most recently by Savatsky and Bell (21).

As already explained (9), the kinetic measurements are easier to interpret quantitatively if done either in a recirculating reactor (CSTR) or in a differential reactor but with measurable conversion. In the typical infrared cell we strive for a close approximation to a differential reactor. The conversion is usually too small to measure. Dwyer (22) and earlier Ueno et al. (19, 20) have used the optical system of Fig. 2. The cell of Fig. 3 permits cancelling gas phase adsorption bands. By operating the cell in the reflection mode as shown, positive control of the temperature of the catalyst disk is achieved, with a very low cell volume (~2 mL) and the possibility of cooling the cell window, as usually required by window material which is transparent over a wide range of frequencies. The temperature is measured in the metal block just behind the mirror. The thermal conductivity of the solid between the thermocouple and the surface is high compared to the effective conductivity of the gas which transfers heat by convection from the surface to the cooler window. Thus the surface temperature is assumed to be close to that measured by the thermocouple. Operation at 2 mL/s gives a residence time of 1s, and at this flow rate the 5 mg catalyst disk gives a negligible conversion for most systems.

Hegedus (23), for the study of adsorbed CO over a limited range of frequencies, was able to use sapphire windows which could be operated at 450°C. His reactor cell thus requires no cooling; it operates in transmission. The cell volume is about 22 mL. A flow rate of 250 mL/s was used so that the residence time was only 0.09s.

Since the flow system can be made with such a fast response, it becomes important to improve the response of the infrared detector. Use of a liquid-nitrogen-cooled Hg-CdTe detector, with 200 to 1000 Hz chopping and a lock-in amplifier, permits the IR

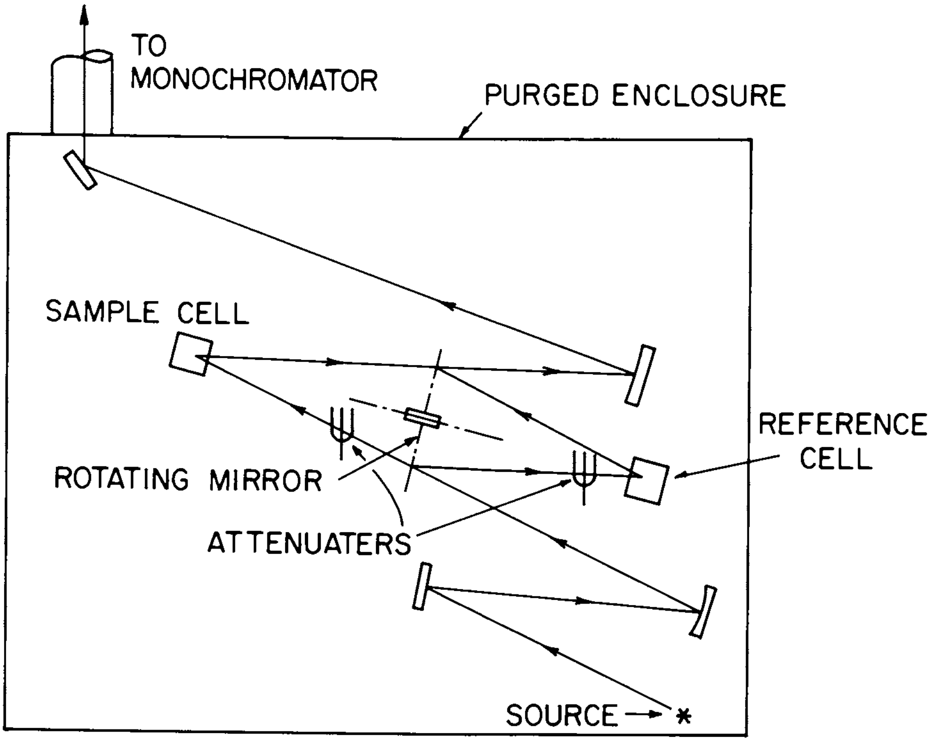

Journal of Catalysis

*Figure 2. IR optical system (*19*).*

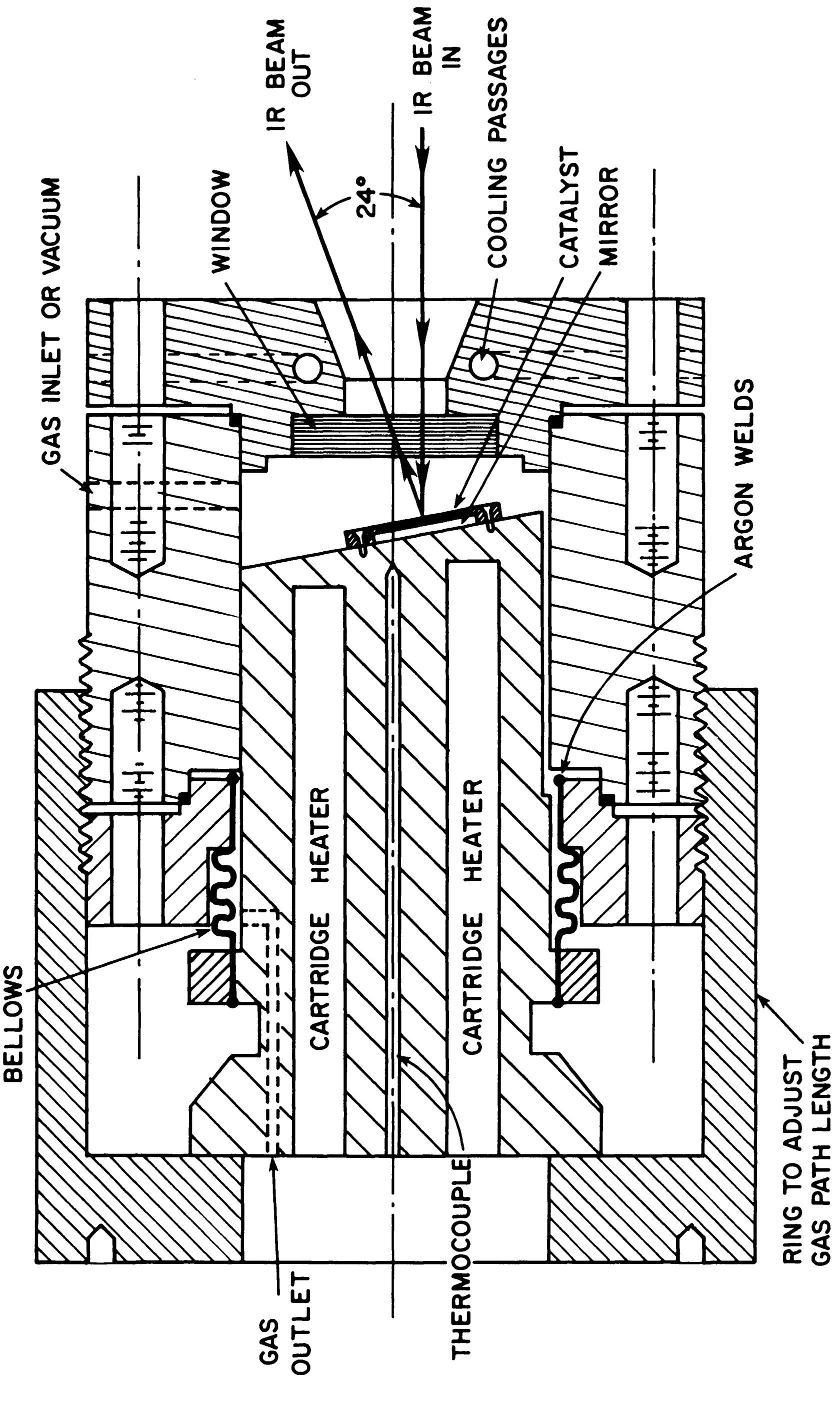

Figure 3. IR cell reactor.

In Catalysis Under Transient Conditions; Bell, A., et al.;
ACS Symposium Series; American Chemical Society: Washington, DC, 1982.

spectrometer to keep up with the imposed signal changes (23). With a dispersion instrument the experiment can be run at several constant wave numbers in repeated experiments. At the signal levels often obtained in studies of the bands of adsorbed species, a Fourier transform instrument may require about 20 scans of 1s each to obtain an adequate interferogram, which of course represents only an average spectrum (21). Software has been developed to resolve this problem through multiplexing in time and mirror position (55, 56). However, this approach only works for a repetitive transient, such as might result from a cycled feed. During each scan the signal, mirror position, and time are stored. The beginning of each scan is offset with reference to the beginning of the transient by a time interval that may be as low as 50μs (55). Then the program sorts the data accumulated over enough repeated cycles for good signal to noise and reconstructs the signal-averaged interferogram corresponding to the chosen time intervals during the transient. This technique has been applied to gas-phase transients (55, 56) but apparently not to surface transients.

With the dispersive IR instrument, it is important to use computer control and data acquisition. For conventional experiments also, the attractiveness of such a system has been pointed out by Peri (24).

Measurements by Electron Spectroscopies. The various electron spectroscopies permit the determination of the surface state of a solid because emitted electrons a few layers beneath the surface do not escape. For example, emitted electrons may be excited by a beam of incident electrons (Auger electron spectroscopy-AES) or by a beam of X-rays (X-ray photoelectron spectroscopy-XPS). The spectrum of intensity of the produced electrons is recorded as a function of the energy of the electrons, leading to a good estimate of surface composition. By XPS even the valence state of a given element can often be determined. Usually XPS is used in connection with transient studies only to measure the surface concentration of non-volatile intermediates like carbon (25); the measurement must be made after the gas phase is removed. However, Matsushima et al. (26) have been able to follow by AES the transient surface concentration of oxygen on platinum as the oxygen reacts with carbon monoxide from the gas phase present at working spectrometer pressures, 1.86×10^{-7} to 4.8×10^{-6} pascals. The limitation of pressures to this range limits the number of systems which can be observed during transients caused by changes in the pressure (concentration) of the gas phase in contact with the solid catalyst.

Some progress has recently been made towards adopting XPS or UPS to in situ measurements during transients. Rubloff (27) has studied the interaction of CO with Ni(111) by directing a pulse of CO (200-300 ms) to the nickel surface while observing the $5\sigma/1\pi$ peak by UPS. The chamber pressure is little affected by

the pulse, but Rubloff estimates that the gas pressure near the sample is about 150 times the system pressure during the pulse (27). The pulse is achieved by a fast acting differentially pumped dosing valve. A result is shown in Fig. 4.

Joyner and Roberts (28) have gone further by constructing a sample cell, differentially pumped, within the spectrometer. Gas is leaked at a constant rate into the sample region. There is a small hole about 2 mm above the surface of the sample through which the electrons excited from the sample pass into the spectrometer. X-rays are directed at the surface through an aluminum window; a second small opening is provided if exitation is by UV radiation. In this way the system pressure can be kept at 10^{-3} Pa while there is a steady pressure of 100 Pa above the sample. There is of course attenuation of the signal, as shown in Fig. 5, taken from Joyner and Roberts (28). The gas phase spectrum will also be obtained, but this usually can be separated easily from the signal of the solid. This sample cell arrangement thus permits the study of the stationary-state surface during catalysis and also its evolution in response to pulses and step functions in the gas composition. The temperature of the sample should be controlled so that the surface can be studied during temperature-programmed desorption and reaction.

Modes of Operation

Steps and Pulses. Supposing that the proper equipment can be devised for measuring gas-phase and--in some cases--surface transients, the question arises as to what kind of forcing function should be used. An important class of experiments involves temperature as the perturbing variable. Temperature programmed desorption or reaction and flash desorption are widely used. Following transients induced by temperature change by mass spectrometric analysis of the gas phase has been highly developed by Madix and his students (29). In the present review we shall limit our discussion to concentration forcing functions.

Step functions up and down as perturbations have been related to many common one- and two-step processes by Kobayashi and Kobayashi (8). Figure 6, from our previous review (9) illustrates the parametric sensitivity of this version of the transient method. A switch is made from a flow of argon to N_2O/Ar over a NiO_2/SiO_2 catalyst at 350°C, and curve (1) of Fig. 6 shows the N_2 response. This curve has been computer-simulated by a model which requires *a* steady-state oxygen surface coverage θ of 0.58. Other values of θ can be used in the simulation, and they can lead to the correct steady-state rate, but as shown, the transient responses would be unambiguously altered from that actually observed. Note that the equilibrium oxygen surface coverage at the steady-state gas-phase oxygen concentration would be lower than 0.58 (5).

All these experiments involve a multicomponent response, ideally of both the gas phase and the surface. The number of

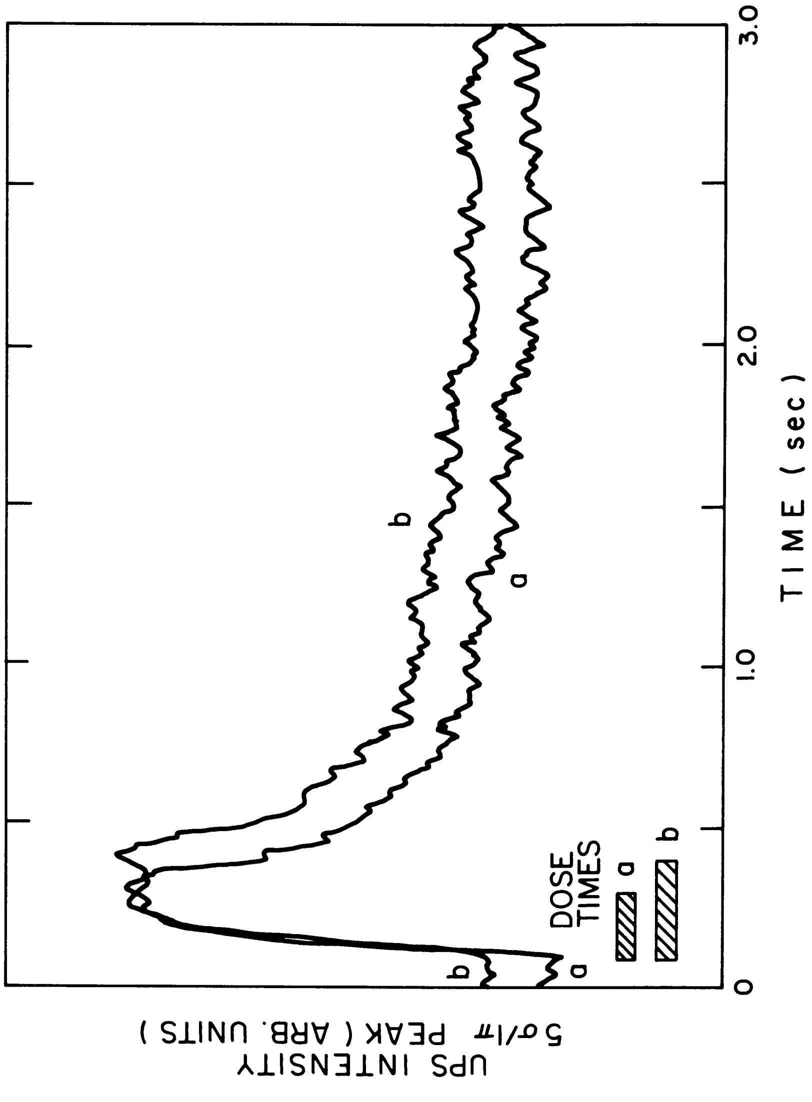

Surface Science

Figure 4. Adsorption–desorption of CO on Ni(111) at 175°C due to 200-ms doses (curve a) starting after 100-ms delays (from $t = 0$) and 300-ms doses (curve b) after similar delays (27).

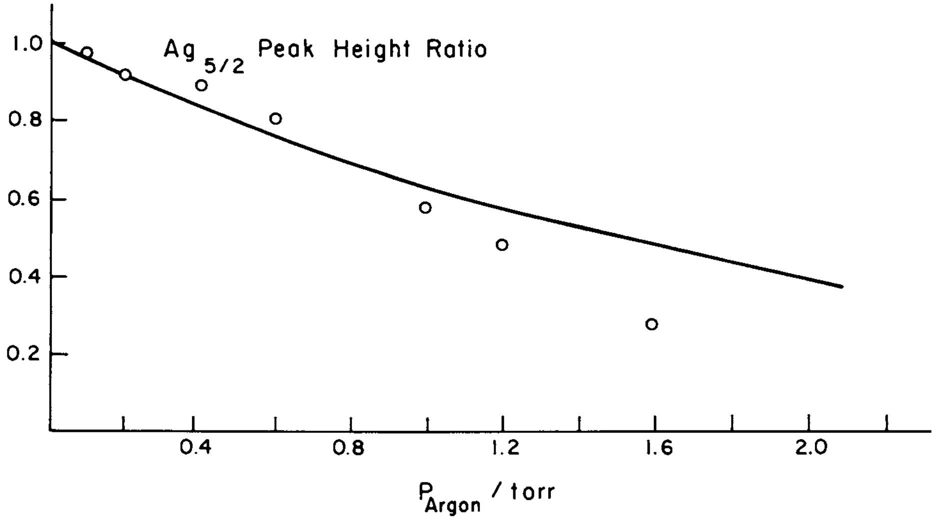

Surface Science

Figure 5. The attenuation of Ag $3d_{5/2}$ signal by Ar. Key: ○, experimental points; and —, theory (28).

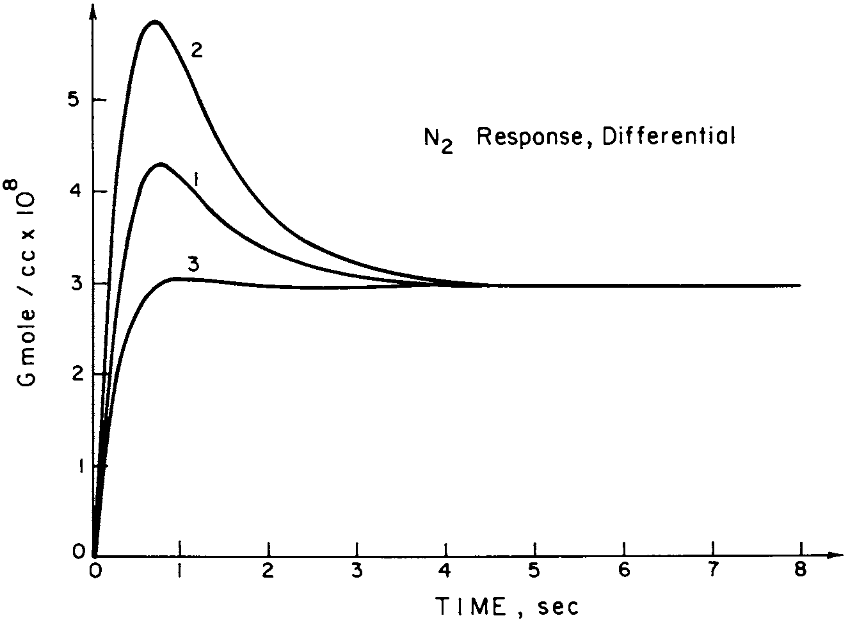

Catalysis Review

Figure 6. Decomposition of N_2O over NiO in a differential reactor. The steady-state surface oxygen coverage θ was 0.58 (curve 1), 0.69 (curve 2), and 0.28 (curve 3) (9).

In Catalysis Under Transient Conditions; Bell, A., et al.;
ACS Symposium Series; American Chemical Society: Washington, DC, 1982.

responses to fit--and thus the reliability of the result--can be increased by using stable isotopes. The quantitative manipulation of such a method has been most highly developed by Happel and co-workers (30). In this paper isotopic tracing is used to make it possible to identify the rate parameters of various steps in a sequence by a linear analysis. Methanation over a nickel catalyst has been studied. In the gas flowing to a gradientless reactor at steady state a step change is made from $H_2/^{12}CO$ to $H_2/^{13}CO$. The response is followed by mass spectrometry. All the chemistry, such as surface rates and coverages, is assumed to be unaltered by the change, so the result of the perturbation is that of a series of first-order processes, each one representing the accumulation of ^{13}C in a particular intermediate or gas component. We can speak of pools for the accumulation of ^{13}C without knowing the complete identity of each intermediate. By this method large concentrations of tracers can be used while retaining a convenient linear analysis. The mathematics of a similar superposition method has also been studied by Le Cardinal et al. (31). He and Happel have exchanged polemics on the matter (32, 33).

A disadvantage of tracer methods is the frequent presence of exchange processes which are difficult to account for. This hampered Happel's work with ^{18}O (30) and complicated the interpretation of the work of Conner and Bennett (34), who used pulses of tracers and a qualitative interpretation of their data on CO oxidation over NiO.

Cycled Feed. The qualitative interpretation of responses to steps and pulses is often possible, but the quantitative exploitation of the data requires the numerical integration of nonlinear differential equations incorporated into a program for the search for the best parameters. A sinusoidal variation of a feed component concentration around a steady state value can be analyzed by the well developed methods of linear analysis if the relative amplitudes of the responses are under about 0.1. The application of these ideas to a modulated molecular beam was developed by Jones et al. (7) in 1972. A number of simple sequences of linear steps produces frequency responses shown in Fig. 7 (7). Here ε is the ratio of product to reactant amplitude, η is the sticking probability, ω is the forcing frequency, and k_d is the desorption rate constant for the product. For the series process k_1 is the rate constant of the surface reaction, and for the branched process P is the fraction reacting through path 1 and desorbing with a rate constant k_{d1}. This method has recently been applied to the decomposition of hydrazine on Ir(111) by Merrill and Sawin (35).

Whether to use as perturbing function a step, pulse, or cycled feed depends on the particular system under study. For expensive tracers, a pulse is often mandatory. However, simple textbook relations based on a Dirac function do not usually apply, for a relatively long pulse may be required to get a good signal. A long enough pulse becomes two step functions, and as already men-

In Catalysis Under Transient Conditions; Bell, A., et al.;
ACS Symposium Series; American Chemical Society: Washington, DC, 1982.

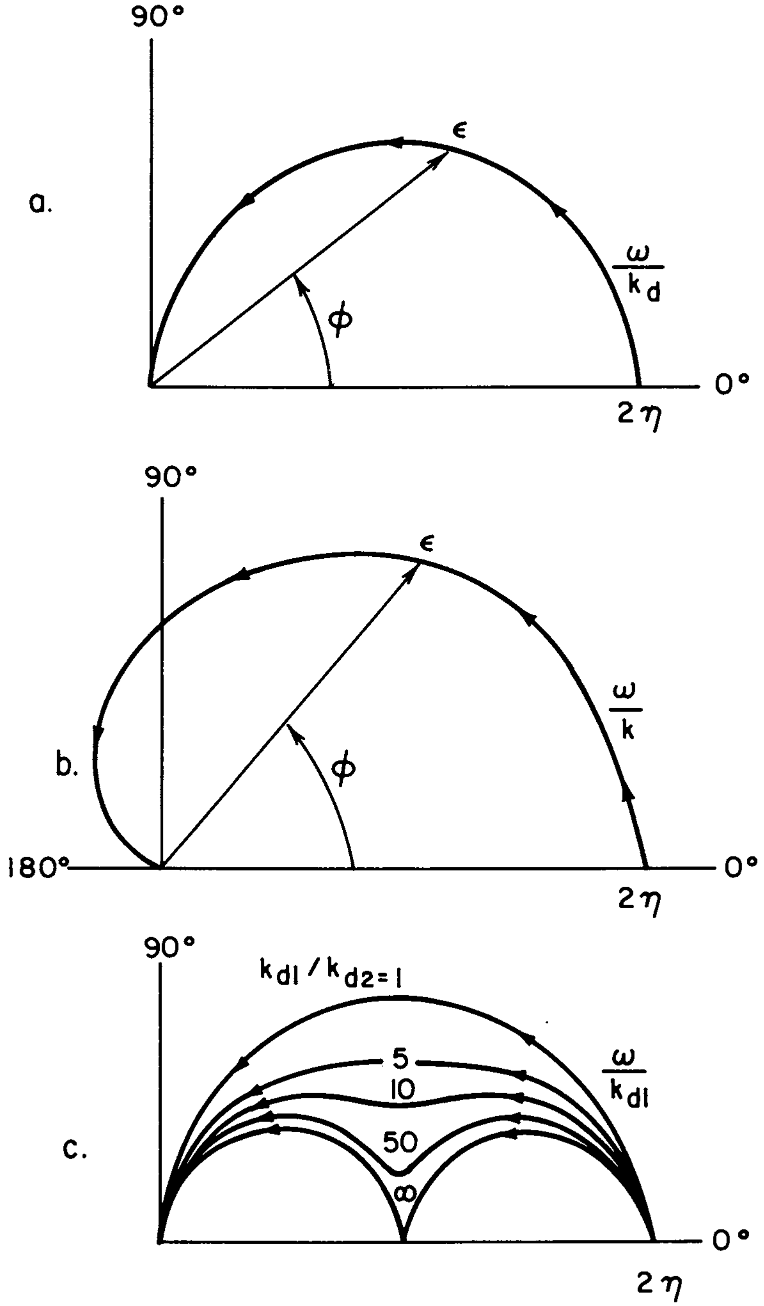

Journal of Vacuum Science and Technology

Figure 7. Polar plots of the reaction product vector for three surface mechanisms. Key: a, simple adsorption–desorption; b, series process, $k_1 = k_d = k$; and c, branch process, $P = 0.5$ (7).

tioned, there is a convenient directory of common responses (8). For a cycled feed (a chain of interfering pulses) the interpretation requires some mathematical transformations, but results such as Fig. 7 can also be used as qualitative indicators of certain processes (35). The complete computer simulation is quite tedious and has so far been done for relatively few reactions; thus the partial exploitation of the data in the spirit of preceding work is often all that is attempted in practice.

Strozier (36) has also used a cycled (pulsed) feed at UHV. As in the molecular beam experiment, the reactor volume, pumping speed, and rate of introduction of reactants have values which lead to a flux of reactants well defined in time. Strozier, however, simply doses gas into the vacuum system (reactor) rather than using a molecular beam. He studied CO oxidation, which has nonlinearities in the surface rate equation, so that computer rather than analytic solutions are necessary. The results are represented at constant frequency and varying temperature as shown in Fig. 8, which is a computer simulation (37).

Cycled-feed experiments are more complicated to analyze if done at atmospheric pressure and at relatively high conversion. Now the surface reaction rates alter the gas-phase reactant concentrations. Cutlip (38) has studied CO oxidation over Pt/Al_2O_3 in a gradientless reactor under conditions often leading to complete conversion. The feed gas alternated between 2% CO and 3% O_2 in argon. Figure 9 shows some typical results. Clearly there is no hope of simulating such data by anthing but a complicated computer model.

Figure 10 (38) shows that under some circumstances the rate is greatly enhanced (20 times) by a cycled feed. At the conditions shown there are no multiple steady states, the only steady state corresponds to a very high CO surface coverage. By alternately switching to pure oxygen, CO_2 is generated at a high rate from the adsorbed CO. The net result is as if the surface were more equally covered with oxygen and carbon monoxide with a Langmuir-Hinschelwood rate equation: $r = k\,(CO_{ads})(O_{ads})$.

Figure 11 shows the effect on CO conversion (oxidation) over two Rh/Al_2O_3 catalysts of cycling at 550°C as studied by Schlatter and Mitchell (39). Steady state operation (high frequency) gives complete conversion of a stoichiometric reactant mixture, and cycling around this steady state ratio must give a lower average conversion. Since the control operation to maintain an average stoichiometric ratio in the reactor feed leads to cycles of frequency about 1 Hz (39), it is of practical interest to understand these effects. Cerium has been added to the catalyst to try to retain oxygen and keep the rate up during the part of the cycle during which there is insufficient gaseous oxygen for complete conversion. As shown, Schlatter and Mitchell (39) found the Ce-containing catalyst superior, but the explanation for its behavior is more complicated than simple oxygen storage.

The possible importance of obtaining improved yield in a

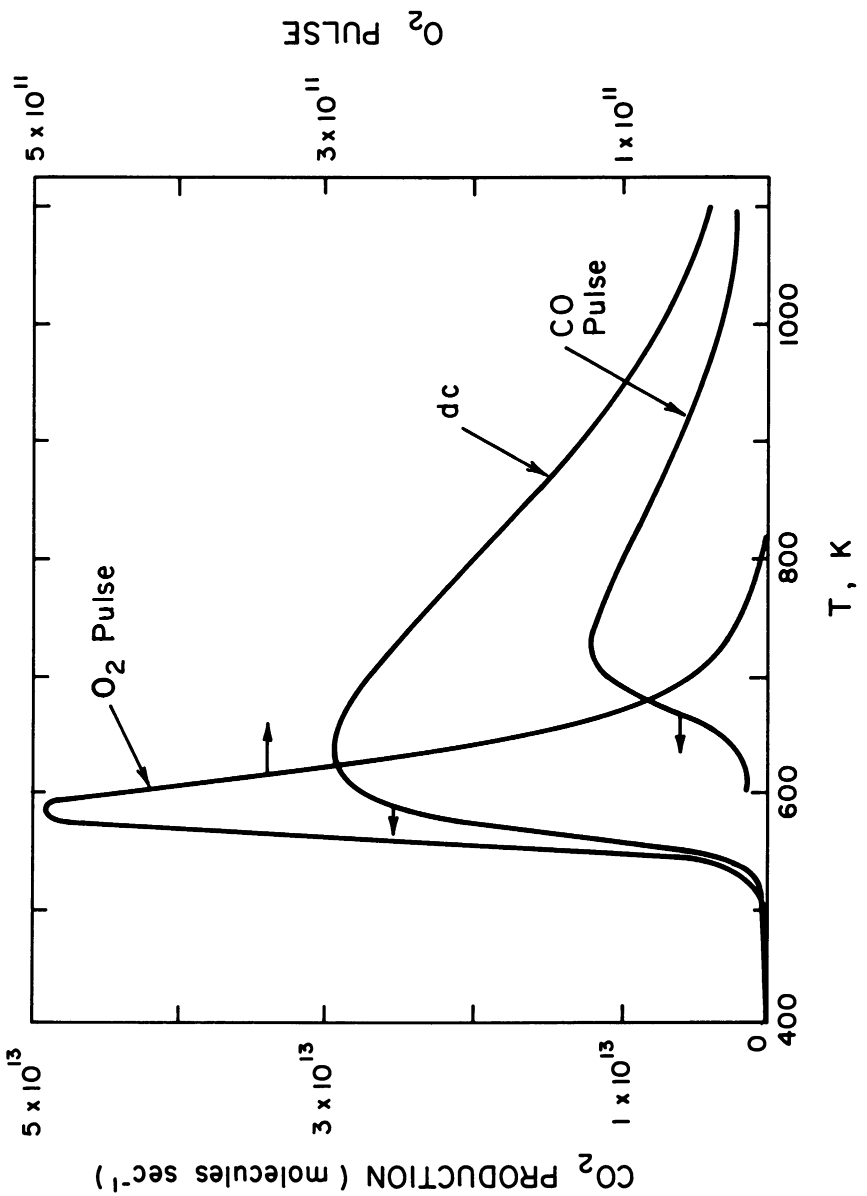

Surface Science

Figure 8. Responses averaged in time to steady and pulsed feeds for CO oxidation over Pt (37).

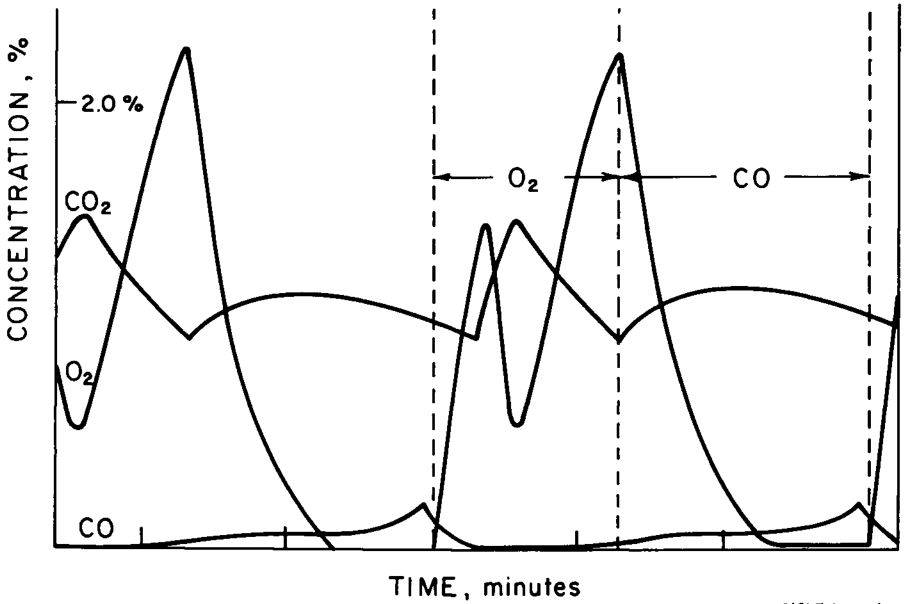

Figure 9. Reactor outlet concentrations during a 3-min period at 60°C (38). Feed is cycled from 2% CO at 80 s to 3% O_2 at 100 s over a Pt/Al_2O_3 catalyst at 60°C.

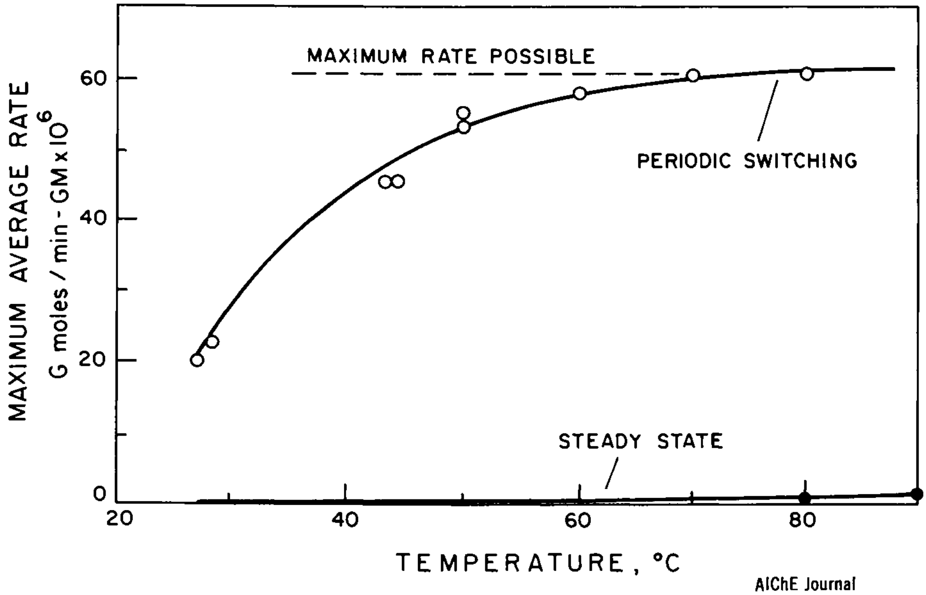

Figure 10. Rate comparison of periodic to steady-state operation for stoichiometric feed of CO/O_2 to Pt/Al_2O_3 catalyst (38).

In Catalysis Under Transient Conditions; Bell, A., et al.;
ACS Symposium Series; American Chemical Society: Washington, DC, 1982.

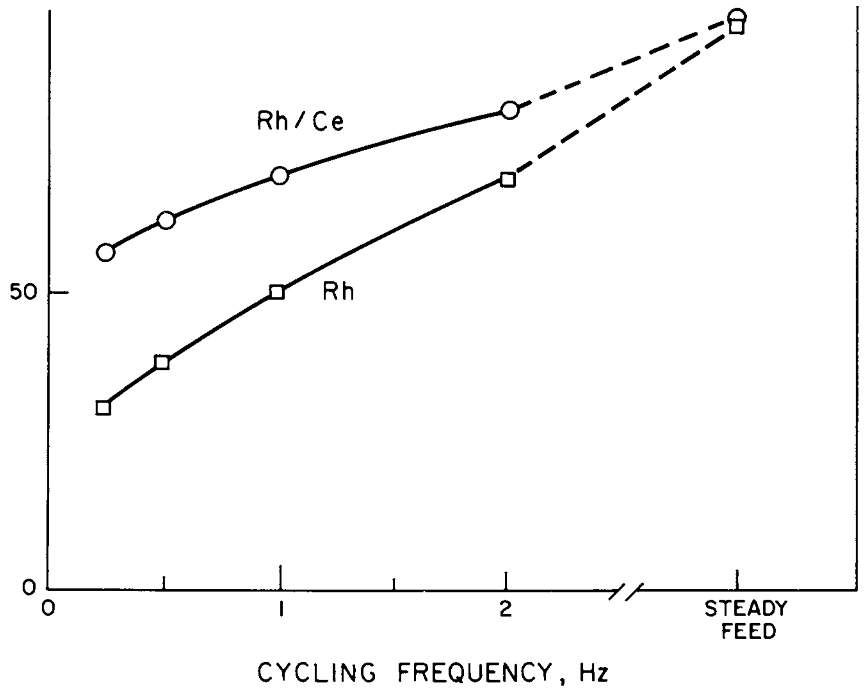

Figure 11. Effect of Ce on the cycled performance of a Rh/Al_2O_3 catalyst fed CO/O_2 mixtures at 550°C and a space velocity of 104,000 h^{-1} (39).

multiproduct catalytic process by feed concentration cycling has already been discussed in our previous review (9). Bilimoria and Bailey (40) have studied the hydrogenation of acetylene to ethylene and ethane, and Al-Taie and Kerschenbaum (41) have studied the hydrogenation of butadiene to butylene and to butane. In the latter work the yield of butylene was improved by cycling for certain reactor conditions. No mechanistic analysis is done in these papers from the Chemical Reaction Engineering Meeting in Houston beyond acknowledging that consideration of surface rates and capacities is essential.

Self-sustained Oscillations. Under certain conditions, isothermal limit cycles in gaseous concentrations over catalysts are observed. These are probably caused by interaction of steps on the surface. Sometimes heat and mass transfer effects intervene, leading to temperature oscillations also. Since this subject has recently been reviewed (42, 43) only a few recent papers will be mentioned here.

Cutlip and Kenney (44) have observed isothermal limit cycles in the oxidation of CO over 0.5% Pt/Al_2O_3 in a gradientless reactor only in the presence of added 1-butene. Without butene there were no oscillations although regions of multiple steady states exist. Dwyer (22) has followed the surface CO infrared adsorption band and found that it was in phase with the gas-phase concentration. Kurtanjek et al. (45) have studied hydrogen oxidation over Ni and have also taken the logical step of following the surface concentration. Contact potential difference was used to follow the oxidation state of the nickel surface. Under some conditions, oscillations were observed on the surface when none were detected in the gas phase. Recently, Sheintuch (46) has made additional studies of CO oxidation over Pt foil.

The N_2O decomposition, CO oxidation, and H_2 oxidation reactions are known to exhibit concentration oscillations over noble metal catalysts. Flytzani-Stephanopoulos et al. (47) have observed oscillations for the oxidation of NH_3 over Pt. The effects are dramatic and lead to large temperature cycles for the catalyst wire. Heat and mass transfer effects are important.

The Oxidation of Carbon Monoxide on Platinum

This subject has been thoroughly reviewed by Engel and Ertl (48) and most recently by White (49). Here the intention is to describe some contributions of the transient method to our understanding of this classical problem. Only the temperature range below 450K is discussed here.

The question of the role of the Eley-Rideal (ER) mechanism in the reaction is usually investigated by the reaction of preadsorbed oxygen with CO from the gas phase. The well known results of Bonzel and Ku (6) are shown in Fig. 12. CO_2 is immediately produced, lending some support to the existance of an ER step. However, Matsushima et al. (26) have used Auger electron spectros-

copy to follow the surface concentration of oxygen (dissociated into adsorbed atoms) during the same process. Although the rate is about first-order in gas-phase CO concentration, it is zero-order in surface O, as shown in Fig. 13. The order does increase as the surface oxygen is depleted. The result is interpreted as showing that CO does not react by impact on oxygen atoms but must adsorb in a mobil precursor state.

In a later article, Matsushima (50) has used a transient tracer method at 301K to study the ER process further. The surface of the Pt was initially exposed to a pulse of a mixture of $^{13}CO/^{12}CO$ so that the CO surface coverage was 0.23 and the ratio of $^{13}CO(a)$ to $^{12}CO(a)$ was 1.6. Then a pulse of $^{12}CO + O_2$ was admitted, and the first CO_2 to be produced had the same $^{13}C/^{12}C$ ratio as the preadsorbed CO. This result is interpreted as meaning that the surface oxygen reacts with surface CO much faster than with the gaseous CO; the ER step plays a minor role.

This process has been studied by infrared spectroscopy by Dwyer (22), using 9% Pt/SiO_2 and the cell used by Ueno et al. (19). The bands arising from gaseous CO_2 and surface CO were followed after a switch in the gas phase composition from 3kPa O_2 in helium, to pure helium for a few seconds and then to 2kPa CO in helium. This is basically the same sequence as that of Fig. 12. The results are shown in Fig. 14. The CO(a) band grows immediately and at the same time CO_2 is produced. Taken with the results of Matsushima et al. (26, 50) it seems reasonable that the ER step plays a minor role in the reaction between CO and O(a).

The process O_2 + CO(a) is also interesting and this can be studied by a gas phase switch from CO to O_2. As mentioned above a short exposure to helium between the CO and O_2 is used. This procedure eliminates the interaction of CO and O_2 during the mixing time (ca 2 s) for the cell. Oxygen does not desorb in helium ($T<450K$) but Dwyer (22) found that CO does, as shown in Fig. 15. The process was studied so that suitable corrections could be made for the CO → He → O_2 experiments. The desorption of Fig. 15 starts from a surface coverage of CO near unity. From the initial rates an activation energy of 8 kcal/mole is obtained. This may be compared with 9 kcal/mole reported by Nashayima and Wise (51). Figure 16 (22) shows that the slight desorption of loosely bound CO has a remarkably large effect on the CO(a) left on the surface.

The results of the CO → He → O_2 experiment (22) are shown in Fig. 17. There is an induction time between the admission of O_2 and start of the reaction of CO(a). Oxygen cannot react from the gas phase, and its adsorption must await the desorption of a trace of CO(a). Bonzel and Ku () found a similar result, as shown in Fig. 18. Their induction times are much longer than those of Dwyer (22), perhaps because of the regularity of their (110) surface.

From these examples it is clear that the transient results add important understanding to our ideas about the oxidation of CO over Pt.

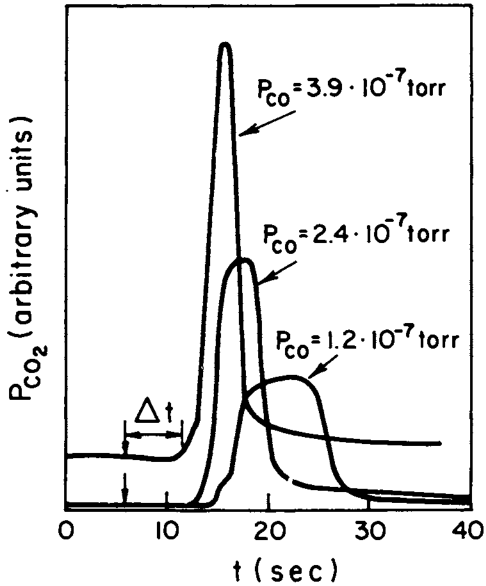

Surface Science

Figure 12. Reaction between CO and preadsorbed oxygen on Pt (110) at 218°C (6).

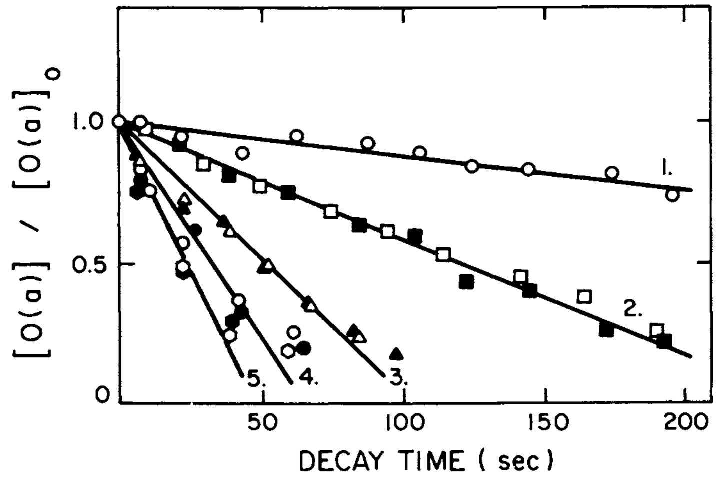

Figure 13. Reaction of surface O with CO for several fixed CO pressures over Pt measured by Auger electron spectroscopy. Key: Fixed CO pressures (Pa) are 1.86 × 10^{-7} (1), 6.27 × 10^{-7} (2), 1.67 × 10^{-6} (3), 2.8 × 10^{-6} (4), and 4.8 × 10^{-6} (5). The light and dark symbols denote separate experiments (26).

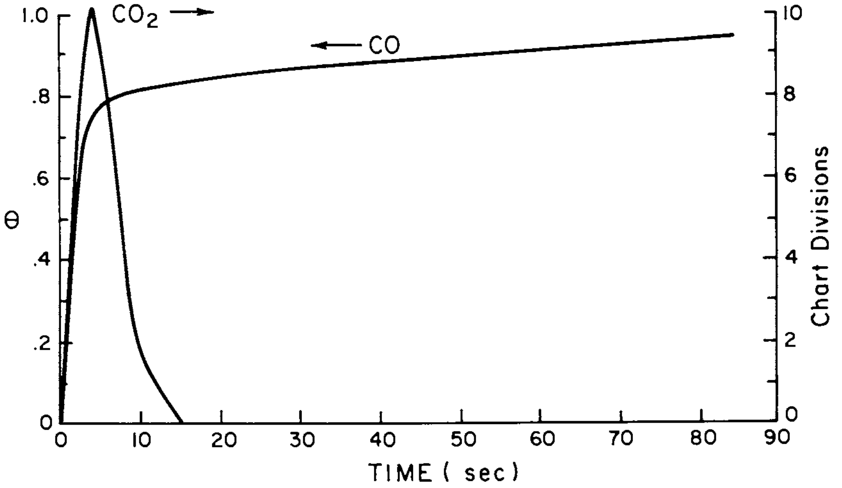

Figure 14. Reaction between CO and O_2 preadsorbed on Pt/SiO_2 (22) at 160°C and flow rate of 9.5 mL/60 s.

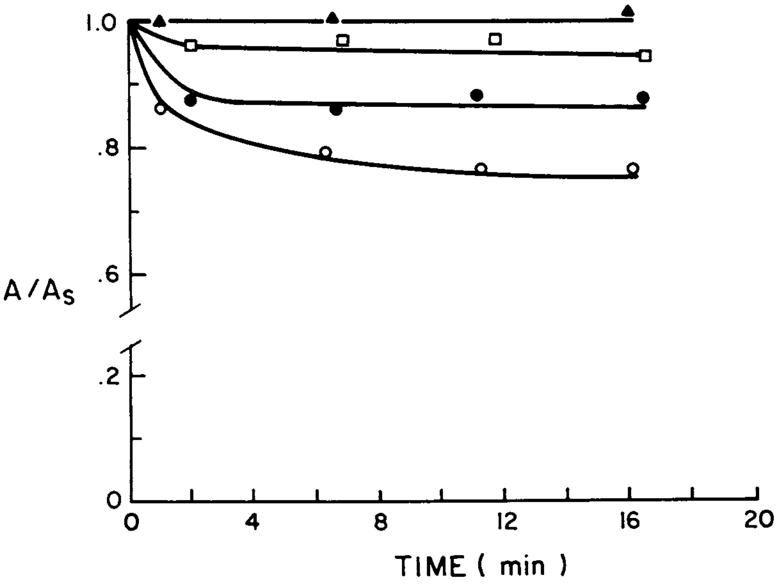

Figure 15. Desorption of CO from Pt/SiO_2 (22). Key: ▲, 100°C; □, 120°C; ●, 140°C; and ○, 160°C.

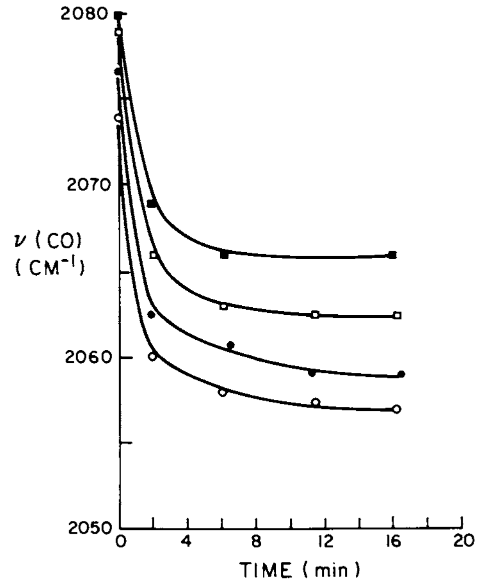

Figure 16. Variation of IR frequency during CO desorption from Pt/SiO₂. Key: ■, 100°C; □, 120°C; ●, 140°C; and ○, 160°C (22).

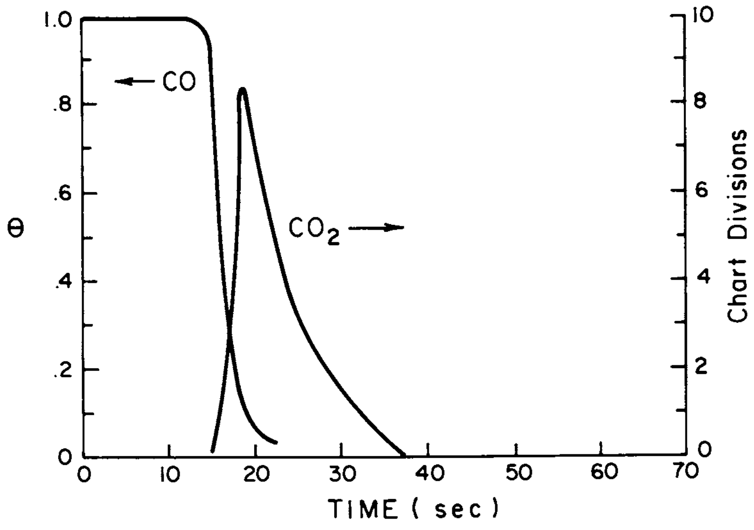

Figure 17. Reaction between O_2 and CO preadsorbed on Pt/SiO_2 (22) at 160°C and flow rate of 9.5 mL/60 s.

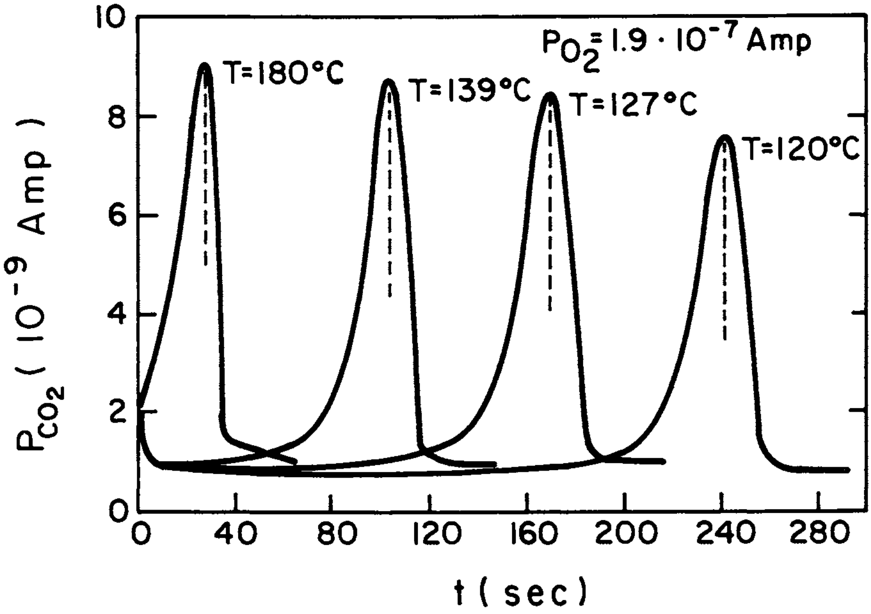

Surface Science

Figure 18. Rate of CO_2 formation on Pt (110). Initially, the Pt (110) surface was exposed to a feed mixture of CO and oxygen. Then at t = 0, the partial pressure of CO was suddenly reduced and the subsequent rate of CO_2 formation was measured (6).

The Reaction of Hydrogen and Carbon Monoxide over Iron

The transient method has contributed to our understanding of H_2/CO reactions, and a few results of studies over iron will show the power of the method. Matsumoto and Bennett (52) worked with a CCI fused iron catalyst (ca 96% iron) which had been reduced in flowing H_2 at 450°C for at least 15 h. Upon switching to a feed of 10% CO in H_2, the data of Fig. 19 were obtained. Large rates of production of H_2O and CO_2 are observed as CO is dissociated on the fresh catalyst. The production of methane and higher hydrocarbons starts at zero and gradually increases. This result was interpreted as evidence that surface carbon reacted preferentially with iron to form a carbide. As this reaction slowed with time, surface carbon built up and led to the production of methane and lower production rates for CO_2 and H_2O. Figure 20, from Reymond et al. (25) shows the evolution of the methane production rate over a longer period. A switch from the H_2/CO feed to pure H_2 produced a peak of methane as shown (250°C). This increase in CH_4 production rate shows that H_2 must be adsorbed (probably dissociated as H) in order to react, and also that the steady-state surface must be largely covered with carbonaceous intermediate. Methane production seems to be governed by the equation $r = k\ C(a)\ H(a)$, with $C(a) > H(a)$ so that an increase in H(a) leads to a higher rate. The second peak in Fig. 20 represents methane generated by the decarburization of the bulk of the iron.

When the freshly reduced catalyst is suddenly exposed to 10% C_2H_4 in H_2 the result is shown in Fig. 21 (25). Chain growth occurs as with CO/H_2, but the reaction rate decreases from an initial maximum as the surface becomes covered with intermediates. A switch to pure H_2 produces only a trace of methane, even on heating to 500°C, so no surface carbon or bulk carbide has been formed. Probably the sequence of steps passes through a CH_2 intermediate, whereas C is needed for carburizing the iron. The rate of reaction of C_2H_4/H_2 is higher than that of CO/H_2, lending weight to the concept of the hydrogenation of C(a) as the rate-determining step for the latter.

Some of these same experiments have been done using 10% Fe/Al_2O_3 rather than the fused iron catalyst (53). Figure 22 shows the result of a switch from H_2 to 10% CO in H_2 over a freshly reduced catalyst. Here a large initial rate of methane formation is observed and water does not appear until most of the initial peak has passed. The probable explanation for the presence of the CH_4 peak is that water produced by methanation is adsorbed on the initially dry γ-Al_2O_3 support (100 m^2/g). Thus the iron remains briefly in a relatively reduced state. For the CCI catalyst the Al_2O_3 promoter is not sufficient to prevent the water from rising quickly as shown in Fig. 19. The H/O ratio on the surface is reduced, and carburization occurs more rapidly than methanation, as for the unsupported catalyst.

When the 10% Fe/Al_2O_3 catalyst is pretreated with water vapor,

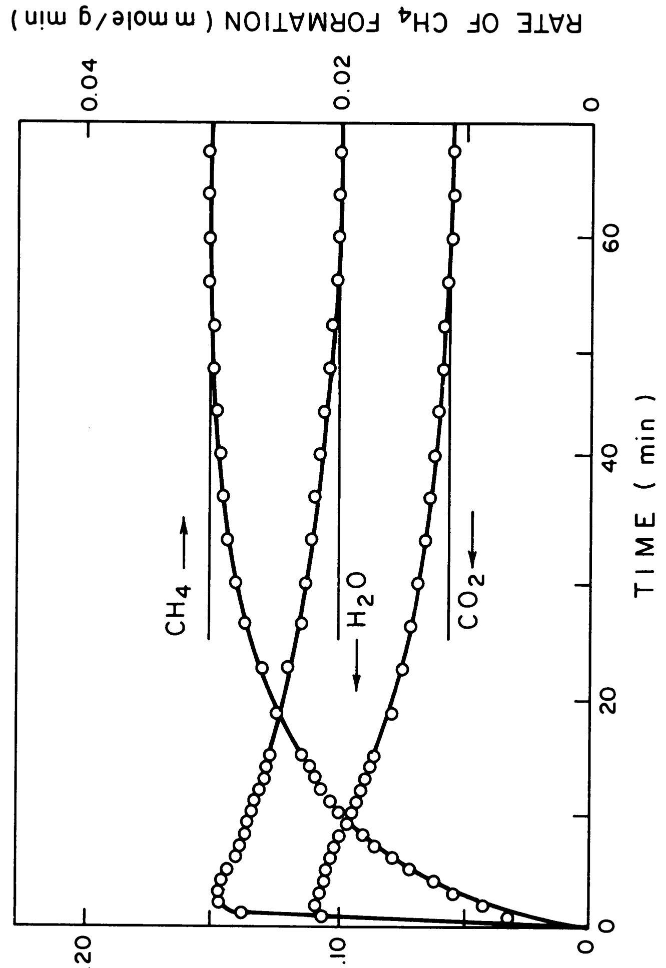

Journal of Catalysis

Figure 19. Formation of major components as a function of exposure time for the reaction of 10% CO/H_2 at 250°C over CCI fused iron catalyst (reduced at 450°C) (52).

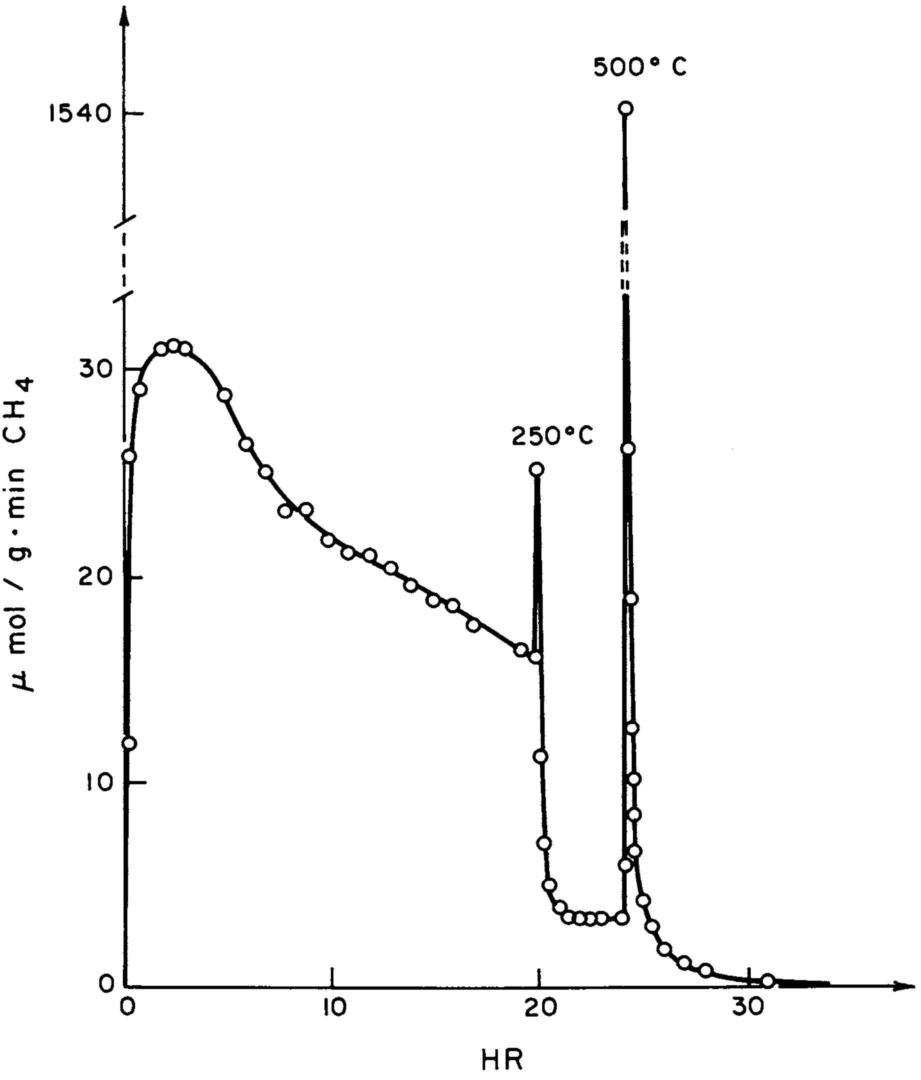

Journal of Catalysis

Figure 20. Hydrogenation of surface carbon over catalyst initially reduced for 15 h at 500°C and then cooled to 250°C. At t = 0 flow is switched to H_2/CO = 9, 250°C. At 20 h feed is switched to pure H_2, 250°C; at 24 h temperature is raised to 500°C (25).

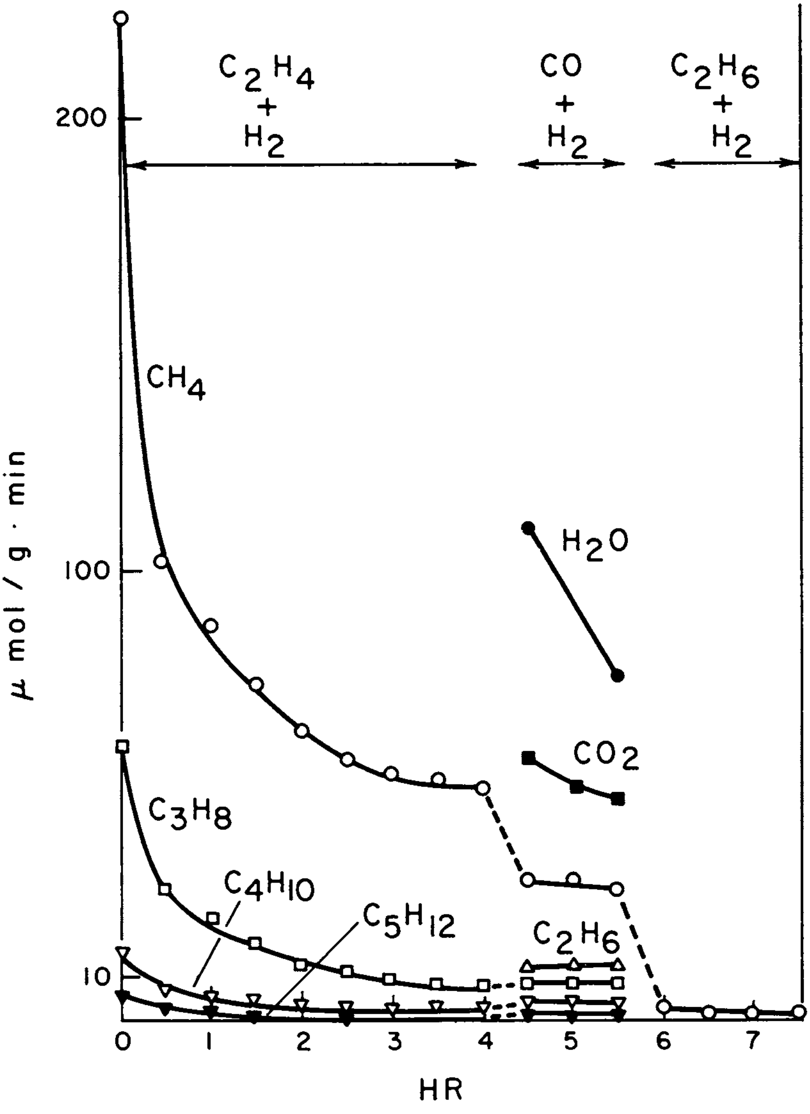

Journal of Catalysis

Figure 21. Reaction of ethylene and hydrogen (1:10) on a reduced catalyst at 250°C, followed by switch to CO/H_2 (1:10) and then C_2H_6/H_2 (1:10) (25).

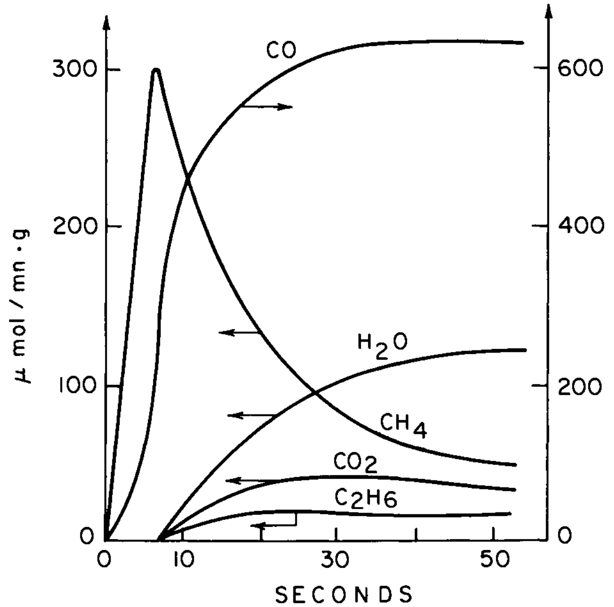

Figure 22. Initial production rates of principal products from a 10% Fe/Al_2O_3 catalyst (53).

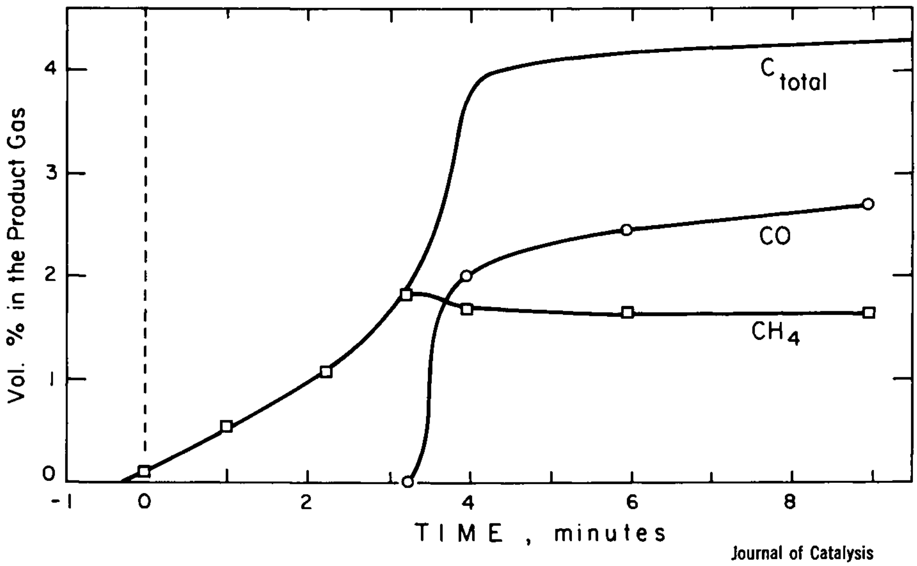

Figure 23. Response of the 10% Ni/SiO_2 catalyst to a step increase in P_{CO} (54). Conditions: 190°C; P_{H_2} 1 atm; $t < 0$, $P_{CO} = 0$; $t > 0$, $P_{CO} = 0.44$ atm; and flow rate = 100 mL/60 s.

the methane production behaves as for the CCI catalyst--it rises from zero as in Fig. 19.

Van Ho and Harriott (54) have done similar transient experiments on H_2/CO over 10% Ni/SiO_2, and a result is shown in Fig. 23. Even though the bulk of the nickel is not carbided, the methane production rate rises from zero, as shown.

The complete discussion of these experiments is beyond the scope of this review. By showing these few results some idea of the richness in information of the transient data is conveyed. Any model which can explain all such complicated results is bound to be nearer the truth than one based on steady state data alone. An understanding improves, it is permitted to hope that this will eventually lead to the development of better catalysts.

Summary

From the examples discussed in this review it is clear that a proper understanding of heterogeneous catalysis is linked to understanding transient effects. The interpretation requires a model based on elementary steps, and various steps may be rate-determining as the conversion and temperature vary. Complicated programs for fitting a steady-state equation to data are not sufficient if the equation itself changes with conversion, for example. Any mathematical control or design calculations in reactor design must take into account the elementary steps and the storage capacity of the catalyst surface.

Understanding catalysis has been emphasized here, but the possible practical effects of deliberate cycling of a reactor feed to improve yield must also be kept in mind. Also, undesired feed oscillations must be taken into account in the design of a reactor. Design for such a situation is not possible based on steady state laboratory data alone.

Acknowledgement

This work was supported by NSF grants #ENG-7921890, and #CPE-7901018 A01.

Literature Cited

1. Wagner, Carl, and Hauffe, Karl. Untersuchungen über den stationären Zustand von Katalysatoren bei heterogenen Reaktionen. I: Ztschr. Elektrochem. 1938, 44 (3) 172; II: ibid. 1939, 45 (5) 409.
2. Tamaru, Kenzi. Adsorption measurements during surface catalysis. Adv. Catal. 1964, 15, 65.
3. Bennett, C. O. A dynamic method for the study of heterogeneous catalytic kinetics. A.I.Ch.E. J. 1967, 13, 890.
4. Kobayashi, M., and Kobayashi H. Application of transient response method to the study of heterogeneous catalysis. J. Catal. 1972, 27, 100, 108, 114.

5. Yang, C. C., Cutlip, M. B., and Bennett, C. O. A study of nitrous oxide decomposition on nickel oxide by a dynamic method. Proc. of the Vth Congr. on Catal., Palm Beach, 1973.
6. Bonzel, H. P., and Ku, R. Mechanisms of the catalytic carbon monoxide oxidation on Pt(110). Surface Sci. 1972, 33, 91.
7. Jones, R. H., Olander, D. R., Siekhaus, W. J., and Schwarz, J.A. Investigation of gas-solid reactions by modulated molecular beam mass spectrometry. J. Vac. Sci. Technol. 1972, 9, 1429.
8. Kobayashi, M., and Kobayashi, M. Transient response method in heterogeneous catalysis. Catal. Rev.-Sci. Eng. 1974, 10 (2), 139.
9. Bennett, C. O. The transient method and elementary steps in heterogeneous catalysis. Catal. Rev.-Sci. Eng. 1976, 13 (2), 121.
10. Temkin, M. I. Relaxation rate of a two-stage catalytic reaction. Kin. and Catal. 1976, 17 (5), 1095.
11. Krylov, O. V. Elementary processes determining the mechanisms of a catalytic reaction. Kin. and Catal. 1980, 21 (1), 79.
12. Dorawala, T. G., and Douglas, J. M. Complex reactions in oscillating reactors. A.I.Ch.E. J.. 1971, 17 (4), 974.
13. Schmitz, Roger A. Multiplicity, stability, and sensitivity of states in chemically reacting systems--A review. Adv. Chem. Sci. 1975, 148, 154.
14. Sheintuch, M., and Schmitz, R. A. Kinetic modeling of oscillatory catalytic reactions. ACS Symp. Ser. 1978, 65, 487.
15. Bennett, C. O., Cutlip, M. B., and Yang, C. C. Gradientless reactors and transient methods in heterogeneous catalysis. Chem. Eng. Sci. 1972, 27, 2255.
16. Heyne, H., and Tomkins, F. C. Application of infrared spectroscopy and surface potential measurements in a study of the oxidation of carbon monoxide on platinum. Proc. Roy. Soc., Ser. A. 1966. 292, 460.
17. Tamaru, K. Recent progress in elucidating the mechanism of heterogeneous catalysis. Pure and Appl. Chem. 1980. 52, 2067.
18. Dent, A. L., and Kokes, R. J. Intermediates in ethylene hydrogenation over zinc oxide. J. Phy. Chem. 1970. 74, 3653.
19. Ueno, A., Hochmuth, J. K., and Bennett, C. O. Interaction of CO_2, CO, and NiO studied by infrared spectroscopy. J. Catal. 1977. 49, 225.
20. Ueno, A., and Bennett, C. O. Infrared study of CO_2 adsorption on SiO_2, J. Catal. 1978. 54, 31.
21. Savatsky, B. J., and Bell, A. T. Studies of NO reduction by H_2 using transient response techniques. This volume.
22. Dwyer, S. M. Transient infrared studies of carbon monoxide oxidation on a supported platinum catalyst. M.S. Thesis, University of Connecticut, 1980.
23. Hegedus, L. L. Infrared spectroscopic reactor system to study the transient operation of heterogeneous catalysts.

24. Peri, J. B. Characterization of catalyst surfaces by computerized infrared spectroscopy. Prepr., Div. Pet. Chem., Am. Chem. Soc. 1978. 23 (4), 1281.
25. Reymond, J. P., Mériaudeau, P., Pommier, B., and Bennett, C. O. Further results on the reaction of H_2/CO on fused iron by the transient method. J. Catal. 1980. 64, 163.
26. Matsushima, T., Almy, D. B., and White, J. M. The reactivity and Auger chemical shift of oxygen adsorbed on platinum. Surface Sci. 1977. 67, 89-108.
27. Rubloff, G. W. Photoemission studies of time-resolved surface reactions: Isothermal desorption of CO from Ni (111). Surface Sci. 1979. 89, 566.
28. Joyner, R. W., and Roberts, M. W. A high-pressure electron spectrometer for surface studies. Surface Sci. 1979. 87, 501.
29. Johnson, S. W., and Madix, R. J. Modification of adsorption and desorption of CO and H_2 and surface reactions of alcohols by sulfur on Ni (100). ACS Symp. Ser. 1981; Madix, R. J. Adv. in Catal. 1980. 29.
30. Happel, J., Suzuki, I., Kokayeff, P., and Fthenakis, V. Multiple isotope tracing of methanation over nickel catalyst. J. Catal. 1980. 65, 59.
31. Le Cardinal, G., Walter, E., Bertrand, P., Zoulalian, A. and Gelas, M. A new operating method for the kinetic study of open systems by means of tracer elements. Chem. Eng. Sci. 1977. 32, 733.
32. Happel, J. Transient tracing. Chem. Eng. Sci. 1978. 33, 1567.
33. Le Cardinal, G. Chem. Eng. Sci. 1978. 33, 1568.
34. Conner, W. C., and Bennett, C. O. Carbon monoxide oxidation on nickel oxide. J. Catal. 1976. 41, 30.
35. Merrill, R. P., and Sawin, H. H. Decomposition of hydrazine on Ir (111). This volume.
36. Strozier, J. A., Jr. Oxidation of CO on Pt by an a.c. pulsing technique. II. Experiment. Surface Sci. 1979. 87, 161.
37. Strozier, J. A., Jr. Cosgrove, G. J., and Fischer, D. A. Oxidation of CO on Pt and Pd. I. Theory. Surface Sci. 1979. 82, 481.
38. Cutlip, M. B. Concentration forcing of catalytic surface rate processes. A.I.Ch.E. J. 1979. 25 (3) 502.
39. Schlatter, J. C., and Mitchell, P. J. Three-way catalyst response to transients. Ind. Eng. Chem. Prod. Res. Dev. 1980. 19, 288.
40. Bilimoria, M. R., and Bailey, J. E. Dynamic studies of acetylene hydrogenation on nickel catalysts. ACS Symp. Ser. 1978. 65, 43.
41. Al-Tai, A. S., and Kerschenbaum, L. S. Effect of periodic operation on the selectivity of catalytic reactions. ACS Symp. Ser. 1978. 65, 42.

42. Sheintuch, M., and Schmitz, R. A. Oscillations in catalytic reactions. Catal. Rev. 1977. 15 (1) 107.
43. Slin'ko, M. G., and Slin'ko, M. M. Self-oscillations of heterogeneous catalytic reaction rates. Catal. Rev.-Sci. Eng. 1978. 17 (1) 119.
44. Cutlip, M. B., and Kenney, C. N. Limit cycle phenomena during catalytic oxidation reactions over a supported platinum catalyst. ACS Symp. Ser. 1978. 65, 39.
45. Kurtanjek, A., Sheintuch, M., and Luss, D. Surface state and kinetic oscillations in the oxidation of hydrogen on nickel. J. Catal. 1980. 66, 11.
46. Sheintuch, M. Oscillatory state in the oxidation of carbon monoxide on platinum. A.I.Ch.E. J. 1981. 27, 20.
47. Flytzani-Stephanopoulos, M., Schmidt, L. D., and Caretta, R. Steady state and transient oscillations in NH_3 oxidation on Pt. J. Catal. 1980. 64, 346.
48. Engle, T., and Ertl, G. Elementary steps in the catalytic oxidation of carbon monoxide on platinum metals. Advances in Catalysis. 28. New York: Academic Press, Inc., New York. 1979.
49. White, J. M. Transient low-pressure studies of catalytic carbon monoxide oxidation. This volume.
50. Matsushima, T. Kinetic studies on the CO oxidation over platinum by means of carbon 13 tracer. Surface Sci. 1979. 79, 63.
51. Nishiyama, Y., and Wise, H. Surface interactions between chemisorbed species on platinum: Carbon monoxide, hydrogen, oxygen, and methanol. J. Catal. 1974. 32, 50.
52. Matsumoto, H., and Bennett, C. O. The transient method applied to the methanation and Fischer-Tropsch reactions over a fused iron catalyst. J. Catal. 1978. 53,331.
53. Teule-Gay, F. Transient studies of the CO/H_2 reaction on various supported iron catalysts. M. S. Thesis, University of Connecticut, 1981.
54. Van Ho, S., and Harriott, P. The kinetics of methanation on nickel catalysts. J. Catal. 1980. 64, 272.
55. Murphy, R. E., Cook, F. H., and Saki, H. J. Opt. Soc. Am. 1975. 65, 600.
56. Mantz, A. W. Appl. Spectroscopy. 1976. 30, 459.

RECEIVED July 28, 1981.

Transient Low-Pressure Studies of Catalytic Carbon Monoxide Oxidation

J. R. CREIGHTON and J. M. WHITE

University of Texas, Department of Chemistry, Austin, TX 78712

The purpose of this article is to review the results of transient low pressure studies of carbon monoxide oxidation over transition metal substrates. Particular emphasis is given to the use of in-situ electron spectroscopy, flash desorption, modulated beam and titration techniques. The strengths and weaknesses of these will be assessed with regard to kinetic insight and quantification. An attempt will be made to identify questions that are ripe for investigation. Although not limited to it, the presentation emphasizes our own work. A very recent review of the carbon monoxide oxidation reaction (1) will be useful to readers who are interested in a more comprehensive view.

The carbon monoxide oxidation reaction has been widely studied over the course of many years. The pioneering work of Langmuir (2) set the tone for much of the subsequent work and we continue to refine many of his ideas. Catalyzed carbon monoxide oxidation is perhaps better understood than any other heterogeneous reaction and, because it shows little variation with crystal plane (3), there is a good correlation of low area single crystal results with high area supported catalyst results. This is particularly true under conditions where CO accumulates and inhibits the rate of CO_2 production (4,5). In the realm of applications, CO oxidation is a significant consideration in systems designed to limit undesirable emissions from combustion processes.

At the outset, it is worth noting how transient data fit into the overall picture of this reaction and what we expect to learn by doing such experiments. With the exception of oscillations (6), transients are induced by rapidly changing one or more of the independent variables of the system. For the case

0097-6156/82/0178-0033$06.50/0
© 1982 American Chemical Society

of CO oxidation, changing the substrate temperature or the partial pressures of CO or O_2 induces such transients. The information generated comes from measurement of the time evolution of surface coverages and gas phase composition. The former are, of course, central to any kinetic description involving adsorbed species; measurements under working conditions give the greatest insight because they are directly related to the CO_2 production rates. The latter provide product formation and adsorption/desorption rates during transients. In addition, when used in conjunction with a model, coverages can be calculated from pressure versus time data. Taken together these measurements in principle provide the rates and coverages needed for a full kinetic description. In practice, there are serious experimental limits on the measurements. In particular the dynamic range over which surface concentrations can be reliably measured is 0.01 to 1 monolayer; the lower end of this range is particularly troublesome. Moreover, because adsorbed species often occupy sites of variable activity on a surface, measurement of the total concentration of an adsorbed species may be insufficient. Improved resolution and measurement of small concentrations of relatively labile surface species lie at the heart of experimental progress in the surface chemistry of heterogeneous catalysis. Succinctly put, the old catalytic chemists' proverb, "if you can see a certain surface species, it is not kinetically important", must be taken seriously. However, in the case of CO oxidation, the kinetically active adsorbed oxygen and carbon monoxide species can in fact be measured under many, but not all, conditions.

Transients Induced by Temperature Changes

One of the standard surface science methods for assessing the concentration and stability of a chemisorbed species is thermal desorption spectroscopy (TDS). An early paper by Redhead (7) developed the conceptual framework for certain cases. Many papers since then have expanded the applicability of this method. Recent work of Madix (8), Weinberg (9) and Schmidt (10) is particularly noteworthy. Most of this work focuses on the desorption of a single molecular species and not on reactions in desorbing systems. However, qualitative features of the temperature dependence of reactions can be assessed using this method. Figures 1 and 2 taken from the

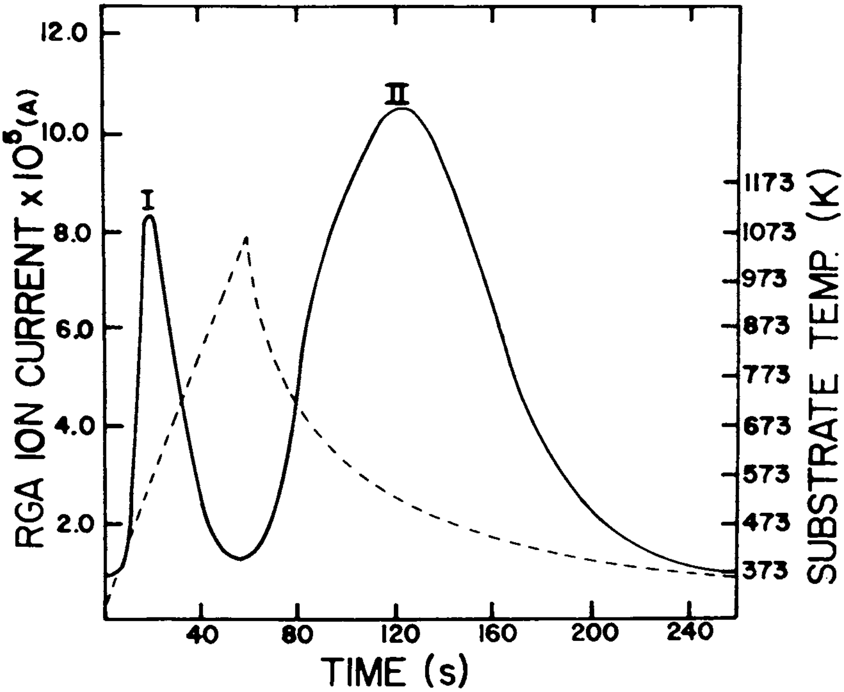

Journal of Catalysis

Figure 1. Variation of CO_2 pressure with time during the flash of a Pd substrate preexposed to oxygen at high temperatures. The total pressure was about 10^{-4} Pa and $O_2/CO \simeq 1.5$. Key: – – –, temperature variation; and ——, CO_2 pressure (11).

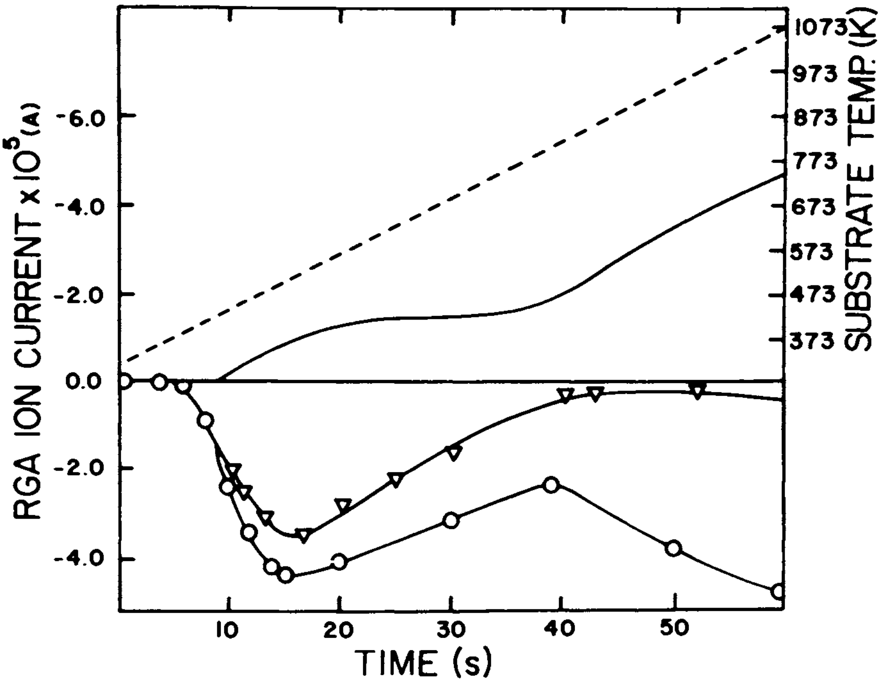

Journal of Catalysis

Figure 2. Non-steady state variation of O_2 pressure with time during flashing of a stable polycrystalline Pd substrate. Initial $O_2/CO = 1.5$. The origin of the ordinate is defined as the O_2 pressure at 300 K. Key: ○, observed O_2; ▽, calculated on the basis of CO_2 production; ——, difference between calculated and observed; and – – –, temperature (11).

work of John Close (11) in our laboratory adequately illustrate the point.

Figure 1 shows the variation of the CO_2 pressure during the flash and subsequent cool down of a polycrystalline Pd foil. The sample, mounted within a continuously pumped UHV system, was exposed to 10^{-6} torr of a mixture characterized by $O_2/CO = 1.5$. After stabilization at 300K, the sample was heated resistively at a rate of $12Ks^{-1}$ while the CO_2 partial pressure was monitored mass spectrometrically. The CO_2 signal, which is a measure of the CO_2 production rate, is strongly peaked on both the heating and cooling cycles. Since the maxima both occur near 573K, we expect to find maxima in the steady-state CO_2 production rates near the same temperature. This data was used as a qualitative guide only. The only significant differences in the rates are the amplitude, which is higher during cool-down, and the peak temperature, which is slightly lower during cool down. These are ascribed to two differences: (1) the absolute rate of temperature change and (2) the amounts of adsorbed CO and oxygen which are present during the transients.

Figure 2 shows data from the variation of P_{O_2} taken under conditions similar to those of Figure 1. The origin of the ordinate is defined as the steady state O_2 pressure measured at 300K. As the sample is heated the O_2 pressure drops (open circles) goes through a local minimum and a maximum between 15 and 40s (500 and 800K). The triangles show a predicted O_2 pressure curve based on CO_2 pressure. Although one might argue that inaccurate relative sensitivities can account for some of the difference in these two curves, it is clear that the local maximum in the experimental O_2 consumption is not reflected in the calculated curve based on CO_2 production. As indicated by the difference spectrum (solid line in the upper portion of Figure 2) there is not a single scaling factor which will bring any significant portion of these two curves into coincidence. From these results we conclude that O penetration into the subsurface region is an important process, particularly at high temperatures. The significance of this process has been confirmed by work in our own (12) and other laboratories (13).

A central point to be made in connection with Figures 1 and 2 is that a great deal of qualitative insight can be gained from relatively simple experiments. The results guide the selection of temperatures for steady-state and transient experiments which can be analyzed more quantitatively.

In Catalysis Under Transient Conditions; Bell, A., et al.;
ACS Symposium Series; American Chemical Society: Washington, DC, 1982.

Another kind of thermally induced transient is illustrated in Figure 3. This data, taken from work of Charles Campbell and Shei-Kung Shi (14), involves the transient production of CO_2 which occurs when a coadsorbed mixture of CO molecules and O atoms on a Rh surface is heated. The various spectra are for different titration times indicated on the figure (0-20 min); a polycrystalline Rh surface presaturated with oxygen was titrated at 360K for x min. by 9.6 x 10^{-7} Pa (133 Pa = 1 Torr) of CO and, after evacuation, was heated to 750K or higher. With titration time (i.e. prior to flashing) CO_2 is produced. This lowers the amount of chemisorbed oxygen and allows increasing amounts of CO to adsorb. Thus, the areas beneath the curves in Figure 3 reflect qualitatively the mathematical product of the coverage of CO times the coverage of oxygen present at the start of the heating cycle. The former is small at short titration times while the latter is small at long titration times. It is important to note the spectra shown in Figure 3 were generated by heating the surface in vacuum. The area beneath the CO_2 pressure transient varies strongly with titration time indicating that CO_2 is readily produced by reaction of coadsorbed CO and O. In fact, companion CO spectra show that all the chemisorbed CO reacts to make CO_2 so long as there is excess oxygen. By analyzing CO_2, CO and O_2 transients like those of Figure 3, the temperature dependence of the rate of CO_2 production can be evaluated for a relatively wide range of CO and O coverages (θ_{co} and θ_o). This analysis shows that the rate is not describable by a simple LH expression of the form

$$R_{co_2} = A \exp \{- (E_{LH}/RT\} \theta_o \theta_{co} \quad (1)$$

Either coverage dependent terms in the rate coefficients or fractional exponents in the coverage terms must be incorporated. Table I summarizes our analysis of several cases using the equation

$$R_{co_2} = A_{LH} \exp \{ - (E_{LH} + \alpha_o \theta_o + \alpha_{co} \theta_{co})/RT\} \theta_o^m \theta_{co}^n \quad (2)$$

Although we cannot demonstrate unambiguously which of these, if any, is physically most satisfactory, we prefer model IV because it preserves the exponents of unity on the coverages, as an elementary equation must, because it gives a good fit to the detailed reaction rate versus titration time at 360K (calcula-

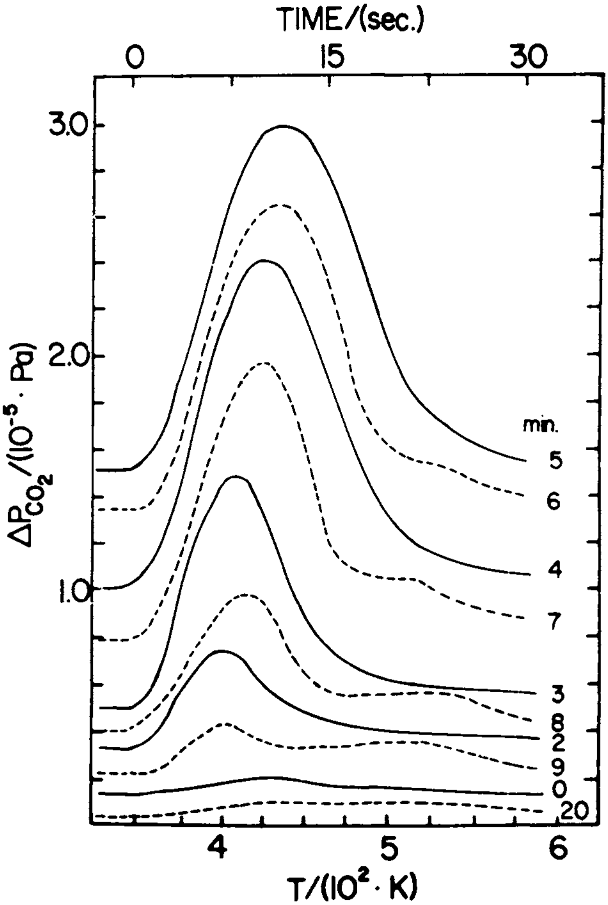

Applications of Surface Science

Figure 3. CO_2 pressure vs. time during heating a polycrystalline Rh sample covered with CO and O. These species were deposited at 360 K in varying amounts by predosing oxygen (15.9 L) and then titrating with CO(g) at 7 × 10^{-9} torr. The heating was then done in vacuo. Titration times are marked in minutes. The small high temperature peak is due to CO interactions with the walls (14).

Table I

Kinetic analysis.

$$R_{CO_2} = A\ \exp[-(E_{LH} + \alpha_O\theta_O + \alpha_{CO}\theta_{CO})/RT]\theta_O^m\theta_{CO}^n$$

Case #	m = order in θ_O	n = order in θ_{CO}	$\frac{\alpha_O}{\text{kcal mole}^{-1}}$	$\frac{\alpha_{CO}}{\text{kcal mole}^{-1}}$	$\ln\frac{A}{\text{molec. cm}^{-2}\text{s}^{-1}}$	$\frac{E_{LH}}{\text{kcal mole}^{-1}}$	Standard deviation α
I	1	1	0	0	41.1 ± 1.02	8.97 ± 0.86	0.299
II	1.6	1	0	0	48.5 ± 0.56	13.31 ± 0.48	0.114[a]
III	1	0.66	0	0	41.0 ± 0.40	8.64 ± 0.34	0.121[a]
IV	1	1	-4.4	0	47.6 ± 0.40	14.30 ± 0.34	0.073[a]
V	1	1	0	2.1	42.1 ± 0.29	8.60 ± 0.24	0.087[a]

[a]Scaled according to E_{LH} for direct comparison with I.

ted from a plot of θ_o versus titration time), and because it gives the best statistical fit to the data. Perhaps some combination of models IV and V would be even better but our data certainly do not require it. In any case, model V alone does not give a large enough CO_2 production rate when the oxygen coverage is high, so it cannot be used alone.

The interpretation of these coverage-dependent effects involves such ideas as island formation, mixed domains of CO and O, the mobility of CO and O and the adsorption of CO on oxygen-covered regions (1,18,26, 27). A deeper understanding of the roles of these processes comes from isothermal experiments involving pressure transients.

All of the results discussed to this point infer surface coverages from gas phase composition measurements. Although these inferences are soundly based in the case of CO oxidation, we would be much more comfortable with direct measurement of the surface coverage.

Transients Induced by Pressure Changes

The most sophisticated and incisive transient experiments are those derived from modulated molecular beam reactive scattering experiments. Results from such experiments will be discussed below after presentation of data from simpler experiments which not only are consistent with the beam results but also extend the range of temperature-coverage conditions and, in some cases, directly assess the coverage.

Figure 4 shows the results of a very simple experiment involving transient CO_2 production on a polycrystalline Pt foil at 540K (15). The transient was set up by establishing a steady-state reaction with $O_2/CO \simeq 10$ and then rapidly closing ($\simeq$3 sec) the O_2 leak valve into the continuously pumped reaction chamber. In the absence of reaction, the CO leak rate gave a partial pressure of 2×10^{-8} torr. The ensuing transient CO_2 comes from the removal of chemisorbed oxygen atoms present at its origin. From Figure 4 it is immediately clear that the CO_2/CO ratio, and therefore the CO_2 production rate per unit CO pressure, remains nearly constant over the first 2 min of the titration while the oxygen coverage drops off more than a factor of 2. This result clearly eliminates the possibility of reaction through a simple ER process of the form

In Catalysis Under Transient Conditions; Bell, A., et al.;
ACS Symposium Series; American Chemical Society: Washington, DC, 1982.

$$CO(g) + O(a) \rightarrow CO_2(g)$$

for which the rate of CO_2 production would be

$$R_{co_2} = k_{ER} P_{co} \theta_o . \qquad (3)$$

According to this expression the rate per unit CO pressure should be proportional to the coverage of oxygen which it is not. Originally (15) this data was interpreted in terms of a physisorbed precursor state largely because no significant accumulation of chemisorbed CO is possible at this temperature and it was felt that the CO residence time was probably very short ($<10^{-5}$ sec). Recent molecular beam data shows that the residence time for reactive CO is actually much longer ($\approx 10^{-2}$ - 10^{-3} sec) (16) meaning that reaction cannot possibly occur in the physisorbed state (lifetime would be less than 10^{-5} sec). Theoretical calculations indicate that the barrier to lateral diffusion of CO across a Pd surface is quite low, at least along certain crystallographic directions, (17) so that chemisorbed CO moves about rapidly and during its surface lifetime will collide with an oxygen atom even when the oxygen coverage is relatively small.

Before moving on, we should describe the experimental procedure by which the oxygen coverages shown in Figure 4 were determined. The total area beneath the CO_2 versus time curve was taken as a measure of the initial coverage, θ_{max}, of oxygen atoms. Integrating this same curve from the beginning of the transient to time, t, provides a measure of the coverage removed. By subtraction

$$\theta_o (t) = \theta_{max} - \int_o^t P_{co_2} (t) \, dt \qquad (4)$$

the time dependent coverage is calculated. This equation assumes that penetration of surface oxygen into the bulk can be ignored on Pt (18).

Other more direct methods of assessing the oxygen coverage are available through AES (18), XPS (19), UPS (20) and other forms of electron spectroscopy. Figure 5 shows a nice example taken from the work of Tatsuo Matsushima and David Almy (18). In this work on polycrystalline Pt, a steady-state reaction was established at various temperatures with $P_{O_2}/P_{co} = 10$. At time t = 0, the O_2 pressure

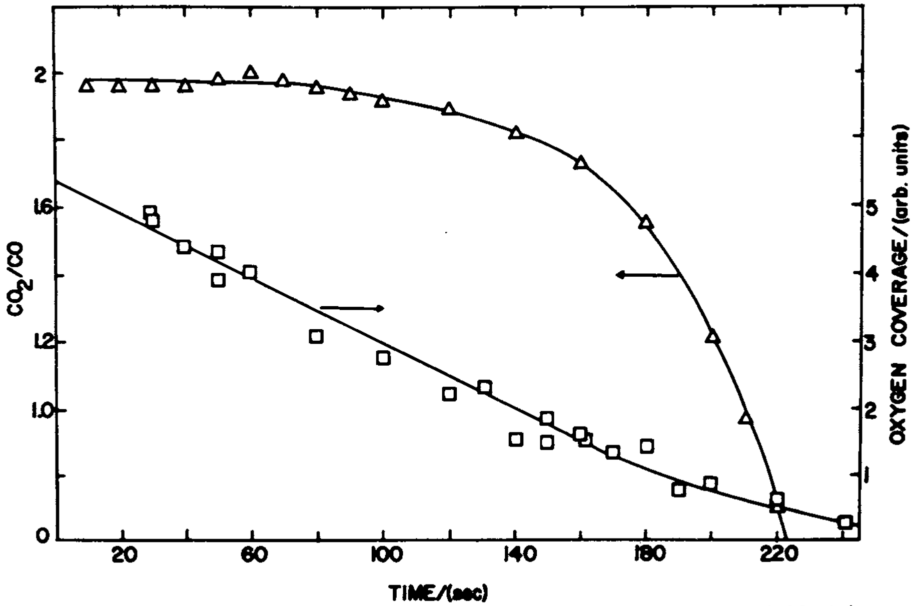

Journal of Catalysis

Figure 4. The time dependence of CO_2/CO (△) and O coverage (□) during the transient titration of chemisorbed oxygen on polycrystalline Pt at 540 K (5).

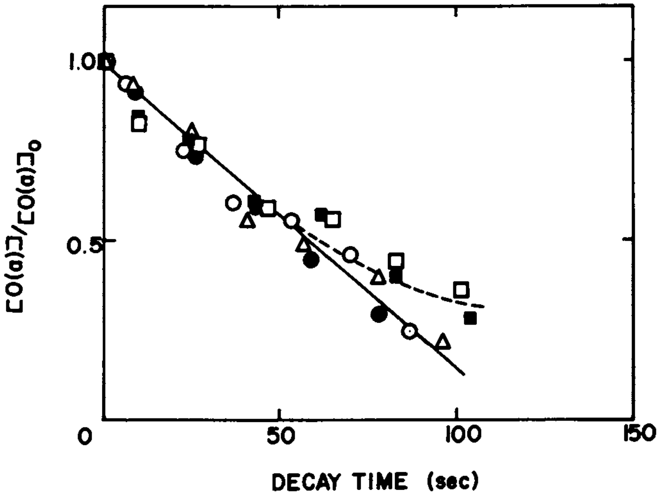

Surface Science

Figure 5. Decay of reactive oxygen, existing at various temperatures in a steady-state $CO/O_2/Pt$ system, after termination of the O_2 supply. The CO pressure was constant at 1×10^{-8} torr (18). $P_{CO} = 1.3 \pm 0.1 \times 10^{-6}$ Pa. Key: ■, 373 K; □, 413 K; △, 473 K; ○, 523 K; and ●, 608 K.

is rapidly reduced to zero and the oxygen Auger signal is measured as a function of time. The results, normalized to the initial Auger signal, are shown in Figure 5 for P_{CO} = 1x10^{-8}torr. Above a relative coverage of 0.5 the decay is linear with time which is consistent with a process that is zero-order in oxygen coverage. At low temperatures and low oxygen coverages the decay becomes more exponential which is consistent with a first order dependence on oxygen coverage. Other transients at a fixed temperature demonstrate that the rate is first order in P_{CO}.

Figure 6 shows that all of the chemisorbed oxygen is reactive. Here, a polycrystalline Pt surface at 370K is exposed to various amounts of O_2 as indicated on the abscissa and, after termination of the O_2 input, titrated with CO. As indicated by the four sets of dashed lines in the figure, all of the oxygen Auger signal vanishes.

A very important non-transient measurement related to the carbon monoxide oxidation reaction is shown in Figure 7. These data show the steady-state oxygen Auger signal for various CO pressures and three fixed oxygen pressures. When taken as a measure of the oxygen coverage these may be compared to the oxygen coverages determined by transient CO_2 production after terminating the O_2 input in a steady-state experiment. Although the details cannot be given here, agreement is very satisfying (18).

Although the use of Auger spectroscopy to detect directly oxygen coverages during the course of a transient or steady-state reaction is very satisfying, there are limitations. One of these is illustrated in Figure 7; the bracketed open triangles indicate the detectable presence of carbon and oxygen on the surface. This, of course, means that the carbon monoxide coverage is significant and must be separated from the oxygen coverage in the analysis. This is not a simple problem and it is compounded by the fact that electron beam damage destroys the carbon-oxygen bond. The solution to this problem lies in the use of some other form of spectroscopy, like x-ray photoelectron spectroscopy (XPS), which does not destroy CO and which can separate chemisorbed oxygen and chemisorbed CO on the basis of chemical shifts.

Figure 8 gives an example of time dependent XPS signals observed during the carbon monoxide titration of chemisorbed oxygen on Ir(111) at 398K. This data from Henry Weinberg's lab (19) was taken by presaturating a clean Ir surface with oxygen and then titrating with 2x10^{-7}torr of CO while following the time

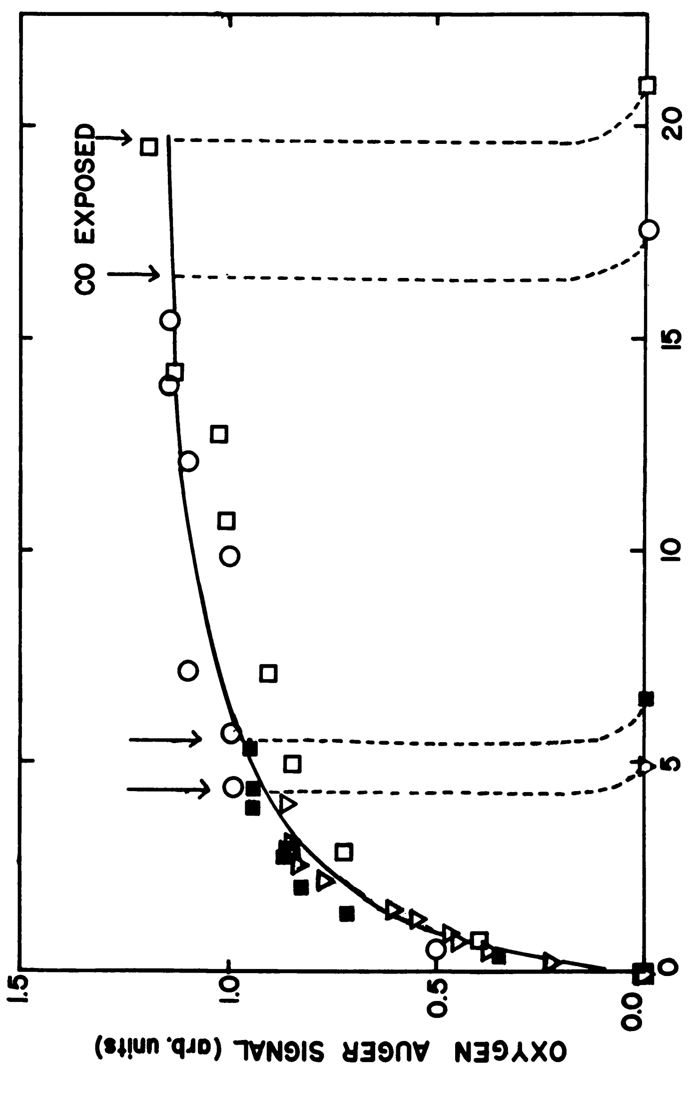

Surface Science

Figure 6. Peak-to-peak oxygen Auger signal (517 eV) as a function of oxygen exposure to polycrystalline Pt at 370 K. Oxygen pressures (Pa) are 1.13 × 10^{-6} (■), 1.29 × 10^{-6} (▽), 2.93 × 10^{-6} (○), and 6.33 × 10^{-6} (□). Vertical arrows indicate points of CO exposure in four separate experiments, and dashed lines connecting to points on the abscissa indicate the loss of the O_2 signal (18).

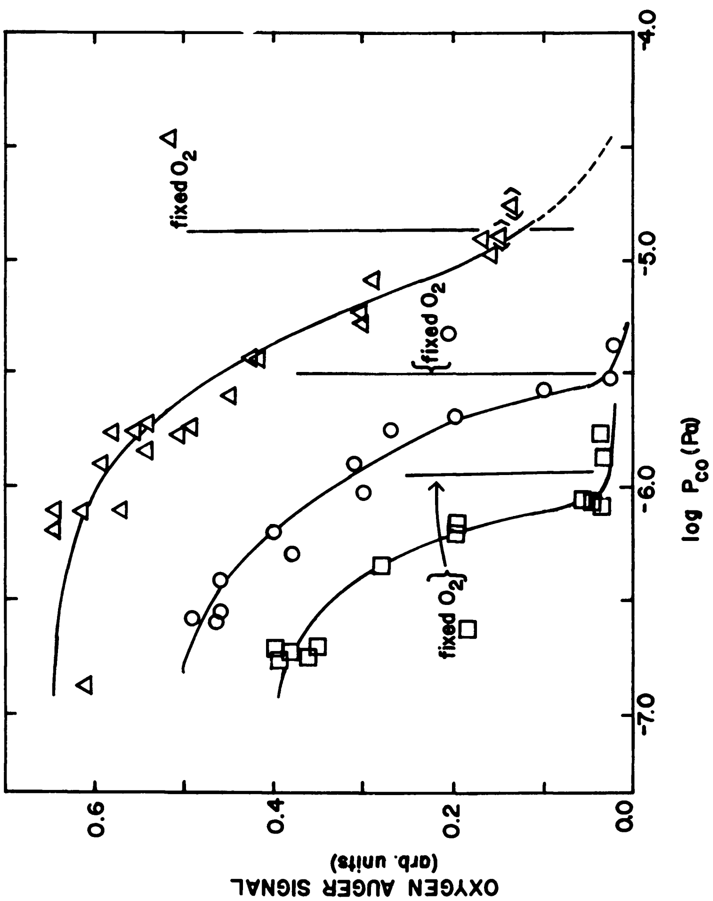

Surface Science

Figure 7. Steady-state oxygen Auger signal on Pt at 483 K as a function of CO pressure for several fixed O pressures. Triangles enclosed in brackets ((△)) indicate the presence of a detectable concentration of adsorbed carbon monoxide. The fixed oxygen pressures (torr) were 10^{-8} (□), 2.5×10^{-8} (○), and 1.1×10^{-7} (△) (18).

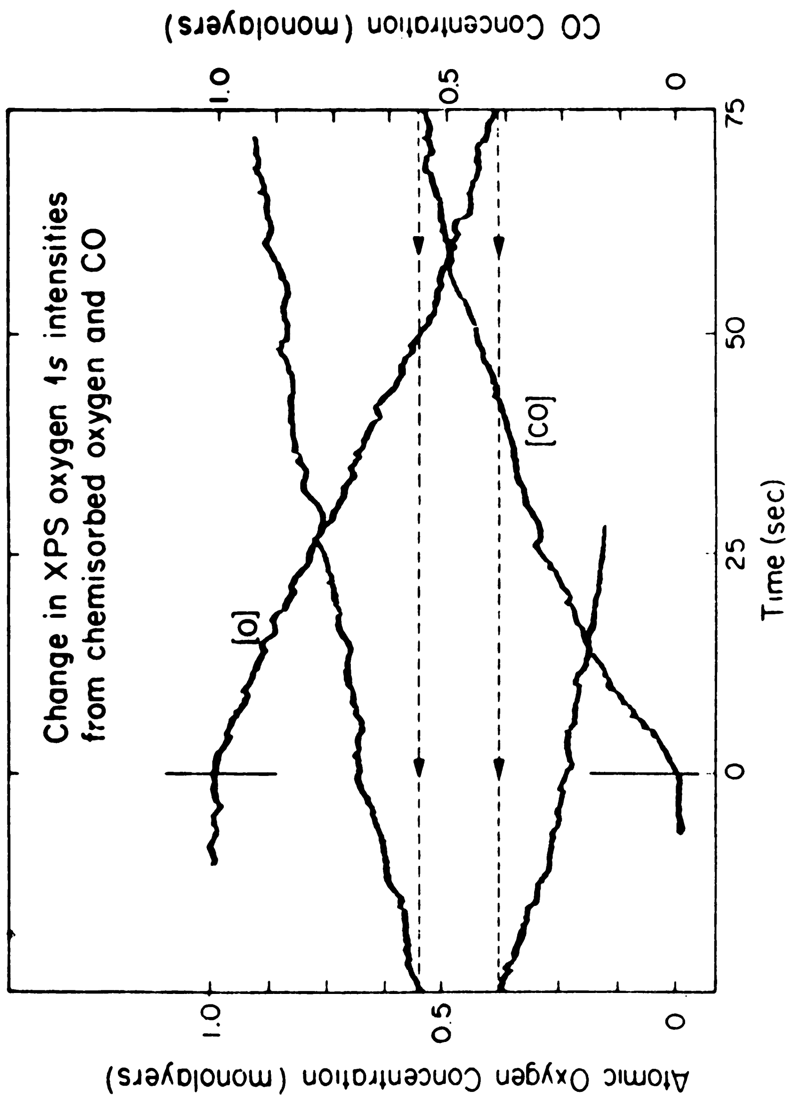

Applications of Surface Science

Figure 8. XPS intensities at 529.8 eV, O(a), and 532.0 eV, CO(a), binding energy vs. time for a titration of O(a) by CO(a) on Ir (111) at 398 K. The CO pressure was fixed at 2 × 10^{-7} torr (19).

American Chemical
Society Library
1155 16th St. N. W.
Washington, D. C. 20036

dependence of XPS signals at 529.8, O(a), and 532.0 eV, CO(a). These results, and others like them, can be used to compute the time dependent coverages of both CO and O for a variety of conditions. From the slope of the oxygen coverage versus time, a CO_2 rate can also be calculated. In Figure 9 the function Rate/[O(a)][CO(a)] is plotted as a function of time. The curvature of this plot shows clearly that a single Langmuir-Hinshelwood expression cannot be used over a broad range of coverages. This same kind of behavior has been reported for Pd (16a) and Rh (14). The interpretation given for Ir (19) involves two competing reaction mechanisms -- one involves CO adsorbed on Ir and the other involves CO adsorbed over oxygen on Ir.

Recently, Shei-Kung Shi and John Schreifels in our laboratory (21) have done an interesting transient experiment involving the titration of adsorbed oxygen with hydrogen on Ru(001). The results indicate the caution with which Auger spectroscopy should be used to follow reactive chemisorbed oxygen concentrations. On Ru, the H_2 + O(a) reaction is characterized by long induction times at high oxygen coverages. Figure 10 shows a comparison of the time dependences of this reaction as followed at 500K using AES and XPS to measure the surface oxygen. The initial oxygen coverages were identical. Unfortunately, the H_2O production rates were so slow that quantitative measurement of them was not possible. The differences in Figure 10 are startling, and indicate a rather strong electron beam effect causing O^+ desorption and/or activation of the surface oxygen. Although the details of this are now being worked out, this example illustrates the care which must be exercised in interpreting kinetic data using Auger for oxygen coverages.

Before considering modulated molecular beam results, we examine a very interesting example of CO_2 production transients from the work of Madix and co-workers (22). An example of the data is given in Figure 11 where the CO_2 mass spectrometer signal is plotted as a function of time upon exposure to CO of a Ag(110) surface partially covered with oxygen. Clearly the slope (proportional to the rate) is higher in magnitude at the lower temperature. From an analysis of such curves over a temperature range from 150 to 400K an apparent activation energy of -1.1 kcal mole^{-1} is calculated. This is interpreted as the difference between the activation energy for reaction and that for desorption of CO, (E_r - E_d).

In Catalysis Under Transient Conditions; Bell, A., et al.;
ACS Symposium Series; American Chemical Society: Washington, DC, 1982.

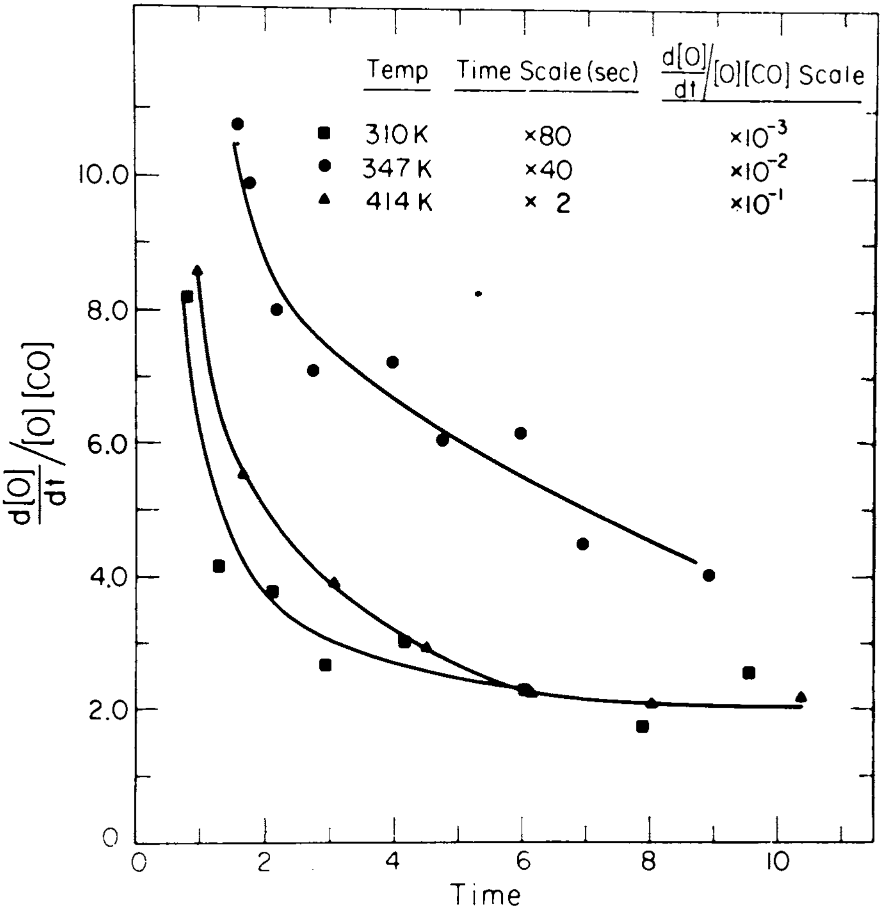

Applications of Surface Science

Figure 9. Plot of the CO_2 production rate (divided by the coverages of oxygen and carbon monoxide) as a function of time for the titration of O by CO on Ir (111).

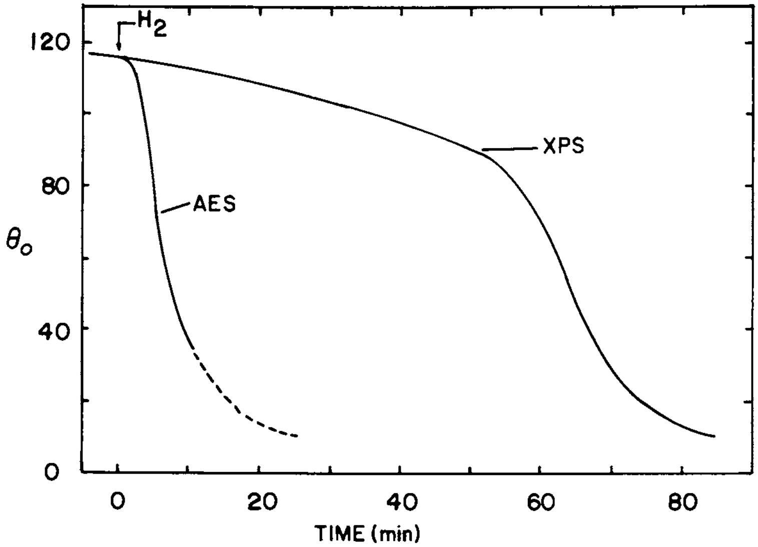

Figure 10. Oxygen AES and XPS signals vs. titration time for the H_2 + O(a) reaction on Ru (001) at 570 K (21).

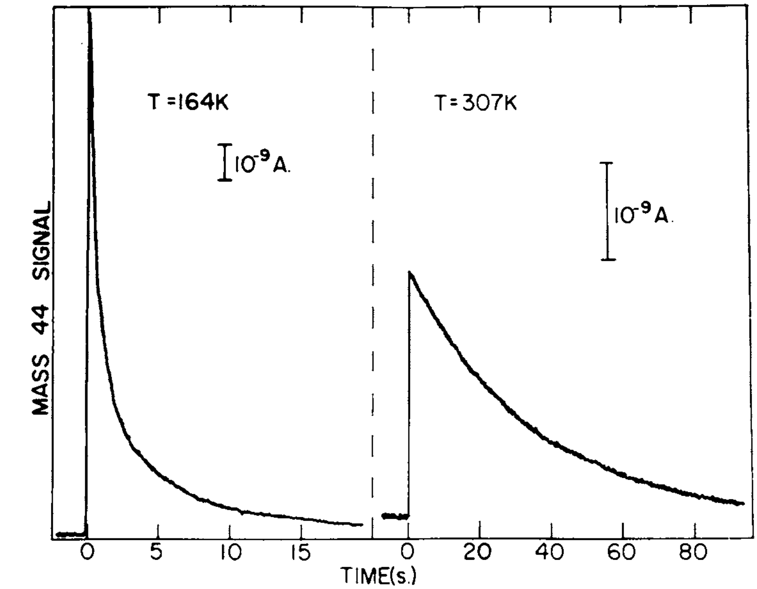

Surface Science

Figure 11. CO_2 signal vs. time for the titration of oxygen chemisorbed on Ag (110) at 164 K and 307 K (22).

If CO is physisorbed then $E_d \simeq 2$ kcal mole^{-1} and $E_r \simeq +1$ kcal mole^{-1}. On the other hand if CO is chemisorbed $E_d \simeq 6$ kcal mole^{-1} and $E_r \simeq 5$kcal mole^{-1}. Since strongly chemisorbed oxygen atoms and slightly perturbed CO molecules are involved, Madix prefers the latter path. Although this is inferential, it is very reasonable and certainly is in agreement with molecular beam work on other transition metals (described below).

Throughout this section on pressure transients we have emphasized electron spectroscopy as a procedure for directly detecting surface species, and, with difficult calibration, their concentration. It is important to keep in mind that the detection limit for these is about 0.01 of a monolayer. Using flash desorption as a complementary technique this limit can be extended to 0.001 monolayer in certain cases. The fact remains that extremely labile chemisorbed species may be present in kinetically important but undetectable concentrations. Since residence times as short as 2×10^{-5} seconds can be determined, molecular beam techniques, as described below, afford an alternative but indirect method of measuring the properties of these very reactive species.

Just as in gas phase kinetics, reactive molecular beam-surface scattering is providing important molecular level insight into reaction dynamics. There is no surface reaction for which such studies have proven more illuminating than the carbon monoxide oxidation reaction. For example Len, Wharton and co-workers (23) found that the product CO_2 exits a 700K Pt surface with speeds characteristic of temperatures near 3000K. This indicates that the CO_2 formed by the reactive encounter of adsorbed species is hurled off the surface along a quite repulsive potential.

A very incisive set of experiments on Pd(111) (16a) and Pt(111) (16b) done in Gerhard Ertl's lab, show that the Eley-Rideal pathway makes no measurable contribution to the CO_2 production rate for many low pressure conditions. In these experiments, a steady-state CO pressure was established, the O_2 pressure was modulated and the phase-lag of the modulated CO_2 product signal was measured. The slope of ln (tanϕ), where ϕ is the phase lag, as a function of T^{-1} can be interpreted in terms of an activation energy difference $(E_r - E_d)$ between reaction and desorption. The result for Pt(111) is -10.8 kcal mole^{-1} as shown in Figure 12 (16b). For an Eley-Rideal pathway in which a gas phase CO molecule makes a direct or impact attack on an oxygen adatom, $E_d = 0$ and we require

In Catalysis Under Transient Conditions; Bell, A., et al.;
ACS Symposium Series; American Chemical Society: Washington, DC, 1982.

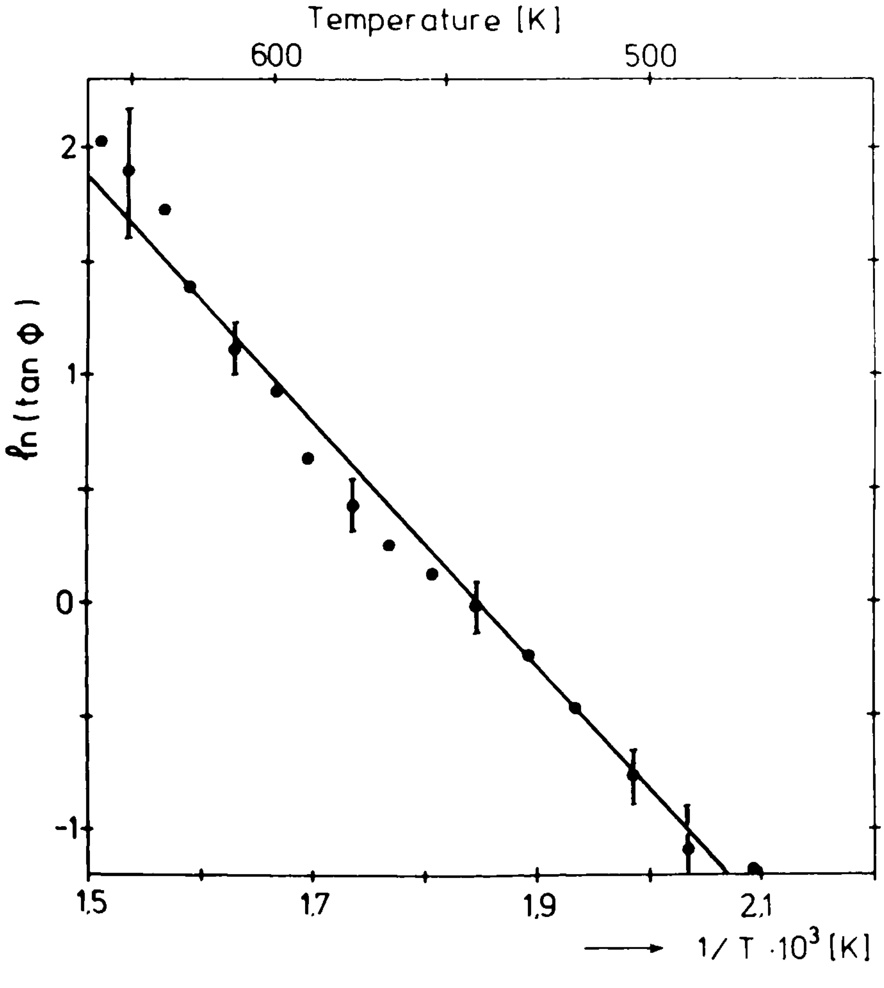

Figure 12. Logarithmic plot of the tangent of the phase lag as a function of temperature for CO_2 reactively scattered from Pt (111). The experiment was run with a background CO pressure of 10^{-7} torr and a modulated O_2 beam (10 Hz) which had an equivalent pressure of 6.3×10^{-7} torr. Key: ●, data; and ——, model, $E_{LH}^* = 24.1$ kcal/mol, $\nu_{\frac{1}{2}} = 0.11$ cm²/particles s (16b).

$E_r < 0$ which is unreasonable. If a physisorbed CO is involved, its binding energy would have to exceed 10 kcal mole^{-1} in order for E_r to become positive and it is not reasonable to expect a binding energy of this magnitude. We are thus led to the conclusion that the reaction occurs through an LH pathway.

The same conclusions hold for Pd(111)(16a) where, on the basis of phase shift measurements, $E_r - E_d = -9.5$ kcal mole^{-1}. In this same very interesting work, transient pressure jump experiments with excellent time resolution were performed. An example is shown in Figure 13 in which a CO beam, with a flux equivalent to $P_{co} = 6x10^{-8}$torr impinges on a Pd(111) substrate immersed in a constant ambient $P_{O_2} = 1x10^{-7}$torr. The important points to note are the induction time at 375K and the transients, with clear maxima noted at 375 and 450K. Since the beam can be turned on in about 1 msec the response shown in Figure 13 is not an artifact of the procedure and we must conclude that more than ER kinetics is involved even under these conditions of high oxygen coverage and relatively low temperatures; an ER path would show no induction time. The maxima observed in Figure 13 are related to the variation of the CO_2 production rate with coverages of CO and O. At short times θ_{co} is low while θ_o is high and the reaction rate grows as CO accumulates. With the passage of time, θ_o declines and θ_{co} continues to grow. The resulting product $\theta_o\theta_{co}$ maximizes when $\theta_o = \theta_{co} = 0.5$. At longer times and lower temperatures θ_{co} inhibits dissociative oxygen adsorption and the rate drops to some steady-state value. At high temperatures, θ_{co} cannot rise to inhibit O_2 adsorption. Consequently, the rate rises upon admission of CO but there is no pronounced maximum.

Finally, we note a very clever isotope experiment done by Tatsuo Matsushima (24). The results are summarized in Figure 14 and show that when ^{13}CO is preadsorbed on Pt and then a mixture of ^{12}CO and O_2 is introduced into the gas phase, the product CO_2 molecules initially formed all are labelled with ^{13}C. In fact the experiment is not quite so simple. An initial $^{13}CO_2/^{12}CO_2$ ratio is measured (unity in Figure 14) which is equal to the $^{13}CO/^{12}CO$ ratio in the preadsorbed CO. The conclusion is that CO_2 is produced by the reaction of adsorbed, rather than gaseous, CO and adsorbed O atoms - i.e. the Langmuir-Hinshelwood process. This conclusion has dominated all of the results presented here and appears to be ubiquitous for all transition metals under all conditions that have been studied to date.

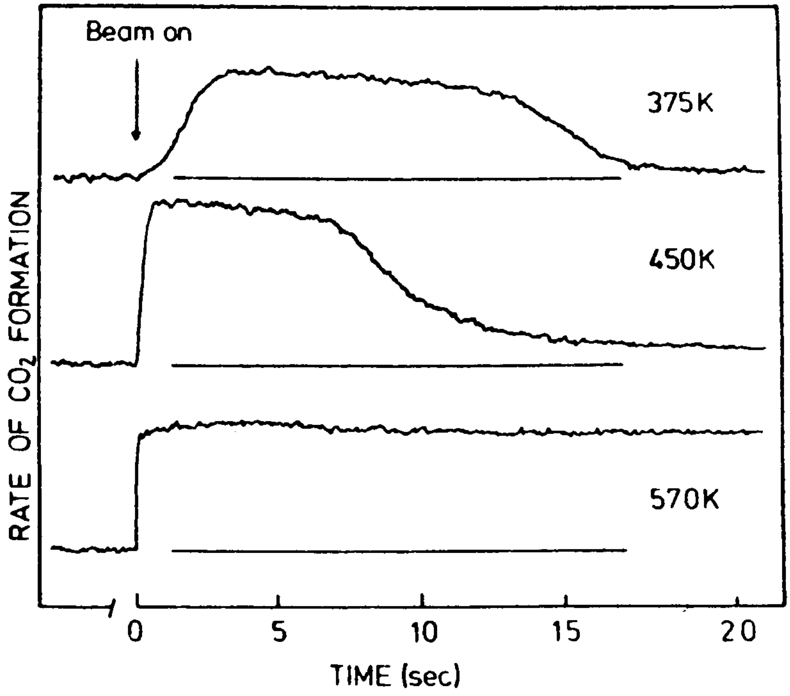

*Figure 13. Transient CO_2 production rates as a function of time for the titration of preadsorbed oxygen on Pd (111) at 375, 450, and 500 K. The experiment was run in a background of 10^{-7} torr of O_2, and the CO pressure 6×10^{-8} torr was introduced at the point indicated (*16a*).*

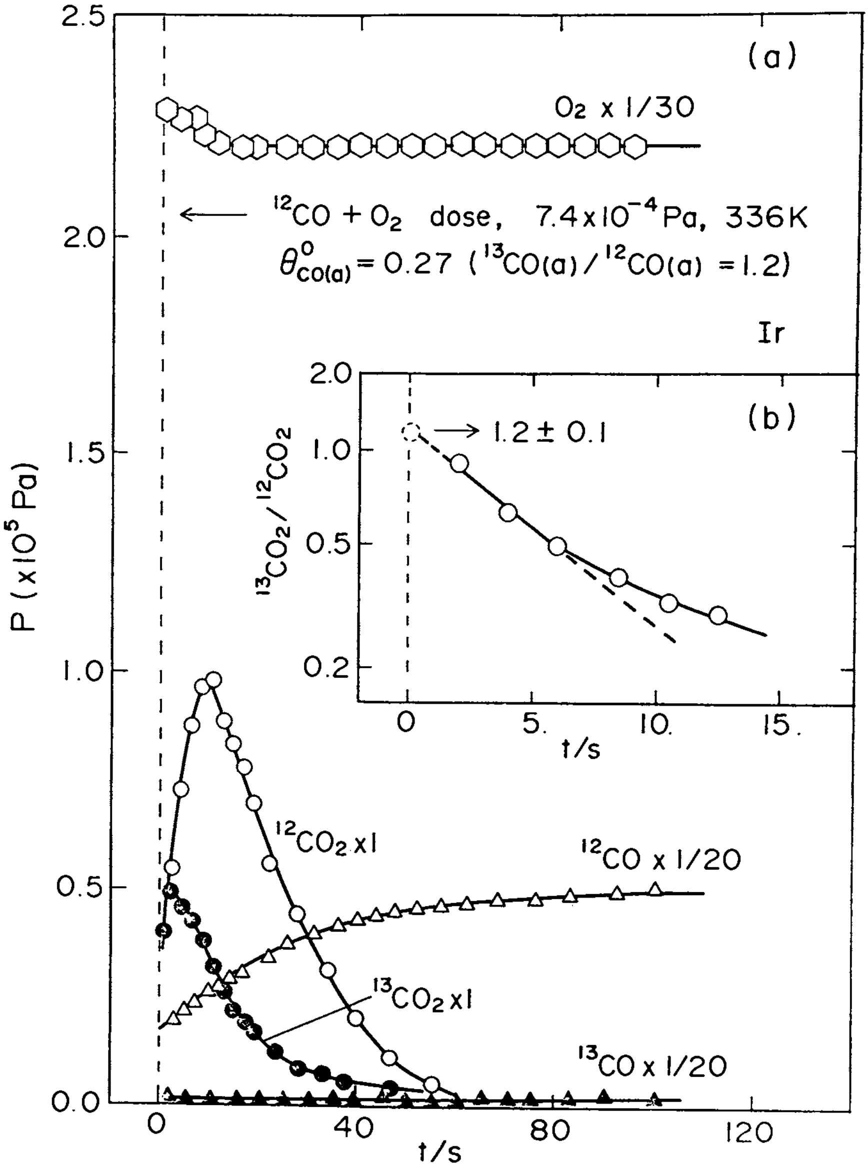

Surface Science

Figure 14. a: Variation of $^{13}CO_2$ and $^{12}CO_2$ produced by reaction of preadsorbed ^{13}CO and ^{12}CO with a $^{12}CO/O_2$ mixture. The catalyst was polycrystalline Pt at 300 K, and the ratio of ^{13}CO to ^{12}CO was 1.0.

b: The ratio of $^{13}CO_2$ to $^{12}CO_2$ observed during the initial stages of the reaction (24).

Questions for Future Study

Among the ripest questions for study are those related to the way various modes of motion participate. For example, it is very important to determine the internal energy distribution of the exiting CO_2 molecule and how this varies with the surface structure of both the underlying metal lattice and the chemisorbed layer. The angular dependence of this distribution is also a question ripe for study.

In connection with practical situations where CO oxidation is important, we must also consider the perennial question of how to connect the low pressure results onto those at high pressure. Qualitatively this has been done for the CO oxidation reaction but it would still be worthwhile to attempt a numerical prediction of high pressure results based on low-pressure rate parameters. A very nice paper modeling steady-state CO oxidation data over a supported Pt catalyst at CO and O_2 pressures of several torr has very recently appeared (25). Extension of this work to other systems in warranted and, even though unresolved questions continue to exist, every indication is that the high and low pressure data can be reliably modeled with the same rate parameters if no adsorption - desorption equilibria are assumed.

The role which mobility of surface metal atoms play and the role of oxygen penetration into the lattice is only now beginning to be examined.

Even though widely studied, this reaction continues to defy a full description. Its simplicity in terms of the species involved and the reproducibility with which many of its characteristics have been established make it remain a model system for a wide variety of studies.

Acknowledgement

This work was supported in part by the Robert A. Welch Foundation and the National Science Foundation (CHE 80-05107). A fellowship to JRC awarded by the New Mexico Section of the American Vacuum Society is gratefully acknowledged.

Literature Cited

1. Engel, T; Ertl, G. Advances in Catalysis, J. Catalysis 1979, 28, 1.
2. a. Langmuir, I. J. Am. Chem. Soc. 1915, 37, 1162.
   b. Langmuir, I. Trans. Faraday Soc. 1922, 17, 621.
   c. Langmuir, I. Trans. Faraday Soc. 1922, 17, 672.
3. a. Ertl, G; Koch, J. "Proc. 5th Int. Congr. on Catalysis"; Hightower, J., Ed.; North Holland: Amsterdam, 1973; p. 969.
   b. Hopster, H; Ibach, H.; Comsa, G; J. Catalysis 1977, 46, 37.
4. Cochran, H. D.; Donnelly, R. G.; Modell, M.; Baddour, R. F. "Colloid and Interface Science", Vol. III; Kerker, M., Ed.; Academic Press: New York, 1976; p. 131.
5. Golchet, A; White, J. M. J. Catalysis 1978, 53, 266.
6. Sheintuch, M.; Schmitz, R. A. Catal. Rev.--Sci. Eng. 1977, 15, 107.
7. Redhead, P. A. Vacuum 1962, 12, 203.
8. Falconer, J. L.; Madix, R. J. J. Catalysis 1977, 48, 262.
9. Taylor, J. L.; Weinberg, W. H. Surface Sci. 1978, 78, 259.
10. Gorte, R.; Schmidt, L. D. Surface Sci. 1978, 76, 559.
11. Close, J. S.; White, J. M. J. Catalysis 1975, 36, 185.
12. Campbell, C. T.; Foyt, D. C.; White, J. M. J. Phys. Chem. 1977, 81, 491.
13. a. Conrad, H.; Ertl, G.; Kuppers, J.; Latta, E. E. Surface Sci. 1977, 65, 245.
    b. Ducros, R.; Merrill, R. P. Surface Sci. 1976, 55, 227.
    c. McCabe, R. W.; Schmidt, L. D. Surface Sci. 1976, 85, 60.
14. Campbell, C. T.; Shi, S. K.; White, J. M. Appl. of Surface Sci. 1979, 2, 382.
15. White, J. M.; Golchet, A. J. Chem. Phys. 1977, 66, 5744.
16. a. Engel, T.; Ertl, G. J. Chem. Phys. 1978, 69, 1267.
    b. Campbell, C. T.; Ertl, G.; Kuipers, H.; Segner, J. J. Chem. Phys. 1980, 73, 5862.
17. Doyen, G.; Ertl, G. Surface Sci. 1977, 69, 157.
18. Matsushima, T.; Almy, D. B.; White, J. M. Surface Sci. 1977, 67, 89.

19. Zhdan, P. A.; Boreskov, G. K.; Boronin, A. I.; Schepelin, A. P.; Withrow, S. P.; Weinberg, W. H. Appl. of Surface Sci. 1979, 3, 145.
20. Matsushima, T.; Hashimoto, M.; Toyoshima, I. J. Catalysis 1979, 58, 303.
21. Shi, S.-K.; Schreifels, J.; White, J. M., in preparation.
22. Bowker, M.; Barteau, M. A.; Madix, R. J. Surface Sci. 1980, 92, 528.
23. Becker, C. A.; Cowin, J. P.; Wharton, L.; Augerbach, D. J. J. Chem. Phys. 1977, 67, 3394.
24. a. Matsushima, T. J. Catalysis 1978, 55, 337.
b. Matsushima, T. Surface Sci. 1979, 87, 665.
25. Herz, R. K.; Marin, S. P. J. Catalysis 1980, 65, 281.
26. Conrad, H.; Ertl, G.; Kuppers, J. Surface Sci. 1981, 76, 323.
27. Barteau, M. A.; Ko, E. I.; Madix, R. J. Surface Sci. 1981, 104, 161.

RECEIVED June 26, 1981.

3

The Dynamic Behavior of Three-Way Automotive Catalysts

RICHARD K. HERZ

General Motors Research Laboratories, Physical Chemistry Department, Warren, MI 48090

The composition of engine exhaust entering a three-way catalytic converter oscillates about the stoichiometric point at frequencies of 0.5 to 2 Hz when the engine is operating under feedback control. Time-averaged conversion measurements have shown that three-way catalysts do not respond instantaneously under these rapidly varying conditions. Recently, time-resolved conversion measurements have permitted direct observation of the dynamic responses of three-way catalysts. After a step change from lean to rich conditions, for example, CO conversions over a catalyst may take several seconds to decay to a new, lower steady-state level. One possible explanation of this response is reaction of the CO in rich exhaust with oxygen that was stored on the catalyst during the preceding exposure to lean exhaust. Other measurements have demonstrated that the oxygen content of a base metal-containing three-way catalyst can vary with exhaust composition at rates which are sufficient to explain the observed dynamic responses of CO conversion.

Three-way catalysts are used in most 1981 gasoline-fueled automobiles to lower the levels of NO, CO, and hydrocarbons in engine exhaust. These catalysts normally operate under dynamic conditions: catalyst temperature increases rapidly after the engine starts (during catalyst "warmup"), and exhaust flowrate and composition fluctuate under most modes of operation. The warmup of automotive catalysts is reasonably well understood (1). The operation of three-way catalysts in the dynamic exhaust environment after warmup is complex and less well understood.

In this paper, we summarize the progress that has been made toward understanding the behavior of three-way catalysts in exhaust of rapidly varying composition. After a brief description of the conditions under which three-way catalysts operate

0097-6156/82/0178-0059$05.00/0
© 1982 American Chemical Society

in an automobile, we discuss time-averaged NO and CO conversions measured under laboratory conditions which simulate actual operation. Next, we discuss time-resolved CO conversions measured during step-response experiments. Some of the step-response results may be explained by changes in the amount of oxygen bound to the catalyst, and measurements of these changes are reviewed. We conclude by suggesting approaches to be taken in future studies.

Conditions During Automobile Operation

Three-way catalysts are able to reduce NO as well as oxidize CO and hydrocarbons when the exhaust composition is held near the stoichiometrically balanced composition, or "stoichiometric point." This control of exhaust composition is accomplished, after the initial warmup period, through the use of the feedback control system illustrated in Figure 1 (2, 3, 4). An oxygen sensor signals whether the exhaust entering the converter is "rich" (net reducing) or "lean" (net oxidizing). The voltage response of an oxygen sensor is shown in Figure 2. A microcomputer periodically reads the sensor signal and adjusts the fuel control signal to bring the air-fuel ratio, and thus the exhaust composition, closer to the stoichiometric point. The exhaust composition cannot be held exactly at the stoichiometric point, however. As a result of the switch-like response of the oxygen sensor and the time required for flow from the fuel metering point through the engine to the sensor, the control system exhibits limit-cycle behavior. The exhaust composition oscillates about the stoichiometric point at a frequency which increases with exhaust flowrate over the range 0.5 to 2 Hz. This oscillation, or cycling, is illustrated by the oxygen sensor signal shown in Figure 3. In addition to these fairly regular oscillations in exhaust composition, transients in composition occur during rapid vehicle acceleration and deceleration. Depending on the response of the catalyst, lean excursions from the stoichiometric point may result in increased NO emissions and rich excursions may result in increased CO and hydrocarbon emissions.

Time-Averaged Conversion Measurements

The performance of a three-way catalyst under dynamic conditions is often studied by measuring the time-averaged reactant conversions that are obtained as the feedstream composition is deliberately cycled. The variables in these cycled studies include time-averaged feedstream composition, cycling frequency, cycling amplitude, and catalyst composition. Cycled studies are performed in engine-dynamometer laboratories by switching the air-fuel ratio between two settings at selected frequencies (5, 6, 7). Cycled studies also have been performed

In Catalysis Under Transient Conditions; Bell, A., et al.;
ACS Symposium Series; American Chemical Society: Washington, DC, 1982.

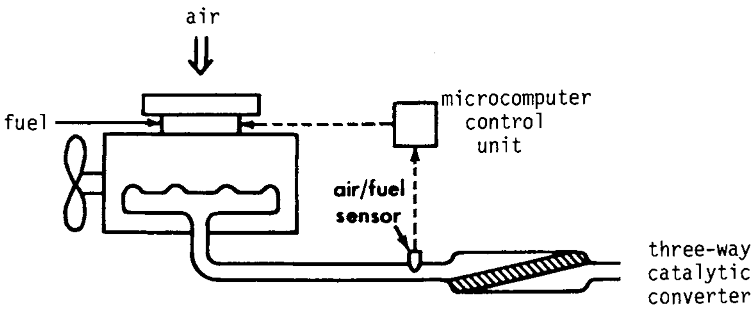

Figure 1. Schematic diagram of an engine and emission control system. The microcomputer also reads signals from sensors measuring other engine operating parameters. In some emission control systems, the three-way catalyst is followed by supplementary air injection and an oxidizing catalyst to provide additional control of CO and hydrocarbon emissions.

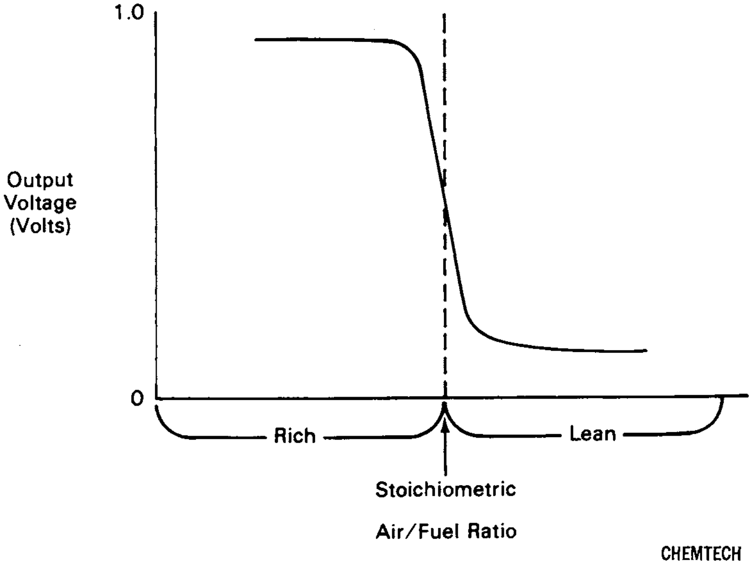

Figure 2. Exhaust oxygen sensor characteristics (4).

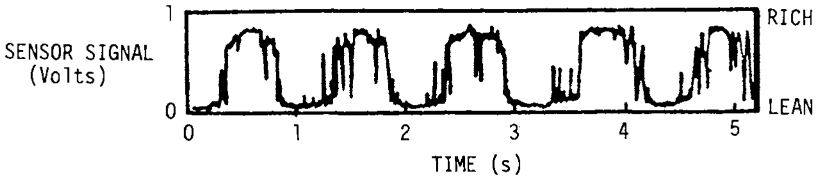

Figure 3. Oxygen sensor signal showing oscillation of the exhaust composition around the stoichiometric point during feedback control of the engine.

(6) using the laboratory reactor system developed by Schlatter, Sinkevitch, and Mitchell (8), shown in Figure 4. Two simulated exhaust streams of different compositions are alternately fed to the reactor in this system. Time-averaged inlet and outlet compositions are measured in these cycled studies because of the limited response rates of conventional exhaust analyzers. Figure 5 presents CO and NO conversion data which are characteristic of the cycled performance of three-way catalysts. Note that cycling results in lower average conversions for mean air-fuel ratios near the stoichiometric point. The extent to which cycling affects average conversions over a catalyst has been found to be sensitive to changes in the composition of the catalyst and to aging of the catalyst in engine exhaust (9). Since cycling often results in the lowering of conversions, there is a substantial incentive to study the dynamic behavior of three-way catalysts. One incentive is that an understanding of the effects of catalyst composition on dynamic behavior may lead to the formulation of catalysts which give required conversions under cycled air-fuel ratio conditions with the use of minimum amounts of noble metals.

Note in Figure 5 that average conversions are dependent on cycling frequency. Some of this effect is related to mixing in the feedstream which decreased the amplitude of the inlet composition oscillations as the frequency was increased. However, this frequency effect does indicate that the dynamic response of the catalyst was complex such that conversions over the catalyst did not change instantaneously as the feedstream composition changed. This complexity is shown more specifically for CO by Figure 6. The solid line gives conversions measured under steady-state conditions. The dotted line represents the average conversions that would be expected if the outlet CO concentration instantaneously reached a new steady-state value as the inlet composition is cycled as a square wave about the mean air-fuel ratio. Actual conversions obtained when cycling at a frequency of 0.25 Hz are given by the dashed line. The result that the measured cycled conversions are higher than the predicted conversions implies that conversions during the rich half of a cycle are higher than would be obtained under these rich conditions at steady-state.

Dynamic Gas-Phase Measurements

Although time-averaged conversion measurements provide valuable information, a detailed analysis of the dynamic behavior of three-way catalysts requires direct observation of catalyst responses to rapid changes in exhaust composition. Some transients over three-way catalysts in simulated exhaust occur slowly enough that they can be observed with conventional exhaust analyzers. Schlatter and Mitchell (9) have studied the step responses of $Pt/Rh/Ce/Al_2O_3$ catalysts in simulated exhaust.

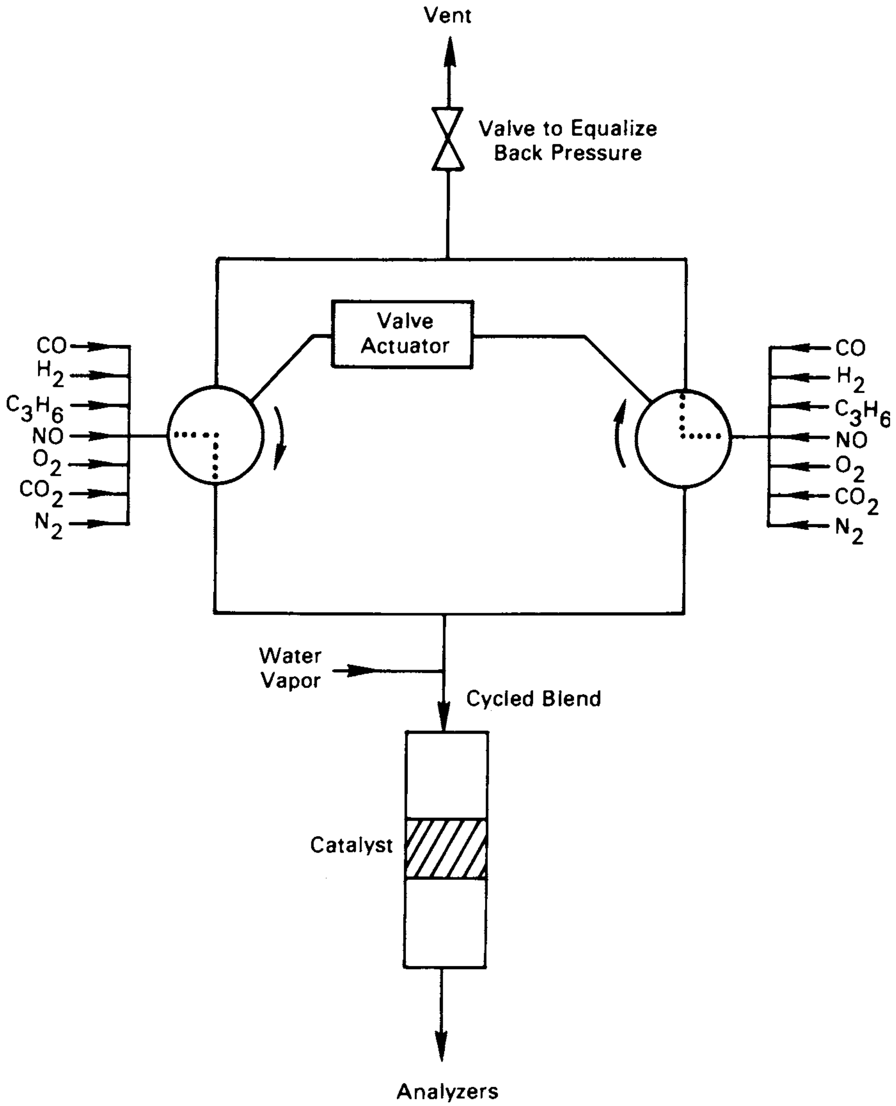

Figure 4. Laboratory reactor system used to measure the performance of catalysts under cycled conditions. Two simulated exhaust streams of differing compositions are alternately fed to the reactor (8).

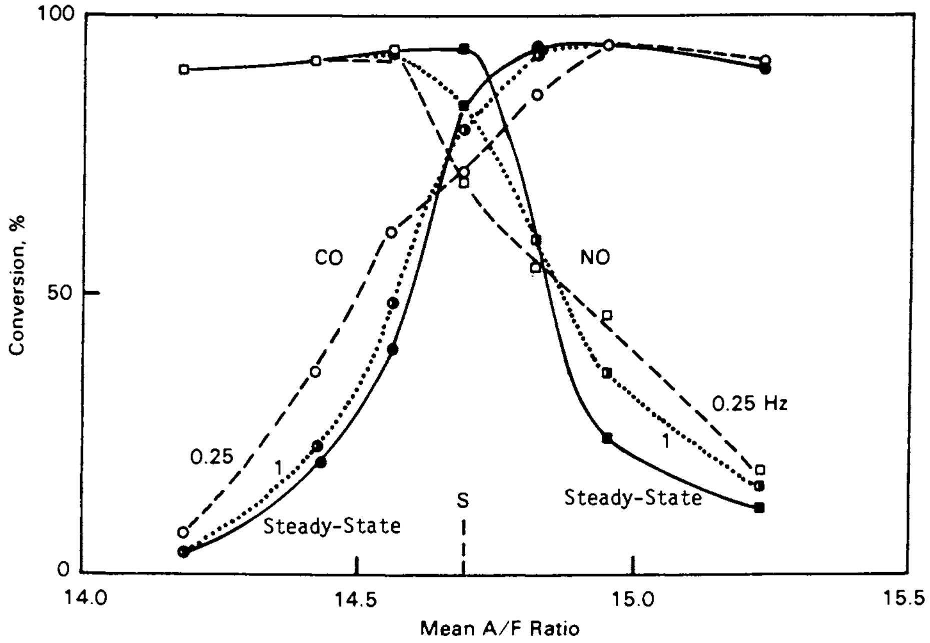

Figure 5. Time-averaged CO and NO conversions measured using the laboratory reactor system shown in Figure 4. A fresh, pelleted Pt/Rh/Al_2O_3 catalyst was operated at a middle-bed temperature of 820 K and a space velocity of 52,000 h^{-1} (STP). The feedstreams simulated exhaust that would be obtained with various engine air–fuel ratios (A/F) but did not contain SO_2. The feedstream compositions were cycled at 0.25 and 1 Hz at an amplitude of ±0.25 A/F about the mean A/F. For the curves labeled Steady-State, conversions were measured with feedstreams at the mean A/F values (8).

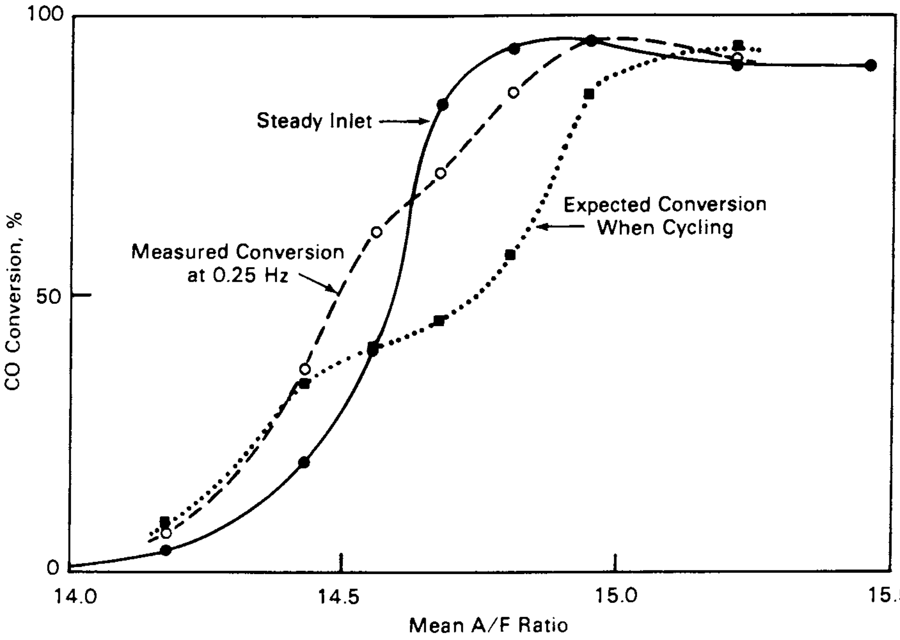

Figure 6. CO conversions measured under steady and cycled (±0.25 A/F) conditions. Expected conversions were calculated by assuming that the catalyst would respond instantaneously to changes in feedstream composition (8).

They found that CO conversions can take up to 15 minutes to decrease to a new steady-state level after a change from lean to rich conditions at a space velocity of 100,000 h^{-1} (STP) and a middle-bed temperature of 823 K. The transient enhancement in CO conversion was found to be due to the water-gas shift reaction catalyzed by Rh. An oxidized form of Rh was proposed to be active for the water gas shift reaction, with reduction of the oxidized Rh occurring slowly in the rich feedstream. Ce prolonged the transient enhancement in CO conversion, apparently by retarding the rate of Rh reduction. When SO_2 was added to the feedstream, CO conversions reached a new steady-state level in less than 10 s, or faster than the response rate of the analysis system. SO_2 is present in exhaust at a level of about 20 ppm and poisons the water-gas shift reaction on the Group VIII transition metals (10). Cooper and Keck (11) have studied the step responses of Ni-containing three-way catalysts in SO_2-free simulated exhaust. At a space velocity of 50,000 h^{-1} (STP) and a catalyst inlet temperature of 813 K, they observed transients in conversion over periods up to 10 minutes long. The water-gas shift activity of the Ni and changes in the amount of oxygen bound to the Ni were proposed to affect the observed step responses of the catalysts.

Conversions over three-way catalysts change more rapidly after a change in inlet composition when the feedstream is actual engine exhaust rather than SO_2-free simulated exhaust. The difference between the catalyst responses in the two feedstreams may be related to factors which are yet unknown in addition to SO_2 poisoning of the water-gas shift reaction. Instruments which have 10%-to-90% response times of less than 0.1 s are required to measure the dynamic response of a catalyst in engine exhaust.

As we have seen in Figure 3, the oxygen sensor used in the engine control system is fast enough to respond to most of the important changes in exhaust composition. However, the oxygen sensor cannot be used to measure concentrations of reactants in exhaust since the sensor's output is a nonlinear function of the ratio of oxidizing species to reducing species. Meitzler (12) has used oxygen sensors placed before and after a catalytic converter to study the dynamic response of a three-way catalyst. The catalyst was found to retain oxidizing species into the initial periods of rich portions of air-fuel ratio cycles.

Infrared diode laser spectroscopy has been used for the measurement of hydrocarbon and CO concentrations in exhaust (13, 14, 15). The adsorption path length, and thus the absorption cell volume, required for hydrocarbon measurement is rather large, limiting the time-resolution of the measurement. The absorption path length required for CO measurement, however, is relatively short and approximately equal to the diameter of a standard exhaust pipe. This allows CO to be measured with high time-resolution by an infrared laser beam passed through an

In Catalysis Under Transient Conditions; Bell, A., et al.;
ACS Symposium Series; American Chemical Society: Washington, DC, 1982.

exhaust pipe. The path length required for NO measurement may be short enough to allow dynamic measurement of this species. O_2 cannot be measured by conventional infrared spectroscopy.

Figure 7 is a schematic diagram of the apparatus used for dynamic CO measurements. An infrared diode laser beam is split and components pass through the exhaust at the inlet and outlet of a standard catalytic converter. The laser beam is chopped at a high frequency and lock-in amplifiers are used to separate the detector signal due to the laser from that due to the high infrared background near the engine. A minicomputer is used to record the carburetor or fuel-injector control signal, the two laser signals, and signals from oxygen sensors placed at various points in the exhaust flow system. The engine can be operated under normal feedback control, or the minicomputer can be used to control the air-fuel ratio. The 10%-to-90% response-time of this system is 0.025 s, which is sufficiently fast to follow accurately any CO concentration change which occurs in automotive exhaust.

Figure 8 shows the CO concentrations measured at the inlet and outlet of the catalytic converter during feedback control of the exhaust composition. The flow time between the inlet and outlet measurement points was 0.06 s at the space velocity of 50,000 h^{-1} (STP) and converter temperature of 773-823 K. The converter contained a pelleted $Pt/Pd/Rh/Ce/Al_2O_3$ catalyst which had been aged for 30,000 km on an automobile. The relatively large, low frequency (ca. 1 Hz) oscillation in the inlet CO level was due to limit-cycling of the control system. The lower amplitude, higher frequency (ca. 10 Hz) oscillations resulted from two superimposed components: (1) a component due to modulation of the fuel-metering rod in the carburetor, and (2) a component due to maldistribution of fuel to the engine's cylinders (15). The exhaust composition fluctuations shown by the CO measurements are also present in the oxygen sensor signal in Figure 3. The high frequency CO oscillations were present at the converter outlet during the rich periods of the limit-cycles; little or no CO broke through the converter when the exhaust was lean.

These results are direct measurements of the CO concentrations which are present at the inlet to a three-way converter under realistic operating conditions. The concentrations of other exhaust components at the converter inlet can be estimated using concentration crossplots, for each component versus CO, obtained from time-averaged measurements at constant air-fuel ratio settings.

One of the goals of an analysis of three-way dynamic behavior is to predict outlet concentrations given rapidly varying inlet concentrations, such as those shown in Figure 8. The analysis is made easier, however, when the dynamic conditions are simplified to step changes and single frequency, constant amplitude oscillations in air-fuel ratio. Figure 9A shows CO

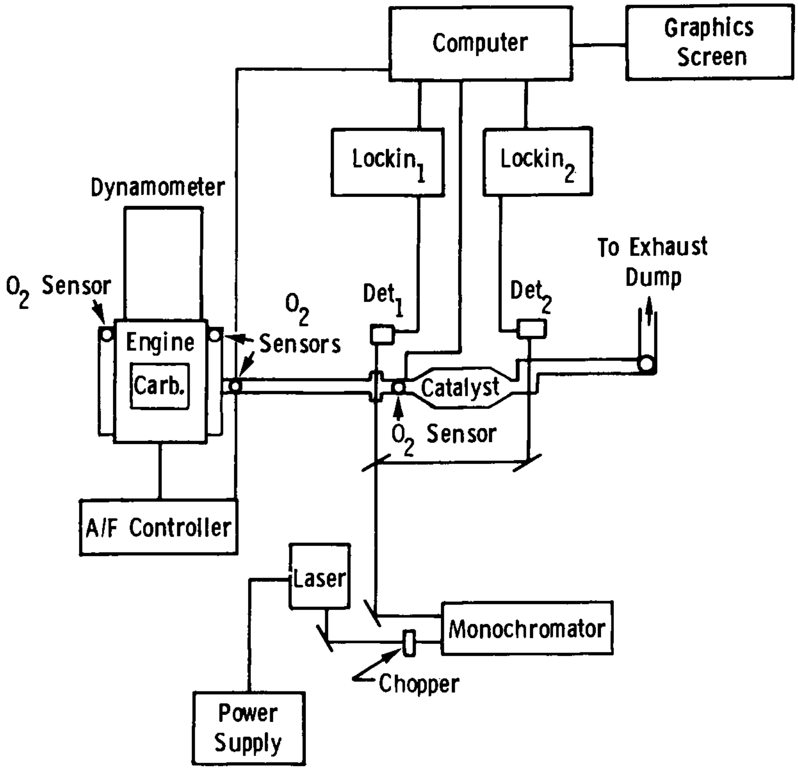

Society of Automotive Engineers

*Figure 7. Schematic diagram of the apparatus used to study the dynamic behavior of three-way catalysts in engine exhaust (*14, 15*). This apparatus was used to make the measurements shown in Figures 8 and 9.*

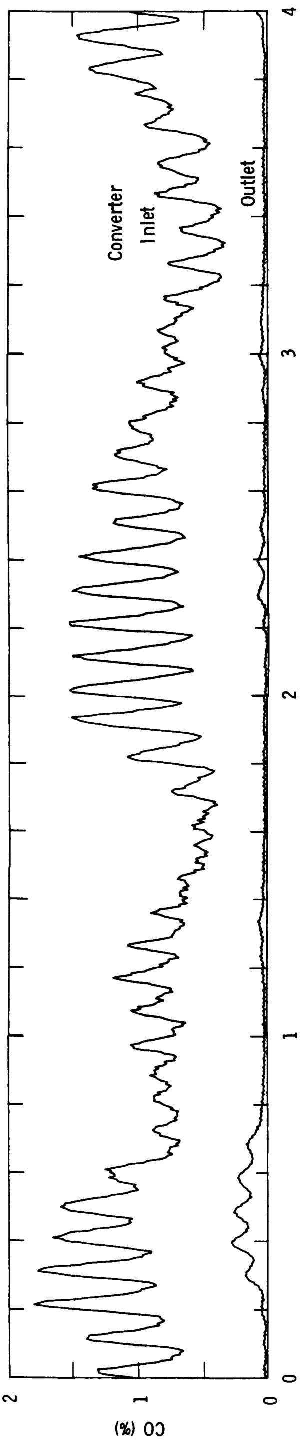

Society of Automotive Engineers

Figure 8. CO concentrations measured at the inlet and outlet of a three-way catalytic converter during feedback control of the exhaust composition (15).

concentrations measured as the air-fuel ratio control signal was stepped from rich to lean over a pelleted $Pt/Pd/Rh/Ce/Al_2O_3$ catalyst at a space velocity of 50,000 h^{-1} (STP). Before use, the catalyst was aged for 100 h on an engine-dynamometer to simulate 6400 km of exposure to automobile exhaust. Although difficult to see in this figure, the CO at the converter outlet actually dropped faster than at the inlet (after considering the flow time between the measurement points). This is because the inlet O_2 concentration (not measured) increased as the inlet CO concentration dropped so that the conversion of CO increased at the same time that CO eluted. This rich-to-lean CO response was found to be insensitive to catalyst composition.

A much more interesting response is shown in Figure 9B. Here, the air-fuel ratio setting was stepped from lean to rich. The inlet CO trace is roughly a mirror image of that in Figure 9A. The outlet CO level, however, took a much longer time to reach a new steady-state level than for the rich-to-lean step. At the maximum time shown in Figure 9B, the outlet CO level had only risen to about 60% of the rich steady-state outlet level, which can be seen on the left side of Figure 9A. Approximately 25 s were required for the outlet CO to reach the new steady-state level after the lean-to-rich step. This time is much shorter than that mentioned above for catalysts in SO_2-free simulated exhaust, but is still long with respect to the periods of the exhaust composition oscillations observed during actual automotive operation.

The dashed curve in Figure 9B gives the approximate, smoothed result that would have been obtained if the catalyst response were instantaneous. The area between the dashed curve and the actual response represents additional CO conversion due to the noninstantaneous dynamic response of the catalyst. This type of response is desirable because it will lead to low CO emissions when the air-fuel ratio cycles about the stoichiometric point.

The additional CO conversion that is observed after a change from lean to rich exhaust may be due to a temporarily enhanced water-gas shift activity as proposed by Schlatter and Mitchell (9), and may also be due to reaction of CO with oxygen bound to Ce in the catalyst.

On the basis of time-averaged conversion measurements and laboratory measurements using single component gases, Shelef and coworkers (5, 16) proposed that the "storage" of oxygen by base metals is an important factor in the dynamic performance of three-way catalysts. If this mechanism is important for a catalyst, then the oxygen content of the catalyst should change by measurable amounts after sudden changes in exhaust composition.

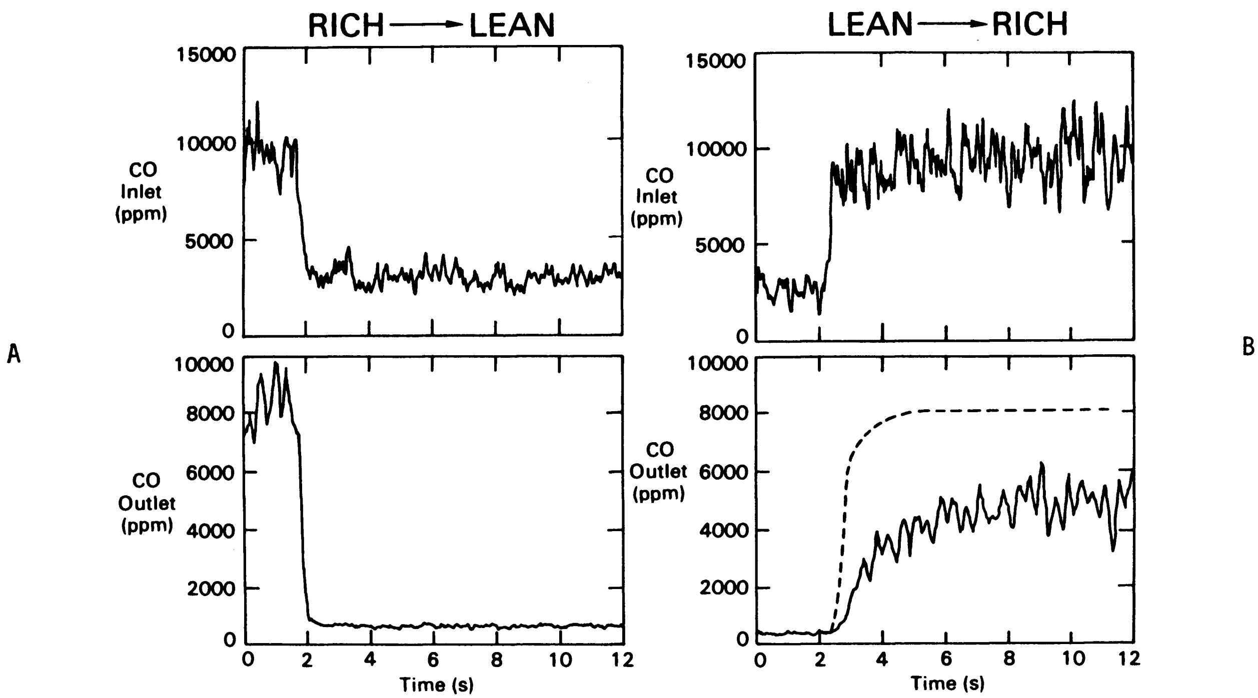

Society of Automotive Engineers

Figure 9. A: CO concentrations measured over a pelleted Pt/Pd/Rh/Ce/Al_2O_3 catalyst at a space velocity of 50,000 h^{-1} (STP) as the engine A/F control setting was stepped from rich (A/F = 14.1) to lean (A/F = 15.5).

*B: CO concentrations measured as the A/F control setting was stepped from lean (A/F = 15.5) to rich (A/F = 14.1) (*14*). The dashed curve gives the approximate, smoothed result that would have been obtained if the catalyst response were instantaneous.*

Measurement of Catalyst Oxygen Content

Kaneko, et al. (17) have made measurements of the oxygen content of a Pt/Rh/Al_2O_3 catalyst after various exposures to exhaust. After reduction of the catalyst with CO, the oxygen content of the catalyst was found to increase with exposure to lean exhaust. The data obtained were used to develop a procedure for calculating emissions under cycled air-fuel ratio conditions. The calculations could explain average conversion measurements that could not be explained by assuming the catalyst responded instantaneously to air-fuel ratio changes.

The catalyst studied by Kaneko and coworkers contained only Pt and Rh. Most three-way catalysts, however, also contain base metals in larger amounts than the precious metals (5, 6, 7, 9, 11). We have measured changes in the oxygen content of a Ce-containing three-way catalyst after various exposures to exhaust (18).

The apparatus that was used in our study is shown in Figure 10. After the desired exposure of the 5 g catalyst bed to exhaust, the reactor was flushed with N_2 for 10 min, and then the oxygen content of the catalyst bed was determined in the following procedure. First, both solenoid valves at the inlet of the reactor were closed and a small flow of N_2 was injected into the reactor through a 4-port switching valve. The switching valve was then turned to inject a stream of 2.3% O_2/0.1% Ar/He into the reactor as the flow from the reactor was analyzed continuously with the mass spectrometer. Ar was monitored to determine the elution curve of an inert species, and it also served as an internal concentration standard in the CO_2 measurement. The elution curve of O_2 relative to that of Ar was used to determine the amount of O_2 that reacted with the catalyst. A small amount of O_2 reacted with carbon on the catalyst to form CO_2, which was also measured (H_2O formation was negligible). The oxygen content of the catalyst after exposure to exhaust was calculated by subtracting the net oxygen uptake (measured uptake less the amount reacted to form CO_2) from the maximum oxygen content, or oxygen capacity of the catalyst bed. The oxygen capacity of the catalyst bed is defined as the maximum amount of oxygen that was retained by the catalyst after treatment with O_2 and that could be removed by reaction with CO.

The rate of increase of oxygen content after a rich-to-lean step change in air-fuel ratio was studied using the following procedure. The reactor flow was switched to N_2 after stabilization of the catalyst in exhaust at an air-fuel ratio of 14.1, a catalyst inlet temperature of 680 K, and a space velocity of 110,000 h^{-1} (STP). Next, the air-fuel ratio was changed to a setting of 15.1 while the exhaust bypassed the reactor. Then the reactor was given a pulse of lean exhaust by switching from N_2 to exhaust for a specified period, and then back to N_2.

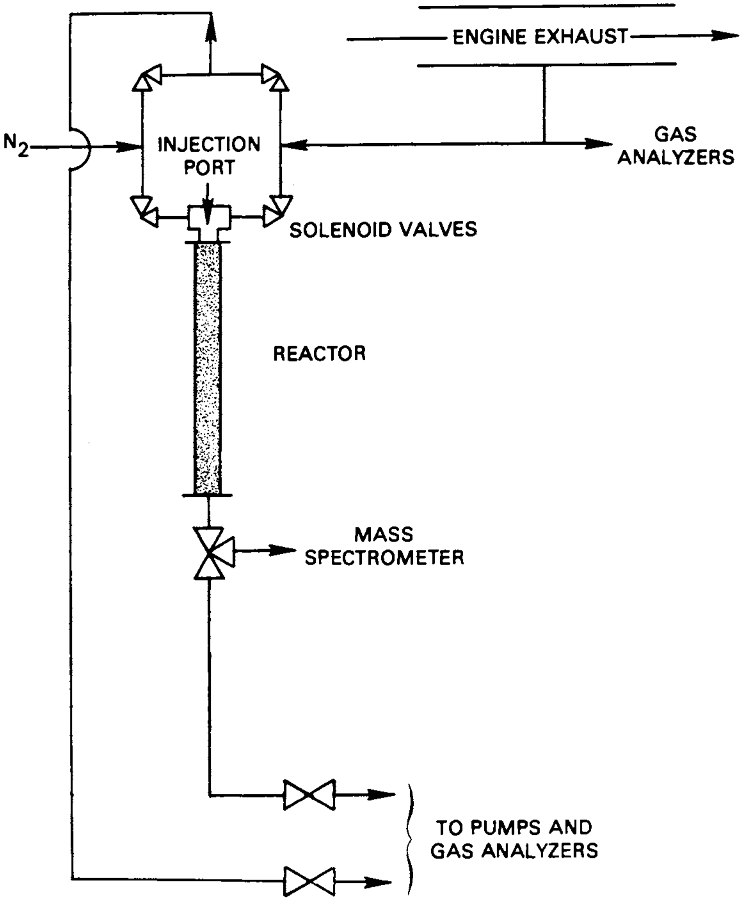

I&EC Product Research and Development

Figure 10. Schematic diagram of the apparatus used to measure changes in the oxygen content of a catalyst with changes in exhaust air–fuel ratio. The 2.54-cm i.d. tubular reactor contained 5 g of catalyst and was heated by an electric furnace (18).

After this exposure, the oxygen content of the catalyst was measured.

Figure 11 shows the results of these experiments for the same pelleted $Pt/Pd/Rh/Ce/Al_2O_3$ catalyst used for the data in Figure 9. The oxygen content of the catalyst bed increased linearly with pulse duration and reached the steady-state lean level within 0.5 s. The oxygen capacity of the catalyst was associated primarily with oxidation of the 190 μmol of Ce contained in each gram of catalyst; the catalyst contained only 8 μmol of precious metal per gram. A comparison of the oxygen capacity to the amount of Ce in the catalyst suggests that about 76% of the Ce could change between the +3 and +4 oxidation states (the most common oxidation states of Ce). The identities of the Ce compounds which undergo oxidation and reduction in exhaust are not known, however, dispersed hydroxides and oxyhydroxides are likely candidates (18).

The rate of decrease of oxygen content of the catalyst after a lean-to-rich step change was studied using the procedure described above with the lean and rich exposures reversed. Figure 12 presents the results of these experiments. After exposure to rich exhaust for 1.0 s, the oxygen content of the catalyst bed decreased 36% of the way from its lean steady-state level to its rich steady-state level. This change in oxygen content could correspond to a conversion of 58% of the CO and H_2 in the 1.0 s pulse of rich exhaust (hydrocarbons are less reactive with the oxygen held by the catalyst than CO and H_2). The difference in catalyst oxygen content between the rich and lean steady-states is sufficiently large to account for the extra conversion obtained in the CO step response experiment shown in Figure 9B. In addition, the rates of change of catalyst oxygen content shown in Figures 11 and 12 are sufficiently fast to affect the performance of the catalyst when the air-fuel ratio is cycled about the stoichiometric point at frequencies on the order of 1 Hz.

Future Studies

The studies described in the preceding two sections have identified several processes that affect the dynamic behavior of three-way catalysts. Further studies are required to identify all of the chemical and physical processes that influence the behavior of these catalysts under cycled air-fuel ratio conditions. The approaches used in future studies should include (1) direct measurement of dynamic responses, (2) mathematical analysis of experimental data, and (3) formulation and validation of mathematical models of dynamic converter operation. Such models must be used in conjunction with a model of converter warmup (1) and a model of catalyst deactivation (6) when designing the distribution of active components in a catalyst and converter and the engine control strategy.

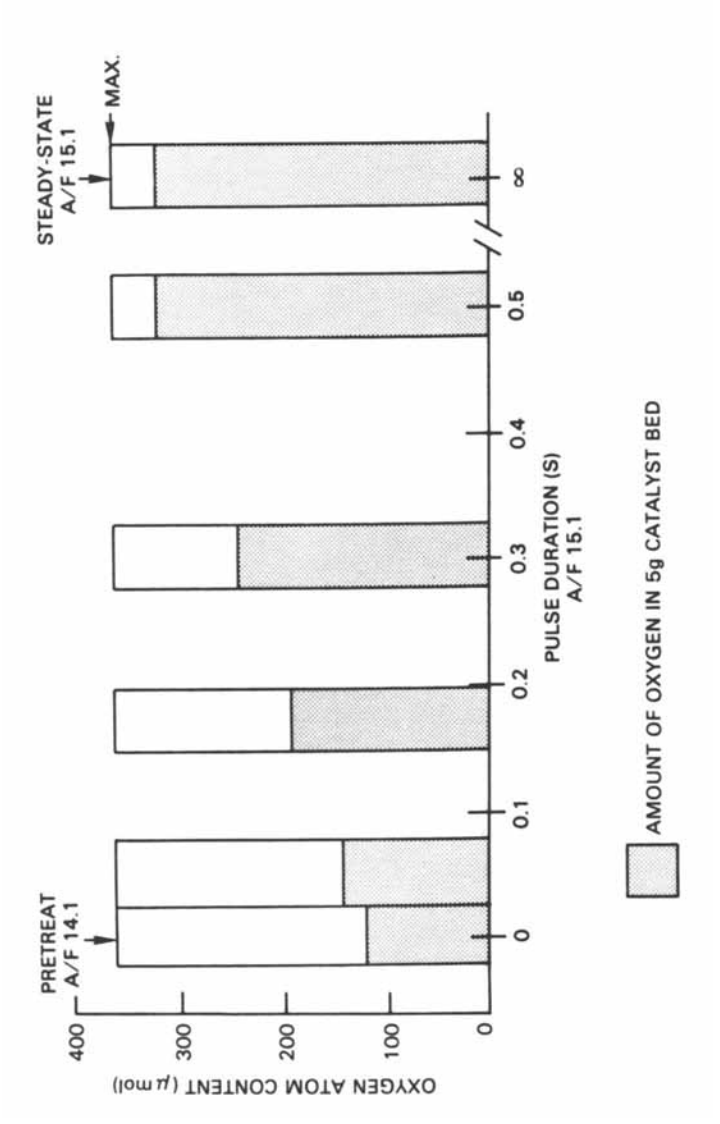

I&EC Product Research and Development

Figure 11. Rate of increase in the oxygen content of a pelleted Pt/Pd/Rh/Ce/Al_2O_3 catalyst in lean exhaust at a space velocity of 110,000 h^{-1} (STP) and a catalyst inlet temperature of 680 K (18).

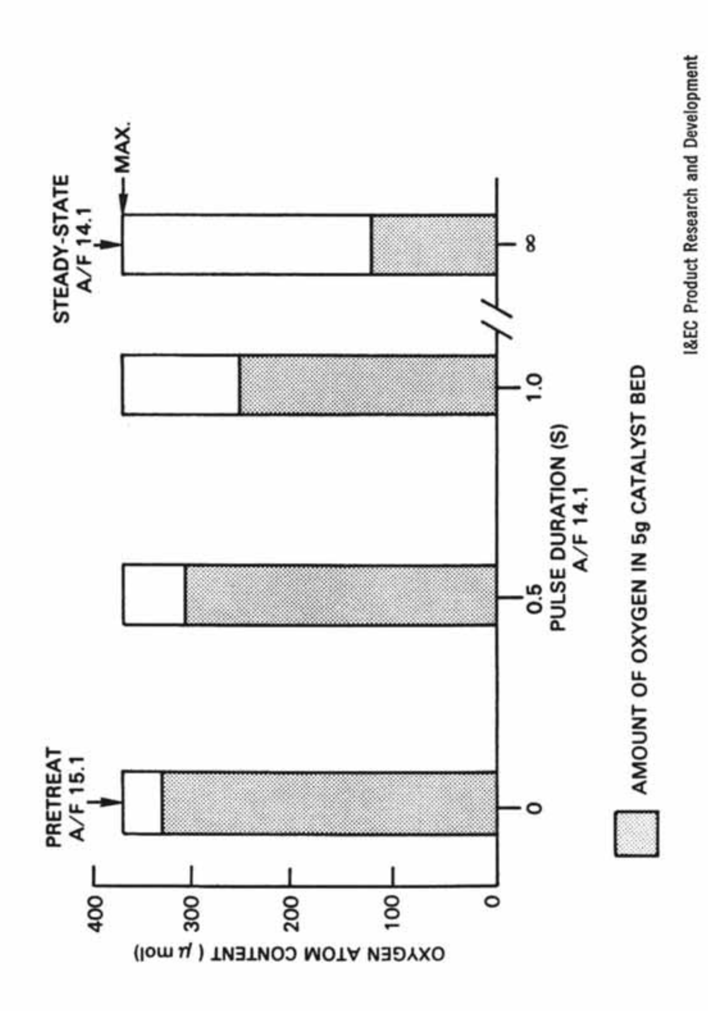

Figure 12. Rate of decrease in the oxygen content of a pelleted $Pt/Pd/Rh/Ce/Al_2O_3$ catalyst in rich exhaust at a space velocity of 110,000 h^{-1} (STP) and a catalyst inlet temperature of 680 K (18).

Literature Cited

1. Oh, S. H.; Cavendish, J. C.; Hegedus, L. L. "Mathematical Modeling of Catalytic Converter Lightoff: Single Pellet Studies"; AIChE J., 1980, 26, 935.

2. Canale, R. P.; Winegarden, S. R.; Carlson, C. R.; Miles, D. L., SAE Paper No. 780205, SAE Trans. 1978, 87, 843.

3. Seiter, R. E.; Clark, R. J., SAE Paper No. 780203, SAE Trans. 1978, 87, 828.

4. Hegedus, L. L.; Gumbleton, J. J. CHEMTECH 1980, 10, 630.

5. Gandhi, H. S.; Piken, A. G.; Shelef, M.; Delosh, R. G., SAE Paper No. 760201, SAE Trans. 1976, 85, 901.

6. Hegedus, L. L.; Summers, J. C.; Schlatter, J. C.; Baron, K. J. Catal. 1979, 56, 321.

7. Falk, C. B.; Mooney, J. J. "Three-Way Conversion Catalysts: Effect of Closed-Loop Feed-Back Control and Other Parameters on Catalyst Efficiency"; SAE Paper No. 800462, 1980.

8. Schlatter, J. C.; Sinkevitch, R. M.; Mitchell, P. J. "A Laboratory Reactor System for Three-Way Catalyst Evaluation"; GM Research Publication GMR-2911; presented at 6th N. Amer. Mtg. Catal. Soc., Chicago, IL, March 1979.

9. Schlatter, J. C.; Mitchell, P. J. Ind. Eng. Chem. Prod. Res. Dev. 1980, 19, 288.

10. Joy, G. C.; Molinaro, F. S.; Lester, G. R. "Water-Gas Shift and Steam-Reforming Ability of Group VIII Metals in Simulated Automotive Exhaust"; UOP Inc. report presented at 6th N. Am. Mtg. Catal. Soc., Chicago, IL, March 1979.

11. Cooper, B. J.; Keck, L. "NiO Incorporation in Three Way Catalyst Systems"; SAE Paper No. 800461, 1980.

12. Meitzler, A. H. "Application of Exhaust-Gas-Oxygen Sensors to the Study of Storage Effects in Automotive Three-Way Catalysts"; SAE Paper No. 800019, 1980.

13. Hill, J. C.; Majkowski, R. F. "Time-Resolved Measurement of Vehicle Sulfate and Methane Emissions with Tunable Diode Lasers"; SAE Paper No. 800510, 1980.

14. Sell, J. A.; Herz, R. K.; Monroe, D. R. "Dynamic Measurement of Carbon Monoxide Concentrations in Automotive Exhaust Using Infrared Diode Laser Spectroscopy"; SAE Paper No. 800463, 1980.

15. Sell, J. A.; Herz, R. K.; Perry, E. C. "Time-Resolved Measurement of Carbon Monoxide in the Exhaust of a Computer Command Controlled Engine"; SAE Paper No. 810276, 1981.

16. Yao, H. C.; Shelef, M. J. Catal. 1976, 44, 392.

17. Kaneko, Y.; Kobayashi, H.; Komagome, R.; Hirako, O.; Nakayama, O., SAE Paper No. 780607, SAE Trans. 1978, 87, 2225.

18. Herz, R. K. "The Dynamic Behavior of Automotive Catalysts. I. Catalyst Oxidation and Reduction"; Ind. Eng. Chem. Prod. Res. Dev. 1981, in press.

RECEIVED July 28, 1981.

4

Dynamics of High-Temperature Carbon Monoxide Chemisorption on Platinum–Alumina by Fast-Response IR Spectroscopy

S. H. OH and L. L. HEGEDUS[1]

General Motors Research Laboratories, Warren, MI 48090

Since the early work of Langmuir (1), the chemisorption of carbon monoxide on platinum surfaces has been the subject of numerous investigations. Besides its scientific interest, an understanding of CO chemisorption on Pt is of considerable practical importance; for example, the catalytic reaction of CO over noble metals (such as Pt) is an essential part of automobile emission control.

There is a wealth of information available on CO chemisorption over single-crystal and polycrystalline platinum surfaces under ultrahigh-vacuum conditions; research efforts in this area have gained a significant momentum with the advent of various surface analysis techniques (e.g., 2-8). In contrast, CO chemisorption on supported platinum catalysts (e.g., 9, 10, 11) is less well understood, due primarily to the inapplicability of most surface-sensitive techniques and to the difficulties involved in characterizing supported metal surfaces. In particular, the effects of transport resistances on the rates of adsorption and desorption over supported catalysts have rarely been studied.

Transmission infrared spectroscopy is one of the few techniques applicable to the in situ study of supported catalyst systems (e.g., 12). Much of the evidence concerning the nature of the adsorbed states of CO over supported Pt catalysts has been obtained from infrared spectroscopic studies. For example, it has been shown (13, 14) that CO can chemisorb on supported Pt catalysts either in a linear or in a bridged form. At high temperatures, however, the absorption band due to the bridge-bonded CO disappears (e.g., 15), and thus the linear form of adsorbed CO represents the dominant state, giving rise to a strong, well-defined infrared band at a frequency of about 2070 cm^{-1}. This provides a convenient means of monitoring the surface concentration of CO under realistic operating conditions by observing the intensity of the associated infrared band.

[1] Current address: W. R. Grace & Company, Washington Research Center, Columbia, MD 21044.

0097-6156/82/0178-0079$06.25/0
© 1982 American Chemical Society

Recently there has been a growing emphasis on the use of transient methods to study the mechanism and kinetics of catalytic reactions (16, 17, 18). These transient studies gained new impetus with the introduction of computer-controlled catalytic converters for automobile emission control (19); in this large-scale catalytic process the composition of the feedstream is oscillated as a result of a feedback control scheme, and the frequency response characteristics of the catalyst appear to play an important role (20). Preliminary studies (e.g., 15) indicate that the transient response of these catalysts is dominated by the relaxation of surface events, and thus it is necessary to use fast-response, surface-sensitive techniques in order to understand the catalyst's behavior under transient conditions.

In this paper we will first describe a fast-response infrared reactor system which is capable of operating at high temperatures and pressures. We will discuss the reactor cell, the feed system which allows concentration step changes or cycling, and the modifications necessary for converting a commercial infrared spectrophotometer to a high-speed instrument. This modified infrared spectroscopic reactor system was then used to study the dynamics of CO adsorption and desorption over a Pt-alumina catalyst at 723 K (450°C). The measured step responses were analyzed using a transient model which accounts for the kinetics of CO adsorption and desorption, extra- and intrapellet diffusion resistances, surface accumulation of CO, and the dynamics of the infrared cell. Finally, we will briefly discuss some of the transient response (i.e., step and cycled) characteristics of the catalyst under reaction conditions (i.e., $CO + O_2$).

Fast-Response Infrared Reactor System

a. Reactor cell. The objective was to construct a rugged infrared cell which can be operated at high temperatures (about 500°C), which has a small enough volume to allow fast response characteristics, and which behaves as a well-mixed reactor (CSTR). The reactor body was manufactured of a pair of Varian nonrotatable blank Conflat flanges, according to a suggestion of Bell (21). These flanges were machined such that a small cavity was created for placement of a thin catalyst disc. A thin thermocouple was placed in direct contact with the disc.

The disc holder was machined to fit into the stainless steel flange in such a way that it directs the gas to consecutively sweep both faces of the catalyst disc, with an expansion volume in-between. This configuration provided good gas-phase mixing in the cell, thus allowing the reactor to be characterized as a CSTR. This mode of internal mixing eliminates the need for internal moving parts or external recycle loops and pumps.

The reactor assembly was heated by electric heaters. The maximum operating temperature is determined by the window construction. Sapphire windows (from EIMAC), brazed into Kovar sleeves, were used; the sleeves were then welded directly into the stainless steel reactor housing. We found that the cell so constructed was capable of trouble-free, continuous operation at 450°C; operations at somewhat higher temperatures are probably still possible but were not explored. Sapphire was chosen as a window material because it is insensitive to water vapor and is transparent in the wave number range of our interest (about 2400 cm^{-1} to 2000 cm^{-1} in these experiments). Moreover, the thermal expansion characteristics of the reactor were found to match well with those of the window fixture.

The catalyst was prepared by impregnating γ-alumina (Alon) to incipient wetness using an aqueous solution of $H_2(PtCl_6)$. After impregnation, the powder was dried, and calcined in air at 773 K (500°C) for 2 h. The infrared disc was prepared by compressing 0.08 g of the catalyst powder at 58 840 N. The properties of the catalyst disc are listed in Table I.

b. Feed system. Figure 1 shows a flow diagram of the feed system. Two feedstreams of differing compositions were employed; these were alternatively interchanged by four, electrically operated high-speed solenoid switching valves (Automatic Switch Co.). In cycled experiments, the amplitude is determined by the concentration difference between the two feedstreams, and the frequency by the valve switching frequency. An electronic clock was used to vary the switching frequency in the range of interest (ranging from single steps to about 10 Hz).

The reactor was preceded by a preheater which had a sufficiently small mixing volume so that it did not contribute significantly to the dispersion of the feedstream pulses.

Steady streams of H_2O vapor or SO_2 could be introduced before the preheater to simulate automobile exhaust. When H_2O was added to the feedstream (we used a liquid chromatographic pump), it was condensed out before the gas entered the vent line. However, no water- or SO_2-containing feedstreams were used in the examples shown in this paper.

The gas-phase composition before or after the reactor was monitored by mass spectroscopy; although no such data are shown here, experience indicated the necessity of a fast-response inlet system.

c. Fast-response IR spectrophotometer. A Perkin-Elmer Model 180 infrared spectrophotometer was modified for these experiments to provide the necessary time response. The modifications included the replacement of the original chopper by a high-speed variety (Laser Precision Corporation, 15-1000 Hz), and redirecting the infrared beam so that it was focused onto a

Table I. Properties of the Catalyst Disc

Pt (wt %)	1.0	BET surface area (m^2/g)	100
Pt dispersion (%)*	64	ρ_s (g/cm^3)	3.67
a (cm^2 Pt/cm^3 pellet)	25 276	ρ_p (g/cm^3)	1.52
V_{macro} (cm^3/g)	0.040	D_{eff} (cm^2/s)**	0.0246
V_{micro} (cm^3/g)	0.346	ε_p	0.586
$\bar{r}_{macro}$ (Å)	211 150	Diameter (cm)	2.0
$\bar{r}_{micro}$ (Å)	130	Thickness (cm)	0.017

*Determined by a CO flow-chemisorption technique.

**Computed from the random pore model of Wakao and Smith (22) and given here at 101.3 kPa and 723 K.

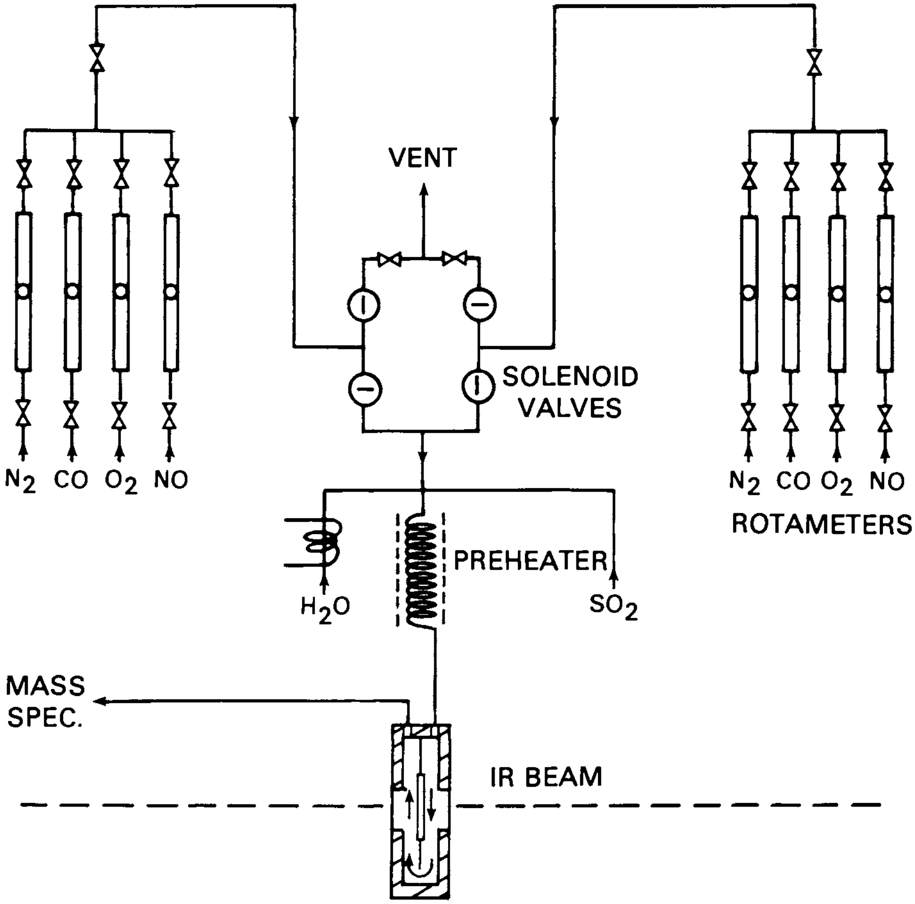

Figure 1. Schematics of the IR reactor system.

In Catalysis Under Transient Conditions; Bell, A., et al.;
ACS Symposium Series; American Chemical Society: Washington, DC, 1982.

solid-state, high-speed detector (Hg-Cd-telluride, Santa Barbara Research). The detector was cooled by liquid N_2, and its listed response time was on the order of 10^{-6} s.

The infrared spectrometer was operated in the single-beam mode. The detector signal was passed through a lock-in amplifier (Princeton Applied Research, 2 Hz-210 kHz) and the amplified signal was monitored by a storage oscilloscope. The photographed patterns were then digitized and appropriately processed. The timer section of the oscilloscope was used to trigger the switching valves in single-step experiments.

The half-scale response time of the modified infrared electronics was 0.02 s, as opposed to the half-scale response time of about 0.5 s for the infrared spectrometer before the above-described modifications.

d. Cell response and mixing characteristics. The gas-phase response and mixing characteristics of the reactor cell were analyzed by observing the responses of the cell to step changes in feedstream composition under nonreactive conditions. About 10 vol % CO in N_2 was employed as the tracer, and the gas-phase CO band (at 2170 cm^{-1}) was monitored. Analysis of the step responses indicated reasonably good mixing behavior in the cell; for a step increase (i.e., $N_2 \rightarrow CO$), a plot of $\ln(1-c_\infty/c_{\infty,in})^{-1}$ vs t yielded a straight line, as shown in Figure 2. From the slope of the straight line, the effective mixing cell volume was calculated to be 30.1 cm^3, with a 50% relaxation time of about 0.08 s. Similar mixing characteristics were observed following a step decrease (i.e., $CO \rightarrow N_2$), giving an effective mixing cell volume of 31.8 cm^3 and a 50% relaxation time of 0.09 s. Since these response times of the reactor are not much faster than the time scale of the adsorption process (a half-scale relaxation time of about 0.2 s), the transients of the reactor cell were included in our analysis. For our simulations, the mixing cell volume was taken to be 31 cm^3.

Theory of Transient, Diffusion-Coupled CO Chemisorption

The balance equation for CO in the intrapellet gas phase is

$$\varepsilon_p \frac{\partial c}{\partial t} = D_{eff} \frac{\partial^2 c}{\partial x^2} - a\,[\tilde{R}_a - \tilde{R}_d] \qquad (1)$$

where $\tilde{R}_a$ and $\tilde{R}_d$ represent the rates of CO adsorption and desorption per unit surface area of Pt, respectively. The boundary conditions for Equation (1) are

$$\frac{\partial c}{\partial x}(0,t) = 0 \qquad (2)$$

$$D_{eff} \frac{\partial c}{\partial x}(L,t) = k_m\,[c_\infty(t) - c(L,t)] \qquad (3)$$

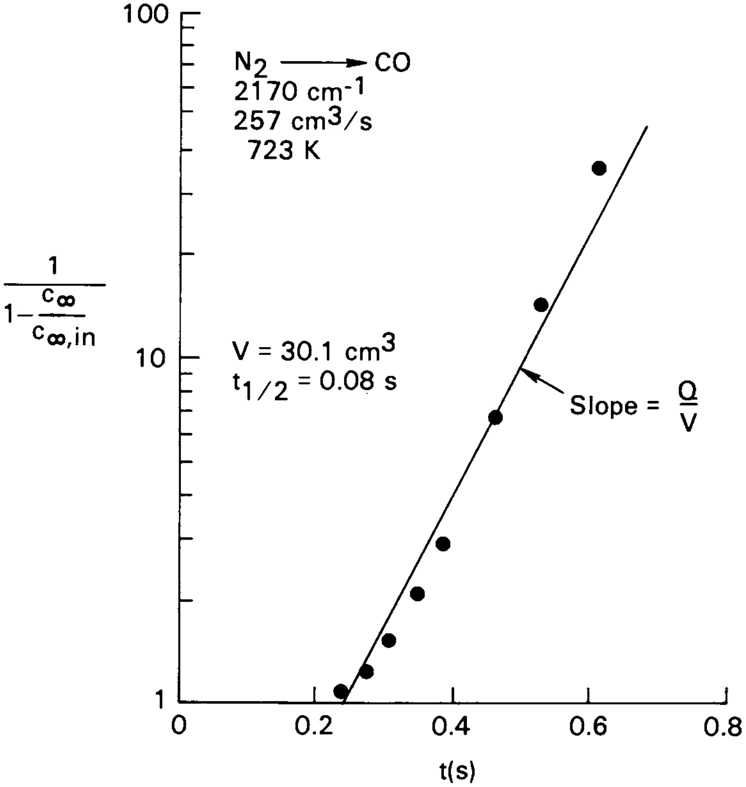

Figure 2. Mixing behavior of the reactor cell: gas phase response to a step increase in inlet CO concentration.

where L is the half-thickness of the catalyst disc. The bulk gas-phase CO concentration in the reactor, c_∞, varies with time, and its time dependency will be described below.

The conservation of adsorbed CO on the Pt surface can be expressed, in terms of its fractional surface coverage Θ, as

$$N_s \frac{\partial \Theta}{\partial t} = \tilde{R}_a - \tilde{R}_d \tag{4}$$

where N_s denotes the surface concentration of CO corresponding to a complete monolayer coverage of the Pt surface. For our computations, N_s was taken to be 2×10^{-9} mol CO/cm^2 Pt (1.2×10^{15} CO molecules/cm^2 Pt), based on the assumption of 1:1 stoichiometry between Pt surface atoms and CO molecules.

The dynamics of the infrared cell can be described by

$$V \frac{dc_\infty}{dt} = Q\,[c_{\infty,in} - c_\infty(t)] - D_{eff}\, A \frac{\partial c}{\partial x}(L,t) \tag{5}$$

In our experiments, the CO concentration at the reactor inlet, $c_{\infty,in}$, was perturbed in a stepwise fashion at t=0.

The initial conditions for Equations (1), (4), and (5) are given by

$$\left.\begin{aligned} c\,(x,0) &= c_o \\ \Theta\,(x,0) &= \Theta_o \\ c_\infty(0) &= c_{\infty,o} \end{aligned}\right\} \tag{6}$$

For the simulation results reported here, $c_o = \Theta_o = c_{\infty,o} = 0$ for CO adsorption, and $c_o = c_{\infty,o} = 1$ vol % and $\Theta_o = 0.78$ for CO desorption. The initial coverage (Θ_o) for the desorption experiments was obtained by calibrating the absorbances in terms of CO coverage, as will be explained later.

The analysis of the system's dynamic behavior requires solving Equations (1) to (6) simultaneously. The rate expressions for $\tilde{R}_a$ and $\tilde{R}_d$ which appear in these equations will be discussed briefly in the following paragraphs.

The rate of adsorption of CO is equal to the product of the flux of CO molecules striking the surface, F, and their scicking probability, S. That is,

$$\tilde{R}_a = F\,S \tag{7}$$

where F can be written from the kinetic theory of gases (e.g., 23) as

$$F = \sqrt{\frac{R\,T}{2\,\pi\,M}}\; c \tag{8}$$

and, assuming that the CO adsorption rate is proportional to the fraction of vacant sites,

$$S = S_o\,(1-\Theta) \tag{9}$$

It should be noted that Equation (9) is not strictly valid for CO/Pt systems; experiments show that the rate of CO adsorption remains essentially constant as Θ increases up to about 0.25 to 0.5 before the rate decreases with a further increase in Θ (8, 24, 25). However, this simple relationship is adopted here because the essential features of the system are not expected to be lost by this approximation. The initial sticking probability for CO, S_o, remains nearly constant up to about 450 K, but at higher temperatures it decreases appreciably with temperature (4, 6). In this study S_o (at 723 K) was taken to be 0.025 (4).

The rate of desorption of an adsorbed species from a surface is usually expressed in the form

$$\tilde{R}_d = \nu c_s^n \exp(-E_d(\Theta)/RT) \tag{10}$$

where c_s is the surface concentration of the adsorbate (mol/cm^2 Pt surface). In view of the nondissociative adsorption of CO, the order of desorption n and the pre-exponential factor ν were taken to be 1 and 10^{13} s^{-1}, respectively (26, 27). A coverage-dependent activation energy for desorption is assumed because the desorption energy has often been observed to decrease with coverage for CO/Pt systems (e.g., 8). Moreover, this coverage dependence has been successfully used in the analysis of thermal desorption data (7, 24, 28, 29). The decrease in the desorption energy with coverage is related physically to the mutual interactions (such as long-range repulsive interactions) between the adsorbed CO molecules (8).

For the present analysis, it is assumed that the activation energy for CO desorption decreases linearly with CO coverage. That is,

$$E_d = E_{do} - \alpha \Theta \tag{11}$$

where the desorption energy at the low-coverage limit, E_{do}, was taken to be 144.4 kJ/mol (34.5 kcal/mol). This desorption energy is compatible with the literature values reported for single-crystal Pt surfaces (8, 24, 30, 31), and for Pt ribbons and wires (3-6). The parameter α, which describes the variation of the desorption energy with coverage, was chosen to be 27.2 kJ/mol (6.5 kcal/mol) (7).

Implicit in the use of Equation (10) is the assumption that desorption occurs from the surface populated by one type of adsorbed species. This single-state model will be shown to be adequate to describe the dynamic behavior of CO desorption at the high temperature (723 K) considered here. The analysis of the more general case of multi-state desorption can be found in Donnelly et al. (32) and Winterbottom (3).

The determination of the external mass transfer coefficient of CO, k_m, (see Equation 3) deserves brief comments. Since the complex geometry and flow characteristics in the reactor cell precluded a reliable estimation of k_m based on correlations given in the literature, the CO oxidation activities of the catalyst

disc, measured independently under mass transfer-limited conditions, were used to determine k_m. Figure 3 shows the CO conversion performance of the reactor as a function of temperature in a large excess of O_2 (i.e., 1 vol % CO and 5 vol % O_2). It can be seen that the CO conversion remains essentially constant (about 60%) above 650 K, indicating that the reaction rate in this regime is limited by mass transfer from the bulk gas to the catalyst's external surface. Similar conversion data, including the same asymptotic conversion level, were obtained with a feedstream composition of 0.5 vol % CO and 5 vol % O_2. In the completely mass transfer-limited regime, the steady-state mass balance equation for the reactor cell can be written as

$$Q\ (c_{\infty,in} - c_{\infty}) = k_m\ A\ c_{\infty} \tag{12}$$

or, in terms of the fractional CO conversion ϕ,

$$k_m = \frac{Q}{A}\left(\frac{\phi}{1-\phi}\right) \tag{13}$$

Using Equation (13), the external mass transfer coefficient at 723 K was calculated to be 60 cm/s. Since the reactor operating conditions at this temperature (723 K, slightly above atmospheric pressure, 247 cm^3/s) were very similar to those of our transient chemisorption experiments, the external mass transfer coefficient calculated above was used for the simulations.

The transmittance observed at 2070 cm^{-1} was converted into absorbance ($A_{CO}=\ln(1/T_{CO})$), since the latter is a direct measure of the surface concentration of CO. In order to quantify the absorbances in terms of surface coverages, the steady-state intensities of the Pt-CO band were measured at several different gas-phase CO concentrations. The results (absorbance vs CO concentration) are shown in Figure 4a. The same data, when plotted in the plane of c/A_{CO} vs c, yield a straight line (see Figure 4b), indicating that these adsorption equilibrium data can be well approximated by a Langmuir isotherm. From the slope of this straight line, the absorbance corresponding to a monolayer coverage of CO, A_{sat}, was calculated to be 0.473.

Once A_{sat} is determined, the surface coverage of CO can be obtained from the relationship $\Theta = A_{CO}/A_{sat}$. This relationship implies that the extinction coefficient of adsorbed CO is independent of CO coverage. While this aspect was not explored here, the agreement of the model's predictions with the experimental data (as will be shown later) indicates that this assumption may not interfere significantly with the essential features of the system.

For the rate expressions $\tilde{R}_a$ and $\tilde{R}_d$ given above, Equations (1) to (6) were solved numerically using the PDEPACK routine of Madsen and Sincovec (33). The computational results as well as their comparison with the experimental data will be discussed in the next section.

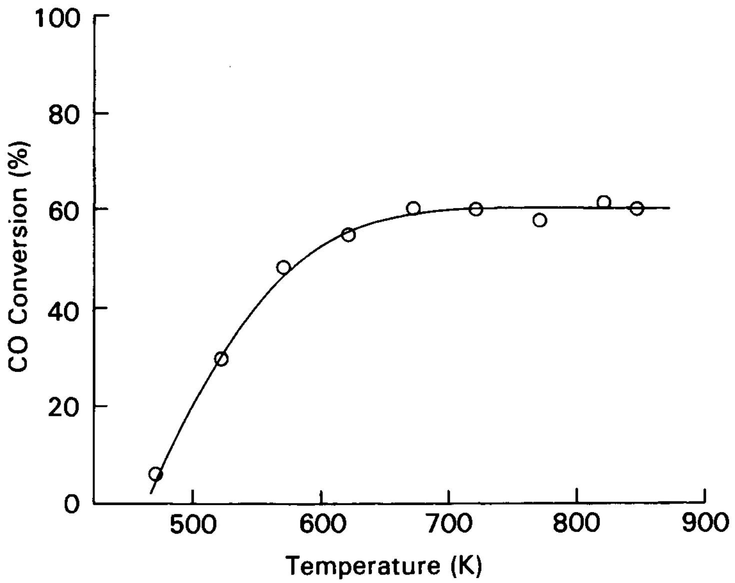

Figure 3. CO conversion in the reactor cell as a function of temperature, measured to determine the external mass transfer coefficient of CO. Conditions: 1% CO, 5% O_2, 93.3 cm^3/s at 273 K and 101.3 kPa.

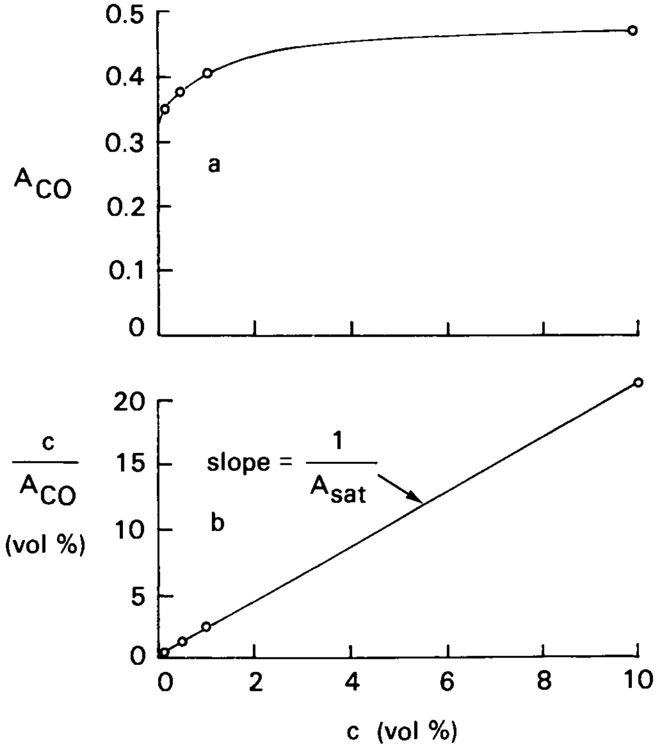

Figure 4. Adsorption isotherm for the CO/Pt system at 723 K and 121.7 kPa, plotted in two different forms. In the lower curve, A_{sat} = 0.473.

Results and Discussion

a. CO chemisorption studies. The step-change experiments for the adsorption and desorption of CO were conducted at a pellet temperature of 723 K and at a reactor pressure of 121.7 kPa (slightly above atmospheric pressure). Such a high temperature was chosen in order to approximate the operating temperature of a fully warmed-up catalytic converter. The gas flow rate was 257 cm^3/s at our experimental conditions. Before the infrared experiments, the Pt-alumina catalyst disc was pretreated with 0.7 vol % O_2 (in N_2), with N_2, with 1 vol % H_2 (in N_2), and then with N_2, each step being at 723 K for 5 min. The adsorption of CO was then studied by suddenly directing a feedstream of 1 vol % CO in N_2 through the reactor (in place of the N_2 stream) and monitoring the resulting time variations of the transmittance at 2070 cm^{-1}, the well-known Pt-CO stretch frequency. After equilibration, the step response of CO desorption was measured by switching the feed back to N_2.

It is interesting to note that at this high temperature the frequency of the Pt-CO band did not shift appreciably as the CO coverage varied, in contrast to observations made on a (111)-oriented platinum ribbon (6) or on a polycrystalline Pt surface (34) at or below room temperature.

As will be shown later, the surface coverages of CO vary with distance into the pellet during CO adsorption and desorption, as a result of intrapellet diffusion resistances. However, the infrared beam monitors the entire pellet, and thus the resulting absorption band reflects the average surface concentration of CO across the pellet's depth. Therefore, for the purpose of direct comparison between theory and experiment, the integral-averaged CO coverage in the pellet

$$\Theta_{av}(t) = \frac{1}{L} \int_0^L \Theta(x,t)\, dx \qquad (14)$$

was computed from the mathematical model.

Figure 5 shows the integral-averaged surface coverage of CO in the catalyst pellet as a function of time during the CO adsorption at 723 K. In this experiment, the reactor inlet concentration was switched from N_2 to 1 vol % CO (in N_2) at t=0, while maintaining the total flow rate and the reactor pressure essentially unperturbed. The measured values (solid line in Figure 5) were obtained based on the relationship $\Theta_{av}=A_{CO}/A_{sat}$ (A_{sat}=0.473). The asymptotic CO coverage reached after the relaxation of the step change was calibrated to be 78% of a complete monolayer coverage. The computational result shown in the dotted line of Figure 5 is in very good agreement with the experimental data.

Figure 6 shows the measured and calculated time variations of the integral-averaged CO coverage following the step change

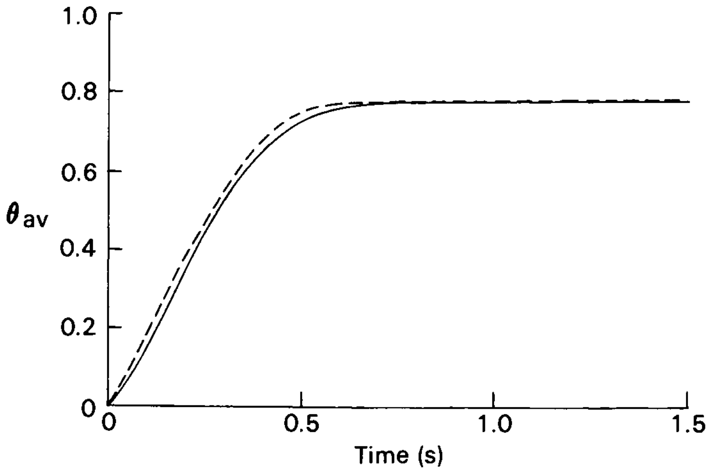

Figure 5. Integral-averaged CO coverage as a function of time during CO adsorption. Key: ——, measured; and – – –, calculated.

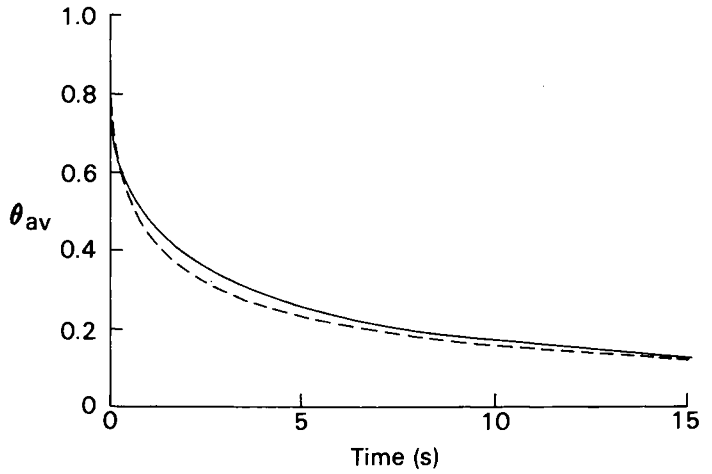

Figure 6. Integral-averaged CO coverage as a function of time during CO desorption. Key: ——, measured; and – – –, calculated.

from 1 vol % CO to N_2 (i.e., during CO desorption at 723 K). Here again, good agreement between theory and experiment was obtained. Notice that the CO desorption occurred much more slowly than the CO adsorption; that is, a ten-fold difference in the 50% relaxation time (2 s vs 0.2 s) was observed.

In view of the possible presence of diffusion resistances in the catalyst pellet, it is of interest to examine the intrapellet concentration profiles established during transient CO adsorption and desorption. Figure 7 shows the calculated intrapellet concentration profiles for CO adsorption at various times. It can be seen that significant gas-phase concentration gradients (see solid lines) are established inside the pellet at the early stages of the transient adsorption process. Also shown in Figure 7 are the corresponding profiles for the fractional surface coverage of CO (dotted lines).

Figure 8 shows how the intrapellet concentration profiles vary with time during the course of CO desorption. Both the gas-phase (solid lines) and surface (dotted lines) CO concentration profiles exhibit relatively mild gradients inside the pellet, in contrast to the steep profiles established during the adsorption process. This can be attributed to the fact that the intrinsic rate of desorption is slower than that of adsorption.

The importance of including mass transport resistances (both internal and external) in the model can be best examined by comparing the exact solution of the model with the predicted responses obtained based on the assumption of negligible mass transport resistances. As Figure 9 shows, the step response of the integral-averaged CO coverage during the adsorption is affected only slightly by the external mass transfer resistance (compare Curves A and B); however, when both internal and external mass transport resistances are assumed to be negligible, the model predicts a considerably faster response (compare Curves A and C). These results demonstrate the importance of accounting for intrapellet diffusion resistances in the analysis of transient chemisorption over supported catalysts. Similar effects are observed for CO desorption, as shown in Figure 10.

It is interesting to note that, although the intrinsic rate of desorption is slower than that of adsorption, both rates were found to be sufficiently fast under our experimental conditions so that the adsorption-desorption process on the Pt surface can be assumed to rapidly equilibrate at all times; that is, even a ten-fold increase in <u>both</u> the adsorption and desorption rate constants (while keeping their ratio constant) did not significantly change the predicted step responses. With the assumption of chemisorption equilibrium, Equations (1) and (4) can be combined into the form (35)

$$[\varepsilon_p + N_s\, a \left(\frac{\partial\theta}{\partial c}\right)] \frac{\partial c}{\partial t} = D_{eff} \frac{\partial^2 c}{\partial x^2} \qquad (15)$$

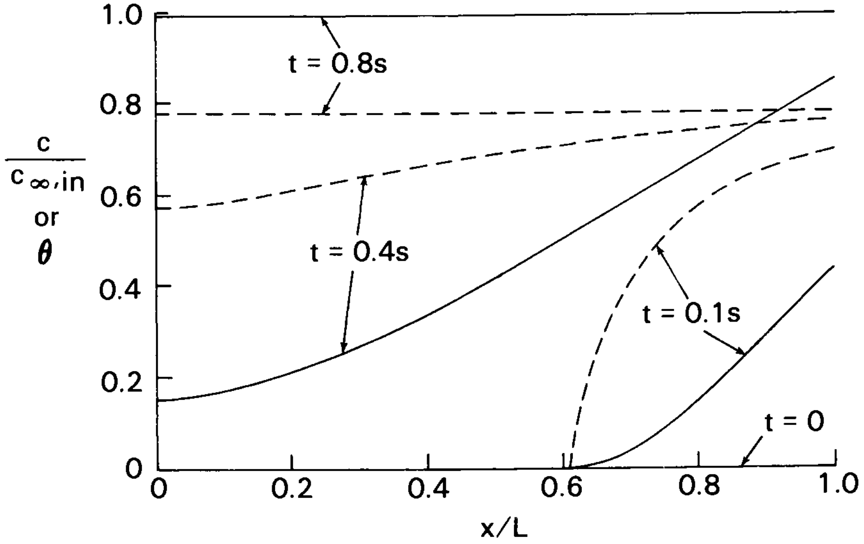

Figure 7. Computed time variation of intrapellet concentration profiles during CO adsorption. Key: ——, gas phase; and – – –, surface.

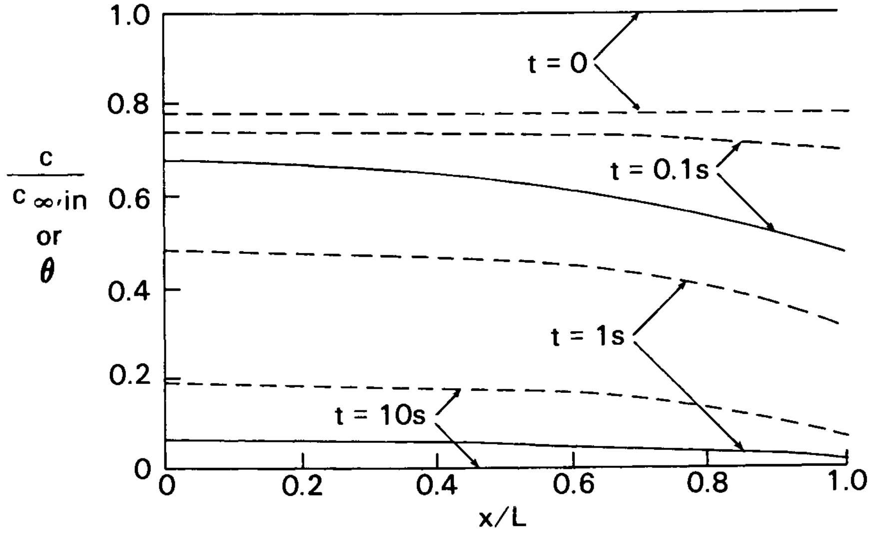

Figure 8. Computed time variation of intrapellet concentration profiles during CO desorption. Key: ——, gas phase; and – – –, surface.

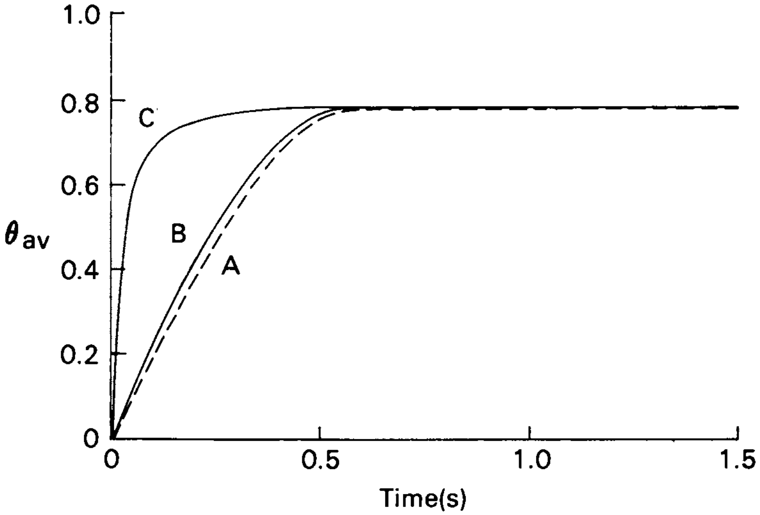

Figure 9. Effects of internal and external transport resistances on the computed step-response of CO adsorption. Curve A corresponds to our experimental conditions. Key: A, $k_m = 60$ cm/s, $D_{eff} = 0.0246$ cm²/s; B, $k_m \rightarrow \infty$, $D_{eff} = 0.246$ cm²/s; and C, $k_m \rightarrow \infty$, $D_{eff} \rightarrow \infty$.

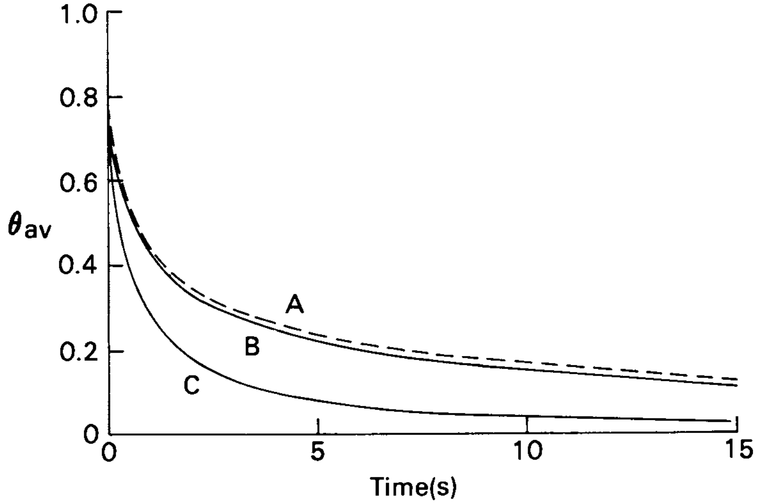

Figure 10. Effects of internal and external transport resistances on the computed step-response of CO desorption. Curve A corresponds to our experimental conditions. Key: A, $k_m = 60$ cm/s, $D_{eff} = 0.0246$ cm²/s; B, $k_m \rightarrow \infty$, $D_{eff} = 0.0246$ cm²/s; and C, $k_m \rightarrow \infty$, $D_{eff} \rightarrow \infty$.

where $(\partial\Theta/\partial c)$ represents the slope of the adsorption isotherm. The quantity $[N_s\ a\ (\partial\Theta/\partial c)]$ in Equation (15) accounts for the capacity of the catalytic surface for the chemisorption of CO. For porous catalyst pellets with practical loadings, this quantity is typically much larger than the pellet void fraction ε_p, indicating that the dynamic behavior of supported catalysts is dominated by the relaxation of surface phenomena (e.g., 35, 36). This implies that a quasi-static approximation for Equation (1) (i.e., $\varepsilon_p \frac{\partial c}{\partial t} = 0$) can often be safely invoked in the transient modeling of porous catalyst pellets. The calculations showed that the quasi-static approximation is indeed valid in our case; the model predicted virtually the same step responses, even when the value of ε_p was reduced by a factor of 10.

It follows directly from Equation (15) that the characteristic response time for the intrapellet gas-phase concentration during the adsorption-desorption process is approximated by $[(L^2/D_{eff})\ N_s\ a\ (\partial\Theta/\partial c)]$. (Note that this characteristic response time represents the product of the characteristic time for intrapellet diffusion, L^2/D_{eff}, and the surface capacity for CO chemisorption, $N_s\ a\ (\partial\Theta/\partial c)$.) The estimation of the response time is complicated by the fact that the slope of the adsorption isotherm $(\partial\Theta/\partial c)$ varies with gas-phase CO concentration; however, when its average value over the CO concentration range of 0 to 1 vol % was taken to be $5\times10^6\ cm^3/mol$ (= 1 (vol %)$^{-1}$; see Figure 4a), the characteristic response time was calculated to be 0.75 s. Inspection of the time variation of the intrapellet gas-phase concentrations shown in Figures 7 and 8 (solid lines) lends support to our estimated response time; that is, the intrapellet gas-phase concentration relaxes on the time scale of 1 s during both the adsorption and desorption processes.

In contrast to the intrapellet gas-phase concentration, the surface concentration of CO in the pellet relaxes at significantly different rates, depending on the direction of the step changes. As shown earlier, the surface concentration of CO decays much more slowly during CO desorption than it increases during CO adsorption (compare Figures 5 and 6). This is, however, merely due to the fact that close to adsorption equilibrium, the surface coverage of CO can be high even at low gas-phase CO concentrations, as shown in Figure 4a.

b. Reactive experiments. In addition to the chemisorption studies described above, we also conducted transient infrared experiments under reaction conditions (i.e., $CO + O_2$ over Pt-alumina). The results of these reactive experiments, though not yet analyzed in quantitative detail, will be nevertheless shown here (in the transmittance mode) because they illustrate some interesting features of the transient response of the $CO/O_2/Pt$ system.

Figure 11 shows how O_2 pretreatment of the catalyst influences the step response during CO adsorption. Prior to this experiment, the catalyst was first pretreated in 0.7 vol % O_2 (in N_2) for 5 min and then flushed with N_2 for 5 min (all at 723 K). After this N_2 flush, the catalyst was suddenly exposed to a step flow of 1 vol % CO (in N_2). As shown in Figure 11, the growth of the 2070 cm^{-1} Pt-CO band is significantly delayed after O_2 pretreatment (Curve B), indicating that at the early stages of the step change, the CO on the Pt surface is rapidly consumed by the strongly chemisorbed oxygen.

The rate of CO removal from the Pt surface is also affected by the presence of O_2 in the gas phase, as demonstrated in Figure 12. In this experiment the catalyst, initially in equilibrium with 1 vol % CO (in N_2), was suddenly exposed to a feedstream of 0.7 vol % O_2 (in N_2). It can be seen from Figure 12 that the Pt-CO band decays much faster in O_2 (Curve B) than in N_2 (Curve A for reference). This indicates that the surface reaction between CO and oxygen is faster than the rate of CO desorption.

Figure 13 shows the time variation of the surface concentration of CO (on the transmittance scale) during feedstream composition cycling. Cycling between two feedstreams, one oxidizing (1 vol % CO, 1.03 vol % O_2) and the other reducing (1 vol % CO, 0.23 vol % O_2), was accomplished by four fast-acting solenoid valves at a switching frequency of 1 Hz. In the oxidizing feedstream, the Pt surface was found to be essentially free of CO, while a significantly higher CO coverage was observed over Pt in equilibrium with the reducing feedstream. It is interesting to note that, as Figure 13 shows, the surface concentration of CO assumed the same stationary pattern after several transitory cycles, regardless of whether the catalyst was initially stabilized in an oxidizing or in a reducing feedstream.

Concluding Remarks

A fast-response infrared spectroscopic reactor system has been described which is capable of operating at high temperatures (e.g., 450-500°C). The infrared reactor system was successfully used to monitor the response of the surface concentration of CO to step changes or oscillations in the feedstream composition, under both reactive and nonreactive conditions.

The dynamics of high-temperature CO adsorption and desorption over Pt-alumina was analyzed in detail using a transient mathematical model. The model combined the mechanism of CO adsorption and desorption (established from ultrahigh-vacuum studies over single-crystal or polycrystalline Pt surfaces) with extra- and intrapellet transport resistances. The numerical values of the parameters which characterize the surface processes were taken from the literature of clean surface studies;

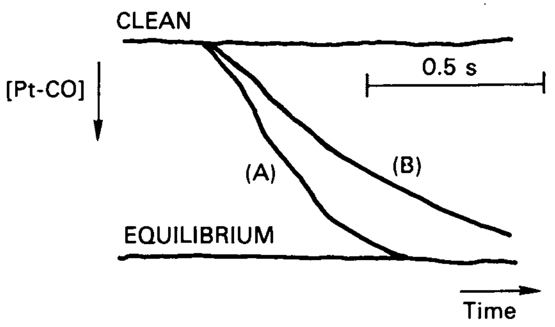

Figure 11. Effect of O_2 pretreatment on the rate of CO adsorption (transmittance mode) at 723 K, 257 cm^3/s, and 2,070 cm^{-1}. Key: A, prereduced Pt; and B, Pt preexposed to O_2 and flushed with N_2.

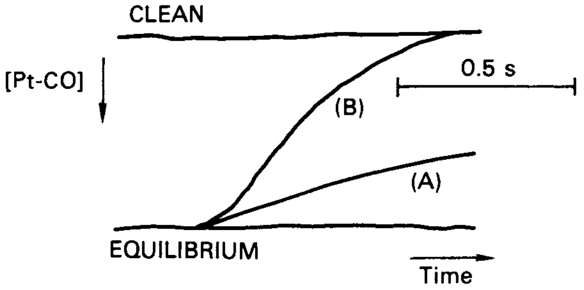

Figure 12. Effect of O_2 on the rate of CO removal (transmittance mode) at 723 K, 257 cm^3/s, and 2,070 cm^{-1}. Key: A, CO removal by N_2; and B, CO removal by 1% O_2.

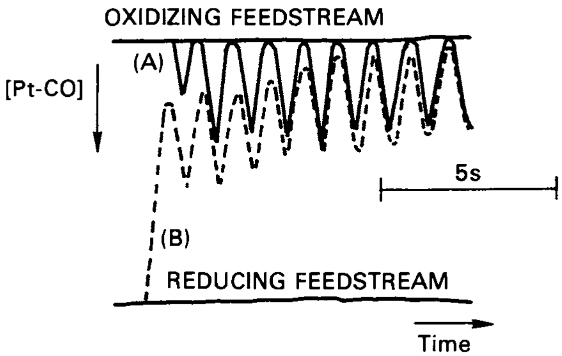

Figure 13. Surface transients over Pt-alumina, starting with an oxidizing feedstream (A) or with a reducing feedstream (B) (transmittance mode) at 723 K, 257 cm^3/s, 2,070 cm^{-1}, and 1 Hz switching frequency.

we found good agreement between the measured and calculated step responses, indicating that, at least in this case, it is possible to apply surface chemistry information to supported catalysts operating at high temperature and pressure (450°C, slightly above atmospheric pressure).

Parametric sensitivity analysis showed that for nonreactive systems, the adsorption equilibrium assumption can be safely invoked for transient CO adsorption and desorption, and that intrapellet diffusion resistances have a strong influence on the time scale of the transients (they tend to slow down the responses). The latter observation has important implications in the analysis of transient adsorption and desorption over supported catalysts; that is, the results of transient chemisorption studies should be viewed with caution, if the effects of intrapellet diffusion resistances are not properly accounted for.

Nomenclature

a	=	local Pt surface area, cm^2 Pt/cm^3 pellet
A	=	total external surface area of the catalyst pellet, cm^2
A_{CO}	=	absorbance for adsorbed CO
A_{sat}	=	absorbance corresponding a complete monolayer coverage of CO
c	=	CO concentration in the intrapellet gas phase, mol/cm^3 or vol %
c_o	=	initial CO concentration in the intrapellet gas phase, mol/cm^3
c_s	=	surface concentration of CO, mol/cm^2 Pt
c_∞	=	CO concentration in the bulk gas phase of the reactor cell, mol/cm^3
$c_{\infty,o}$	=	initial CO concentration in the reactor cell, mol/cm^3
$c_{\infty,in}$	=	CO concentration at the inlet of the reactor cell, mol/cm^3
₵	=	fractional conversion of CO
D_{eff}	=	effective diffusivity of CO in the catalyst pellet, cm^2/s

E_d	=	activation energy for desorption, kJ/mol
E_{do}	=	activation energy for desorption extrapolated to zero surface coverage of CO, kJ/mol
F	=	flux of CO molecules striking the surface, mol/ $(s \cdot cm^2\ Pt)$
k_m	=	external mass transfer coefficient of CO, cm/s
L	=	half-thickness of the catalyst pellet, cm
M	=	molecular weight of CO, g/mol
N_s	=	saturation CO concentration over the active sites, mol/cm^2 Pt
Q	=	gas volumetric flow rate, cm^3/s
R	=	gas constant, 8.3144×10^7 g $cm^2/(s^2 \cdot mol \cdot K)$ or 8.32×10^{-3} kJ/(mol·K)
$\tilde{R}_a$	=	rate of CO adsorption, $mol/(s \cdot cm^2\ Pt)$
$\tilde{R}_d$	=	rate of CO desorption, $mol/(s \cdot cm^2\ Pt)$
$\bar{r}_{macro\ or\ micro}$	=	integral-averaged pore radii, Å
S	=	sticking probability for CO
S_o	=	initial sticking probability for CO
T	=	temperature, K or °C
T_{CO}	=	transmittance for adsorbed CO
t	=	time, s
V	=	volume of the reactor cell, cm^3
$V_{macro\ or\ micro}$	=	pellet macro- or micropore volumes, cm^3/g
x	=	distance from the pellet center, cm

Greek Letters

α	=	parameter describing the variation of the desorption energy with fractional surface coverage (see Equation 11), kJ/mol

ε_p = pellet void fraction

Θ = fractional surface coverage of CO

Θ_{av} = integral-averaged fractional surface coverage of CO in the pellet

Θ_o = initial CO coverage

ν = pre-exponential factor for the rate of desorption, s^{-1}

ρ_p = pellet density, g/cm^3 pellet

ρ_s = pellet solid density, g/cm^3 solid

Acknowledgments

E. J. Shinouskis built the infrared reactor cell and conducted the infrared reactor experiments. The authors are indebted to J. A. Sell for the modifications of the infrared spectrophotometer, and to Professor A. T. Bell for sharing his experience with infrared reactor construction. The CO conversion data of Figure 3 were obtained by J. E. Carpenter.

Literature Cited

1. Langmuir, I. Trans. Faraday Soc. 1922, 17, 621.

2. Morgan, A. E.; Somorjai, G. A. J. Chem. Phys. 1969, 51, 3309.

3. Winterbottom, W. L. Surface Sci. 1973, 37, 195.

4. Nishiyama, Y.; Wise, H. J. Catal. 1974, 32, 50.

5. Collins, D. M.; Lee, J. B.; Spicer, W. E. Surface Sci. 1976, 55, 389.

6. Shigeishi, R. A.; King, D. A. Surface Sci. 1976, 58, 379.

7. McCabe, R. W.; Schmidt, L. D. Surface Sci. 1977, 65, 189.

8. Ertl, G.; Neumann, M.; Streit, K. M. Surface Sci. 1977, 64, 393.

9. Cormack, D.; Moss, R. L. J. Catal. 1969, 13, 1.

10. Bain, F. T.; Jackson, S. D.; Thomson, S. J.; Webb, G.; Willocks, E. J. Chem. Soc. Faraday Trans. I 1976, 72, 2516.

11. Foger, K.; Anderson, J. R. Appl. Surface Sci. 1979, 2, 335.

12. Delgass, W. N.; Haller, G. L.; Kellerman, R.; Lunsford, J. H. "Spectroscopy in Heterogeneous Catalysis," Academic Press: New York, 1979.

13. Eischens, R. P.; Francis, S. A.; Pliskin, W. A. J. Phys. Chem. 1956, 60, 194.

14. Heyne, H.; Tompkins, F. C. Proc. Roy. Soc. (London) 1966, A292, 460.

15. Hegedus, L. L.; Chang, C. C.; McEwen, D. J.; Sloan, E. M. Ind. Eng. Chem. Fundam. 1980, 19, 367.

16. Kobayashi, H.; Kobayashi, M. Catal. Rev.-Sci. Eng. 1974, 10, 139.

17. Bennett, C. O. Catal. Rev.-Sci. Eng. 1976, 13, 121.

18. Tamaru, K. "Dynamic Heterogeneous Catalysis," Academic Press: New York, 1978.

19. Hegedus, L. L.; Gumbleton, J. J. ChemTech 1980, 10, 630.

20. Hegedus, L. L.; Summers, J. C.; Schlatter, J. C.; Baron, K. J. Catal. 1979, 56, 321.

21. Bell, A. T., personal communications (1980).

22. Smith, J. M. "Chemical Engineering Kinetics," McGraw-Hill: New York, 1970.

23. Somorjai, G. A. "Principles of Surface Chemistry," Prentice-Hall: Englewood Cliffs, New Jersey, 1972.

24. McCabe, R. W.; Schmidt, L. D. Surface Sci. 1977, 66, 101.

25. Weinberg, W. H.; Comrie, C. M. J. Catal. 1976, 41, 489.

26. Menzel, D. "Desorption Phenomena," in "Topics in Applied Physics," Vol. 4; Gomer R., Ed.; Springer-Verlag: New York, 1975.

27. Baetzold, R. C.; Somorjai, G. A. J. Catal. 1976, 45, 94.

28. Falconer, J. L.; Madix, R. J. J. Catal. 1977, 48, 262.

29. Taylor, J. L.; Weinberg, W. H. Surface Sci. 1978, 78, 259.

30. Bonzel, H. P.; Burton, J. J. Surface Sci. 1975, 52, 223.

31. Lambert, R. M.; Comrie, C. M. Surface Sci. 1974, 46, 61.

32. Donnelly, R. G.; Modell, M.; Baddour, R. F. J. Catal. 1978, 52, 239.

33. Madsen, N. K.; Sincovec, R. F. "PDEPACK: Partial Differential Equations Package," Scientific Computing Consulting Services, Livermore, California, 1975.

34. Hoffmann, F. M.,; Bradshaw, A. M. J. Catal. 1976, 44, 328.

35. Oh, S. H.; Baron, K.; Cavendish, J. C.; Hegedus, L. L. Paper No. 38, ACS Symposium Series, No. 65, "Chemical Reaction Engineering-Houston," ACS: Washington, D.C., 1978.

36. Sheintuch, M.; Schmitz, R. A. Catal. Rev.-Sci. Eng. 1977, 15, 107.

RECEIVED July 28, 1981.

5

Nitric Oxide Reduction by Hydrogen over Rhodium Using Transient Response Techniques

BRUCE J. SAVATSKY and ALEXIS T. BELL

University of California, Department of Chemical Engineering, Berkeley, CA 94720

The catalyzed reduction of nitric oxide over rhodium is of considerable interest in view of extensive research (1-7) showing that catalytic convertors containing rhodium are particularly effective for controlling the emission of nitric oxide from automobiles. While it has been established that carbon monoxide and hydrogen are the primary agents participating in NO reduction, little is known thus far concerning the mechanism and kinetics of the reduction process. Studies by Kobylinski and Taylor (1) with Rh/Al_2O_3 have shown that H_2 is a more effective reducing agent than CO, as evidenced by the fact that the temperature required to achieve a given degree of conversion is lower using H_2 rather than CO as the reducing agent. It was also demonstrated that even when H_2 and CO are combined, H_2 is still the preferred reducing agent. A more detailed investigation of NO reduction by H_2 has been reported by Yao et al. (6). These authors noted that the global activation energy for NO reduction decreased from 14.7 to 8.8 kcal/ mole as the Rh loading increased from 0.34 to 12.4%. Nitrogen and N_2O were observed as the major products with N_2O being the dominant product under all conditions studied. It was also noted that the ratio of N_2/N_2O was not very much affected by either the reactant concentrations or the catalyst temperature. Although not observed directly, the authors proposed that a surface complex containing two NO molecules and two H atoms could be an important reaction intermediate. More recently, Myers and Bell (8) have investigated the interaction of NO with H_2 over Rh/SiO_2 using temperature programmed reaction (TPR). Their results suggest that NO dissociation to form N and O atoms is the first step of the reaction sequence. Ammonia and H_2O are believed to be formed by the stepwise hydrogenation of the atomic species and the small amount of N_2 observed is formed by the recombination of N atoms.

The present work was undertaken to investigate the applicability of transient response techniques [e.g., ref. (9-11)] for characterizing the mechanism and kinetics of NO reduction. Mass spectrometry was used to trace the dynamics of product formation and in situ infrared spectroscopy was used to

0097-6156/82/0178-0105$09.25/0
© 1982 American Chemical Society

observe the state of adsorbed NO. Two types of experiment were performed. The first involved the reduction of preadsorbed NO in a constant flow of H_2. The second type of experiment involved the substitution of ^{15}NO for ^{14}NO, either during steady-state reduction or just prior to the addition of H_2 to a flowing stream of NO. It will be shown that the data obtained from these experiments can be interpreted in terms of a mechanism of NO deduced from evidence presented in the recent literature.

Experimental

Catalyst. A 4.4% Rh/SiO_2 catalyst was used for all of the work presented here. The catalyst was prepared by impregnation of Davison 70 silica gel with an aqueous solution of $RhCl_3$. The freshly prepared material was dried and then reduced in flowing H_2 at 673K for 2 hr. The dispersion of the catalyst was determined to be 25% by H_2 chemisorption.

Apparatus. Figure 1 shows a schematic of the reactor. The reactor body was made of stainless steel flanges. To eliminate the catalytic activity of the reactor, the interior walls were coated with aluminum and then oxidized to produce an alumina surface. Calcium fluoride windows were mounted in each half of the body so that an infrared beam can be passed through the reactor. These windows were sealed to the stainless steel flanges by compression between two Graphoil gaskets. The seal between the two halves of the reactor was made through a copper gasket, gold plated to eliminate its catalytic activity. The catalyst, a 15 mm diameter disk, weighing 51 mg, was held in place between two aluminum rings. The assembled reactor is compact and has a dead volume of only 1.6 cm^3. The reactor was heated by two 200W disk heaters (Thermal Circuits, Inc.), placed over the circular faces, and the catalyst temperature was measured with a 1/16" stainless-steel sheathed thermocouple, fed through a port (not shown) in the reactor body.

The reactor was connected to the balance of the apparatus as shown in Fig. 2. One of two premixed gas streams could be fed to the reactor. By switching the indicated valve, a step change in either reactant or isotope concentration could be achieved. The effluent from the reactor was sampled through a differentially pumped inlet system into an EAI 250B quadrupole mass spectrometer. The signal from the mass spectrometer was then fed to a microprocessor-based data acquisition system. This unit was designed to monitor as many as ten preselected mass peaks, as well as the catalyst temperature and the gas flow rate. The time required for the collection of one data set depended on the number of mass peaks tracked and the dwell time on each peak. The shortest cycle time used in the present work was 0.5 s, during which the intensities of four mass peaks were read, together with the catalyst temperature and the gas flow rate.

In Catalysis Under Transient Conditions; Bell, A., et al.;
ACS Symposium Series; American Chemical Society: Washington, DC, 1982.

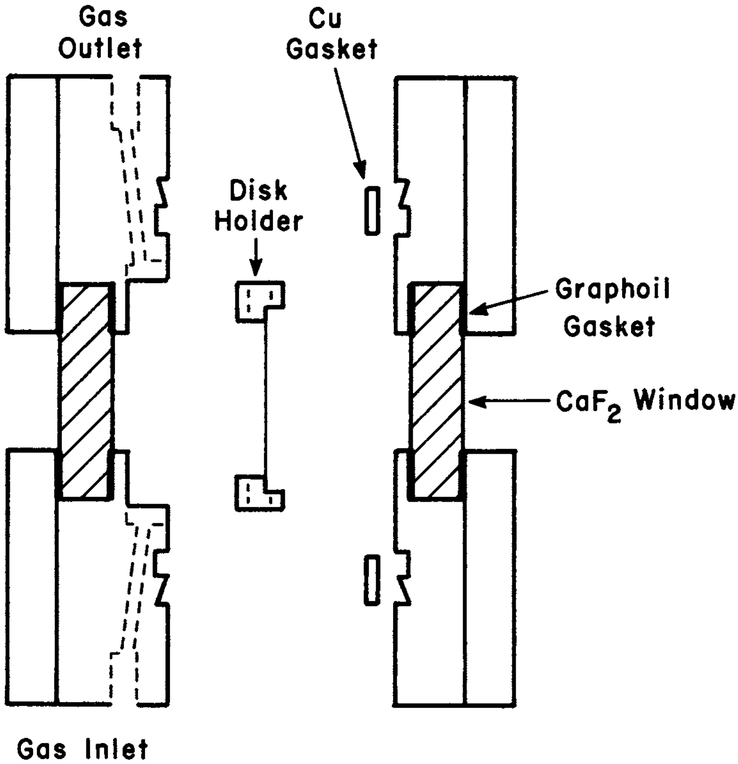

Figure 1. Schematic of the reactor — IR cell.

In Catalysis Under Transient Conditions; Bell, A., et al.;
ACS Symposium Series; American Chemical Society: Washington, DC, 1982.

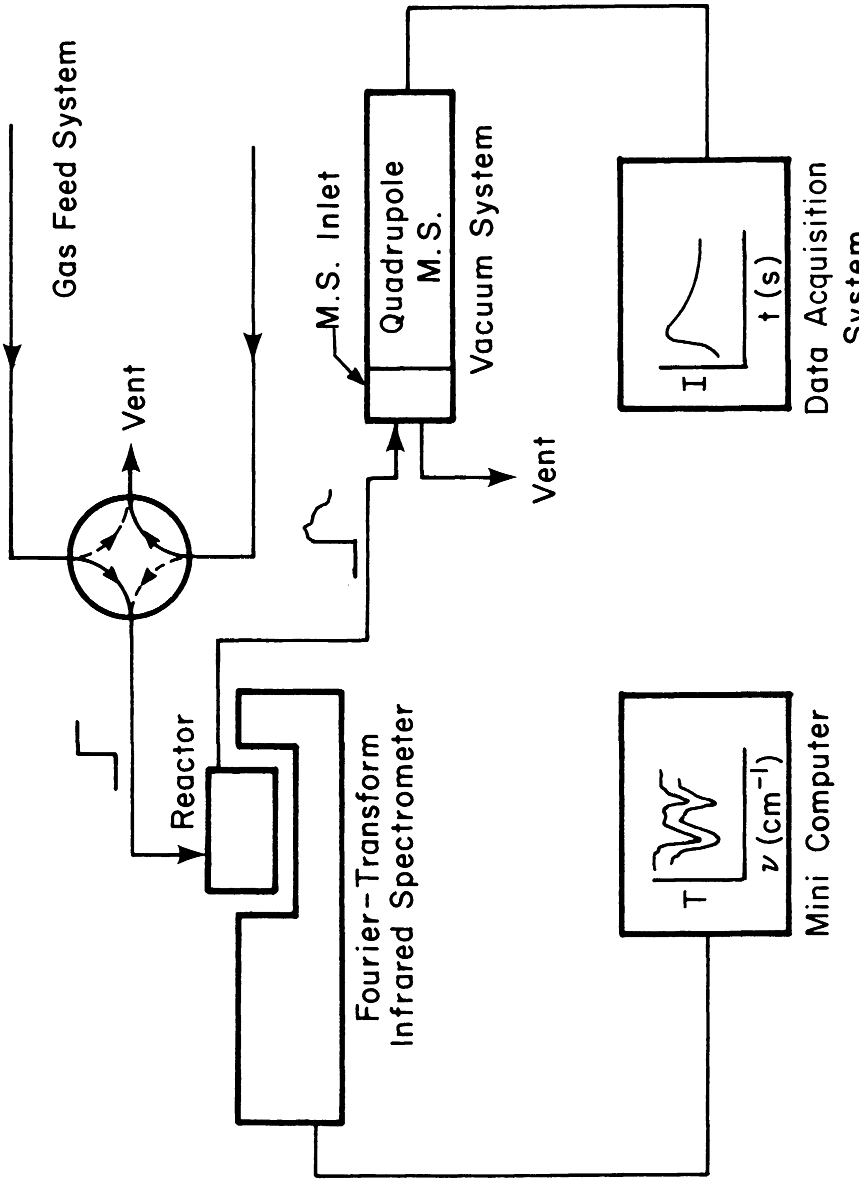

Figure 2. Schematic of the experimental apparatus.

Transmission infrared spectra of species adsorbed on the catalyst were taken with a Digilab FTS-10M Fourier-transform infrared spectrometer, using a resolution of 4 cm^{-1}. To improve the signal-to-noise ratio, between 10 and 100 interferograms were co-added. Spectra of the catalyst taken following reduction in H_2 were subtracted from spectra taken in the presence of NO to eliminate the spectrum of the support. Because of the very short optical path through the gas in the reactor and the low NO partial pressures used in these studies, the spectrum of gas-phase NO was extremely weak and did not interfere with the observation of the spectrum of adsorbed species.

Results

Reaction of Preadsorbed NO. These experiments were carried out using the following procedure. Prior to each experiment, the catalyst was reduced in H_2 for 5 min at 423 K. The catalyst was then exposed to a 0.28% NO/Ar mixture for 5 to 60 s. It was noted that NO adsorption was accompanied by a partial reduction of the adsorbing NO with adsorbed H_2 left on the catalyst surface from the period of reduction. Infrared spectra taken at the end of the NO adsorption period showed an intense band at 1660-1680 cm^{-1}, the position of the band shifting upscale with the duration of adsorption, and a much weaker band at 1830 cm^{-1}. Based on previous studies of NO adsorption on supported Rh catalysts (12-14) and analogy with the spectra of Rh nitrosyls (15-17), the band at 1660-1680 cm^{-1} can be assigned to a $NO_a^{\delta-}$ structure and the band at 1830 cm^{-1} to a NO_a structure. The reduction of adsorbed NO was initiated by substituting a 10% H_2/Ar mixture for the NO/Ar mixture. While the formation of products began immediately, no change in the catalyst temperature was observed during the course of the reaction.

Figure 3 illustrates a typical series of product responses. Nitrogen and N_2O were formed immediately upon contact of the catalyst with H_2 and the maximum in the signals for these products was observed in about 1.2 s. The hydrogen-containing products, NH_3 and H_2O, also appeared as sharp peaks, but the maximum in the signals for these products occurred at 2.5 s. Changes in the experimental conditions did not alter the qualitative features of the responses. In all cases the peaks for N_2 and N_2O occurred simultaneously and preceded the peaks for NH_3 and H_2O. It was further observed that the reaction temperature, duration of NO exposure, and the H_2 partial pressure during NO reduction affected the intensities of the product peaks and the time delay between the N_2/N_2O peaks and the NH_3/H_2O peaks. To a much lesser degree, the reaction conditions also affected the time at which the N_2 and N_2O signals reached a maximum.

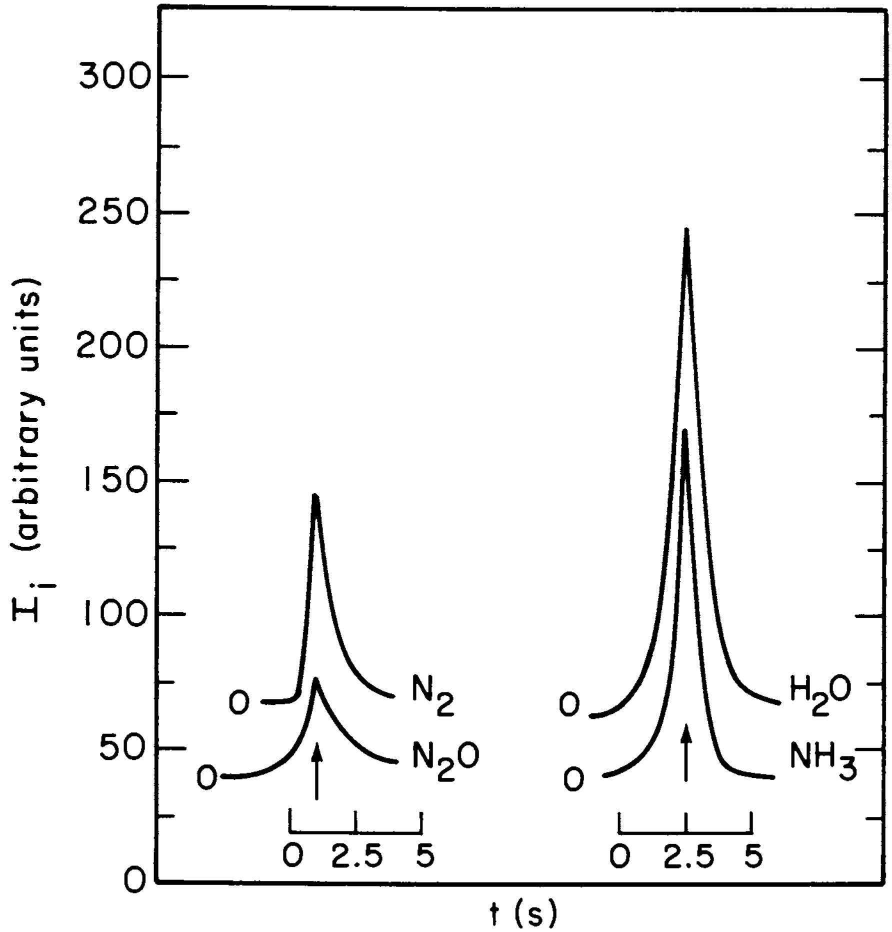

Figure 3. The transient responses for N_2, N_2O, H_2O, and NH_3, during the reduction of preadsorbed NO. Before reaction, NO was adsorbed for 15 s: $P_{H_2} = 1.0 \times 10^{-1}$ atm, $P_{NO} = 2.8 \times 10^{-3}$ atm, and $T = 423$ K.

Figure 4 shows the effects of NO exposure time on the absorbance of the band at 1660-1680 cm^{-1}, observed prior to reaction, and the maximum intensities of the NH_3, N_2, N_2O, and H_2O signals, observed during reaction. The absorbance of the infrared band provides a measure of the quantity of NO adsorbed on the Rh surface. As may be seen, the coverage by adsorbed NO increases rapidly for NO exposures up to 15 s and then levels off at a plateau. The product maxima show a similar trend, but for NO exposures greater than 20 s, the signals for H_2O, NH_3, and N_2 show a slight decline. Assuming that the maximum signal intensity for each product is proportional to the total amount of product formed, the results presented in Fig. 4 indicate that for NO exposure times greater than 20 s the amount of adsorbed NO undergoing reduction decreases slightly with increasing NO coverage. Such a trend suggests that at high NO coverages, a fraction of the adsorbed NO desorbs and, hence, is not reduced.

The time of exposure to NO had no effect on the time required for the N_2 and N_2O signals to reach a maximum during NO reduction. However, the NO exposure time did affect the time at which the NH_3 and H_2O signals attained a maximum. As shown in Fig. 5, the delay between the maximum for the N_2 peak and the maximum for the NH_3 peak was the same as the delay between the N_2 peak and the H_2O peak. In both cases, as the exposure time increases, the delay increases from 0 to 2.5 s and then levels off for NO exposures of more than 20 s.

Results similar to those shown in Figs. 4 and 5 were also obtained at other temperatures. Increasing the temperature from 398 to 473 K had two principal effects. The first was to produce narrower but more intense product peaks. The second effect was to reduce the delay between the N_2 peak and either the NH_3 or H_2O peak. Thus, for example, for NO exposure times of greater than 20 s, the delay decreased from 7.5 s at 398 K to 0.5 s at 473 K.

The effects of the H_2 partial pressure, used to reduce the adsorbed NO, on the maximum product signal intensities and the times at which the product peaks appeared was explored for a constant NO exposure time of 35 s and a temperature of 423 K. The results in Fig. 6 show that the maximum intensity of each product signal increases slightly as the partial pressure of H_2 is increased. Both the time at which N_2 and N_2O signals reach a maximum and the delay of the NH_3 and H_2O signals are affected by the H_2 partial pressure. Figure 7 show that the time for maximum production of N_2 and N_2O decreases from 3 to 1.5 s as the H_2 partial pressure increases from 0.01 to 0.1 atm and Fig. 8 shows that the time delay for the maximum production of NH_3 and H_2O decreases from 5.5 to 3.0 s.

Isotopic Tracing with ^{15}NO. To trace out the dynamics of nitrogen incorporation into the products under conditions where the surface coverage by adsorbed NO remains constant, experiments

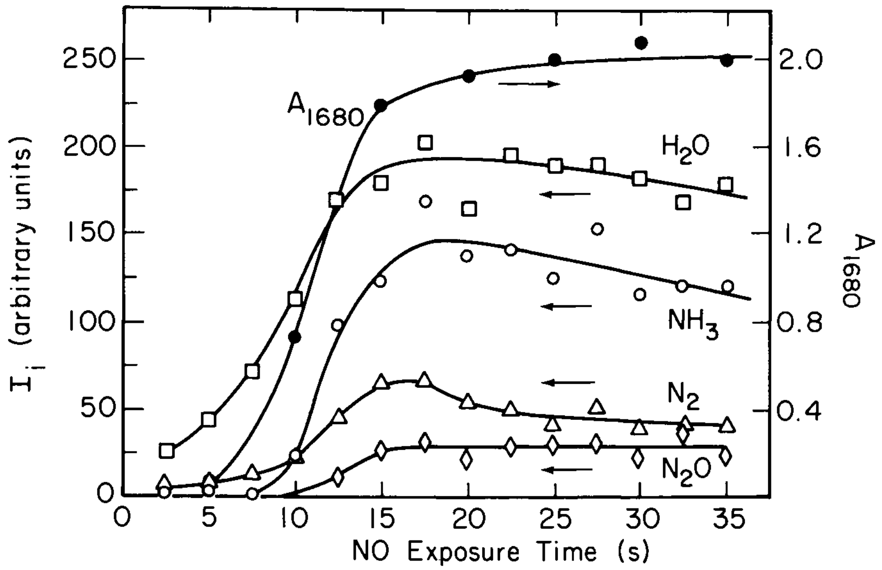

Figure 4. The maximum intensity of the reaction products and the absorbance of the IR band at 1680 cm^{-1}, as a function of NO exposure time during the reduction of preadsorbed NO_2: $P_H = 1.0 \times 10^{-1}$ atm, $P_{NO} = 2.8 \times 10^{-3}$ atm, and $T = 423$ K.

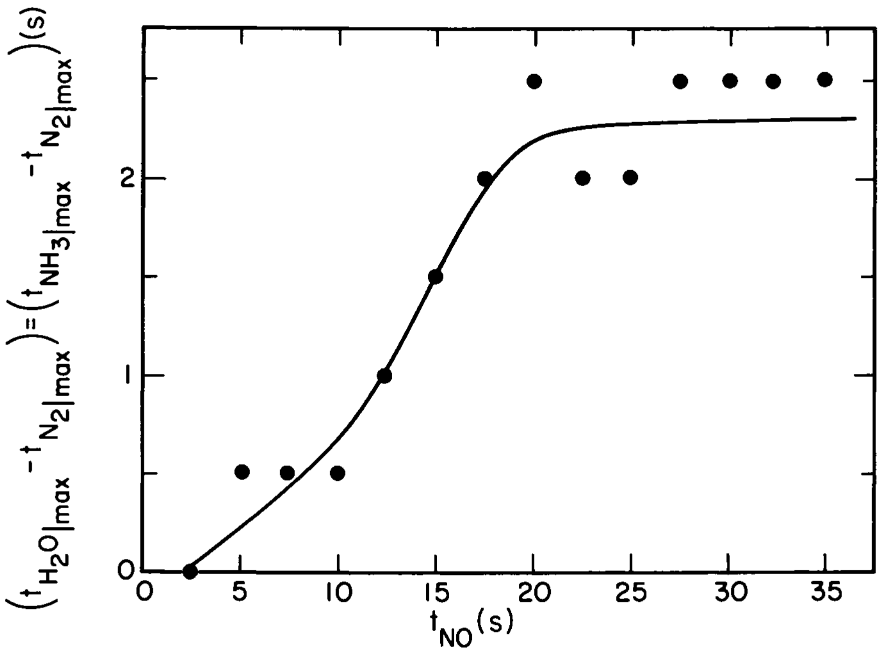

Figure 5. The effect of NO exposure time on the time delay in the maximum production of H_2O and NH_3 relative to N_2, during the reduction of preadsorbed NO: $P_{H_2} = 10 \times 10^{-1}$ atm, $P_{NO} = 2.8 \times 10^{-3}$ atm, and $T = 423$ K.

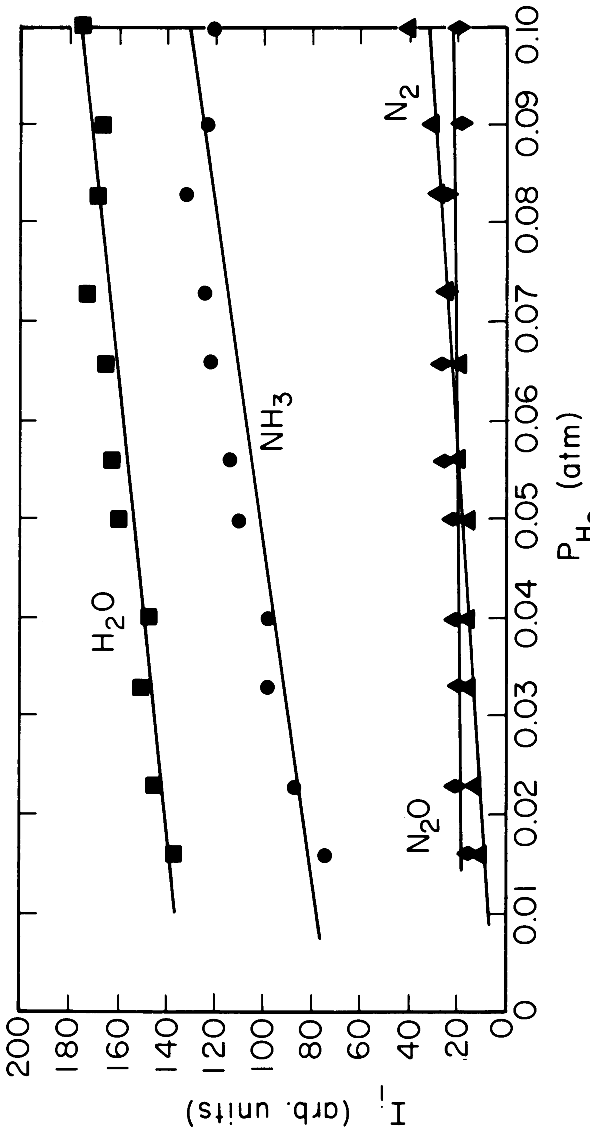

Figure 6. The effect of H_2 partial pressure on the maximum intensities of H_2O, NH_3, N_2O, and N_2, during the reduction of preadsorbed NO: $P_{NO} = 2.8 \times 10^{-3}$ atm, $T = 423$ K, and $t_{NO} = 30$ s.

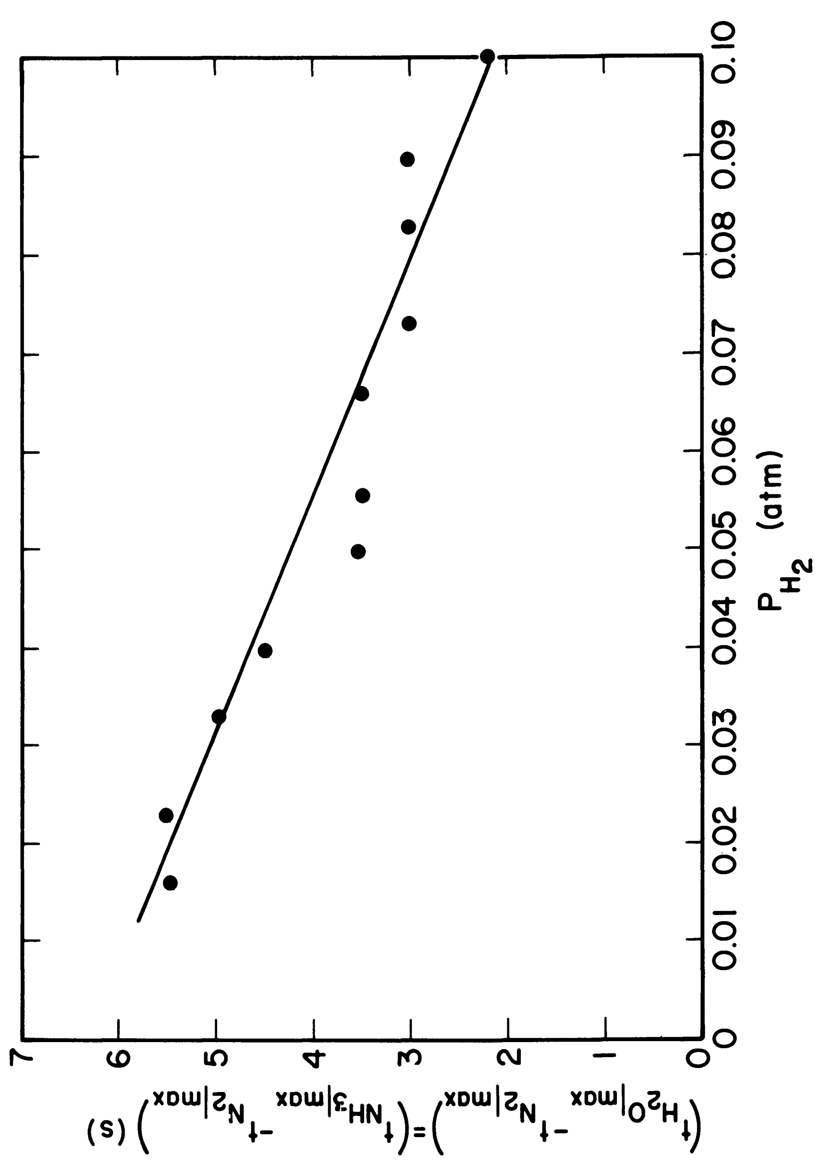

Figure 7. The effect of H_2 partial pressure on the time delay in the maximum production of H_2O and NH_3 relative to N_2, during the reduction of preadsorbed NO: $P_{NO} = 2.8 \times 10^{-3}$ atm, $T = 423$ K, and $t_{NO} = 30$ s.

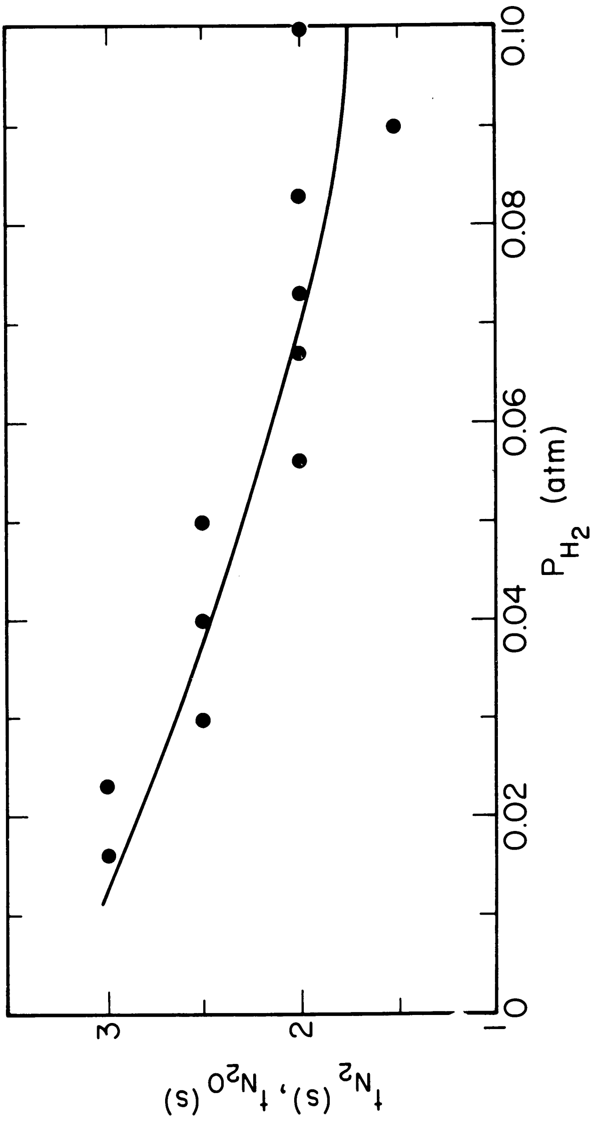

Figure 8. The effect of H_2 partial pressure on the time for the maximum production of N_2 and N_2O, during the reduction of preadsorbed NO: $P_{NO} = 2.8 \times 10^{-3}$ atm, $T = 423$ K, and $t_{NO} = 30$ s.

were performed in which ^{15}NO was substituted for ^{14}NO. Because of problems in resolving products with very nearly identical molecular weights, only the responses for the isotopes of N_2 were followed.

Two experiments were performed. In the first, the catalyst was initially exposed to a $^{15}NO/Ar$ mixture for 60 s after which this mixture was replaced by a $^{14}NO/H_2/Ar$ mixture. The responses for $^{14}N_2$ and $^{14}N^{15}N$ were recorded as functions of time, but the responses for $^{15}N_2$ could not be resolved from that for ^{14}NO, since the two species have nearly the same value of m/e. To establish the $^{15}N_2$ response, the experiment was performed a second time but now reversing the order in which ^{14}NO and ^{15}NO were introduced. The response for the $^{14}N_2$ signal in this case is identical to that for $^{15}N_2$ in the first case. Figure 9 illustrates the partial pressure responses for $^{14}N_2$, $^{14}N^{15}N$, and $^{15}N_2$ observed following introduction of the H_2-containing stream. The $^{15}N_2$ response begins immediately but then passes through a maximum as the adsorbed ^{15}NO is consumed. The $^{14}N^{15}N$ response exhibits an induction period of about 2.5 s, after which it also rises rapidly and then passes through a maximum. The $^{14}N_2$ response begins after a 2 s delay and rises monotonically to a maximum value in about 9 s.

The second experiment was performed to determine the responses of $^{14}N_2$, $^{14}N^{15}N$, and $^{15}N_2$ after a $^{14}NO/H_2/Ar$ mixture was replaced by a $^{15}NO/H_2/Ar$ mixture. This experiment was initiated by exposing the catalyst to a $^{14}NO/Ar$ mixture for 60 s and then replacing this mixture by a $^{14}NO/H_2/Ar$ mixture. After 2 min of reaction, the $^{14}NO/H_2/Ar$ mixture was replaced by a $^{15}NO/H_2/Ar$ mixture, and the responses for $^{14}N_2$ and $^{14}N^{15}N$ were followed as functions of time. For the same reason discussed earlier, the response of $^{15}N_2$ could not be resolved from that for ^{14}NO. To determine the $^{15}N_2$ response, the experiment just described was repeated, but the sequence in which ^{14}NO and ^{15}NO were introduced was reversed. The $^{14}N_2$ response obtained in this case was used to represent the $^{15}N_2$ response for the first case. Figure 10 illustrates the responses for $^{14}N_2$, $^{14}N^{15}N$, and $^{15}N_2$, following the substitution of ^{15}NO for ^{14}NO. The $^{14}N_2$ signal is unaffected during the first second after the isotopic substitution but then declines monotonically to zero. It is significant to observe that the shape of the $^{14}N_2$ response for $t > 2$ s and the shapes of the $^{14}N^{15}N$ and $^{15}N_2$ responses are virtually identical to those observed in Fig. 9.

Discussion

Two general features of the reaction mechanism can be deduced from the observations made during the reduction of adsorbed NO by H_2. First, the close coincidence of the N_2

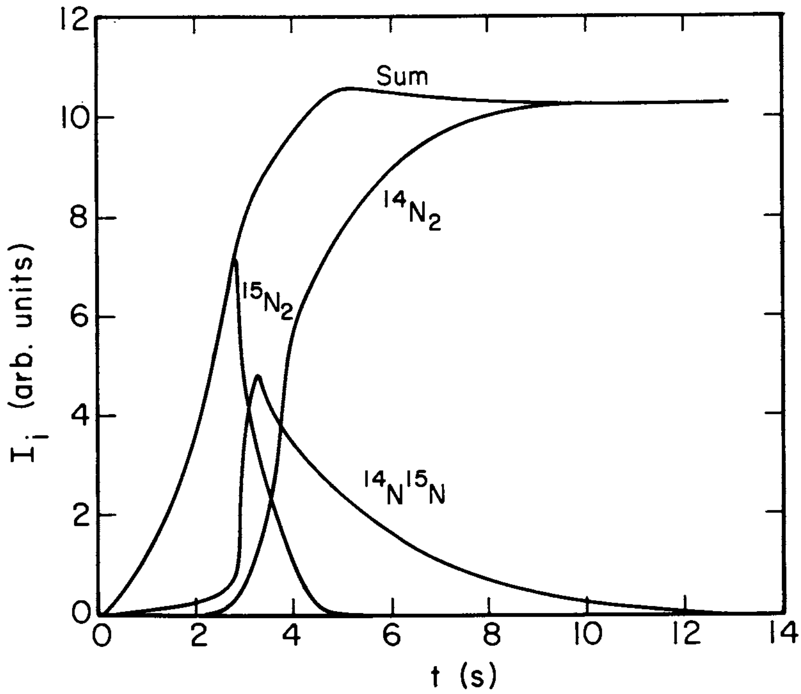

Figure 9. The gas phase responses for $^{15}N_2$, $^{14}N_2$ and $^{14}N^{15}N$ obtained after substitution of a feedstream containing $^{15}NO/Ar$ by a stream containing $^{14}NO/H_2/Ar$: $P_{NO} = 8 \times 10^{-3}$ atm, $P_{H_2} = 7 \times 10^{-2}$ atm, and $T = 438$ K.

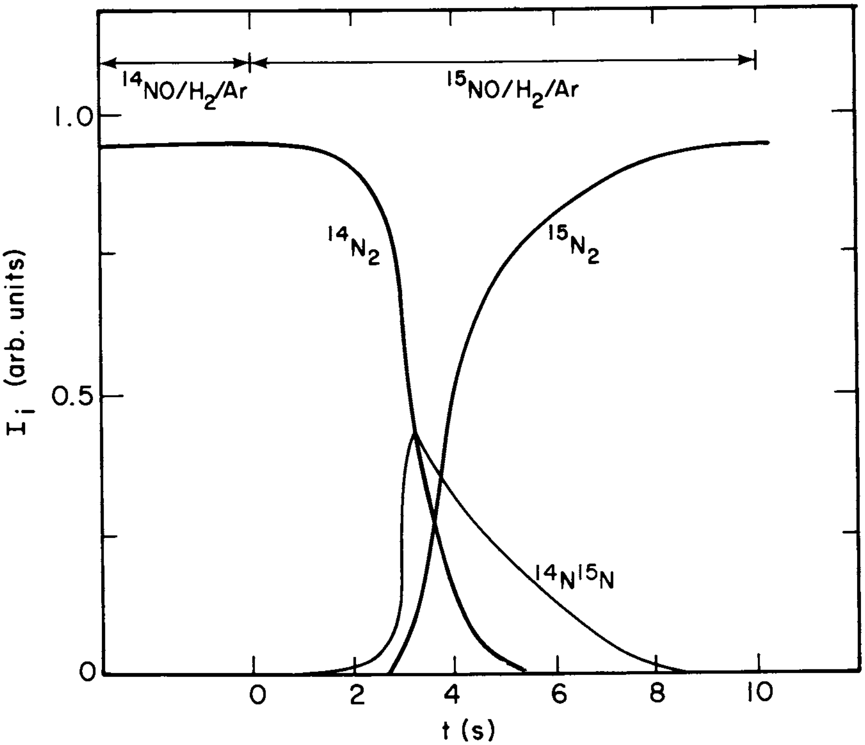

Figure 10. The gas phase responses for $^{15}N_2$, $^{14}N_2$, and $^{14}N^{15}N$ obtained after substitution of a feedstream containing $^{14}NO/H_2/Ar$ by a feedstream containing $^{15}NO/H_2/Ar$: $P_{NO} = 8 \times 10^{-3}$ atm, $P_{H_2} = 8 \times 10^{-2}$ atm, and $T = 438$ K.

and N_2O peaks suggests that these products share a common rate limiting step, such as, for example, the dissociation of adsorbed NO. Second, the delay in the appearance of the NH_3 and H_2O peaks relative to the N_2 and N_2O peaks suggests that formation of the former pair of products involves adsorbed rather than gaseous hydrogen. This deduction is further supported by the manner in which changes in NO exposure time, H_2 partial pressure, and reaction temperature affect the magnitude of the delay. Figure 11 illustrates a possible mechanism for NO reduction, which is consistent with the qualitative features of the present results and information available in the literature. A discussion of the justification for including specific elementary steps will be presented next.

The associative adsorption of NO is supported by several infrared studies (12-14). Spectra of NO adsorbed on reduced Rh show an intense band at 1660-1740 cm^{-1} and a weaker band at 1830 cm^{-1}. These features are associated with NO adsorbed as $NO_a^{\delta-}$ and NO_a, respectively. If the surface is partially oxidized, a third band is observed at 1910 cm^{-1}, associated with $NO_a^{\delta+}$. During steady-state reduction of NO by H_2, only the $NO_a^{\delta-}$ form of adsorbed NO is observed (10). The reversibility of NO adsorbtion into this state has been examined by Savatsky and Bell (14). Their work shows that at temperatures above 293 K, equilibrium desorption occurs when a stream of argon is passed over a Rh/SiO_2 catalyst bearing preadsorbed NO.

Evidence for dissociative chemisorption comes from several sources (8,19-21). TPD studies conducted with Rh single crystals (19-21) suggest that a portion of the NO adsorbed at ambient temperatures occurs dissociatively. Further dissociation is presumed to occur at elevated temperatures since N_2 and N_2O are observed during TPD at temperatures slightly above the threshold for NO desorption. A similar behavior has also been observed in TPD studies conducted with Rh/SiO_2 (8). While the exact mechanism of dissociation is not established by these investigations, it seems plausible to propose that dissociation proceeds as indicated by reaction 2 in Fig. 11.

Studies by a number of authors (8,22-27) have shown that H_2 adsorbs dissociatively on Rh and that this process is reversible at the temperatures used in the present studies. As noted earlier, the atomic hydrogen formed by this means is believed to be responsible for the formation of NH_3 and H_2O. Consequently, these products are assumed to be formed by a sequence of Langmuir-Hinshelwood steps. While there is no independent evidence to support this hypothesis for the synthesis of NH_3, recent results reported by Thiel et al. (27) indicate that the formation of H_2O from H_2 and adsorbed O-atoms does proceed via a two step sequence such as that represented by reactions 6 and 7 in Fig. 11.

(1)	$NO + S$	$\rightleftharpoons$	NO_a
(2)	$NO_a + S$	$\longrightarrow$	$N_a + O_a$
(3)	$H_2 + 2S$	$\rightleftharpoons$	$2H_a$
(4)	$NO_a + N_a$	$\longrightarrow$	$N_2O + 2S$
(5)	$2N_a$	$\longrightarrow$	$N_2 + 2S$
(6)	$O_a + H_a$	$\longrightarrow$	$OH_a + S$
(7)	$OH_a + H_a$	$\longrightarrow$	$H_2O + 2S$
(8)	$N_a + H_a$	$\longrightarrow$	$NH_a + S$
(9)	$NH_a + H_a$	$\longrightarrow$	$NH_{2a} + S$
(10)	$NH_{2a} + H_a$	$\longrightarrow$	$NH_3 + 2S$

Figure 11. The reaction mechanism proposed for the interpretation of transient response experiments.

In Catalysis Under Transient Conditions; Bell, A., et al.;
ACS Symposium Series; American Chemical Society: Washington, DC, 1982.

The specification of reactions 4 and 5 for the formation of N_2O and N_2 is based on the TPD studies reported by Castner et al. (19), Campbell and White (20), Baird et al. (21) and Myers and Bell (8). The work of Myers and Bell has shown specifically that the formation of N_2O does not occur via a Rideal-Eley process. It appears more likely that this product is formed via a Langmuir-Hinshelwood process. To determine whether the mechanism in Fig. 11 could explain the experimental observation reported here, a model of the reduction process was developed and examined. The kinetics of NO adsorption and reduction of the adsorbed NO by H_2 can be described by eqns. 1 and 2.

$$\frac{d\overline{P}_i}{dt} = \frac{Q}{\varepsilon V_r}(P_i^o - P_i) + \rho_c RTM_m \frac{(1-\varepsilon)}{\varepsilon} \sum_j \nu_{ij} r_j \qquad (1)$$

$$\frac{d\overline{\theta}_i}{dt} = \sum_j \nu_{ij} r_j \qquad (2)$$

Definitions for the variables and constants appearing in eqns. 1 and 2 are given in the nomenclature section at the end of this paper. The first of these equations represents a mass balance around the reactor, assuming that it operates in a differential manner. The second equation is a species balance written for the catalyst surface. The rate of elementary reaction j is represented by r_j, and ν_{ij} is the stoichiometric coefficient for component i in reaction j. The relationship of r_j to the reactant partial pressures and surface species coverages are given by expressions of the form

$$r_j = k_j \overline{P}_\ell \overline{\theta}_m \qquad (3)$$

and

$$r_j = k_j \overline{\theta}_m \overline{\theta}_n \qquad (4)$$

for Rideal-Eley and Langmuir-Hinshelwood steps, respectively.

Equations 1 and 2 can be solved numerically using an algorithm which handles stiff differential equations (28). Two sets of boundary conditions are required. For $0<t<t_{NO}$, corresponding to the period during which the reduced catalyst is exposed to NO, the inlet gas composition is given by

$$P^o_{H_2} = P^o_{N_2} = P^o_{NO_2} = P^o_{NH_3} = P^o_{H_2O} = 0 \qquad (5)$$
$$P^o_{NO} = P^a_{NO}$$

and the initial conditions are specified as

$$\bar{P}_{H_2} = 1/2P^r_{H_2}$$
$$\bar{P}_{NO} = 1/2P^a_{NO}$$
$$\bar{P}_{N_2} = \bar{P}_{N_2O} = \bar{P}_{NH_3} = \bar{P}_{H_2O} = 0 \qquad (6)$$
$$\bar{\theta}_H = \sqrt{K_3P^r_{H_2}}/(1 + \sqrt{K_3P^r_{H_2}})$$

In eqn. 6, $P^r_{H_2}$ represents the H_2 partial pressure used for the initial reduction of the catalyst and the subsequent reduction of adsorbed NO, and P^a_{NO} represents the NO partial pressure in the feed during NO adsorption. For $t > t_{NO}$, corresponding to the period of NO reduction, the values of $P^o_{H_2}$ and P^o_{NO} are changed so that

$$P^o_{H_2} = 1/2\ P^r_{H_2} \qquad (7)$$
$$P^o_{NO} = 0$$

Table I lists the values of the rate coefficients used to simulate the transient response experiments shown in Figs. 3 through 8. These values were obtained in the following manner (29). Starting from a set of initial guesses, the values of k were varied systematically to obtain a fit between the predicted product responses and those obtained from experiments in which H_2 was added suddenly to a flow of NO. These experiments while not described here were identical to that presented in Fig. 9, with the exception that only ^{14}NO was used. Because of the large number of parameters in the model, only a rough agreement could be achieved between experiment and theory even after 500 iterations of the optimization routine (30). The parameter values obtained at this point were now used to calculate the responses expected during the reduction of adsorbed NO. These computations produced responses similar to those observed experimentally (i.e., Fig. 3) but the appearance of the product peaks in time did not coincide with those observed. To correct for this, the values of k_6, k_7, and k_8 were adjusted in an empirical manner. The criteria used at this point were that the predicted dependences of the delays between the appearance of the NH_3 and H_2O peaks and the N_2 and N_2O peaks on the duration of NO adsorption and the H_2 partial pressure during reduction agree as closely as possible with the dependences found experimentally and shown in Figs. 5 and 8.

The rate parameters presented in Table I were used together with the parameter values listed in Table II to predict the product responses during the adsorption of NO on a hydrogen covered Rh surface and the subsequent reduction of the adsorbed

Table I. Rate Coefficients Used to Simulate the Transient Response Experiments

Step #	k_j
1.	2.8×10^{-4} s^{-1} atm^{-1}
-1.	1.6 s^{-1}
2.	9.3×10^{-1} s^{-1}
3.	2.8×10^{2} s^{-1} atm^{-1}
-3.	1.9×10^{-1} s^{-1}
4.	3.7×10^{-1} s^{-1}
5.	9.9×10^{-1} s^{-1}
6.	6.8 s^{-1}
7.	1.1×10^{1} s^{-1}
8.	6.0 s^{-1}
9.	1.4×10^{3} s^{-1}
10.	1.8×10^{2} s^{-1}

Table II Parameters and Variables Used to Simulate the Transient Response Experiments

Q	=	$9.55\ cm^3$ (STP)/s
ε	=	0.96
V_r	=	$1.6\ cm^3$
ρ_c	=	$0.8\ gm/cm^3$
M_m	=	10^{-5} mol Rh sites/gm catalyst

In Catalysis Under Transient Conditions; Bell, A., et al.;
ACS Symposium Series; American Chemical Society: Washington, DC, 1982.

NO. The same parameters were then used to predict the responses for the isotopic tracer experiments reported in Figs. 9 and 10. The results of these calculations are presented below.

Figure 12 is representative of the responses predicted for the product partial pressures both during the period of NO adsorption and the subsequent reduction of adsorbed NO. Prior to the addition of NO, the surface is considered to be at equilibrium with the partial pressure of H_2 used to reduce the catalyst. At time zero the H_2 flow is terminated and NO is added to the Ar carrier. Reaction products appear immediately due to the reduction of NO by adsorbed H-atoms. After 30 s of NO exposure, the flow of NO is terminated and the flow of H_2 is restored. The introduction of H_2 causes a sudden increase in the product partial pressures, which then pass through a maximum as the adsorbed NO is consumed. It is noted that in agreement with experimental observation (i.e., see Figs. 3 and 4) the calculations predict that NH_3 is the dominant nitrogen-containing product and that N_2 and N_2O are formed in successively lower concentrations. The curves in Fig. 12 show further that the production of N_2O and N_2 attain maxima within about 1 to 1.5 s after the introduction of H_2 but that the production of NH_3 and H_2O occurs about 2 s later. Both of these features are in good agreement with the behavior of the experimental data.

The responses for $\bar{\theta}_H$, $\bar{\theta}_{NO}$, and $\bar{\theta}_v$ are shown in Fig. 12. The value of $\bar{\theta}_H$, which is initially 0.925, decreased during the period of NO exposure at the same time that the value of $\bar{\theta}_{NO}$ increases rapidly from zero. It should be noted that the predicted rate of accumulation of adsorbed NO is qualitatively consistent with the dynamics of the band appearing at 1680 cm^{-1}, associated with $No_a^{\delta-}$ shown in Fig. 4. It is seen, though, that while the experimental results exhibit a short induction period followed by a rapid rise in the absorbance of the 1680 cm^{-1} band to a saturation level, the predicted curve shows a smooth monotonic increase in $\bar{\theta}_{NO}$.

The vacancy coverage, $\bar{\theta}_v$, which is initially equal to 0.075, rapidly decreases during the initial period of NO exposure but then very slowly increases. This behavior can be attributed to the following factors. The first is that $\bar{\theta}_v$ in equilibrium with 0.10 atm of H_2 is larger than $\bar{\theta}_v$ in equilibrium with 0.0028 atm of NO. Calculating the equilibrium constants for H_2 and NO adsorption and desorption of these gases, given in Table I, one concludes that $\bar{\theta}_v^{H_2} = 0.075$ and $\bar{\theta}_v^{NO} = 0.2$. It is this difference in the strength of adsorption which drives the decrease in $\bar{\theta}_v$. Figure 13 shows, though, that during the adsorption of NO, $\bar{\theta}_v$ falls below 0.02 and then gradually climbs back up. This increase is due to formation of a variety of surface intermediates formed during the initial moments of NO adsorption, which are not released instantaneously as reaction products. The surface

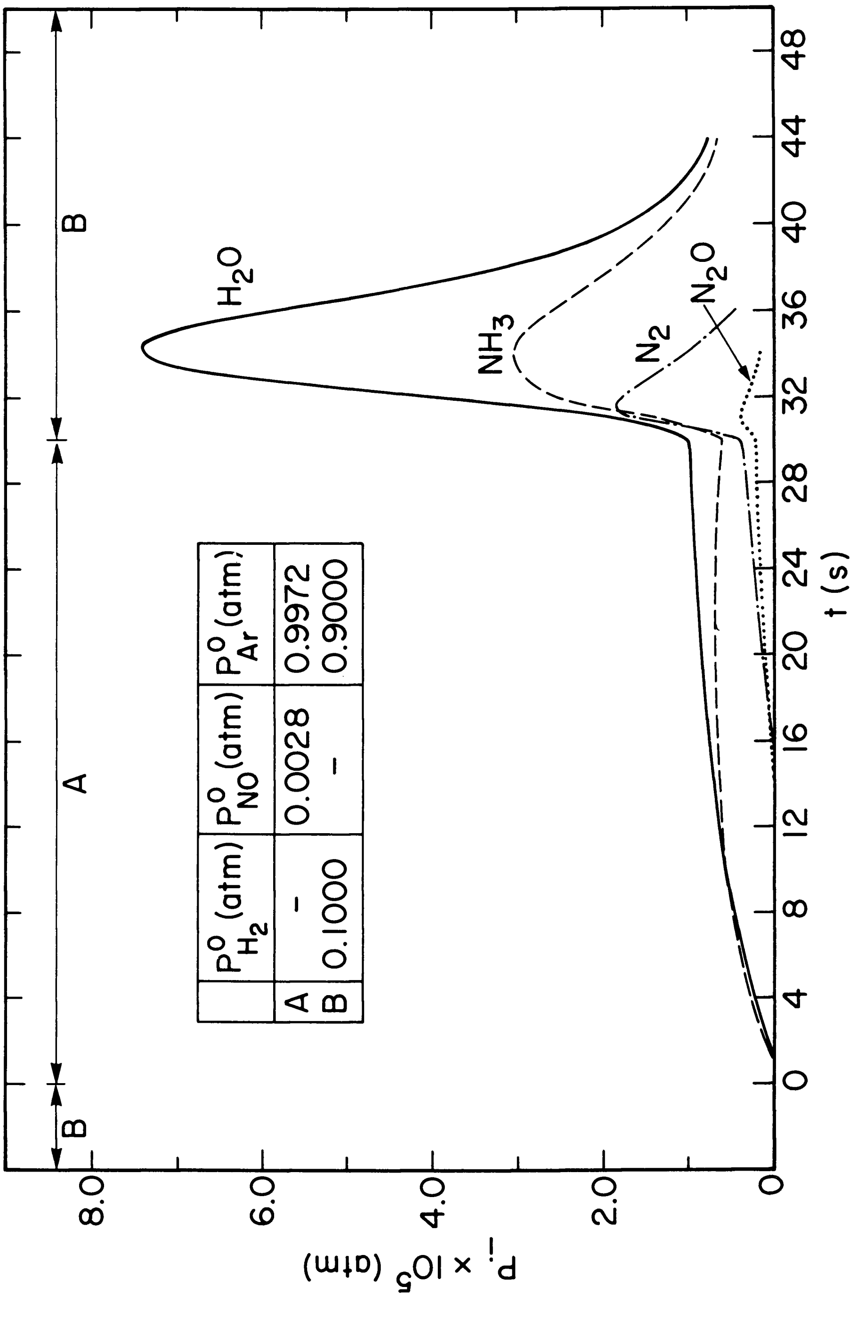

Figure 12. Predictions of the responses for P_{H_2O}, P_{NH_3}, P_{N_2}, and P_{N_2O} during the reduction of preadsorbed NO: $P_{H_2} = 1.0 \times 10^{-1}$ atm, $P_{NO} = 2.8 \times 10^{-3}$ atm, $T = 423$ K, and $t_{NO} = 30$ s.

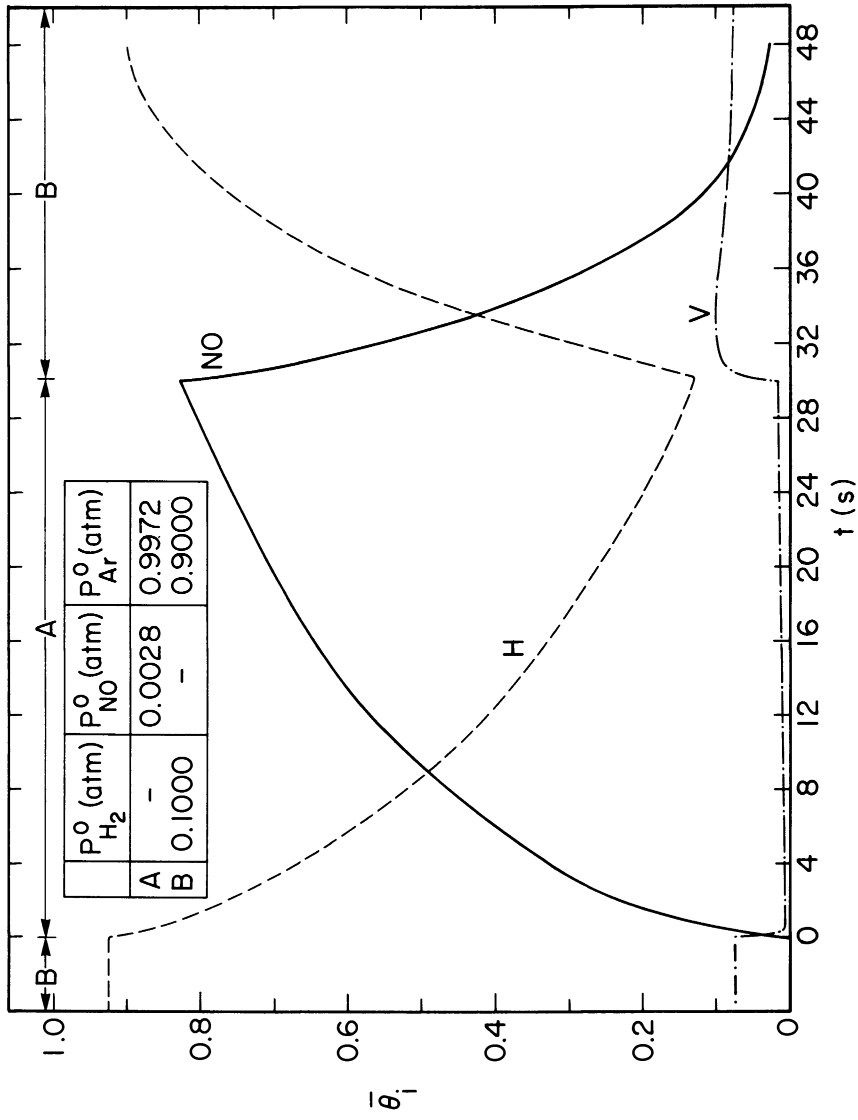

Figure 13. Predictions of the responses for θ_H, θ_V and θ_{NO} during the reduction of preadsorbed NO: $P_{H_2} = 1.0 \times 10^{-1}$ atm, $P_{NO} = 2.7 \times 10^{-3}$, $T = 423$ K, and $t_{NO} = 30$ s.

coverage by these species reduces the vacancy fraction. As time progresses the intermediates are consumed, and the surface gradually exposes a greater number of vacant sites.

Upon introduction of H_2, following NO adsorption, the magnitude of $\bar{\theta}_H$ immediately increases while that of $\bar{\theta}_{NO}$ decreases. The first of these changes reflects the difference between the rates of H_2 adsorption and consumption in the reduction of NO. The decrease in $\bar{\theta}_{NO}$ occurs for two reasons: a) inhibition of the readsorption of desorbing NO as a consequence of H_2 adsorption; and b) the consumption of adsorbed NO by reduction. It should be noted that the dissociation of NO, and hence the rate of NO reduction is accelerated by the creation of vacant sites. The increase in θ_v, seen in Fig. 13, can be ascribed to a consumption of chemisorbed NO and the fact that $\bar{\theta}_v^{H_2}$ is greater than $\bar{\theta}_v^{NO}$, as was discussed earlier.

Figure 14 shows the computed responses for $\bar{\theta}_N$, $\bar{\theta}_O$, and $\bar{\theta}_{OH}$. These coverages increase slowly during NO adsorption but rise rapidly and pass through a maximum when H_2 is added to the flow. The responses for $\bar{\theta}_{NH}$ and $\bar{\theta}_{NH_2}$ are similar in shape to the response for θ_{OH} but are significantly smaller in magnitue and, hence, have not been shown in Fig. 14. It is significant to note that the maxima in $\bar{\theta}_O$ and $\bar{\theta}_N$ occur at times which coincide with the time at which the rates of N_2 and N_2O reach a maximum. Similarly, the maxima in $\bar{\theta}_{OH}$ and θ_{NH_2} appear at times nearly identical to the times at which the rates of H_2O and NH_3 formation reach a maximum.

Calculations similar to those just discussed were also carried out for NO exposure times between 5 and 30 s. Figure 15 illustrates the effects of NO exposure time on the predicted maximum intensity of each product peak. The curves appearing in this figure may be compared with the experimental results shown in Fig. 4. It is noted that while the distribution of products predicted for each NO exposure time is qualitatively consistent with that observed experimentally, the shape of the product peak intensity curves is not. The experimental data show a rapid initial increase which is followed by the attainment of a broad maximum. By contrast, the predicted curves show a slow monotonic increase.

The effect of NO exposure time on the time at which the N_2 and N_2O signals attain a maximum is shown in Fig. 16. It is seen that the model of NO reduction predicts that N_2 formation peaks about 0.5 s after the peak in the N_2O formation and that the peak times for both products decline by about 0.5 s as the NO exposure time is increased from 5 to 30 s. These trends are in good agreement with the data. It should be noted that since a product analysis could be taken only once every 0.5 s, it was not possible to determine product peak positions with an accuracy of better than 0.5 s. Consequently, both the predicted difference between

In Catalysis Under Transient Conditions; Bell, A., et al.;
ACS Symposium Series; American Chemical Society: Washington, DC, 1982.

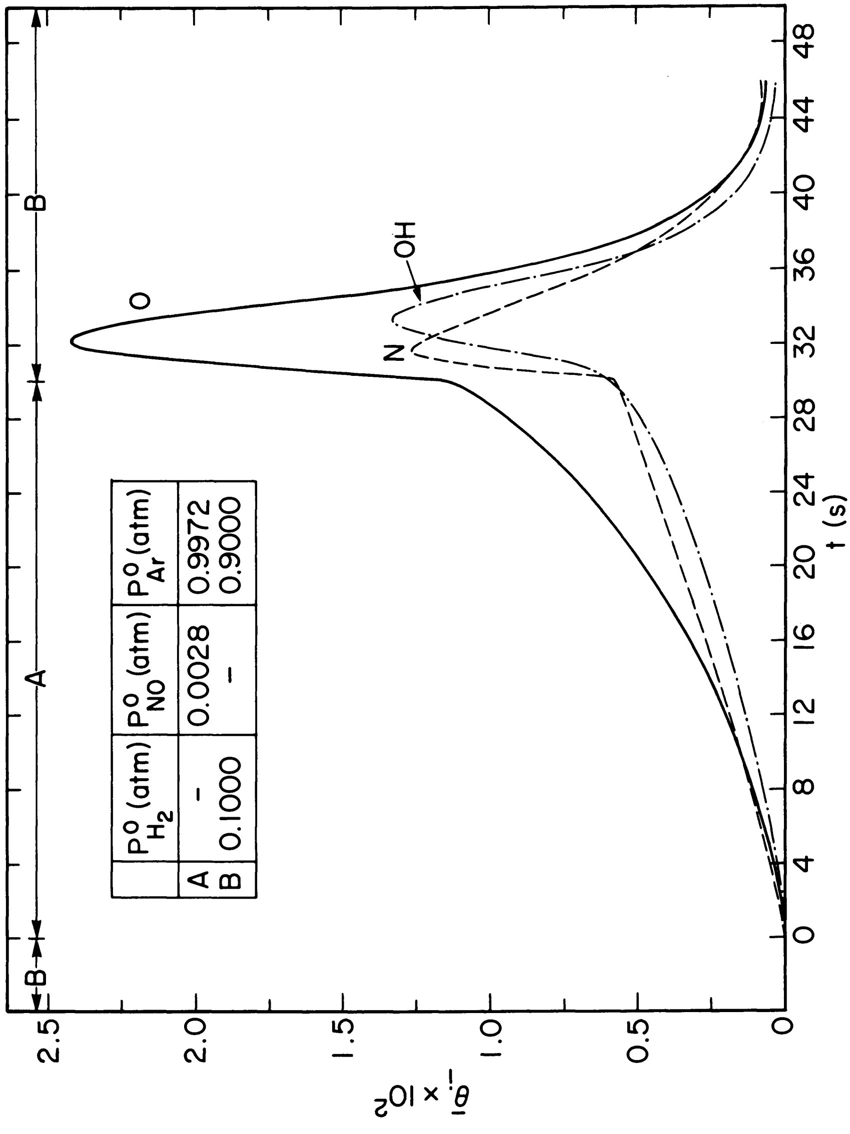

Figure 14. Predictions of the responses for θ_O, θ_N, and θ_{OH} during the reduction of preadsorbed NO: $P_{H_2} = 1.0 \times 10^{-1}$ atm, $P_{NO} = 2.8 \times 10^{-3}$ atm, $T = 423$ K, and $t_{NO} = 30$ s.

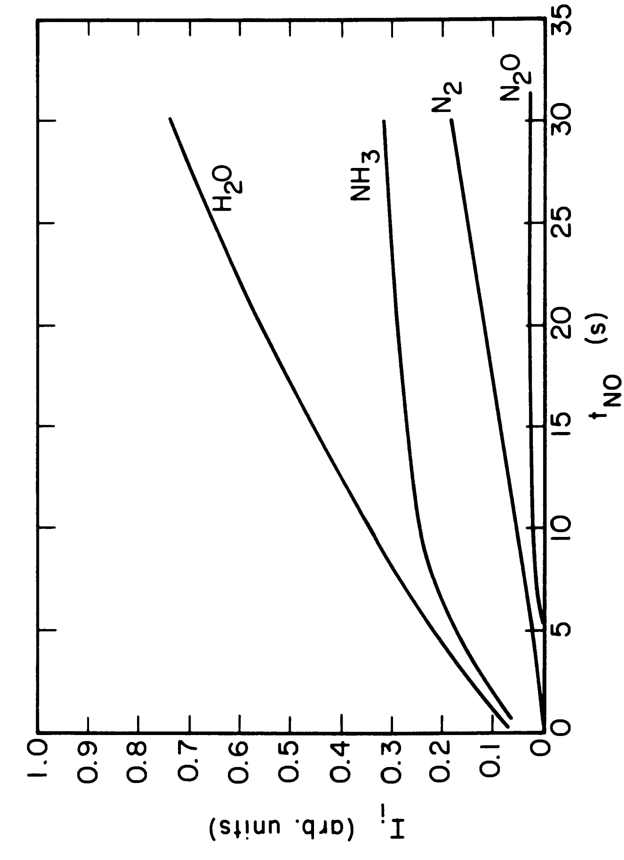

Figure 15. The predicted effects of NO exposure time on the maximum intensities of H_2O, NH_3, N_2, and N_2O, during the reduction of preadsorbed NO: $P_{H_2} = 1.0 \times 10^{-1}$ atm, $P_{NO} = 2.8 \times 10^{-3}$ atm, and $T = 423$ K.

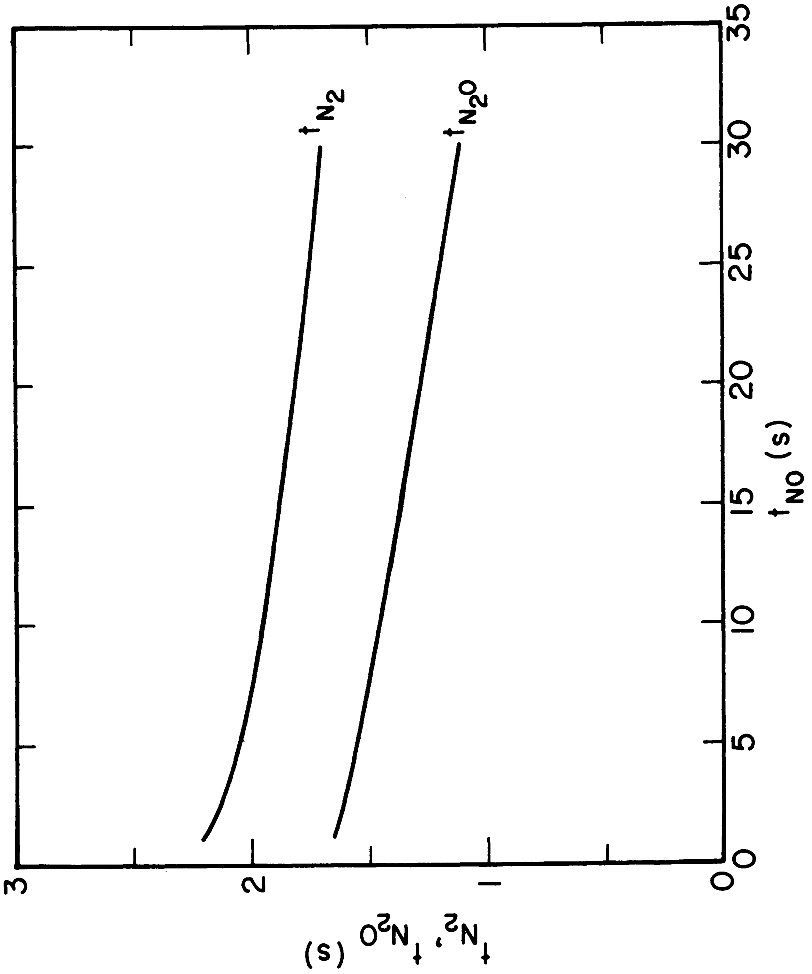

Figure 16. The predicted effects of NO exposure time on the time at which the production of N_2 and N_2O reach a maximum, during the reduction of preadsorbed NO: $P_{H_2} = 1.0 \times 10^{-1}$ atm, $P_{NO} = 2.8 \times 10^{-3}$ atm, and $T = 423$ K.

t_{N_2} and t_{N_2O} and the change in these times with the duration of NO adsorption lie within the limits of uncertainty for the experimental data.

The predicted effects of NO adsorption time on the time delay between the maxima in NH_3 and N_2 production and the maxima in H_2O and N_2 production are shown in Fig. 17. It is seen that the predictions bound the experimental observations and show the the proper trend with increasing NO exposure.

Calculations were also performed to assess the ability of the model to properly predict the effects of H_2 partial pressure on the product peak intensities and the time at which each peak occurs. Figure 18 shows the predicted effect of H_2 partial pressure on the product peak intensities. In contrast to the trend observed experimentally and illustrated in Fig. 6, the model predicts that intensities decline with increasing parital pressure. Nevertheless, the model does show that the changes are small, and it provides a qualitatively correct picture of the product distribution.

Figure 19 shows the predicted and experimentally observed time at which the formation of N_2 reaches a maximum. As may be seen, the model provides a reasonably good description of the experimentally observed trend. The effect of H_2 partial pressure on the time delay between the maximum in the production of H_2O or NH_3, and the maximum production of N_2 is illustrated in Fig. 20. Here too, the calculated curves are in reasonable agreement with the experimental data and it is noted that the model predicts the same time delay for both NH_3 and H_2O under most circumstances.

To further test the model, calculations were performed to simulate the isotopic tracer experiments presented in Figs. 9 and 10. It should be noted that while the tracer experiments were performed at 438K, the rate coefficients used in the model were chosen to fit the experiments in which chemisorbed NO was reduced at 423 K. Figures 21 and 22 illustrate the nitrogen partial pressure and surface coverage responses predicted for an experiment in which ^{15}NO is substituted for ^{14}NO at the same time that H_2 is added to the NO flow. Similar plots are shown in Figs. 23 and 24 for an experiment in which ^{14}NO is substituted for ^{15}NO during steady-state reduction.

Comparison of Figs. 21 and 23 with Figs. 9 and 10 shows that the predicted partial pressure responses for the N_2 isotopes are in fair agreement with those observed experimentally. The principal differences are that the experimental $^{14}N^{15}N$ response is significantly more asymmetric than the corresponding theoretical response and that all of the experimental transients occur over a shorter time frame than would be deduced from the theoretical results. The strong asymmetry of the experimentally observed $^{14}N^{15}N$ response may be due to the fact that ^{14}N and ^{15}N containing adspecies are not randomly mixed but, rather, exist

In Catalysis Under Transient Conditions; Bell, A., et al.;
ACS Symposium Series; American Chemical Society: Washington, DC, 1982.

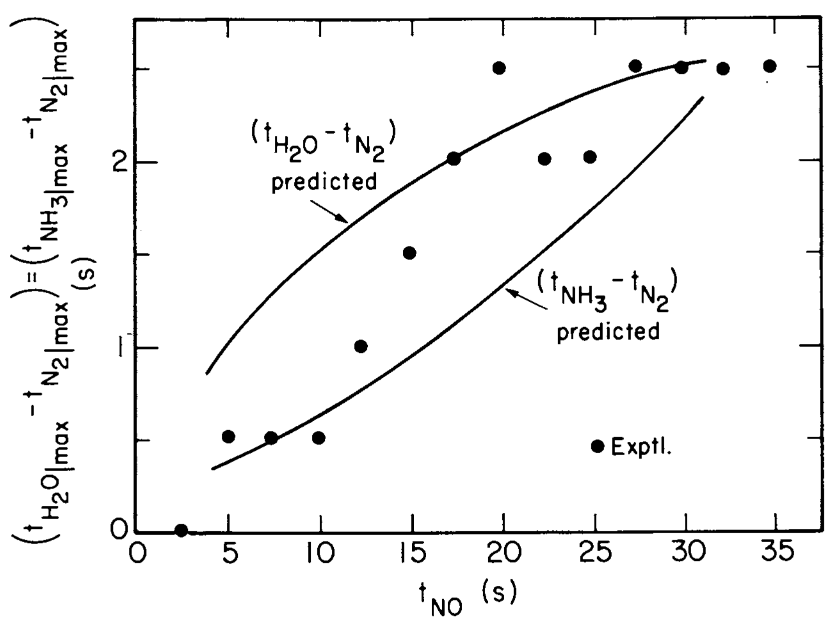

Figure 17. Comparison of the predicted and the observed effects of NO exposure time on time delay in the maximum production of H_2O and NH_3 relative to N_2, during the reduction of preadsorbed NO: $P_{H_2} = 1.0 \times 10^{-1}$ atm, $P_{NO} = 2.8 \times 10^{-3}$ atm, and $T = 423$ K.

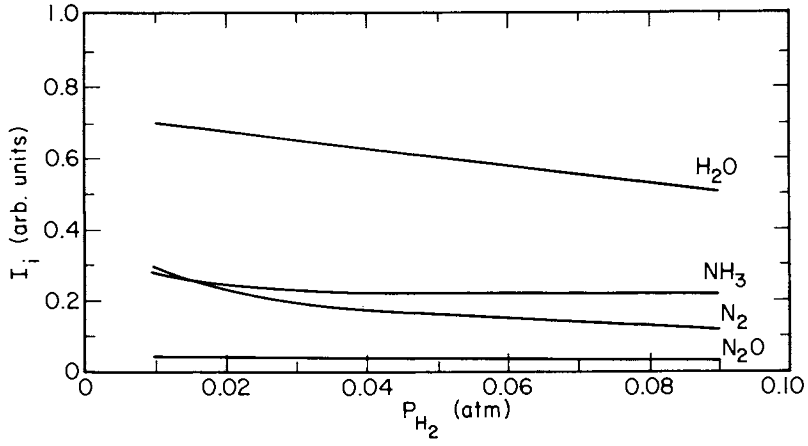

Figure 18. The predicted effects of P_{H_2} on the intensities of H_2O, NH_3, N_2, and N_2O at maximum production, during the reduction of preadsorbed NO: $P_{NO} = 2.8 \times 10^{-3}$ atm; $T = 423$ K; and $t_{NO} = 30$ s.

In Catalysis Under Transient Conditions; Bell, A., et al.;
ACS Symposium Series; American Chemical Society: Washington, DC, 1982.

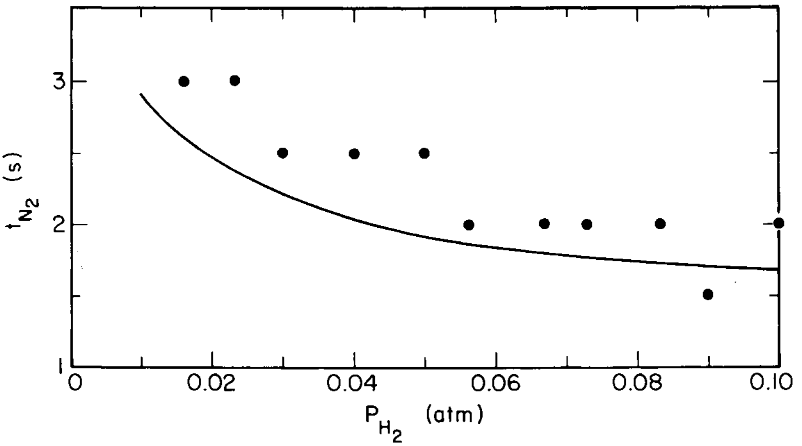

Figure 19. Comparison of the predicted and the observed effects of P_{H_2} on the time of maximum N_2 production, during the reduction of preadsorbed NO: $P_{NO} = 2.8 \times 10^{-3}$ atm, $T = 423$ K, and $t_{NO} = 30$ s.

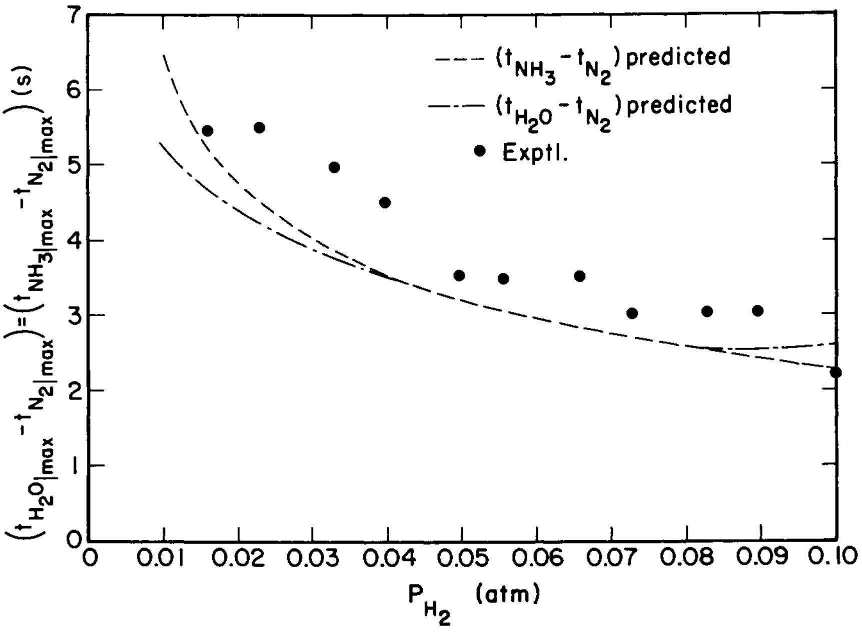

Figure 20. Comparison of the predicted and the observed effects of P_H on the time delay in the maximum production of H_2O and NH_3 relative to N_2, during the reduction of preadsorbed NO: $P_{NO} = 2.8 \times 10^{-3}$ atm, $T = 423$ K, and $t_{NO} = 30$ s.

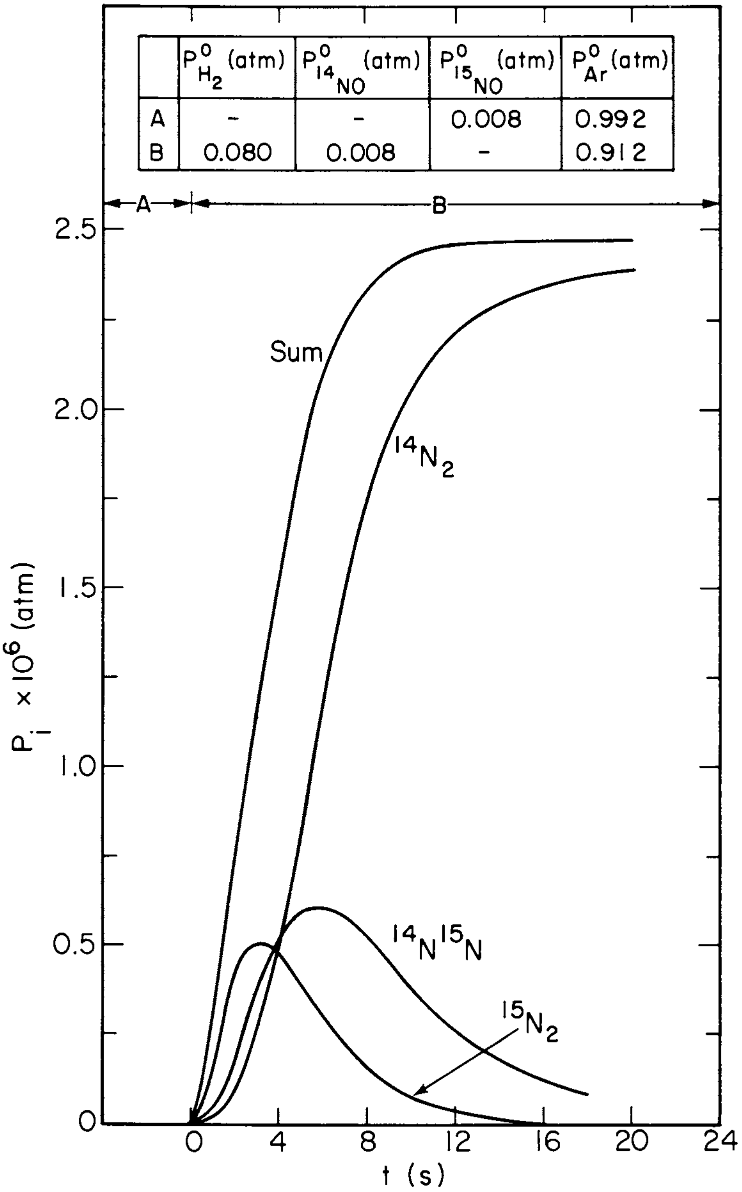

Figure 21. Predictions of the partial pressure responses for $^{14}N_2$, $^{15}N_2$, and $^{14}N^{15}N$ following substitution of a feedstream containing $^{15}NO/Ar$ by a stream containing $^{14}NO/H_2/Ar$: $P_H = 8.0 \times 10^{-2}$ atm, $P_{NO} = 8.0 \times 10^{-3}$ atm, and T = 423 K.

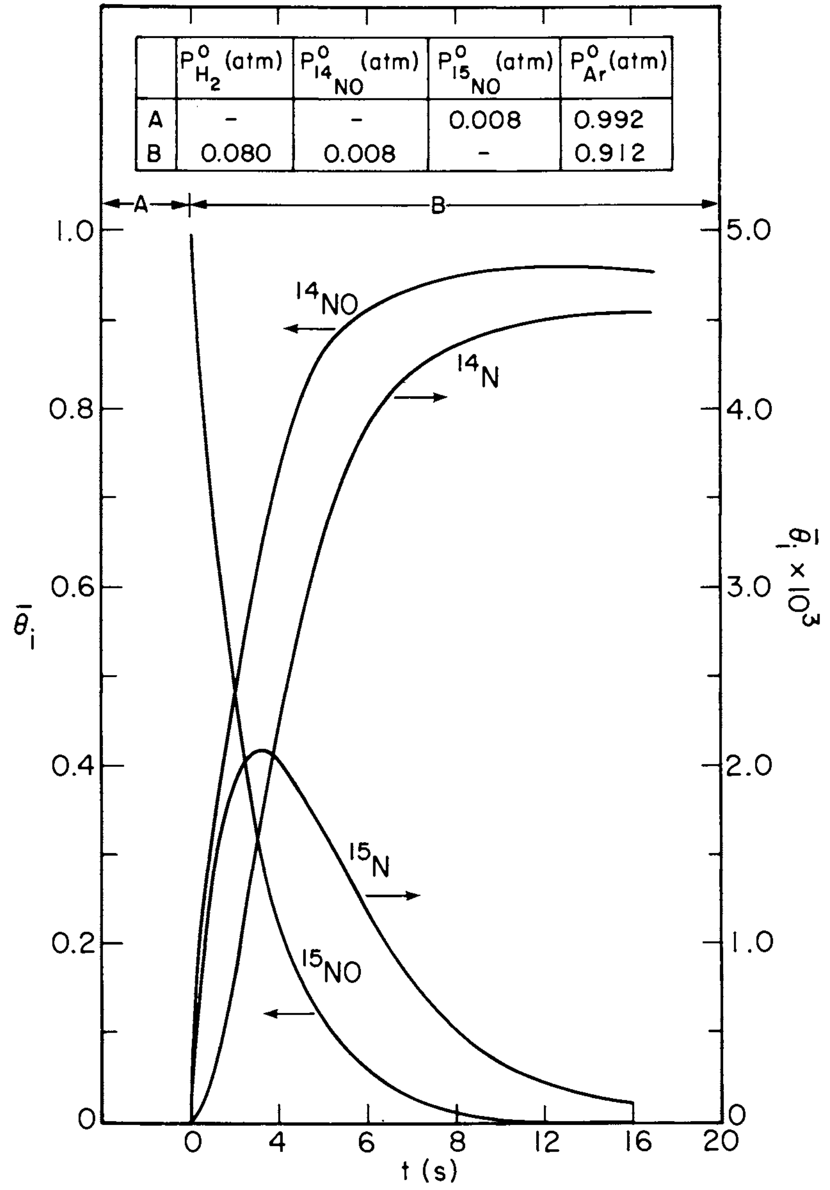

Figure 22. Predictions of the surface coverage responses for $\bar{\theta}_{^{14}NO}$, $\bar{\theta}_{^{15}NO}$, $\bar{\theta}_{^{14}N}$, and $\bar{\theta}_{^{14}N}$ following substitution of a feedstream containing $^{15}NO/Ar$ by a stream containing $^{14}NO/H_2/Ar$: $P_{H_2} = 8.0 \times 10^{-2}$ atm, $P_{NO} = 8.0 \times 10^{-3}$ atm, and $T = 423$ K.

In Catalysis Under Transient Conditions; Bell, A., et al.;
ACS Symposium Series; American Chemical Society: Washington, DC, 1982.

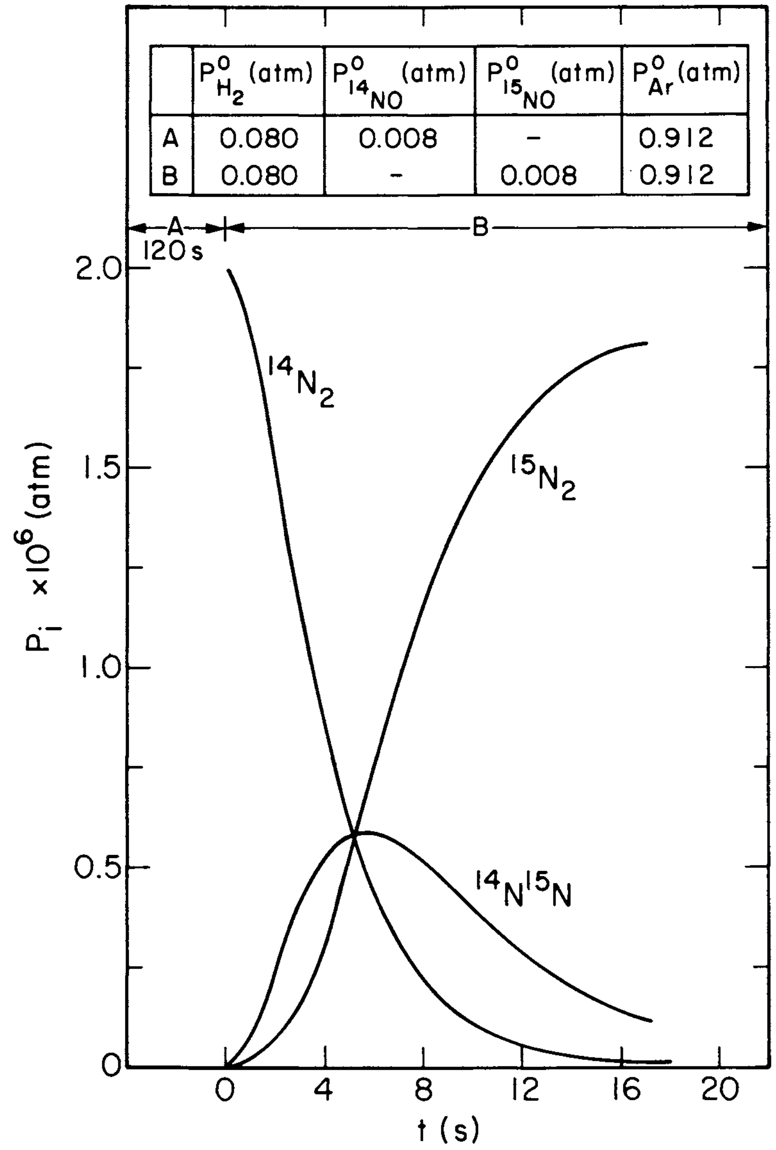

	$P^0_{H_2}$ (atm)	$P^0_{^{14}NO}$ (atm)	$P^0_{^{15}NO}$ (atm)	P^0_{Ar} (atm)
A	0.080	0.008	-	0.912
B	0.080	-	0.008	0.912

Figure 23. Predictions of the partial pressure responses for $^{14}N_2$, $^{15}N_2$, and $^{14}N^{15}N$ following substitution of a feedstream containing $^{14}NO/H_2/Ar$ by a feedstream containing $^{15}NO/H_2/Ar$: $P_{H_2} = 8.0 \times 10^{-2}$ atm, $P_{NO} = 8.0 \times 10^{-3}$ atm, and $T = 423$ K.

In Catalysis Under Transient Conditions; Bell, A., et al.;
ACS Symposium Series; American Chemical Society: Washington, DC, 1982.

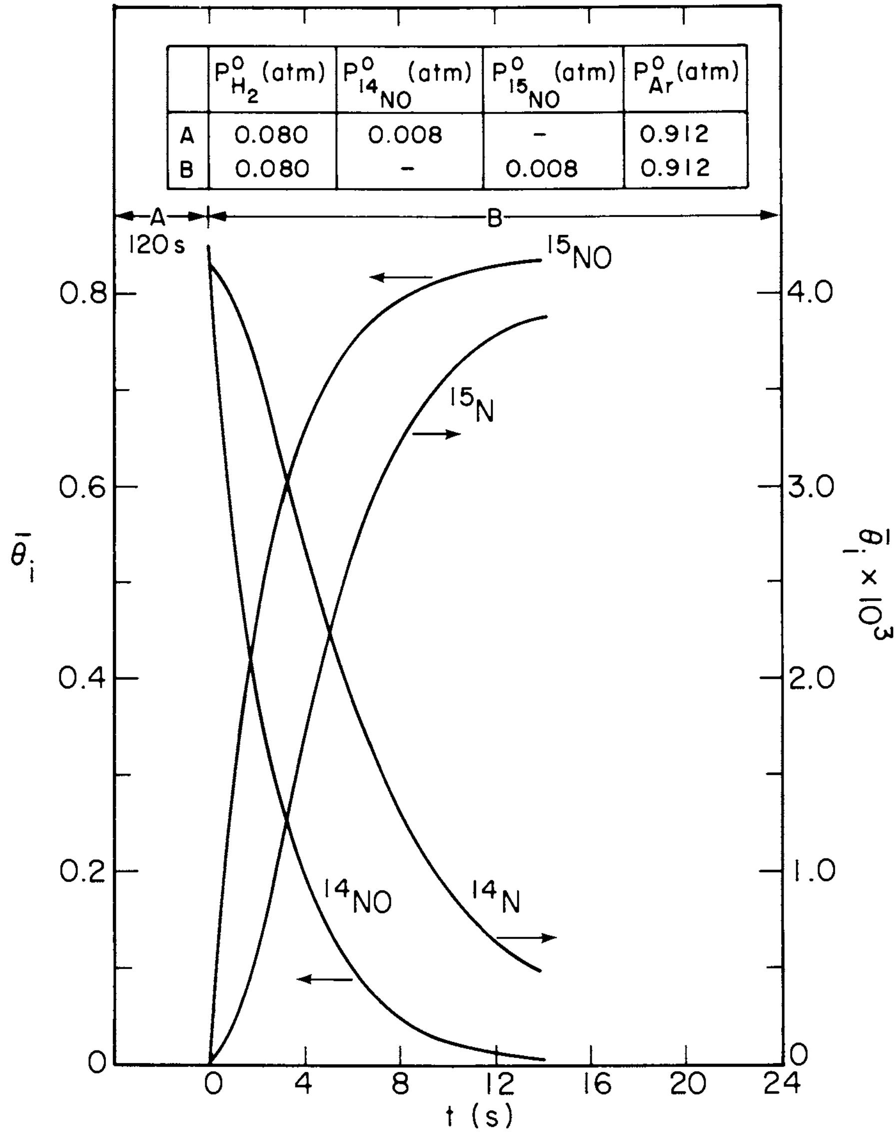

Figure 24. Predictions of the responses for $\bar{\theta}_{^{15}NO}$, $\bar{\theta}_{^{14}NO}$, $\bar{\theta}_{^{15}N}$, and $\bar{\theta}_{^{14}N}$ following substitution of a feedstream containing $^{14}NO/H_2/Ar$ by a feedstream containing $^{15}NO/H_2/Ar$: $P_{H_2} = 8.0 \times 10^{-2}$ atm, $P_{NO} = 8.0 \times 10^{-3}$ atm, and T = 423 K.

in small patches. Such non-uniform mixing would impede the initial formation of the isotopically mixed N_2. The shorter duration of the experimentally observed resonses is not surprising in view of the fact that the experiments were performed at 438 K whereas the calculations were done for a temperature of 423 K.

Conclusions

Transient response experiments have revealed that the formation of N_2 and N_2O during NO reduction by H_2 over Rh proceeds without the intervention of H_2. By contrast, the formation of NH_3 and H_2O involves the reactions of dissociatively chemisorbed H_2 with N and O atoms, respectively. The results obtained from experiments involving the reduction of adsorbed NO and isotopic substitution of ^{15}NO for ^{14}NO can be interpreted on the basis of the reaction mechanism presented in Fig. 11. Key elements of this mechanism are that NO is adsorbed reversibly into a molecular state, that reduction is initiated by the dissociation of molecularly adsorbed NO, and that all products are formed via Langmuir-Hinshelwood process.

Acknowledgment

This work was supported by a grant from the NSF (CPE-7826352).

Nomenclature

k_j - Rate coefficient for reaction j.
M_m - Moles of Rh surface sites per gram of catalyst [mol/gm].
P_i^o - Partial pressure of component i at the reactor inlet [atm].
P_i - Partial pressure of component i at the reactor outlet [atm].
$\overline{P}_i$ - Average partial pressure of component i in the reactor, $\overline{P}_i \equiv (P_i^o + P_i)/2$ [atm].
Q - Total volumetric flow rate [cm^3/s].
r_j - Rate of reaction j [s^{-1}].
R - Gas constant [atm • cm^3/K • mol].
t - Time [s].
T - Temperature [K].
V_r - Reactor volume [cm^3].
ε - Reactor void fraction.
$\overline{\theta}_m$ - Surface coverage.
ν_{ij} - Stoichiometric coefficient for component i in reaction j.
ρ_c - Catalyst density [gm/cm^3].

Literature Cited

1. Kobylinski, T. P. and Taylor, B. W., J. Catal. 33, 376 (1974).
2. Klimisch, R. J and Larson, J. G., Eds., "The Catalytic Chemistry of Nitrogen Oxides", Plenum Press, New York, 1975.
3. Shelef, M., Cat. Rev.-Sci. Eng. 11, 1 (1975).
4. Schlatter, J. C. and Taylor, K. C., J. Catal. 49, 42 (1977).
5. Hegedus, L. L., Summers, J. C., Schlatter, J. C., and Baron, K., J. Catal. 56, 321 (1979).
6. Yao, H. C., Yu Yao, Y. F., and Otto, K., J. Catal. 56, 21 (1979).
7. Summers, J. C. and Baron, K., J. Catal. 57, 380 (1979).
8. Myers, E. C. and Bell, A. T., subbmitted to J. Catal.
9. Kobayashi, H. and Kobayashi, M., Catal. Rv.-Sci. Eng., 10, 139 (1974).
10. Bennett, C. O., Catal. Rev.-Sci. Eng. 13, 121 (1976).
11. Tamaru, K., "Dynamic Heterogeneous Catalysis", Academic Press, New York, 1978.
12. Arai, H. and Tominaga, H., J. Catal. 43, 131 (1976).
13. Solymosi, F. and Sarkany, J., Appl. Surface Sci. 3, 68 (1979).
14. Savatsky, B. J. and Bell, A. T., submitted to J. Catal.
15. Connely, N. G., Inorg. Chim. Acta Rev., 47 (1972).
16. Nappier, Jr., T. E., Meek, D. W., Kirchner, R. H. and Ibers, J. A., J. Am. Chem. Soc. 95, 4194 (1973).
17. Goldberg, S. Z., Kubiak, C., Meyer, C. D. and Eisenberg, R., Inorg. Chem. 14, 1650 (1975).
18. Hecker, W. C. and Bell, A. T., unpublished results.
19. Castner, D. G., Sexton, B. A. and Somorjai, G. A., Surface Sci. 71, 519 (1978).
20. Campbell, C. T. and White, J. M., Appl. Surface Sci. 1, 347 (1978).
21. Baird, R. J., Ku, R. C. and Wynblatt, P., Surface Sci. 97, 346 (1980).
22. Mimeault, V. J. and Hansen, R. S., J. Phys. Chem. 45, 2240 (1966).
23. Zakumbaeva, G. D. and Omaskev, Kh. G., Kin. Katal. 18, 450 (1977).
24. Edwards, S. M., Gasser, R. P. H., Green, D. P., Hawkins, D. S. and Stevens, A. J., Surface Sci. 72, 213 (1978).
25. Kawasaki, K., Shibata, M., Miki, H., and Kioka, T., Surface Sci. 81, 370 (1979).
26. Yates, Jr., J. T., Thiel, P. A. and Weinberg, W. H., Surface Sci. 84, 427 (1979).
27. Thiel, P. A. Yates, Jr., J. T., and Weinberg, W H., Surface Sci. 90, 121 (1979).

In Catalysis Under Transient Conditions; Bell, A., et al.;
ACS Symposium Series; American Chemical Society: Washington, DC, 1982.

28. Hindmarsh, A., "Gear: Ordinary Differential Equation Solver", UDID-3001, Rev. 1, August 20, 1972, Computer Center Library, University of California, Berkeley, CA.
29. Savatsky, B. J., Ph.D. Thesis, Department of Chemical Engineering, University of California, Berkeley, CA, 1981.
30. Nelder, J. A. and Mead, R., Computer J. 7, 308 (1964).

RECEIVED August 6, 1981.

The Use of Molybdenum in Automotive Three-Way Catalysts

H. S. GANDHI, H. C. YAO, and H. K. STEPIEN

Ford Motor Company, Dearborn, MI 48121

Abstract

Recent developments in three-way catalyst (TWC) technology may have potential to decrease the amount of rhodium needed in TWC formulations. Current TWC formulations contain platinum (Pt) and rhodium (Rh). The amount of Rh used in the TWCs, that have desired durability, is considerably higher than the mine ratio of Pt/Rh of 17-19. For large scale vehicle application, it is necessary to find ways to minimize the use of this scarce material. Recent findings show that improved net NO_x activity, with minimum NH_3 formation, is accomplished by the incorporation of molybdenum oxide in Pt and Pt-Rh catalysts. Temperature programmed reduction and IR studies were carried out to investigate the interaction of MoO_3 with PtO_2 and with the γ-Al_2O_3 support. The results are used to explain the improved selectivity for the NO to N_2 reaction and the decreased CO poisoning of molybdenum-containing Pt catalysts when compared to pure Pt catalysts.

Introduction

Three-way catalysts (TWC), or equilibrium catalysts are designed for the simultaneous control of three automotive pollutants: NO, CO, and hydrocarbons (HC). Since rhodium has the desired selectivity for the reduction of NO to N_2 with minimum NH_3 formation and is also selective in reducing NO near stoichiometry or under slightly oxidizing conditions[1, 2, 3], it is one of the active metal components used in TWC formulations.[4] The amount of rhodium used in the TWCs having the desired durability is considerably higher than the mine ratio of Pt/Rh of 17-19. Therefore, for large-scale vehicle application it is necessary to find ways to minimize the use of this scarce material. Ruthenium, which has

0097-6156/82/0178-0143$05.00/0
© 1982 American Chemical Society

the desired selectivity for the NO to N_2 reaction, has not found use in TWC formulations because of the potential loss of Ru as RuO_3. The attempts to stabilize Ru against volatilization have been partially successful.(5, 6, 7) However, the uncertainty of being able to achieve virtually zero ruthenium emissions, under varying driving conditions, has discouraged the use of Ru in TWC.

This paper describes studies on the use of molybdenum in TWC formulations as a substitute for part of the amount of Rh needed.

Experimental

Catalysts: Catalysts used in the flow reactor study for activity and selectivity measurements are described in Table I. They were monolithic catalysts with a fresh BET area of 15 m^2/g.

Catalysts used in the temperature programmed reduction (TPR) study were granular and are described in Table II. These catalysts were made by agglomerating Dispal-M γ-Al_2O_3 powder (180 m^2/g BET area, Continental Oil Co.) and subsequently wetting, drying and calcining at 600°C for 5 h. The resulting solid mass was crushed and sieved and the 0.5 - 1.0 mm diam. fraction was impregnated with an $(NH_4)_2Mo_2O_7$ solution of desired concentration, dried and calcined at 500°C in air for 2 h to obtain the MoO_3/γ-Al_2O_3 sample. Part of this sample was impregnated again with a H_2PtCl_6 solution of desired concentration, dried and calcined at 500°C in air for 2 h to get the PtO_2-MoO_3/γ-Al_2O_3 sample. For supported Pt catalysts, the granular γ-Al_2O_3 support was impregnated with a H_2PtCl_6 solution, dried and calcined at 500°C in air for 5 h to obtain the PtO_2/γ-Al_2O_3 sample. The pure PtO_2 powder (40 mesh) was a commercial sample obtained from Alpha Chemicals, Ventron Corporation.

Apparatus and Procedure: Flow Reactor for Activity and Selectivity Measurements: The experimental apparatus, testing procedures and methods for analyzing the gas streams were identical to those used in ref. (4). The activity and selectivity of the catalysts were measured with a simulated exhaust gas mixture containing NO, CO, O_2, H_2, C_3H_6, C_3H_8, CO_2, H_2O, and N_2. The CO/H_2 ratio was kept at 3. Propylene and propane were used to represent fast-burning and slow-burning hydrocarbons, respectively. The C_3H_6/C_3H_8 ratio was 2. The synthetic exhaust gas composition and a schematic diagram of the flow-reactor used are also given in ref. (4). In addition, the gas mixture also contained 20 ppm of SO_2.

TABLE I

DESCRIPTION OF MONOLITHIC CATALYSTS* USED IN FLOW REACTOR STUDY

Catalyst	Composition wt %			
	Pt	Pd	Rh	Mo
Pt	0.18	-	-	-
MoO_3	-		-	2
Pt-MoO_3	0.25		-	2
Pd-MoO_3		0.2	-	2
Pt-Rh-MoO_3	0.25	-	0.03	2
Pt-Rh	0.12		0.012	-

TABLE II

DESCRIPTION OF THE GRANULAR CATALYST USED IN TPR STUDY

Catalyst	Composition, wt %	
	Pt	Mo
Pt/γ-Al_2O_3(A)	13.8	-
Pt/γ-Al_2O_3(B)	1.6	-
Mo/γ-Al_2O_3(A)	-	10.1
Mo/γ-Al_2O_3(B)	-	3.4
Pt-Mo/γ-Al_2O_3(A)	1.6	3.4
Pt-Mo/γ-Al_2O_3(B)	3.2	3.4
Pt-Mo/γ-Al_2O_3(C)	13.4	3.4

* Catalysts were prepared on Corning monoliths with 300 square cells/in^2. The fresh BET area of catalyst was 15 m^2/g. (γ-Al_2O_3= 10 wt % of the uncoated monolith). Active metal composition as wt % of the total monolith weight including washcoal.

In Catalysis Under Transient Conditions; Bell, A., et al.;
ACS Symposium Series; American Chemical Society: Washington, DC, 1982.

The redox ratio R, used to express the oxidizing or reducing characteristics of the exhaust gas mixture, is defined as follows:

$$R = \frac{p_{CO} + p_{H_2} + 3np_{C_nH_{2n}} + (3n+1)p_{C_nH_{2n+2}}}{p_{NO} + 2p_{O_2}}$$

where p is the partial pressure of the indicated species. Therefore, R > 1 represents an overall reducing gas mixture and R = 1 represents a stoichiometric gas mixture. The activity and the selectivity measurements were made in a flow reactor with the synthetic gas mixture at 1022°F (550°C) and a space-velocity of 60,000 h^{-1}, unless otherwise noted.

Temperature Programmed Reduction (TPR): The apparatus and procedure used in the TPR were reported in a previous paper.[8] A small amount of sample (0.02 to 0.20g) was placed in a Vycor glass cell and a gas mixture of 15% H_2 and 85% Ar was passed over the catalyst at a rate of 25 cc/min. The H_2 uptake during the reduction was measured by a thermo-conductivity detector. During the reduction the programmed temperature rise of the sample was controlled at a constant rate of 10°C/min.

Infrared (IR) Study: The apparatus and procedure used in the IR study were reported in a previous paper.[9] The sample wafers were prepared by pressing about 200 mg of the Pt/Mo/γ-Al_2O_3 catalyst (3.2 wt % Pt and 3.4 wt % Mo) in a 2.86 cm diam. metal die and cutting to a size of 6 mm x 20 mm.

Results and Discussion

NO, CO And HC Conversions

The steady-state activity and selectivity characteristics of a monolithic MoO_3 (2 wt % Mo) catalyst are shown in Figure 1A. Percent conversions of CO, NO, HC and ammonia formation are shown as a function of redox ratio, R. Clearly molybdenum oxide itself does not have any activity for NO reduction over the entire range of R values from R = 0.8 to R = 2. The CO and HC conversions are ~ 15% over this range.

Platinum and palladium catalysts are known to have poor selectivity for the NO to N_2 reaction under reducing conditions. Under these conditions a large fraction of NO is converted to NH_3.[10] Figure 1B shows the characteristic high NH_3 formation over a fresh monolithic 0.18 wt % Pt catalyst. For example, at R = 1.6 gross NO conversion is 58%, however, the net NO conversion is ~1%.

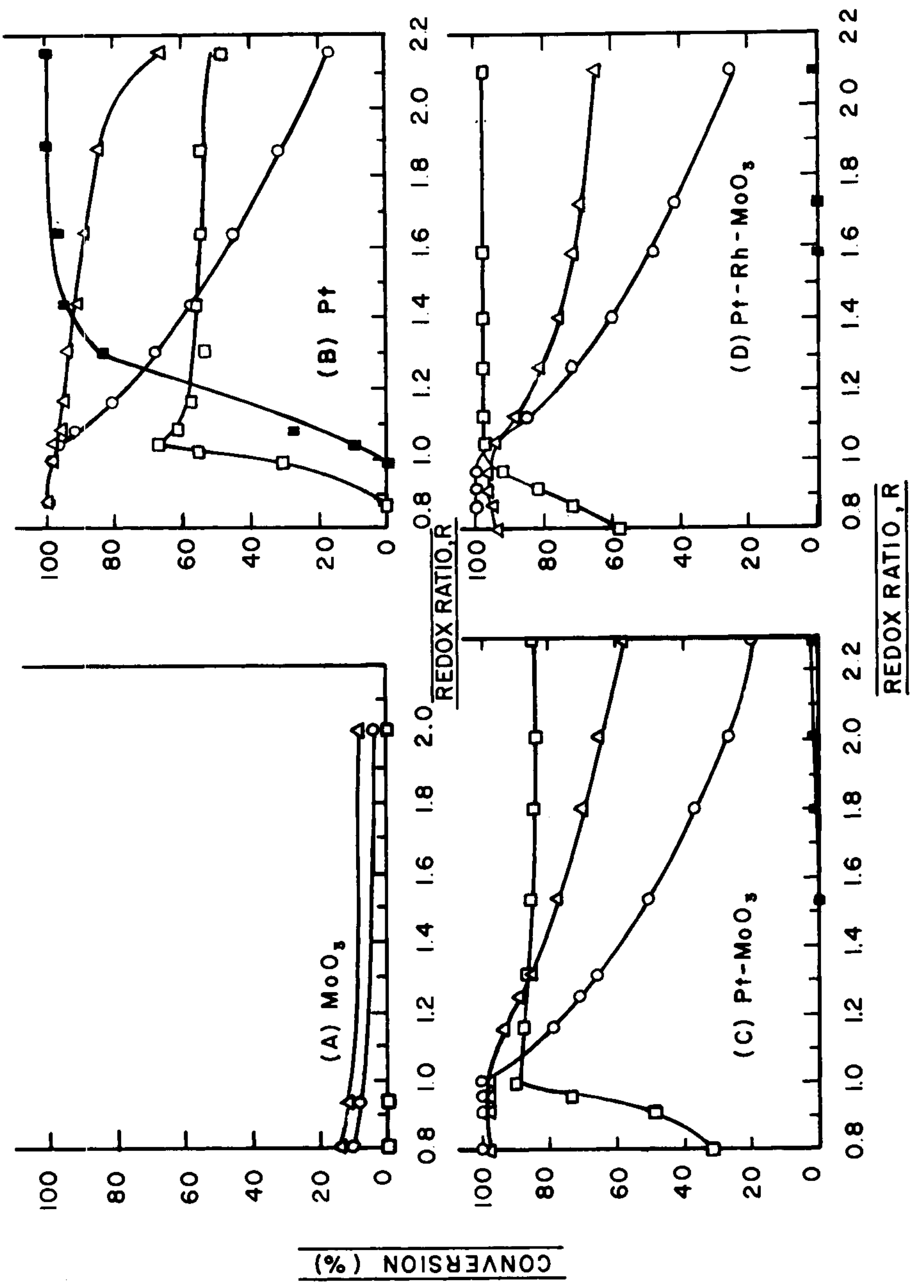

Figure 1. Percent conversion as a function of redox ratio. Key: ○, CO; △, HC; □, NO; and ■, NH_3 as a percent of NO conversion.

American Chemical Society Library
1155 16th St. N. W.
Washington, D. C. 20036

Figure 1C shows the activity and selectivity characteristics of a monolithic catalyst containing 2 wt% Mo in the form of MoO_3 and 0.25 wt% Pt. The addition of MoO_3 to the Pt catalyst significantly improves the net NO conversion over the entire range of R values. For example, at R = 1.6, 86% net NO conversion is achieved, compared to zero and 1% net NO conversion for MoO_3 only, and Pt only catalysts respectively. The Pt-MoO_3 catalyst also maintains good CO and HC activities.

Similarly the incorporation of 2% Mo in the form of MoO_3 in a 0.2 wt% Pd catalyst significantly improves the net NO_x conversion in the rich region. For example, at R = 1.6, 92% net NO conversion is achieved and the NH_3 formation is only 2% of the converted NO.

The addition of molybdenum oxide to Pt and Pd changes the selectivity characteristic of these catalysts for the NO to N_2 reaction. In the rich region, Pt-MoO_3 and Pd-MoO_3 catalysts suppress NH_3 formation almost completely and thereby yield over 80% net NO_x conversion for R values as high as 1.9 over the Pd-MoO_3 catalyst and as high as 2.3 over the Pt-MoO_3 catalyst. In the lean region ($R < 1$), the Pt-MoO_3 catalyst is able to reduce NO by CO (and H_2) in the presence of excess O_2. For example, at R = 0.9 the Pt-MoO_3 catalyst converts 50% of the NO compared to no conversion for MoO_3 and ~ 5% conversion for Pt catalysts, respectively. At R = 0.9 the Pd-MoO_3 catalyst exhibits 70% NO conversion. Thus, Pt-MoO_3 and Pd-MoO_3 catalysts minimize NH_3 formation under reducing conditions and improve NO conversion under somewhat oxidizing conditions.

The addition of Rh to Pt-MoO_3 further improves the NO conversion throughout the range of R values. At R = 1 peak NO conversion for the Pt-Rh-MoO_3 catalyst is 98% (Figure 1D) compared to 90% for the Pt-MoO_3 catalyst (Figure 1C).

In addition, the incorporation of MoO_3 substantially decreases NH_3 formation over Pt-Rh catalysts. For example, a catalyst containing 0.19% Pt and 0.017% Rh shows a decrease in NH_3 formation, at R = 1.8, from 20% to ~ 2% by the incorporation of 2% Mo as MoO_3. However, when the amount of Mo is decreased from 2 to 0.3 wt % (i.e. to Mo/Pt atomic ratio of 3) this improvement in the activity or selectivity behavior is lost. This effect suggests the necessity for the Pt and Mo ions to be present in close proximity. By having a large excess of Mo with respect to Pt, the statistical probability for Pt to be located near Mo ions is greatly increased.

In Catalysis Under Transient Conditions; Bell, A., et al.;
ACS Symposium Series; American Chemical Society: Washington, DC, 1982.

Additional experiments were performed to quantify the effect of varying the Mo/Pt ratio on the selectivity for reduction of NO to N_2(or N_2O). The Pt concentration on the monolithic support was maintained at 0.2 wt % and Mo concentration was varied from 0 to 3.4 wt %. The NO-H_2-CO reaction was done over these catalysts at 60,000 h^{-1} space-velocity. The selectivity is defined as:

$$S = \frac{2N_2 + 2N_2O}{2N_2 + 2N_2O + NH_3} \times 100 = \frac{\text{Net NO Conversion}}{\text{Gross NO Conversion}} \times 100$$

The results for NO to N_2 conversion as a function of varying Mo/Pt atomic ratio at 500°C (Figure 2) show the increase of selectivity with Mo concentration, leveling off at Mo/Pt atomic ratio of 15.

Model Reactions Study over Pt and Pt-MoO_3 Catalysts: In order to further understand the activity and selectivity behavior of Mo-containing Pt catalysts, NO-H_2, NO-CO-H_2, and NO-CO model reactions were studied over Pt (0.25 wt %) and Pt-MoO_3 (Pt = 0.25 wt % and Mo = 2 wt %) catalysts.

The study was carried out over a temperature range of 25°C to 600°C at a space-velocity of 60,000 h^{-1}. The relative catalyst activity as expressed by the temperature required for 50% and 80% NO conversion is given in Table III. For both Pt and Pt-MoO_3 catalysts, the presence of CO in the feedgas poisons the Pt sites, as evidenced by an increase in the 50% and 80% NO conversion temperatures. However, the CO poisoning effect is much stronger for pure Pt catalysts than for a mixed Pt-MoO_3 catalyst. For example, for the NO-CO reaction, 50% NO conversion can not be reached over the Pt catalyst, while 345°C and 360°C temperatures are required for 50% and 80% NO conversions, respectively, over the Pt-MoO_3 catalyst.

Table IV shows the striking difference in selectivity behavior between Pt and Pt-MoO_3 catalysts for NO-H_2 and NO-H_2 and NO-H_2-CO reactions. For the NO-H_2-CO reaction at 600°C,only 12% of the reacted NO is converted to N_2 over the Pt catalyst compared to 100% for the Pt-MoO_3 catalyst.

Sulfur Dioxide and Propane Oxidation

Platinum catalysts are known for their good activity for SO_2 (11,12) and C_3H_8 (13,14) oxidation. Rhodium on the other hand is a poor catalyst for these reactions. Therefore, these reactions were studied on Pt and Pt-

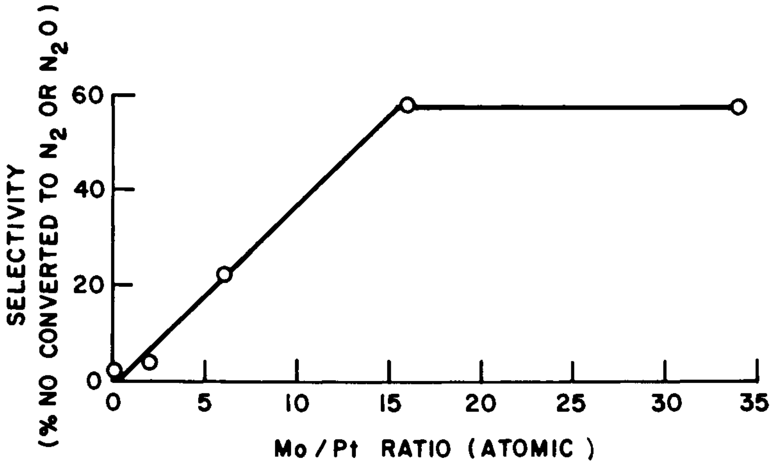

Figure 2. Selectivity as a function of Mo to Pt ratio (Pt, 0.2 wt %; R, 1.6) at 500°C.

In Catalysis Under Transient Conditions; Bell, A., et al.;
ACS Symposium Series; American Chemical Society: Washington, DC, 1982.

TABLE III

TEMPERATURE (°C) FOR 50% AND 80% GROSS NO CONVERSION IN $NO-H_2$, $NO-H_2-CO$ AND NO-CO REACTIONS

Catalysts	$NO-H_2$		$NO-H_2-CO$		NO-CO	
	$T_{50\%}$	$T_{80\%}$	$T_{50\%}$	$T_{80\%}$	$T_{50\%}$	$T_{80\%}$
Pt(0.25%)	60	100	360	500	NR	NR
$Pt-MoO_3$ (Pt=0.25%, Mo=2%)	175	185	250	350	345	360
Feedgas	NO = 0.1%		NO = 0.1%		NO = 0.1%	
	CO = 0		CO = 0.75%		CO = 1%	
	H_2 = 1%		H_2 = 0.25%		H_2 = 0	

TABLE IV

SELECTIVITY (%) FOR NO TO N_2(or N_2O) REACTION IN $NO-H_2$ $NO-H_2-CO$ REACTIONS AS A FUNCTION OF TEMPERATURE °C

T°C	Pt		$Pt-MoO_3$	
	$NO-H_2$	$NO-H_2-CO$	$NO-H_2$	$NO-H_2-CO$
250	0	0	0	30
300	0	0	0	43
350	0	0	0	53
400	0	0	12	60
450	0	0	22	67
500	0	2	30	73
550	0	8	38	80
600	0	12	46	100

MoO_3 catalysts to determine whether the Pt-MoO_3 catalyst exhibits Pt-like or Rh-like behavior. The results for SO_2 oxidation over supported Pt and Pt-MoO_3 catalysts are shown in Table V. The Rh-like behavior, i.e., poor SO_2 oxidation activity, is evident. For example, at 500°C and 60,000 h^{-1} space-velocity, SO_2 conversion is 45% for the Pt catalyst compared to 11% for the Pt-MoO_3 catalyst. Table VI shows similarly the extreme difference in propane oxidation activity for these catalysts.

Effect of Oxygen Pulse on Steam-Reforming Activity

The effect of an oxygen pulse on the steam-reforming activity of fresh Pt, Rh, Pt-Rh, and Pt-MoO_3 catalysts was studied both in the presence and absence of 20 ppm SO_2 in the feed-gas (Table VII). The good steam-reforming activity of Pt, Rh, and Pt-Rh catalysts is severely reduced by the addition of 20 ppm of SO_2 in the feed-gas. The incorporation of MoO_3 significantly suppresses the steam-reforming activity of Pt catalysts even in the absence of the SO_2 in the feed-gas. In this case, the Pt-MoO_3 catalyst performance is similar neither to Pt nor Rh catalysts. Upon adding a 30 sec 1% O_2 pulse, the HC conversion improves for all the catalysts. The average values of percent HC converted during five consecutive 30 sec O_2 pulses, both in the presence and absence of SO_2 in the feed-gas, also are given in Table VII. The improved HC conversion lasts for several minutes after the 30 sec O_2 pulse is terminated. The HC conversion values at t = 10, 15, 20 and 30 sec, after the O_2 pulse was ended, are shown in Table VIII. A comparison of HC conversion values shows that the Pt-MoO_3 catalyst performance is somewhat inferior to that of the Pt catalyst under these cyclic conditions.

These results show that incorporation of MoO_3 into a Pt catalyst changes the basic characteristics of the Pt catalyst and suggest the possibility of an interaction between Pt and Mo oxides on the surface of the support. This possibility was investigated by a TPR study with a Pt-MoO_3 catalyst.

Temperature Programmed Reduction (TPR)

The rates of H_2 uptake (in arbitrary units) as a function of temperature for the γ-Al_2O_3 supported PtO_2, MoO_3, and PtO_2-MoO_3 mixtures of various concentrations are plotted in Fig. 3. TPR of pure PtO_2 and MoO_3 supported on γ-Al_2O_3 have been reported.[15,16] Curve A is the TPR of the PtO_2 sample of high concentration (13.8 wt % Pt) in which two

TABLE V

SO_2 OXIDATION OVER Pt AND Pt-MoO_3 CATALYSTS

Catalyst	% SO_2 Conversion[a]		
	400°C	500°C	600°C
Pt (0.2 wt %)	10	45	59
Pt-MoO_3 (Pt = 0.2 wt %) (Mo = 2 wt %)	3	11	16

[a] Feedgas: SO_2 = 0.02%
O_2 = 1%
S.V. = 60,000 h^{-1}

TABLE VI

PROPANE OXIDATION OVER Pt AND Pt-MoO_3 CATALYSTS

Catalyst	$T_{25\%}$	$T_{50\%}$	$T_{75\%}$
Pt (0.2%)	230	267	298
Pt-MoO_3 (Pt = 0.2%, Mo = 2%)	450	640	N.R.

Feedgas: C_3H_8 = 0.05%
O_2 = 2.25%
SO_2 = 20 ppm
N_2 = Balance

S. V. = 60,000 h^{-1}

In Catalysis Under Transient Conditions; Bell, A., et al.;
ACS Symposium Series; American Chemical Society: Washington, DC, 1982.

TABLE VII

EFFECT OF OXYGEN PULSE ON STEAM REFORMING ACTIVITY

Catalyst	% HC Conversion[A] Steady-State 0 ppm SO_2	Steady-State 20 ppm SO_2	Oxygen Pulse[B] 0 ppm SO_2	Oxygen Pulse[B] 20 ppm SO_2
Pt (0.2%)	70	20	90	73
Rh (0.02%)	80	8	93	72
Pt (0.2%), Rh (0.02%)	89	3	98	84
Pt (0.2%), Mo (2%)	12	4	57	57

[A] Feedgas: C_3H_6 = 0.036%, C_3H_8 = 0.018%, H_2 = 0.5%, CO_2 = 8%, H_2O = 8%, SO_2 = 0 or 0.002%, N_2 = Balance

T = 600°C, S.V. = 60,000 h^{-1}

[B] Average % HC converted during 5 consecutive 30 sec 1% O_2 pulses.

rate maxima are observed. The one at 10°C has been assigned to the reduction of PtO_2 in the particulate phase and the one near 90°C to the reduction of PtO_2 in the saturated dispersed phase.(15) Curve B is TPR of the PtO_2 sample of low concentration (1.6 wt % Pt or 0.48 μmol/m^2 BET), which is far below the saturation concentration of the dispersed phase (2.2 μmol/m^2 BET). The rate maximum in Curve B has shifted to a higher temperature, ~ 250°C, indicating a stronger PtO_2-γ-Al_2O_3 interaction in this sample. Curve C is the TPR of the MoO_3 sample of high concentration (10.1 wt % Mo). The surface concentration of MoO_3 in this sample is 8.2 μmol/m^2 (BET), of which about 50% is present in the particulate phase.(16) The TPR of this sample shows three rate maxima, indicating the difference in the ease of removal for the different oxygen atoms in MoO_3 by H_2. The first rate maximum at 450°C has been assigned(16) to the removal of only

In Catalysis Under Transient Conditions; Bell, A., et al.;
ACS Symposium Series; American Chemical Society: Washington, DC, 1982.

TABLE VIII

STEAM REFORMING WITH EFFECT OF OXYGEN PULSE (T = 600°C, S.V. = 60,000 h^{-1})

Catalyst	Feedgas HC (ppm)	HC Conv. %	10 sec	15 sec	20 sec	30 sec
			after (first) 30 sec O_2 pulse (O_2 = 1%)			
W/O SO_2			HC Conv.(%)			
0.2% Pt	1500	70	-	-	-	-
0.02% Rh	1600	81	95	94	93	92
0.2% Pt + 0.02% Rh	1500	89	98	97	97	97
0.2% Pt + 2% Mo	1620	12	85	44	17	9
With 20 ppm SO_2						
0.2% Pt	1500	21	77	68	61	54
0.02% Rh	1600	8	86	78	69	56
0.2% Pt + 0.02% Rh	1500	3	82	70	62	55
0.2% Pt + 2% Mo	1620	4	72	61	43	32

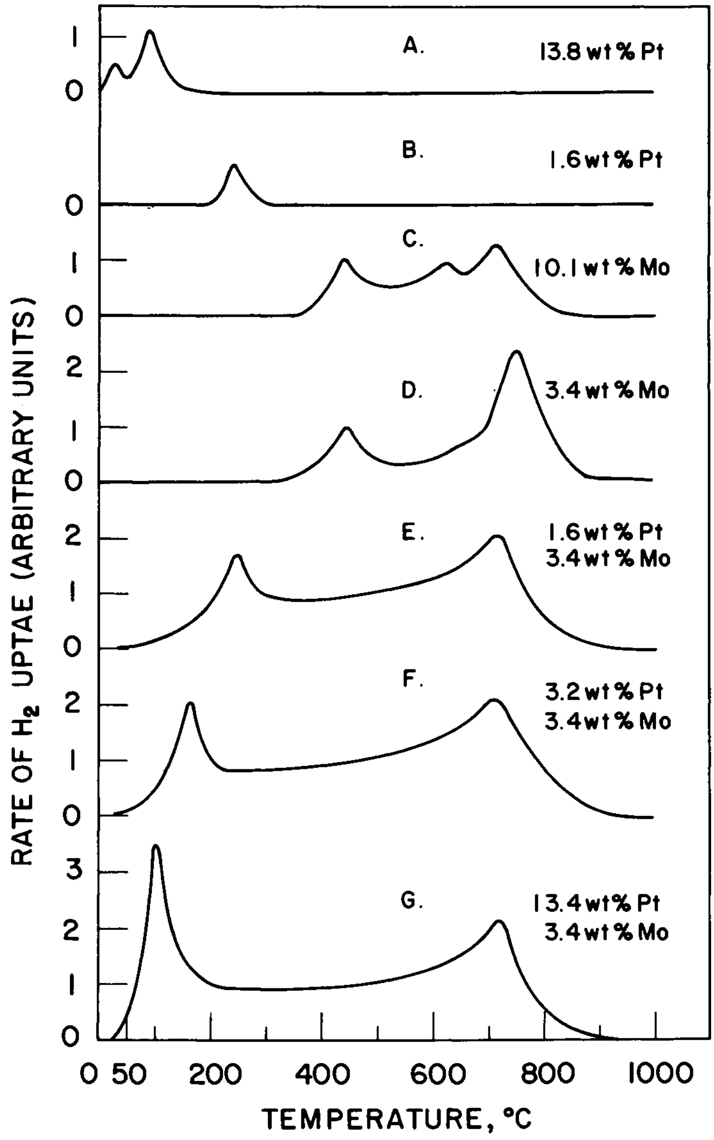

Figure 3. Rate of H_2 uptake as a function of temperature in the TPR of PtO_2, MoO_3, and PtO_2–MoO_3 supported on γ-Al_2O_3.

surface capping oxygen atoms. The other two rate maxima at 580°C and 720°C have been assigned to the removal of the other oxygen atoms in the sublayer and in the bulk of MoO_3 in the particulate phase.

In $MoO_3/\gamma-Al_2O_3$ of low concentration (3.4 wt % Mo, curve D), all of the MoO_3 is present in the dispersed phase.(16) The TPR of this sample gives only two rate maxima. The first one at 450°C is the same as that in curve C and has been assigned to the removal of the surface capping oxygen.(16) The second rate maximum at higher temperature (750°C) has been assigned to the oxygen atoms other than the capping oxygen atoms in the dispersed (Figure 3D) phase of MoO_3 on $\gamma-Al_2O_3$.

The presence of PtO_2 in the $Pt-Mo/\gamma-Al_2O_3$ catalyst lowers the reduction temperature of the first rate maximum from 450°C down to 250°C, 160°C or 100°C depending upon the concentration of PtO_2 (curves E-G); however, it does not affect significantly the second rate maximum at about 750°C. Also, note that the rate maximum for the reduction of PtO_2 coincides with the first rate maximum. These results suggest that the interaction between the PtO_2 and the dispersed MoO_3 on $\gamma-Al_2O_3$ is responsible for lowering the temperature for the removal of the capping oxygen atoms and rule out the mechanism of hydrogen spillover contributing to the observed effect. If hydrogen spillover predominates, then it should also lower the temperature for the removal of other oxygen atoms in the dispersed phase of MoO_3. In fact, the interaction lowers only the temperature for the removal of surface capping oxygen indicating that the interaction of PtO_2 involves only the capping oxygen of the dispersed MoO_3. After this reduction the Pt atoms may form a surface complex with the partially reduced Mo ions. For the $Pt-Mo/\gamma-Al_2O_3$ catalysts which are used at temperatures < 600°C, the active complex may be the dispersed $PtMoO_x$ (where X = 2-3), under the reducing conditions. For temperatures > 600°C, the catalyst can have the surface complex of $PtMoO_{2-x}$ where x ranges from 0 to 2 depending upon the temperature of reduction.

Infrared (IR) Study

IR spectra of CO chemisorbed on a $Pt-Mo/\gamma-Al_2O_3$ sample (3.2 wt % Pt, 3.4 wt % Mo) are presented in Figure 4. Spectrum A was taken after the $Pt-Mo/\gamma-Al_2O_3$ sample was degassed at 300°C and followed by CO chemisorption at 25°C. The weaker band at 2180 cm^{-1} has been assigned

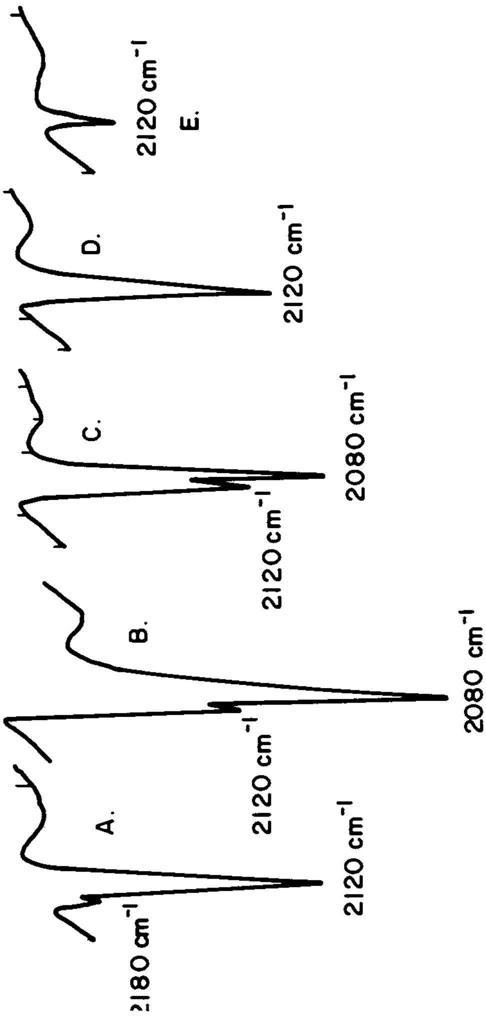

Figure 4. IR data of CO chemisorbed on a Pt–Mo/γ-Al_2O_3 catalyst.

to CO on Pt ions (Pt oxide) and the stronger band at 2120 cm^{-1} to chemisorbed CO on Pt.[17,18] The sample was subsequently heated in 60 torr CO at 300°C for 30 min and cooled to 25°C, giving spectrum B in Figure 4. In spectrum B, the band at 2180 cm^{-1} has disappeared, the band at 2120 cm^{-1} has weakened, and a strong band at 2080 cm^{-1} has emerged. This strong new band was also found in the spectrum (not shown) taken after CO chemisorption on a reduced (500°C, H_2) $MoO_3/\gamma\text{-}Al_2O_3$ sample and was assigned to the CO chemisorbed on reduced Mo ions. Apparently at 300°C, PtO_2 is reduced to Pt^o, and surface MoO_3 is reduced primarily to MoO_2.[19] The CO chemisorbed on the reduced molybdenum oxide is easier to remove when degassed at 200°C and is more reactive with O_2 at elevated temperatures. By exposing this sample to air at 25°C, the band at 2080 cm^{-1} decreases, whereas the band at 2120 cm^{-1} increases slightly (spectrum C). After heating the sample in air at 100°C for 20 min, the band at 2080 cm^{-1} disappears completely while the band at 2120 cm^{-1} further increases (spectrum D). Only after heating in air at 300°C, will the band at 2120 cm^{-1} gradually disappear (spectrum E). At 350°C, the band at 2120 cm^{-1} disappears completely. These results show that CO chemisorbed on Mo ions is more reactive and can be oxidized by air at 25° - 100°C while the CO chemisorbed on Pt is held strongly and can only be oxidized after it is heated near 300°C.

Conclusion

Previously, Ermakov et al.[20,21] studied $Pt\text{-}Mo/SiO_2$ catalysts and found that the presence of Mo in $Pt\text{-}Mo/SiO_2$ catalysts increased the rate of hydrogenolysis by 4 orders of magnitude compared to Pt/SiO_2 catalysts and decreased the electron density of Pt as observed from x-ray electron spectroscopy. They interpreted these data in terms of chemical bonding between Pt and Mo and suggested a $Pt^o\text{-}Mo^{2+}$ complex on silica which has catalytic activity and selectivity similar to Rh or Ir rather than to Pt.

Our activity and selectivity results are in good agreement with their findings. Our model reactions study showed that the presence of Mo in a

Pt-Mo/γ-Al_1O_3 catalyst (1) lowers the activity but increases the selectivity of the Pt catalyst for the NO reduction by H_2, and (2) increases the activity for the NO reduction by CO and the activity and selectivity for the NO reduction by CO + H_2. Based on the TPR and IR data, we attribute these results to a strong interaction between Pt and Mo oxides on the γ-Al_2O_3 support. Such interaction facilitates the removal of the surface oxygen atom of the dispersed MoO_3 to form a surface Pt^o-Mo^{4+} complex which has activity and selectivity characteristics similar to that of Rh/γ-Al_2O_3 or Ir/γ-Al_2O_3 rather than Pt/γ-Al_2O_3 in the reduction of NO by H_2. Both Pt^o and Mo^{4+} sites in the Pt^o-Mo^{4+} complex chemisorb CO, but CO molecules chemisorbed on Mo^{4+} sites are more reactive than CO on the Pt^o sites. Also, CO chemisorbed on Mo^{4+} decreases the affinity of CO for Pt^o sites probably due to the dipole-dipole repulsion between the adsorbed CO molecules on both Pt and Mo^{4+} sites in the Pt^o-Mo^{4+} complex. Both of these effects enhance the activity of the catalyst for NO reduction by CO and the activity and the selectivity by H_2 + CO.

Practical Considerations

While the ability of Pt-MoO_3 or Pd-MoO_3 catalysts to suppress NH_3 formation must be preserved, stabilization of MoO_3 in these catalysts from volatilization at higher temperatures is necessary under cyclic conditions around a stoichiometric A/F ratio. MoO_3 volatilizes at temperatures ~ 600°C under oxidizing conditions, as can be inferred from the vapor pressure values for MoO_3 given in Table IX.[(22)] Although molybdenum oxides are not considered toxic[(23)] compared to the noble metal oxides (e.g., RuO_4 and OsO_4), it is nevertheless desirable to minimize loss of molybdenum by volatilization while maintaining an optimum level of activity and selectivity.

Stabilization of MoO_3 is achieved by incorporation of alkaline-earth metal oxides (e.g. BaO, MgO) or rare-earth metal oxides (e.g., La_2O_3) or by reaction with base metal oxides (e.g., NiO, CoO, CuO etc.). Since MoO_3 is an acidic oxide, its reaction with a basic oxide should lead to a mixed oxide

In Catalysis Under Transient Conditions; Bell, A., et al.;
ACS Symposium Series; American Chemical Society: Washington, DC, 1982.

TABLE IX

VAPOR PRESSURE OF MoO_3

T^oC	V.P. (torr)
627	3.9×10^{-3}
727	0.13
827	1.9
929	11.7
1027	53.2

which should be more stable than MoO_3 against volatilization. Interaction between MoO_3 in the dispersed phase[16] and the γ-Al_2O_3 support also lower the lovatility of MoO_3. Work is currently in progress to optimize the incorporation of MoO_3 into TWCs without sacrificing the desired activity and selectivity.

Acknowledgements

We would like to thank Dr. J. T. Kummer for providing helpful consultation throughout this work and Dr. K. M. Adams for obtaining SO_2 and C_3H_8 oxidation data.

Literature Cited

1. Kobylinski, T. P. and Taylor, B. W., J. Catal. 33, 376 (1974).

2. Ashmead, D. R., Campbell, J. S., Davies, P. and Farmery, K., SAE (Soc. Automotive Eng.) Paper 74039 (1974).

3. Taylor, K. C. in "The Catalytic Chemistry of Nitrogen Oxides," R. L. Klimisch and J. G. Larson (Eds.), Plenum Press, New York, 1975, p. 173.

4. Gandhi, H. S., Piken, A. G., Shelef, M. and Delosh, R. G., SAE Transactions, 85, Paper 760201, 901 (1976).

5. Shelef, M. and Gandhi, H. S., Platinum Metals Review 18(1), 1 (1974).

6. Gandhi, H. S., Stepien, H. K. and Shelef, M., SAE Paper 750157 (1975).

7. Gandhi, H. S., Stepien, H. K. and Shelef, M., Material Research Bulletin, 10, 837 (1975).

8. Yao, H. C., Japar, S. and Shelef, M., J. Catal. 50, 407 (1977).

9. Yao, H. C. and Rothschild, W. G., J. Chem. Phys. 68, 4775 (1978).

10. Shelef, M. and Gandhi, H. S., Ind. Eng. Chem., Prod. Res. Develop. 13, 80 (1974).

11. Gandhi, H. S., Yao, H. C., Stepien, H. K. and Shelef, M., SAE Paper 780606 (1978).

12. Williamsom, W. B., Truex, T. J., Gandhi, H. S. Ku, R. C. and Wynblatt, P., AIChE Symposium Series No. 201, 76, 212 (1980).

13. Williamson, W. B., Stepien, H. K. and Gandhi, H. S.; Environ. Sci. & Tech. 14, 319, 1980.

14. Cooper, B. J., Harrison, B., Shutt, E. and Lichtenstein, I., SAE Paper 770367 (1977).

15. Yao, H. C., Sieg, M. and Plummer, H. K., Jr., J. Catal. 59, 365 (1979).

16. Yao, H. C., J. Catal. (in Press).

17. Heyne, H. and Tompkins, F. C., Trans. Faraday Soc. 63, 1274 (1967).

18. Summers, J. C. and Ausen, S. A., J. Catal. 58, 131 (1979).

19. Hall, W. K. and Lo Jacono, M., Proceedings of the Sixth Int. Cong. on Catal. 1, 246 (1977).

20. Ermakov, Yu. I., Ioffe, M . S., Ryndin, Yu. A. and Kuznetsov, B. N., Kinetika i kataliz 16, 807 (!975).

21. Ermakov, Yu. I., Kuznetsov, B. N., Rydin, Yu. A. and Kuplyakin, V. K., Kinetika i Kataliz 15, 1093 (1974).

22. Thermodynamic Properties of Molybdenum Compounds, Bulletin CDB-2 Climax Molybdenum Company, Sept., 1954.

23. Sax, N. I., "Dangerous Properties of Industrial Materials," Van Nostrand Reinhold, p. 939, New York, 1975.

RECEIVED June 26, 1981.

Decomposition of Nitrous Oxide on Magnesium Oxide Compared to That on Cupric Oxide

H. KOBAYASHI and K. HARA

Hokkaido University, Department of Chemical Process Engineering, Sapporo 060, Japan

The decomposition of nitrous oxide over various metal oxides has been widely investigated by many investigators (1-3). Dell, Stone and Tiley (4) have compared the reactivity of metal oxides and shown that in general p-type oxides were the best catalysts and n-type the worst, with insulators occupying an intermediate position. It has been generally accepted (5) that this correlation indicates that the electronic structure of the catalyst is an important factor in the mechanism of the decomposition of nitrous oxide over metal oxides catalysts. The reaction is usually written (4) as

$$N_2O + e^- \text{ (from catalyst)} \rightarrow N_2 + O^- \text{ (ads)} \qquad (1)$$

$$2\,O^-\text{(ads)} \rightleftarrows O_2 + 2\,e^- \text{ (to catalyst)} \qquad (2)$$

or $$O^- \text{ (ads)} + N_2O \rightarrow N_2 + O_2 + e^- \text{ (to catalyst)} \qquad (3)$$

More recently Vijh (6) has shown that the existing data on the catalytic decomposition of nitrous oxide can be fit to an interpretation very similar to that involved in the Sabatier-Balandin concept. The fundamental idea behind Sabatier-Balandin approach is that the reactants get adsorbed on the catalyst to form a surface compound and the energy of the bond between the catalyst and the reactant is related to the catalytic activity in a volcanic manner; i.e., there is a maximum in activity with increasing bond energy. Based on this interpretation, Vijh has suggested that in the ascending branch of the volcano, the activity decreases with increasing bond energy, indicating that the rate-determining step in the N_2O decomposition on these oxides such as CuO, NiO and CoO probably involves rupture of a bond between the catalyst and the reactant. On the other hand, in the descending branch of the volcano, the activity increases with increasing bond energy and this indicates a rate-determining step involving the formation of a bond between the catalyst and the reactant.

0097-6156/82/0178-0163$05.00/0
© 1982 American Chemical Society

Since the insulator oxides such as MgO, CaO and Al_2O_3 are involved in this branch, it would be worth examining whether the mechanism of N_2O decomposition on these insulator oxides is different from that on p-type oxides.

In the present paper, the reactions on CuO and MgO are examined and compared.

Experimental

Catalysts. Cupric oxide was prepared by thermal decomposition of reagent grade copper nitrate (Wako Pure Chem.Inc.Ltd.) at 400°C in air for 4 hrs. Magnesium oxide was commercially available reagent grade powder (Kanto Chemical Co.Ltd.). The oxides powders were pressed into tablets and crushed and 24-42 mesh granules were used as catalysts.

Apparatus and Procedure. The kinetic studies of the catalysts were carried out by means of the transient response method (7) and the apparatus and the procedure were the same as had been used previously (8). A flow system was employed in all the experiments and the total flow rate of the gas stream was always kept constant at 160 ml STP/min. In applying the transient response method, the concentration of a component in the inlet gas stream was changed stepwise by using helium as a balancing gas. A Pyrex glass tube microreactor having 5 mm i.d. was used in a differential mode, i.e. in no case the conversion of N_2O exceeded 7 %. The reactor was immersed in a fluidized bed of sand and the reaction temperature was controlled within ± 1°C.

The composition of the gas stream before and after contact with the catalyst was monitored by subjecting aliquots to gas chromatographic analysis using a Ohkura Model 701 gas chromatograph and two columns. For N_2 and O_2, a 1 meter molecular sieve 5A column operating at 65°C was employed ; for N_2O, a 2 meter Porapak Q column operating at 89°C was used.

Reaction. The effect of external diffusion on the kinetics was examined at same W/F over different bed size and was found to be negligible at the gas velocity and temperatures used in the kinetic experiments. By varying the gas velocity of a constant composition gas mixture through a bed, no appreciable change in percentage of N_2O decomposition was observed. The effect of internal diffusion was investigated by measuring the rate of reaction under indentical feed and flow rate conditions for beds of (a) 28-36 mesh and (b) 20-28 mesh catalyst granules. The reaction rates on both catalyst beds were essentially the same, showing evidence of the absence of pore diffusion control. The reactor wall was found to be catalytically inactive at temperatures employed.

Nitrous oxide (N_2O 99.0 %) and helium (He 99.999 %) from commerical cylinders were purified through a dry ice-methanol trap to remove water vapor.

Results

The response of the component B in the effluent stream to a step change in the concentration of A in the feed gas stream is designated as A-B response. When A is increased from nil, A(inc., 0)-B, and decreased to nil, A(dec.,0)-B.

CuO Catalyst. 70.9 g of CuO catalyst was used in the experiments. The temperature at which the decomposition of N_2O became appreciable at steady state was 230°C and the reaction experiments were carried out at 256°C. In Figure 1 is shown a response of N_2, O_2 and N_2O in the outlet flow stream to the step change of N_2O in the inlet gas stream, i.e. N_2O(dec.,0)-N_2, 0, N_2O. The response of O_2 and N_2O was found to tail considerably, indicating that these species were adsorbed on the catalyst surface during the reaction at steady state. On the contrary, the N_2 response is quite rapid and sunddenly dropped down to nil. It is worth noting that nitrogen did not evolve in spite of the presence of adsorbed nitrous oxide. It would be reasonable to suggest from this findings, therefore, that the decomposition of nitrous oxide is taking place through the immediate reaction of gaseous nitrous oxide impinging on the active site on the surface.

The slow desorption of oxygen will also suggest that the desorption of oxygen from the catalyst could be the slowest step during the steady state reaction.

After the catalyst had been kept in a helium stream for a surfficient time to remove oxygen, the feed was switched over to a stream of N_2O(17%)-He mixture and the N_2O(inc.,0)-N_2,O_2 response was followed. The results were shown in Figure 2. Upon changing the stream, the N_2O-N_2 response showed an instantaneous maximum which was followed by a steep decrease showing an overshoot-type response. The N_2O-O_2 response, on the other hand, showed a monotonic increase to attain a new steay state value. This delayed increase of oxygen concentration in the effluent stream indicates that the oxygen produced by the decomposition of nitrous oxide is accumulatively adsorbed on the catalyst surface until a new steady state is attained. These results clearly indicate that the oxygen adsorbed on the surface inhibits the reaction, and that N_2O can decompose only on sites which are free from adsorbed oxygen. In support of this, the effect of oxygen on the rate of N_2O decomposition was examined and the results were shown in Figure 3. The presence of oxygen in the gas phase markedly inhibited the reaction substantiating that the sites which are active for the N_2O decomposition reaction are also active for the adsorption of oxygen. The instantaneous maximum in the N_2O-N_2 response curve, therefore, can be attributed to the high concentration of vacant sites in the initial steady state in the helium stream, and the steep decrease which follows will be caused by blocking of active sites with accumulatively adsorbed oxygen.

Since gaseous nitrous oxide decomposes directly on the active

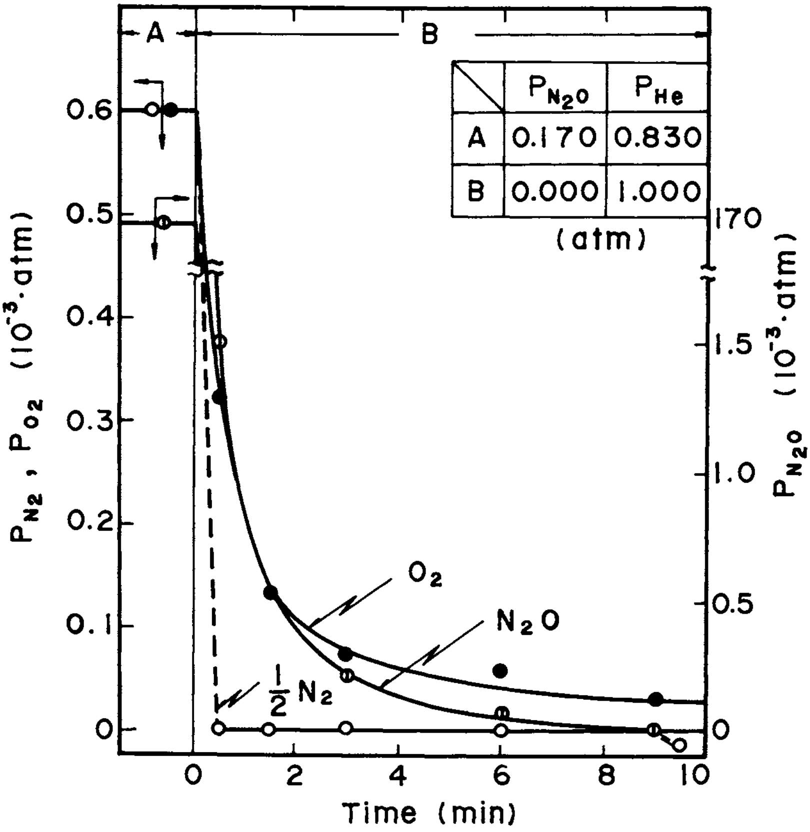

Figure 1. N_2O(dec. O)–N_2, O_2, N_2O response on CuO at 256°C.

In Catalysis Under Transient Conditions; Bell, A., et al.;
ACS Symposium Series; American Chemical Society: Washington, DC, 1982.

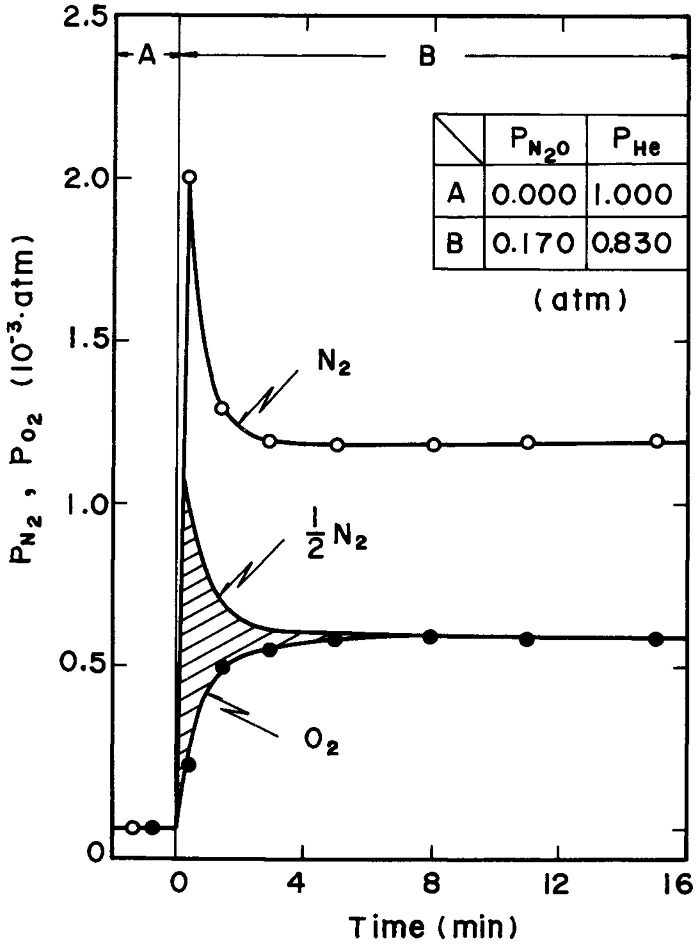

Figure 2. N_2O(inc. O)–N_2, O_2 response on CuO at 256°C.

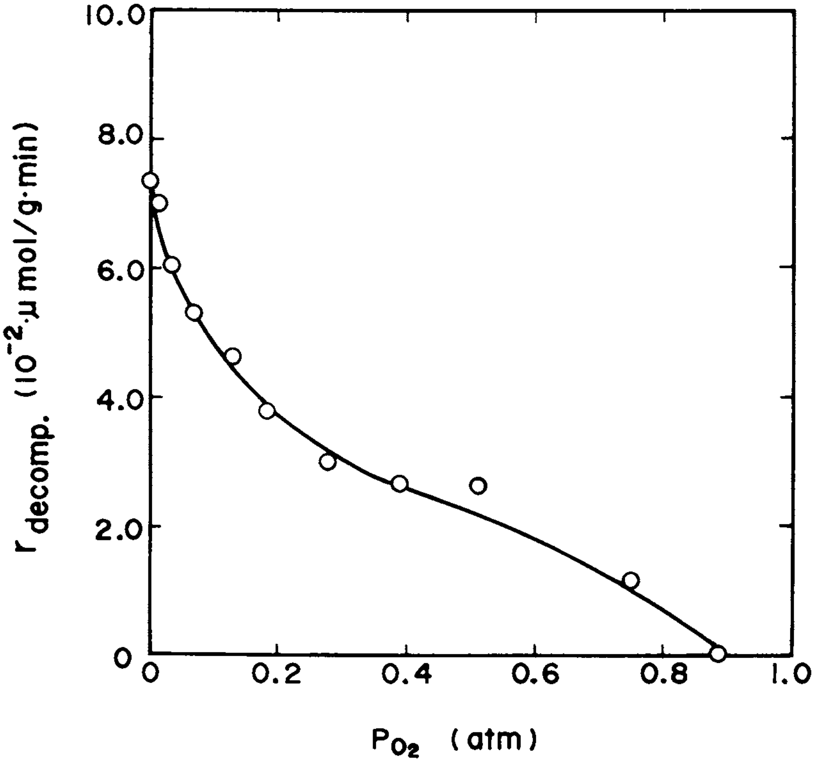

Figure 3. Effect of oxygen on the rate of decomposition on CuO at 256°C and P_{N_2O} 0.113.

sites and the nitrogen produced is not adsorbed on the surface, the N_2O-N_2 response curve will represent the decomposition rate of nitrous oxide at each instance. Therefore the graphical integration of the N_2O-N_2 response curve up to the new steady sate gives the total amount of nitrogen produced by the reaction, and hence the amount of oxygen produced by the reaction can be easily estimated by a stoichimetric relationship. The analogous graphical integration of N_2O-O_2 response curve, on the other hand, will give the amount of oxygen desorbed from the catalyst surface. The difference of those amounts of oxygen gives the amount of retained oxygen on the surface in excess to that at initial steady state, and this procedure is visualized in Figure 2. The amounts of adsorbed oxygen at steady states thus estimated in the stream of various partial pressure of nitrous oxide, as designated as $q^{re}(O_2)$, were plotted against corresponding partial pressure of nitrous oxide in the inlet stream. The results are shown in Figure 4 together with the amounts of adsorbed N_2O at steady states which were estimated by the graphical integration of N_2O (dec.,0)-N_2O curves. The measurements of isothermal adsorption of oxygen on the same catalyst were accomplished in separate experiments and the equilibrium amounts of adsorbed oxygen, $q^{eq}(2)$, are also plotted in the same figure. The corresponding oxygen pressure on the abscissa were so chosen that the oxygen pressure is equal to the average partial pressure of oxygen across the catalyst bed curing the reaction with the inlet concentration of the corresponding partial pressure of nitrous oxide on the abscissa. Since the adsorption of gaseous oxygen on this catalyst was revealed to be dissociative at 256°C and obeyed the Langmuir isotherm, the maximum amount of adsorption can be easily estimated. Based on this value, the fraction of vacant site, θ_V, was also estimated at various P_{N_2O} and plotted in the same figure.

It can be seen from the figure that the $q^{re}(O_2)$ is much higher than $q^{eq}(O_2)$, which strongly suggests that the desorption of oxygen from the catalyst surface is the slowest step in this reaction.

According to the results obtained above, the following mechanism seems to be reasonable for this reaction. This mechanism, in which oxygen desorption is the slowest step, has been suggested by many investigators.

$$N_2O + e^- \text{ (from catalyst)} \rightarrow N_2 + O^- \text{ (ads)} \quad (1)$$

$$2\,O^- \text{ (ads)} \rightleftarrows O_2 + 2\,e^- \text{ (to catalyst)} \quad (2)$$

As has been noticed above nitrogen was not produced unless N_2O existed in the gas phase even though the adsorbed N_2O existed on the surface. This fact may imply the possibility of the following steps which have been suggested by several investigators.

$$N_2O + O^- \text{ (ads)} \rightarrow N_2 + O_2 + e^- \text{ (to catalyst)} \quad (3)$$

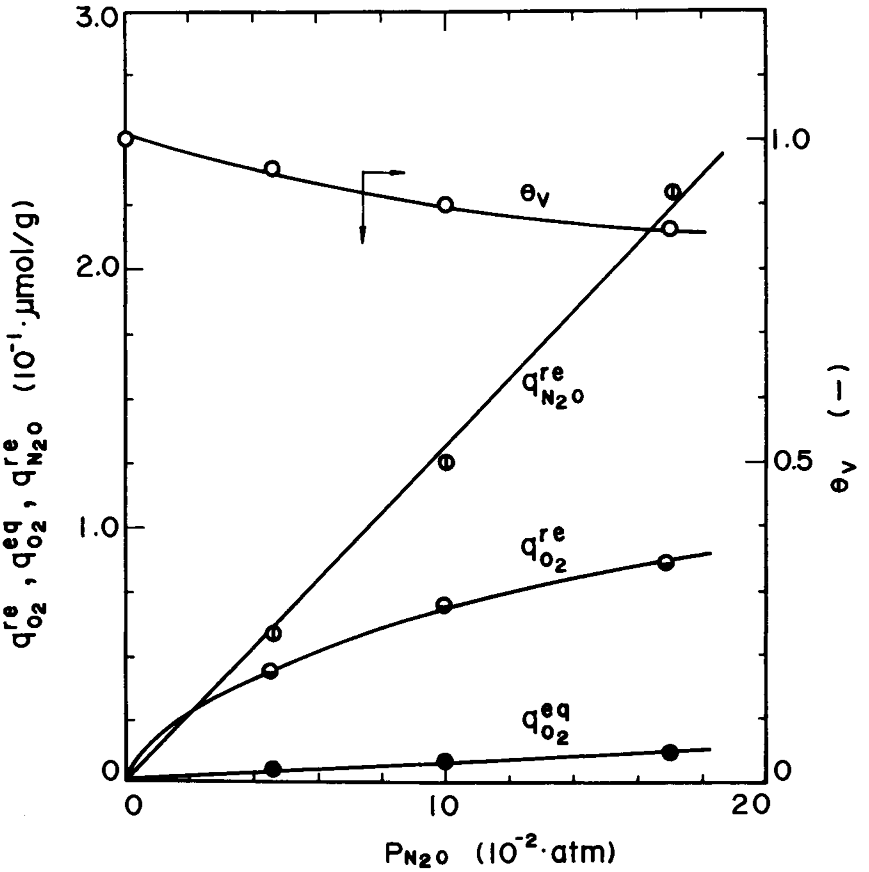

Figure 4. Amounts of adsorbed O_2 $q^{re}(O_2)$ and N_2O $q^{re}(N_2)$ during the reaction and equilibrium amount of adsorbed O_2 $q^{eq}(O_2)$ obtained by O_2 adsorption at 256°C. θ_V is the vacant fraction of active sites during the reaction at steady state on CuO.

$$N_2O + N_2O^- \text{ (ads)} \rightarrow N_2 + O_2 + e^- \text{ (to catalyst)} \qquad (4)$$

For the examination of the possibility of these reactions, the reaction rates were examined kinetically by using the values of θ_V, $q^{re}(N_2O)$ and $q^{re}(O_2)$ which have been estimated from the results of transient response measurements. Since there are three possible reaction routes (1), (3) and (4), the reaction rates as measured by the formation rates of nitrogen can be tested by checking the fitness of rate equations developed for these different reaction routes. These rate equations are :

$$r_{decomp.}\ (1) = k_1 P_{N_2O} \bullet \theta_V \qquad (5)$$

$$r_{decomp.}\ (3) = k_3 P_{N_2O} \bullet q^{re}(O_2) \qquad (6)$$

$$r_{decomp.}\ (4) = k_4 P_{N_2O} \bullet q^{re}(N_2O) \qquad (7)$$

In Figure 5 were shown the relationships between $r_{decomp.}$ and P_{N_2O} and $P_{N_2O} \bullet \theta_V$. A fairly good linear relation between $r_{decomp.}$ and $P_{N_2O} \bullet \theta_V$ is seen and this will also support the above conclusion that the decomposition of nitrous oxide proceeds though reaction (1). If reaction (3) or (4) is taking place, judging from the relationship between $r_{decomp.}$ and P_{N_2O} in Figure 5, $q(O_2)$ and $q(N_2O)$ should decrease with increasing P_{N_2O}. But this is not the case as can see from Figure 4. This will exclude the possibility of reaction (3) and (4).

It will, therefore, be plausible to conclude that the decomposition of nitrous oxide on CuO is taking place predominantly through the reaction step (1) with the desorption of oxygen as the slowest step.

MgO Catalyst. A charge of 42.6 g MgO catalyst was used in this experiment and kinetic measurements were made at 409°C. The response of a MgO catalyst equilibrated with helium stream to a step inflow of nitrous oxide was followed by monitoring N_2 and O_2 in the downflow stream and the results were presented in Figure 6.

As can be seen from the figure, the shape of the response curve of nitrogen is quite different from that obtained with a CuO catalyst, which showed a typical overshoot-type response. In the case of MgO, on the contrary, N_2 response showed a typical monotonic increasing response in the same fashion with that of oxygen. In this case, however, the time required to attain steady state is much shorter than in the case of CuO. Taking into account the fact that nitrogen can not be adsorbed on the catalyst surface, the lag in attaining steady state would suggest the slow adsorption of nitrous oxide. The ratio of evolved nitrogen and oxygen was approximately equal to the stoichiometric ratio indicating that the oxygen can scarcely be adsorbed on the surface or the adsorbed amount must be very small if any.

Figure 7 represents the results of N_2O(dec.,O)-N_2,O_2,N_2O

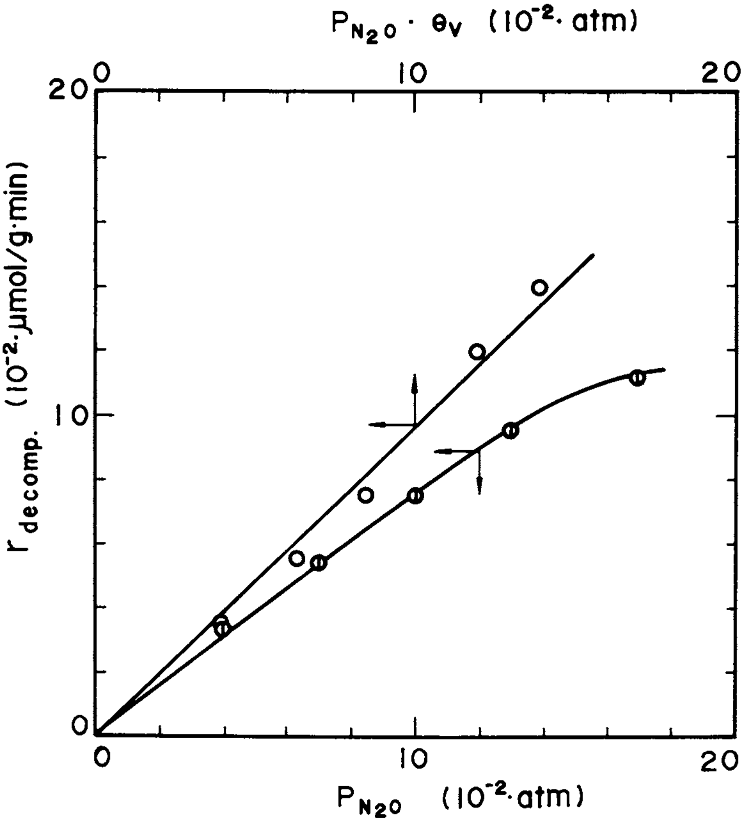

Figure 5. Relationship between the rate of decomposition and $P_{N_2O} \cdot \theta_V$ or P_{N_2O} at 256°C.

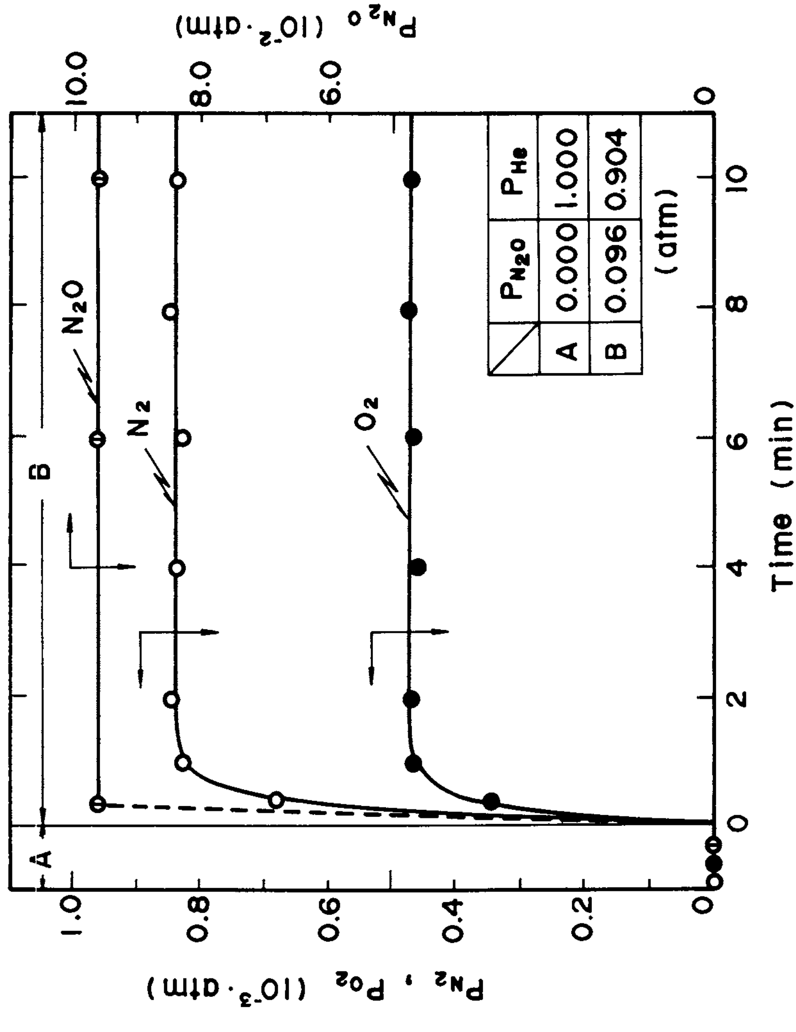

Figure 6. N_2O(inc. O)–N_2, O_2, N_2O response on MgO at 409°C.

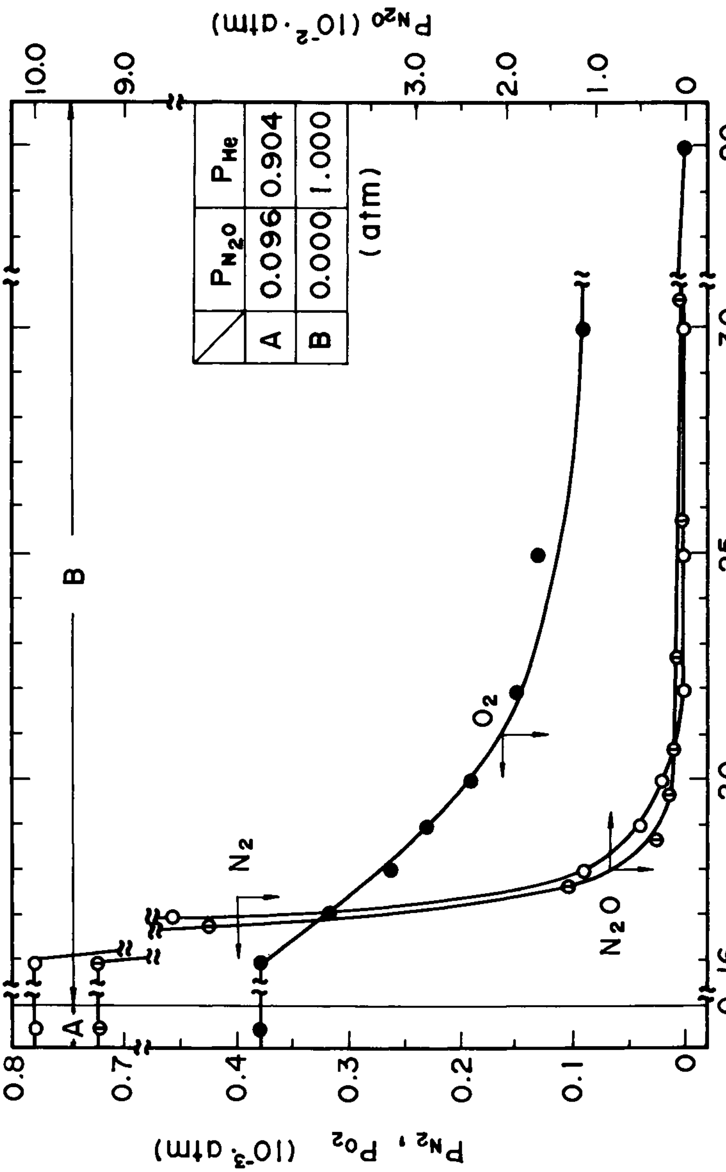

Figure 7. N_2O(dec. O)–N_2, O_2, N_2O response on MgO at 409°C.

response. Transient periods for these species were extremely short compared to those on CuO and this is clearly indicating the very small adsorption amounts of these species on the MgO catalyst in the stationary state of the reaction. It should be worth noted in this case that the evolution of nitrogen was observed even without nitrous oxide in the gas phase and that the evolution of both nitrogen and nitrous oxide ceased simultaneously. This fact strongly suggests that nitrous oxide decomposes after once adsorbed on the surface.

Since nitrous oxide was cut off from the feed stream, the sum of evolved nitrous oxide and nitrogen is equal to the adsorbed amount of nitrous oxide on the catalyst in stationary state of the reaction. This amount is extremely small compared to that on CuO and this fact also implys that the adsorption of nitrous oxide could be the slowest step in the overall reaction of nitrous oxide decomposition on MgO.

A linear relationship was observed between P_{N_2O} and the rates of decomposition as is shown in Figure 8.

The values of $q^{re}(N_2O)$ were estimated from the N_2O(dec.,0)-N_2O response curve and were plotted against $r_{decomp.}$ as shown in Figure 9. As can be seen from the figure, the data were plotted almost in a linear form and the slope is approximately equal to 2.

These kinetic relationships suggest the following reaction mechanism including the adsorption of nitrous oxide as the slowest step.

$$N_2O + e^- \text{ (from catalyst) } \rightleftarrows N_2O^- \text{ (ads)} \quad (8)$$

$$2\ N_2O^- \text{ (ads)} \rightarrow 2\ N_2 + 2\ O^- \text{ (ads)} \quad (9)$$

$$2\ O^- \text{(ads)} \rightleftarrows O_2 + 2\ e^- \text{ (to catalyst)} \quad (10)$$

Discussion

Reaction mechanisms which are capable of explaining the experimental results on CuO and MgO are represented by Equations (1) and (2) for CuO and Equations (8),(9) and (10) for MgO.

In the experiments of transient response on CuO catalyst, it was found that no nitrogen was produced even with the adsorbed nitrous oxide still present on the surface. Although direct evidence was not provided in this study, based on the results and discussion presented by London and Bell (9), we inclined to believe that nitrous oxide adsorbed on sites through its nitrogen end will meet the steric problems in splitting N-O bond to produce nitrogen leaving an oxygen atom on the surface. When nitrous oxide hit the surface sites with its oxygen, on the other hand, this configuration does not meet such steric difficulties but may lead to the rapid breaking of N-O bond by facilitating the addition of electron from the catalyst which is necessary for weakening the bond due to the higher electronegativity of oxygen.

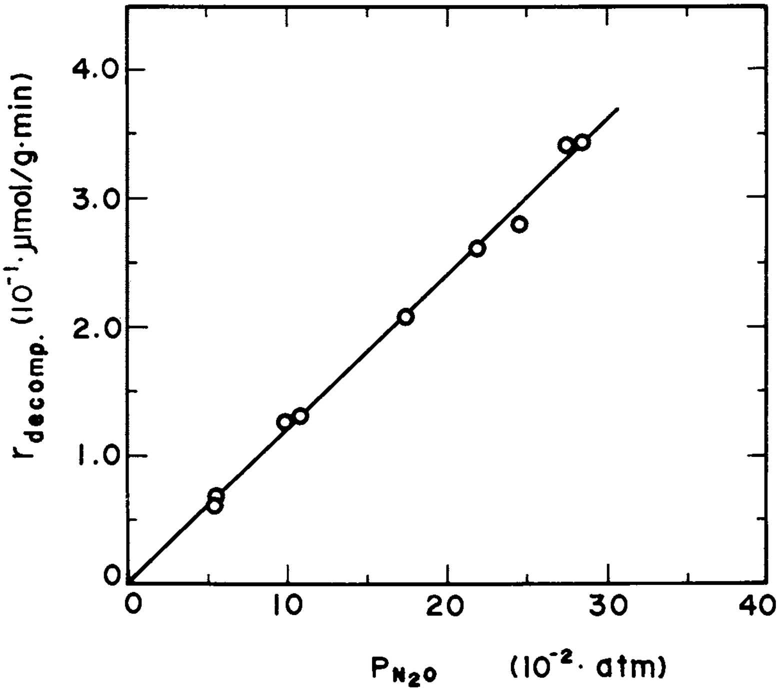

Figure 8. Relationship between P_{N_2O} and the rate of decomposition at steady state on MgO at 412°C.

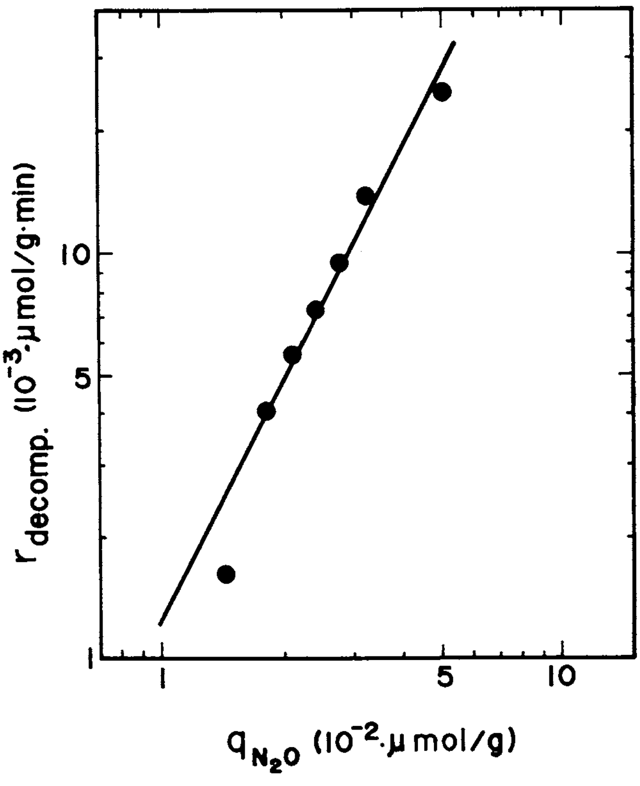

Figure 9. Relationship between the amount of adsorbed nitrous oxide and the rate of decomposition at steady state on MgO at 409°C.

The faster desorption of nitrous oxide than oxygen as shown in Figure 1 may also be explained by this interpretation because the adsorption of nitrous oxide through its nitrogen end would be weaker than adsorption through its oxygen end as had been pointed out by Zecchina, Cerruti and Borello for adsorption of N_2O on Chromia (10).

London and Bell (9) have concluded in their study on the reaction between NO and CO over copper oxide that Cu^+ rather than Cu acts as the receipient of the oxygen atom produced by the dissociation of nitrogen oxide while Cu serves as the adsorption sites for nitrogen oxide through nitorgen end. In our experiments, however, there was no reducing reagent such as CO in their experiments, and hence the oxidation state of the catalyst would be different from that in their experiments. Therefore the further investigation would be necessary to see whether or not the valency state of copper plays a role in acting either as an active site for the decomposition of nitrous oxide or just as a site for the adsorpiton of nitrous oxide.

Relatively little has been done about the kinetics and mechanism of this reaction on MgO. Cimino and Indovina (11) and Cimino and Pepe (12) have investigated the decomposition of nitrous oxide on transient metal ions dispersed in MgO and suggested the possible role of the MgO matrix surface in releasing oxygen. They drew attention to the peroxide ion, which had been known to be formed on MgO and was posturated by Dowden (13) and by Birkley and Stone (14) to be responsible for the oxygen migration on the surface which leads to the desorption of oxygen. However, little has been discussed about the contribution of MgO surface to the adsorption or the decomposition step of nitrous oxide.

Vijh (6) has suggested more recently that if one assumes the adsorbed species formed in this reaction to be a covalent one, the available data can be interpreted in terms of the Sabatier-Balandin views on heterogeneous catalysis. According to his interpretation, he has indicated a volcanic relationship between the catalytic activity (defind as the temperature at which the reaction first becomes appreciable) against the heat of formation per equivalent of the oxide catalyst, ΔH_e. Based on this volcanic relationship, he has concluded that the rate-determining step (r.d.s.) of the reaction on the oxide catalysts such as CiO, NiO and CoO probably involves rupture of a M-O bond. On the other hand, r.d.s. on oxides such as MgO, CaO and CeO_2 would involve the formation of a M-O bond.

The desorption of oxygen which was suggested as the slowest step on CuO catalyst is the rupture of a M-O bond in its nature and the adsorption of nitrous oxide through oxygen end which was suggested as the slowest step on MgO catalyst is the formation of a M-O bond. Therefore, the results we have obtained in the present study appears to be consistent to the conclusion proposed by Vijh.

As has been discussed by Vijh (15) and Vijh and Lenfant (16),

In Catalysis Under Transient Conditions; Bell, A., et al.;
ACS Symposium Series; American Chemical Society: Washington, DC, 1982.

the activity seems to be related volvanically to the band gaps of the oxides and this would tend to emphasize the importance of semiconductivity as has been suggested by previous investigation (4).

Conclusions

The decomposition of nitrous oxide on CuO proceeds by the following reaction steps involving the desorption of oxygen as the slowest step.

$$N_2O + e^- \text{ (from catalyst)} \rightarrow N_2 + O^- \text{ (ads)}$$

$$2\ O^- \text{ (ads)} \rightleftarrows O_2 + 2\ e^- \text{ (to catalyst)}$$

The reaction on MgO, on the other hand, proceeds by the following mechanism involving the adsorption of nitrous oxide as the slowest step.

$$N_2O + e^- \text{ (from catalyst)} \rightarrow N_2O^- \text{ (ads)}$$

$$2\ N_2O^- \text{ (ads)} \rightarrow 2\ N_2 + 2\ O^- \text{ (ads)}$$

$$2\ O^- \text{(ads)} \rightleftarrows O_2 + 2\ e^- \text{ (to catalyst)}$$

The mechanisms suggested in this study are consistent with that proposed by Vijh.

Literature Cited

1. Schwab, G. M. Z. Phys. Chem. 1938 25, 411, 418.
2. Wagner, C.; Hauffe, K. J. Chem. Phys. 1950, 18, 69.
3. Schmid, G. ; Keller, N. Naturwissenschaften 1950, 37, 43.
4. Dell, R. M. ; Stone, F.S.; Tiley, P. F. Trans. Faraday Soc. 1953, 49, 201.
5. Winter, E. R. S. Advance in Catal. 1958, 10, 232.
6. Vijh, A. K. J. Catal. 1973, 31, 51.
7. Kobayashi, H.; Kobayashi, M. Cat. Rev.-Sci. Eng. 1974, 10, 39.
8. Kobayashi, M.; Kobayashi, H. J. Catal. 1972, 27, 100.
6. London, J. W.; Bell, A. T. J. Catal. 1973, 31, 96.
10. Zecchina, A.; Cerrti, I.; Borello, F. J. Catal. 1972, 25, 55.
11. Cimino, A.; Indovina, V. J. Catal. 1970, 17, 54.
12. Cimino, A.; Pepe, F. J. Catal. 1972, 25, 362.
13. Dowden, D. A. Catal. Rev.-Sci. Eng. 1971, 5, 1.
14. Birkley, R. I.; Stone, F. S. Trans. Faraday Soc. 1968, 64, 3393.
15. Vijh, A. K. J. Catal. 1973, 28, 329.
16. Vijh, A. K.; Lenfant, P. Can. J. Chem. 1971, 49, 809.

RECEIVED July 28, 1981.

8

Transient and Steady-State Vapor Phase Electrocatalytic Ethylene Epoxidation

Voltage, Electrode Surface Area, and Temperature Effects

MICHAEL STOUKIDES and COSTAS G. VAYENAS

Massachusetts Institute of Technology, Department of Chemical Engineering, Cambridge, MA 02139

The catalytic activity and selectivity of polycrystalline silver catalysts used for ethylene epoxidation can be affected significantly by electrochemical O^{2-} pumping. This new phenomenon was studied in the solid electrolyte cell

$$C_2H_4,C_2H_4O,CO_2,O_2,Ag|ZrO_2(Y_2O_3)|Ag,air$$

at temperatures between 300° and 420° and atmospheric pressure. In the present communication we report on the effects of voltage, temperature and electrode surface area on the transient and steady-state behavior of the system. The change in the rate of C_2H_4O production can exceed the rate of O^{2-} pumping by a factor of 400 and is proportional to the anodic overvoltage both at steady state and during transients.

The catalytic epoxidation of ethylene on silver has been studied extensively over the last thirty years. The literature in this area is very broad and has been reviewed by several authors (1,2,3). In recent years considerable progress has been made towards a satisfactory understanding of the mechanism of this important and complex catalytic system.

Force and Bell have studied the infrared spectra of species adsorbed on silver during ethylene oxidation (4) and examined the relationship of these species to the reaction mechanism (5). Several authors have studied the effects of catalyst support and crystal size on activity and selectivity (6,7). Cant and Hall (8) used ^{14}C to study oxygen exchange between ethylene and ethylene oxide and found that C_2H_4O oxidation is much slower than direct CO_2 formation from ethylene oxidation in agreement with independent kinetic studies (1,6,12). Recent UHV studies have shown conclusively that CO_2 is the only product of C_2H_4 reaction with atomic oxygen (9) in agreement with previous studies on the interaction of N_2O and ethylene on silver (10). Kinetic measurements in a well mixed reactor have been recently combined with simultaneous in situ measurement of the thermodynamic activity of oxygen on

0097-6156/82/0178-0181$07.00/0
© 1982 American Chemical Society

porous silver catalyst films (11,12). These results showed that thermodynamic equilibrium is not generally established between gaseous and surface oxygen during reaction and provided some additional evidence for the existence of at least two active adsorbed oxygen species (12) in agreement with previous work (2). However even one type of adsorbed oxygen only suffices to explain many of the existing results (5) and there is considerable uncertainty about the exact nature of surface and subsurface oxygen on silver during reaction (2,9). There is some evidence for surface oxide formation from the work of Seo and Sato (13) who observed a continuous exo-electron emission during reaction which parallels the rate of ethylene oxide production.

Despite the existing uncertainty about the exact nature of the oxygen species present during reaction several different approaches have been reported which lead to an increase in the selectivity to ethylene oxide. These include alloying silver with other metals (14) and using different catalyst supports and various promoters (6,15). It is also known and industrially proven that the addition of few PPM of chlorinated hydrocarbon "moderators" to the gas feed improves the selectivity to ethylene oxide but decreases the catalyst activity (15). It has also been found recently by Carberry et al that selectivity increases with γ-irradiation of the catalyst (16).

In a recent communication a new electrochemical technique was described for altering the intrinsic activity and selectivity of silver for ethylene epoxidation (17). The new technique utilizes a stabilized zirconia solid electrolyte cell with a porous silver film electrode exposed to ethylene/O_2 mixtures and functioning both as an electrode and as a catalyst for ethylene epoxidation (Fig. 1). When the circuit is open the silver film acts as a regular catalyst for ethylene epoxidation. When the circuit is closed and an external voltage V is applied to the oxygen concentration cell, O^{2-} is pumped electrochemically to the silver catalyst through the zirconia electrolyte. The activity of oxygen species on silver can thus be altered dramatically. This was shown to cause a significant change in catalyst activity and selectivity (17). It was found that both catalyst activity and selectivity increase when O^{2-} is pumped to the catalyst and decrease when O^{2-} is electrochemically pumped from the catalyst by reversing the applied voltage. It was also found that the increase in the rate of ethylene oxide production can exceed the rate of O^{2-} transport through the electrolyte by a factor of 400. This increase varies linearly with applied current i for low values of current density (<30 $\mu A/cm^2$) and becomes independent of i for current densities exceeding roughly 50 $\mu A/cm$. The relaxation time constants of the system showed conclusively that the new phenomenon is due to some type of surface rather than bulk oxidation of the silver crystallites (17).

In the present communication we establish the effect of cell voltage, temperature and catalyst-electrode surface area on the

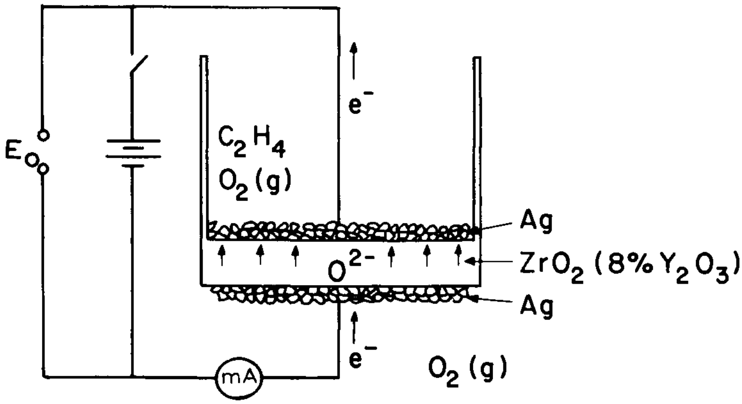

Figure 1. Schematic diagram of the cell reactor.

transient and steady-state behavior of the system. It will be shown that the increase in the rates of ethylene oxide and CO_2 production is proportional to the cell overvoltage ΔV both during transients and at steady state. The implications of this observation upon the reaction mechanism will be discussed.

Zirconia cells similar to the ones employed in the present study, have been used i) by Mason et al (18) to electrochemically remove oxygen from Pt and Au catalysts used for NO decomposition. It was shown that electrochemical oxygen pumping causes a dramatic increase in the rate of NO decomposition (18,19), ii) by Farr and Vayenas to electrochemically oxidize ammonia and cogenerate NO and electrical energy (20,21), iii) by Vayenas et al (11,12,22,23) to study the mechanism of several metal catalyzed oxidations under open circuit (potentiometric) conditions.

The anodic oxidation of ethylene in a low temperature aqueous electrolyte electrochemical cell has been studied by Holbrook and Wise (24). It was found that product selectivity (carbonate, vs. ethylene glycol) depends on the potential of the silver anode.

Experimental Methods

The experimental apparatus has been described in detail elsewhere (11,12,22). In previous communications we have also described the porous silver catalyst film deposition and characterization procedure (11,12). Ten different reactor-cells were used in the present investigation. The cells differed in the silver catalyst surface area as shown in Table I. Catalysts 2 through 5 had been also used in a previous study (17). The reactor-cells also differed in the zirconia electrolyte thickness which could not be measured accurately. The electrolyte thickness varies roughly between 150 and 300 μm.

All reactor-cells used had a volume of 30 ml and have been shown to be well mixed over the range of flowrates employed in the present study (22). Both external and internal mass and heat transfer limitations have been shown to be negligible (12,22). Reactants were certified standards of ethylene diluted in N_2 and Matheson zero grade air. They could be further diluted in N_2. Reactants and products were analyzed by one line Gas Chromatography. The carbon dioxide concentration in the product stream was also continuously monitored using a non-dispersive IR CO_2 Analyzer (Beckman 864).

All runs reported here were done galvanostatically, i.e. by maintaining the imposed current constant and monitoring the cell voltage. Constant currents were applied to the cell using an AMEL 594 galvanostat.

Table I

Catalyst-electrode surface areas

Reactor - Cell #	Reactive oxygen uptake Q (moles O_2)
RC 2	$2.3\cdot10^{-7}$
RC 3	$.4\cdot10^{-7}$
RC 4	$2.5\cdot10^{-7}$
RC 5	$20.\cdot10^{-7}$
RC 6	$6.5\cdot10^{-7}$
RC 7	$9.4\cdot10^{-7}$
RC 8	$5.2\cdot10^{-7}$
RC 9	$.4\cdot10^{-7}$
RC 10	$10.\cdot10^{-7}$
RC 11	$2.6\cdot10^{-7}$

Results

The pure anionic conductivity of the zirconia electrolyte was verified by passing through the reactor-cell mixtures of O_2, N_2 and He of known P_{O_2} and observing close agreement ($\pm$2mV) between measured and theoretical emf values. However when ethylene /O_2 mixtures are fed to the reactor the open circuit emf E which reflects the oxygen activity a_O^2 on the catalyst (11,12) according to

$$E = \frac{RT}{4F} \ln a_O^2 /(.21) \quad (1)$$

takes values between -10 and -80 mV, indicating that $a_O^2 < P_{O_2}$. This implies that thermodynamic equilibrium is not established in general between gaseous and adsorbed oxygen during reaction, because the intrinsic rate of oxygen adsorption is comparable to the rate of the surface oxidation step (11,12).

When a freshly calcined silver catalyst is placed on stream in an ethylene/O_2 mixture the catalyst activity and selectivity as well as the surface oxygen activity a_O change considerably during the first 10 h and approach steady state only after 30 h on stream. The selectivity usually passes through a maximum. A typical case is shown in figure 2. The catalyst activity, selectivity and oxygen activity were then found to remain practically constant over periods of several weeks. All the oxygen pumping experiments

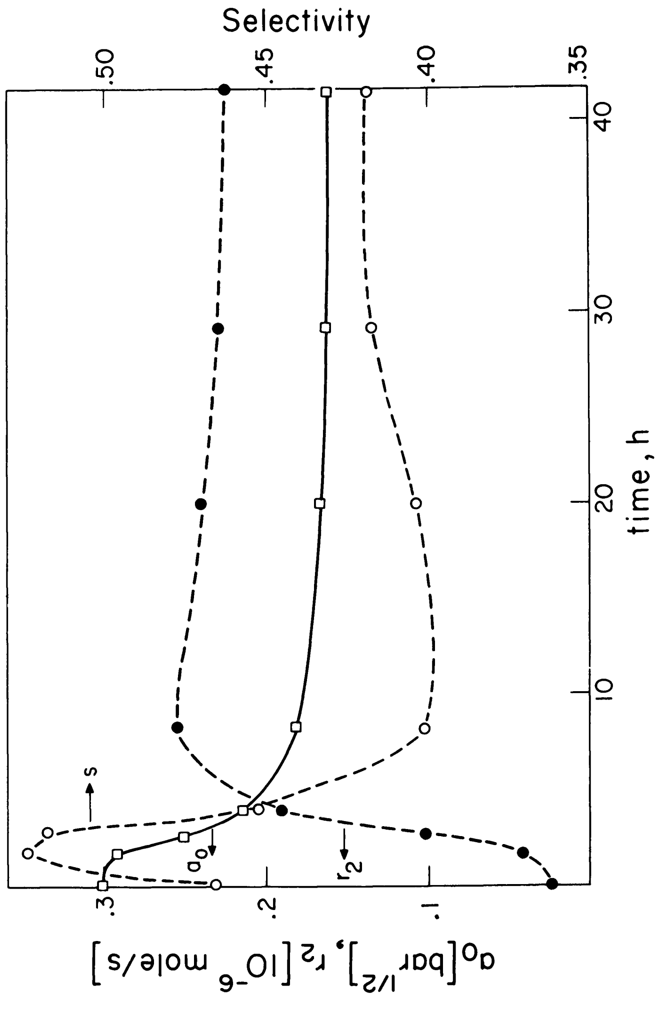

Figure 2. Transient catalytic activity, selectivity, and surface oxygen activity of a freshly calcined silver catalyst during the first 40 h on stream. Catalyst is exposed to reactive gas mixture at t = 0, 410°C, P_{ET} = 0.015 bar, and P_{O_2} = 0.10 bar.

reported here were performed after the silver catalysts had reached steady state.

The effect of electrochemical oxygen pumping on the rates of ethylene epoxidation r_1 and deep oxidation r_2 is shown in figure 3. At time t<o the circuit is open and the catalyst is at a steady state characterized by $r_{10} = 7.6 \cdot 10^{-8}$ mole/s and $r_{20} = 8.9 \cdot 10^{-8}$ mole/s. At t = o a constant current of +25 mA is applied to the cell and O^{2-} is pumped electrochemically to the catalyst at a rate $G_{O^{2-}} = i/2F = 1.3 \cdot 10^{-10}$ mole/s. If the applied voltage had no effect on the Ag catalyst and each O^{2-} pumped to the catalyst yielded one C_2H_4O molecule then the maximum expected relative increase $\Delta r_1/r_{10}$ is $G_{O^{2-}}/r_{10} = 1.7 \cdot 10^{-3}$. As figure 3 shows $\Delta r_1/r_{10}$ = .2, i.e. Δr_1 is two orders of magnitude larger than $G_{O^{2-}}$, indicating a dramatic change in the properties of the Ag catalyst. During the transient as well as at steady state the ratio $\Delta r_1/\Delta r_2$ remains practically constant at 1.7. At time t = 90 min the circuit is opened and the catalyst returns to its initial state indicating the reversibility of the phenomenon. At t = 180 min a constant current of -25 μA is applied through the cell so that oxygen is pumped from the catalyst. The rates r_1, r_2 as well as the selectivity drop. When the circuit is opened again the rates return to the original steady state values r_{10} and r_{20}.

Overvoltage effects: Figure 4 shows a typical transient cell voltage response when a constant current i is imposed to the cell at time t = 0. At t<o the cell voltage equals the open circuit emf E given by (1). The initial rapid rise at t = 0 is caused by the ohmic drop iR_c, where R_c is the ohmic resistance of the cell which is primarily due to the zirconia electrolyte resistance. The subsequent gradual increase ΔV to a final asymptotic value, corresponds to charging of the electrode-electrolyte double layers and formation of surface intermediates on the silver electrode (25). These surface intermediates must be adsorbed oxygen species, possibly surface silver oxide (17). The increase ΔV is the cell overpotential; ΔV as well as the relaxation time constant τ_o, defined as the time required for ΔV to reach 63% of its final steady state value (17,25) were both found to be strongly dependent on gas phase composition. They both vanish as P_{O_2}/P_{ET} approaches zero. It can thus be concluded that double layer charging of the electrode-electrolyte interface happens quite fastly and has a negligible contribution to the ΔV transient.

Within the accuracy of the experimental data the galvanostatic transient response of ΔV is identical to the transient rate response Δr_1 and Δr_2, i.e. $\tau_o = \tau_c$ where τ_c is the relaxation time constant for the two rates (17). This is shown in figure 5 for two different reactors under similar operating conditions and also in figure 6 where the transient and the steady state Δr_i values from four reactors are plotted vs. the cell overvoltage ΔV. In view of the fact that r_{io} is proportional to the surface area Q it follows from figure 6 that for constant gas phase composition

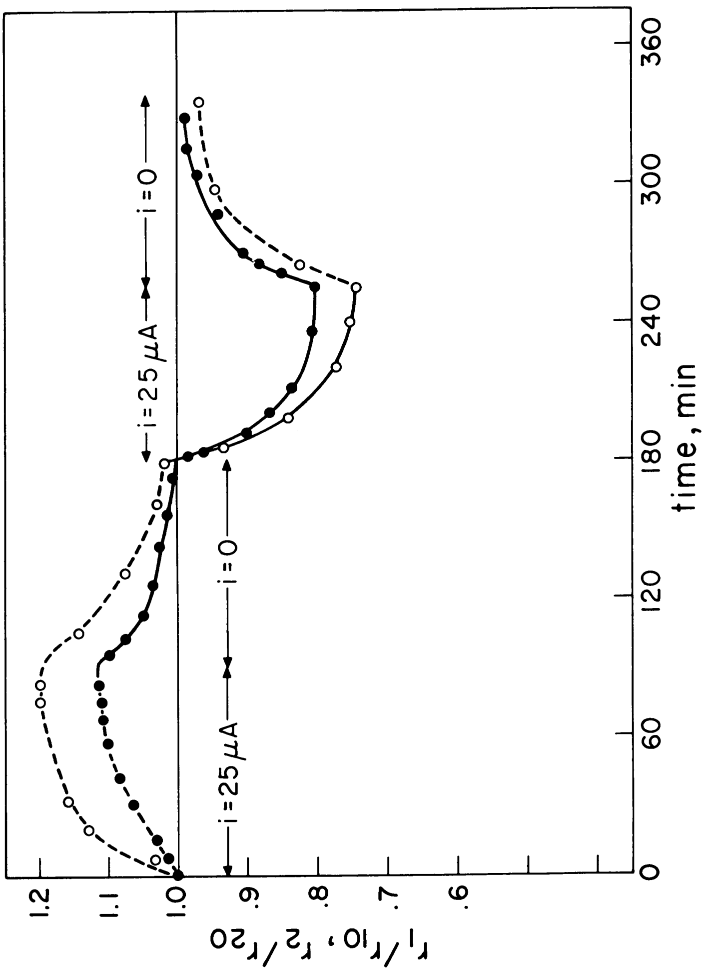

Figure 3. Transient effect of electrochemical oxygen pumping. Conditions: RC 2, P_{ET} = 1.6 × 10^{-2} bar, P_{O_2} = 9.5 × 10^{-2} bar, and 400°C.

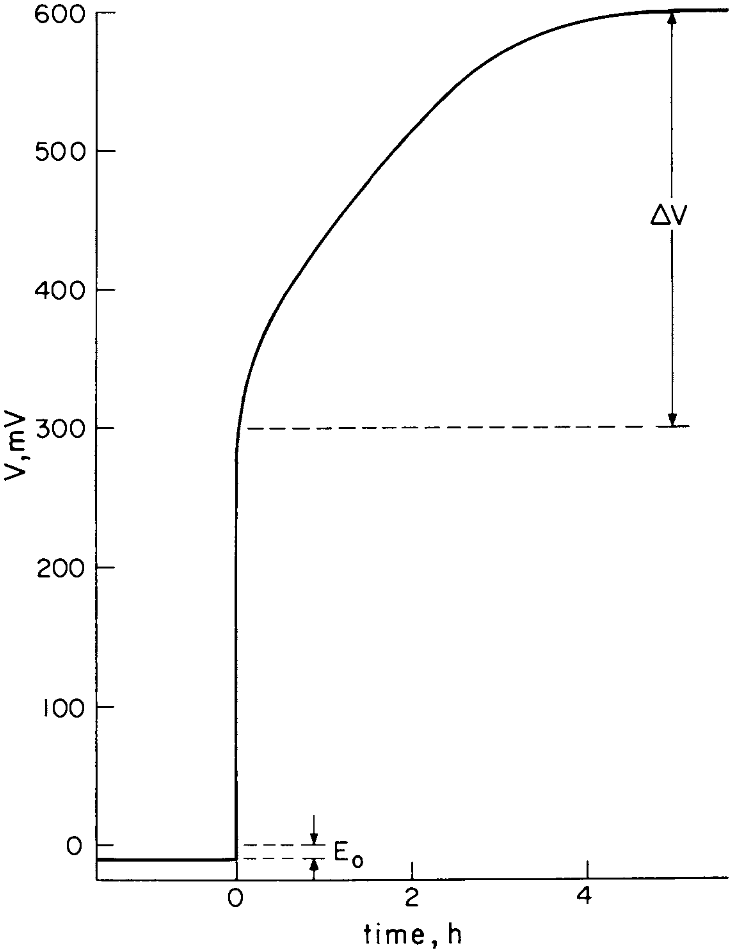

Figure 4. Transient cell voltage response when a constant current $i = +100\ \mu A$ is applied at $t = 0$, $P_{O_2} = 0.140$ bar, and $P_{ET} = 0.008$ bar. Conditions: RC 8, $i = 100\ \mu A$, and 400°C.

In Catalysis Under Transient Conditions; Bell, A., et al.;
ACS Symposium Series; American Chemical Society: Washington, DC, 1982.

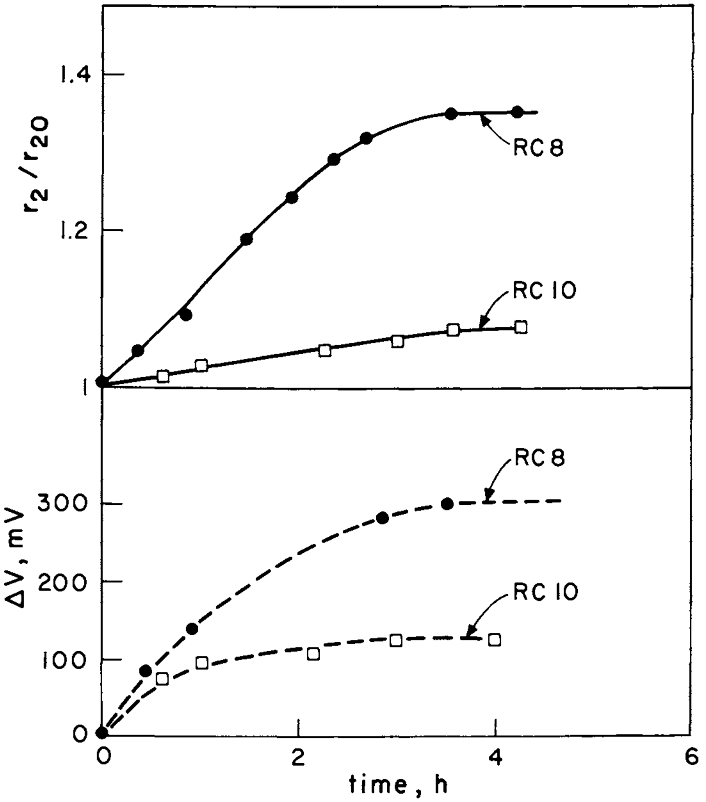

Figure 5. Galvanostatic transients of the rate of ethylene deep oxidation r_2 and of the cell overvoltage. The rate of epoxidation r_1 parallels r_2. Conditions: $i = 100\ \mu A$, $P_{O_2} = 0.14$ bar at 400°C. Key: ●, RC 8, $P_{ET} \approx 0.008$ bar; □, RC 10, $P_{ET} \approx 0.0068$ bar.

In Catalysis Under Transient Conditions; Bell, A., et al.;
ACS Symposium Series; American Chemical Society: Washington, DC, 1982.

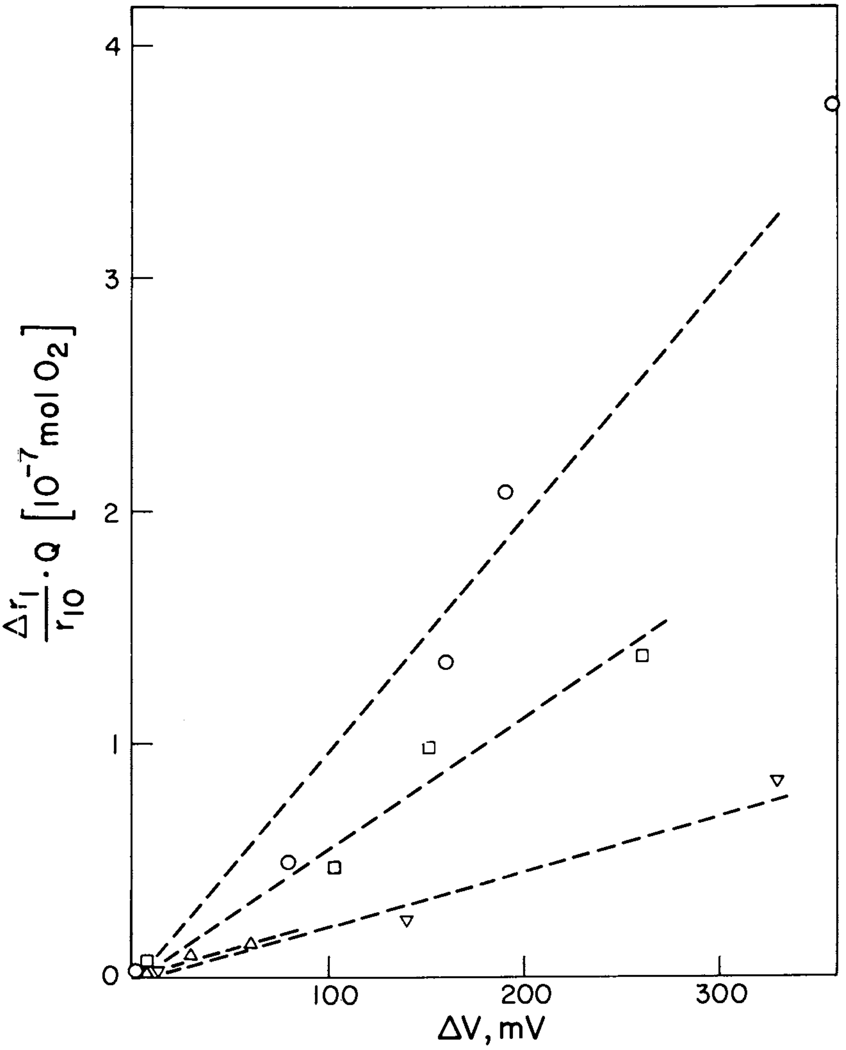

Figure 6. Overvoltage effect on the increase in the rate of ethylene epoxidation at constant gas phase composition and i = 100 μA. Key: ○, RC 7, P_{O_2}/P_{ET} ≈ 21.0, 400°C; □, RC 8, P_{O_2}/P_{ET} ≈ 12.1, 400°C; ▽, RC 9, P_{O_2}/P_{ET} ≈ 7.9, 420°C; and △, RC 10, P_{O_2}/P_{ET} ≈ 6.8, 400°C.

$$\Delta r_i \ \alpha \ \Delta V \tag{2}$$

Equation (2) is valid both during transients as well as at steady state in which case

$$(\Delta r_i)_{max} \ \alpha \ \Delta V_{max}$$

As noted earlier the increase in the rates Δr_i can exceed the rate of oxygen transport through the electrolyte $I/4F$ by more than two orders of magnitude (Fig. 7).

Gas phase composition effects: As shown in figure 6 the increase in the rates Δr_i depends not only on the overvoltage ΔV but also on gas phase composition. This has been reported also in a previous communication where $\Delta r_i/r_{io}$ as well as τ_c were found to increase with decreasing P_{ET} (17). A series of runs performed at constant P_{ET} showed that $\Delta r_i/r_{io}$ is proportional to P_{O_2}. It was then established that $\Delta r_i/r_{io}$ is proportional to P_{O_2}/P_{ET} and that all the data, transient and steady state, obtained with ten different reactors, each having different electrode surface area can be correlated in terms of one surprisingly simple equation,

$$\frac{\Delta r_i}{r_{io}} \cdot Q \cdot \frac{P_{ET}}{P_{O_2}} = \alpha_i \Delta V \tag{3}$$

where α_1, α_2 (i=1,2) are constants with a ratio $\alpha_1/\alpha_2 = 1.65 \pm .3$. This is shown in figure 8. Equation (3) contains as a limiting case equation (2) which is valid for constant gas phase composition.

It should be noted that at temperatures above 350°C r_{io} is first order in ethylene and zero order in oxygen (12), i.e.

$$r_{io} = k_{io} \cdot Q \cdot P_{ET} \tag{4}$$

It thus follows that equation (3) can be written as

$$\Delta r_i = k_{io} \cdot \alpha_i \cdot P_{O_2} \cdot \Delta V \tag{5}$$

which contains as a limiting case the observation that Δr_i vanishes when $P_{O_2} \to 0$, i.e. when the reactor is run as a fuel cell (17). Equations (3), (4) and (5) are also valid both during transients and at steady state.

Most galvanostatic transients followed a first order response with reasonable accuracy, in agreement with (25):

$$\Delta V = \Delta V_{max}(1 - e^{-t/\tau_o}) \tag{6}$$

Table II shows the dependence of τ_o on gas phase composition. For constant surface area and current the time constant τ_o is roughly proportional to $\Delta V_{max} \cdot P_{O_2}/P_{ET}$. It is also shown that τ_o

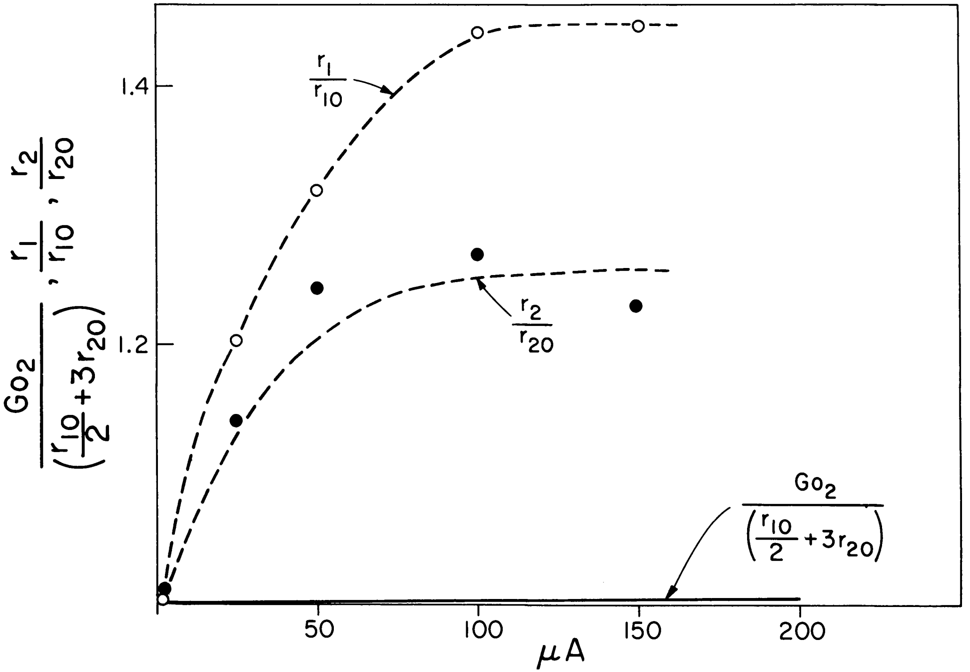

Figure 7. Effect of current on the steady-state increase in the rates of epoxidation (r_1) and deep oxidation (r_2). Comparison with the rate of oxygen transport through the electrolyte $G_{O_2} = i/4F$. Intrinsic selectivity $r_{10}/r_{20} = 0.49$. Conditions: RC 2 at 400°C, $P_{ET} \simeq 0.016$ bar, $P_{O_2} \simeq 0.1$ bar.

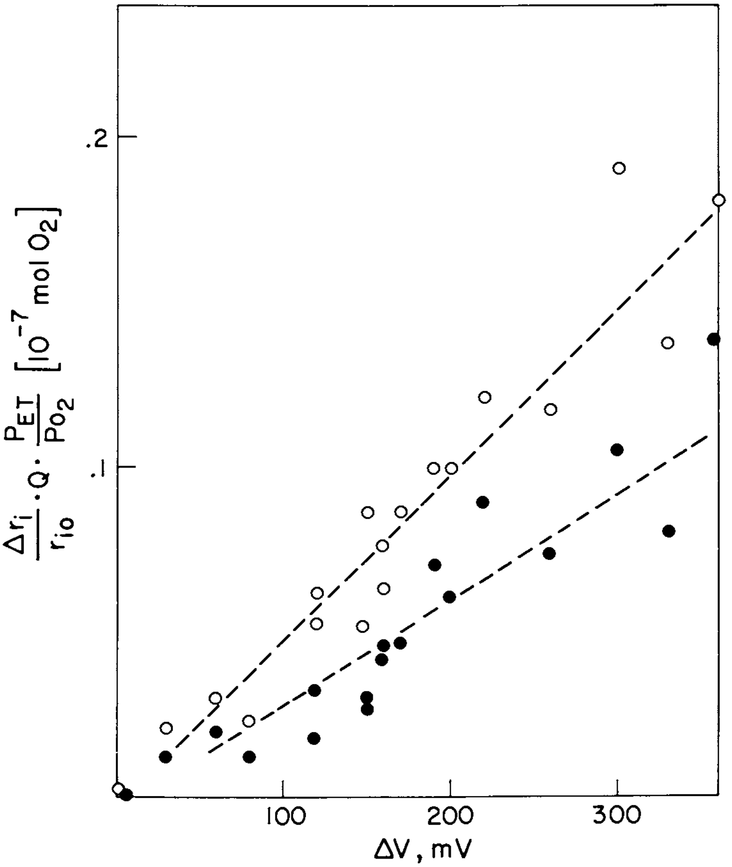

Figure 8. Overvoltage effect on the rates of ethylene epoxidation (i = 1, ○) and deep oxidation (i = 2, ●). At constant overvoltage the relative rate increases are proportional to P_{O_2}/P_{ET} at 400°C.

is proportional to $\Delta r_i/r_{io}$ in agreement with equation (3). The decrease in $\tau_c \approx \tau_o$ with increasing P_{ET} has been also reported previously (17).

Table II

Gas phase composition effect on the relaxation time constant τ_o for i=100 A and T=400°C

Reactor #	Q	P_{O_2}/P_{ET}	ΔV_{max}	r_1/r_{10}	r_2/r_{20}	τ_o
	moles O_2		mV			min
RC 8	$5.2 \cdot 10^{-7}$	17.5	300	.64	.35	150
RC 8	$5.2 \cdot 10^{-7}$	12.1	250	.27	.17	75
RC 8	$5.2 \cdot 10^{-7}$	7.9	180	.15	.09	35
RC 10	$10 \cdot 10^{-7}$	6.9	60	.02	.015	20
RC 10	$10 \cdot 10^{-7}$	20.5	160	.16	.085	130

Catalyst-Electrode Surface Area Effects: At constant temperature, gas phase composition and current, therefore constant overvoltage, the relative increase in the reaction rates $\Delta r_i/r_{io}$ is inversely proportional to the electrode surface area. This is a consequence of equation (3) and is shown in figure 9 for five different reactors. Thus in order to maximize the relative effect of oxygen pumping on r_1 and r_2, i.e. in order to maximize yield and selectivity of ethylene oxide one must minimize the electrode surface area, i.e. minimize the porous silver film thickness without causing a major decrease in its conductivity. A decrease in the electrode surface area also causes a moderate decrease in the relaxation time constant τ_c. This is shown in figure 10 which contains data from 5 reactors obtained at $P_{O_2}/P_{ET} \approx 7$ and T = 400°C and shows that $1/\tau_o$ is a linear increasing function of i/4FQ. An explanation for these observations is given in the discussion section.

Figure 11 demonstrates a problem frequently encountered during the oxygen pumping experiments. The galvanostatic transient was obtained with reactor RC9 which had the lowest electrode surface area Q(Table 1), therefore exhibited the largest relative effect $\Delta r_i/r_{io}$, i.e. a threefold increase in ethylene oxide yield and a 210% increase in CO_2 production with a corresponding 20% increasing in selectivity. As shown on the figure the constant current i = 100 μA was applied at t=o. At t=40 min and long before the reactor would reach steady state the cell resistance suddenly dropped from a few KΩ to 1-2 Ohms indicating electrolysis of the zirconia electrolyte and metallic zirconium formation. This is possible since the total cell voltage ($\Delta V + iR_c$) at t=40 min had reached approximately 2.5 V. As shown on the figure subse-

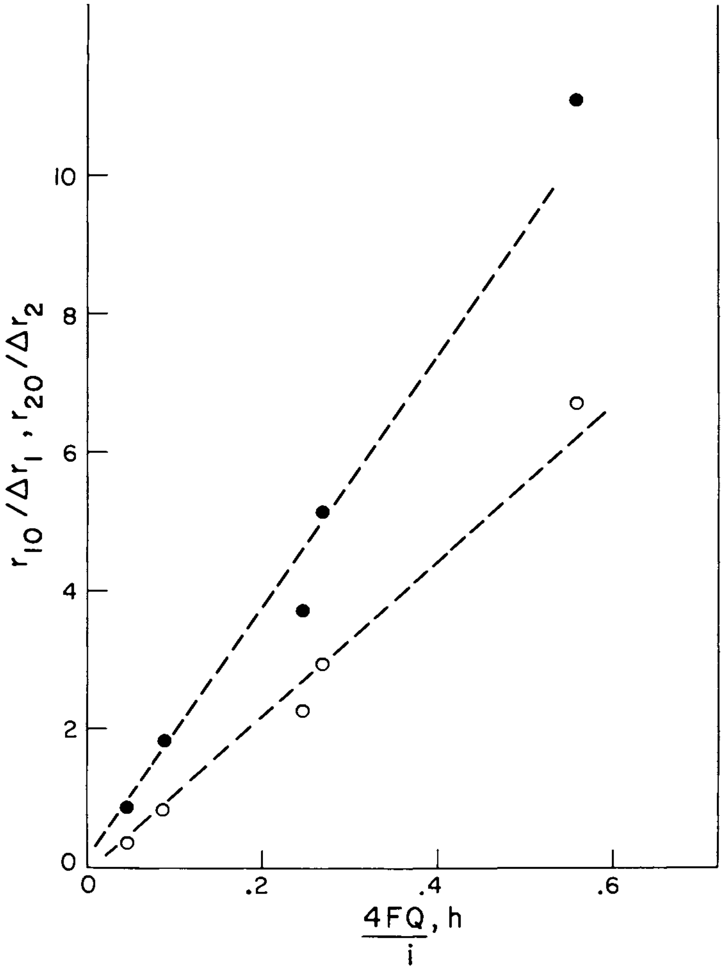

Figure 9. Effect of Ag catalyst–electrode surface area Q on the relative steady-state increase in the rates of epoxidation r_1 and deep oxidation r_2 at constant imposed current $i = 100$ μA, constant gas composition, 400°C, $P_{O_2}/P_{ET} \sim 7$. Key: ○, $r_{10}/\Delta r_1$; and ●, $r_{20}/\Delta r_2$.

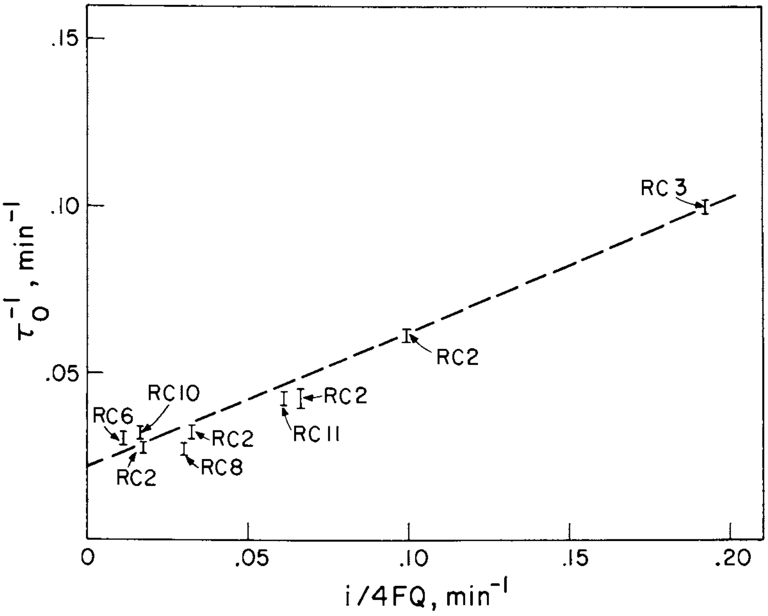

Figure 10. Effect of Ag catalyst–electrode surface area Q on the cell relaxation time constant. Conditions: 400°C, $P_{O_2}/P_{ET} \simeq 7$.

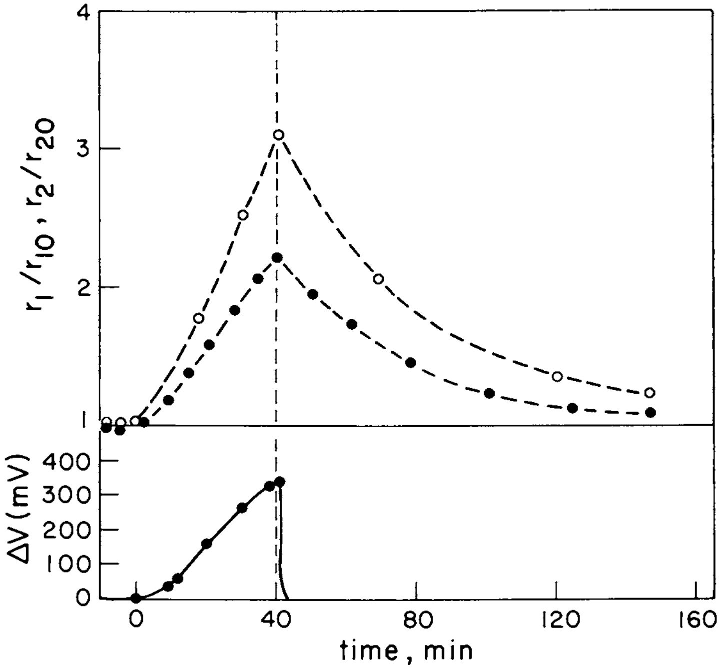

Figure 11. Transient galvanostatic response of the rates of ethylene oxidation r_1 (○) and deep oxidation r_2 (●) and of the cell overvoltage ΔV for reactor RC 9. Electrolyte breakdown occurred at 40 min. Conditions: RC 9, 420°C, $i = 100\ \mu A$, $P_{O_2} = 0.095$ bar, $P_{ET} = 0.012$ bar.

quently to the electrolyte breakdown both r_1 and r_2 slowly return towards their intrinsic values r_{10} and r_{20} since electronic rather than ionic conduction is now occuring across the cell. The cell cannot function as an oxygen concentration cell anymore since the electrolyte has been destroyed; the open circuit emf E always remains equal to zero regardless of the reactor gas composition. It was thus concluded that total voltages in excess of 2.5 V should not be applied to the cell at these relatively low temperatures.

Temperature effects: At constant current and gas composition, temperature has an interesting effect on the steady state rate increases Δr_1 and Δr_2 (Fig. 12). At temperatures below 350°C both Δr_1 and Δr_2 increase rapidly with an activation energy $E^*=33\pm3$ Kcal/mole. However at temperatures above 350°C Δr_1 and Δr_2 decrease with an apparent negative activation energy $E^{**} = 19 \pm 2$ Kcal/mole. The overvoltage ΔV decreased monotonically from 90 mV at 320°C to 3-5 mV at 400°C. It thus appears that the behavior of ΔV parallels the behavior of Δr_1 and Δr_2 at high T but not at temperatures below 350°C. A possible explanation is given in the discussion section. Figure 12 also shows that within the accuracy of the experimental data the ratio $\Delta r_1/\Delta r_2$ remains practically constant at $1.75\pm.25$ which corresponds to $.64\pm.04$ selectivity on the oxide.

Discussion

The nature of the silver catalyst is clearly altered significantly during electrochemical oxygen pumping. The increase or decrease in the rates of ethylene epoxidation and combustion is more than two orders of magnitude higher than the rate of oxygen transport through the electrolyte. The selectivity also changes considerably.

When oxygen is pumped to the catalyst the activity of oxygen on the silver catalyst-electrode increases considerably because of the applied voltage. It thus becomes possible to at least partly oxidize the silver catalyst electrode. In a previous communication it has been shown that the phenomenon involves surface rather than bulk oxidation of the silver crystallites (17). The present results establish the direct dependence of the change in the rates of epoxidation and combustion Δr_1 and Δr_2 on the cell overvoltage (Equations 2,3, and 5) which is directly related to the surface oxygen activity.

Furthermore, the observation that the transient rate change behavior parallels the transient overvoltage behavior (Figures 5, 6 and equations 2,3 and 5) proves undoubtedly that the increase or decrease in the rates is caused by a corresponding increase or decrease in the surface concentration of an adsorbed oxygen species or surface silver oxide. In a previous communication we have denoted this unknown surface oxygen species by AgO_2^* with a concentration c(moles/cm^2). There is previous evidence in the liter-

In Catalysis Under Transient Conditions; Bell, A., et al.;
ACS Symposium Series; American Chemical Society: Washington, DC, 1982.

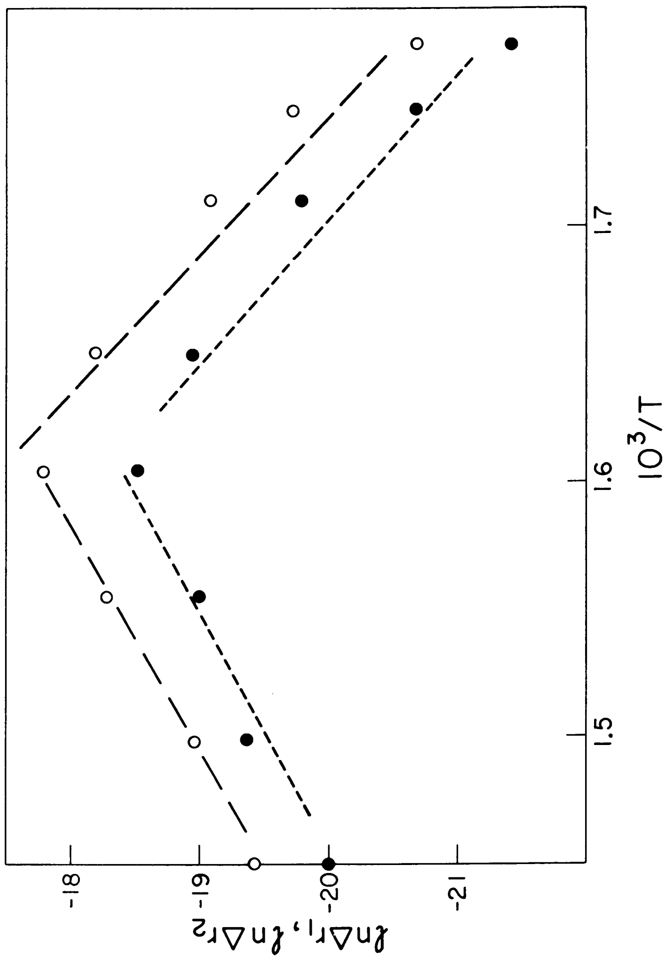

Figure 12. Temperature effect on the steady-state rate increase in Δr_1 (○) and Δr_2 (●) at constant current $i = 50$ μA and gas composition. Conditions: $P_{O_2} = 0.10$ bar, $P_{ET} = 0.015$ bar.

ature for the existence of surface silver oxides including the work of Seo and Sato (13) who observed a continuous exoelectron emission from silver catalysts during ethylene epoxidation which was proportional to the rate of ethylene oxide formation. They explained their results in terms of formation of surface silver oxide Ag_2O with molecular oxygen ion O_2^- adsorbed on it (13). This picture seems to be in excellent agreement with the present results, i.e. with equation (5)

$$\Delta r_i = k_{io} \cdot \alpha_i \cdot \Delta V \cdot P_{O_2} \tag{5}$$

if the change in the amount of surface silver oxide is proportional to ΔV and the coverage of molecular oxygen adsorbed on the oxide is proportional to P_{O_2}, or at least if the rates of epoxidation and combustion on the silver oxide are first order in oxygen.

Equations (2), (3) and (5) which describe the dependence of Δr_i on the overvoltage are extremely simple but deserve some special attention. They all indicate that Δr_i is proportional to ΔV but independent of the surface area of silver electrode. This is why the relative increase in the rates $\Delta r_i/r_{io}$ is highest for reactors with small surface area (Fig. 11) and becomes insignificant for reactors with large surface area. It thus appears that although ΔV is an intensive variable it is nevertheless a measure of the chang $S \cdot \Delta c$ in the mole number of silver oxide and not of the concentration change Δc. This is because all the reactors used had the same electrolyte area $A = 2cm^2$ as explained in detail below: Neglecting the double layer capacitance of the electrode electrolyte interface the constant current i imposed during the transient can be split in two parts (25):

$$i = C_{ad} \frac{d(\Delta V)}{dt} + i_{CTR} \tag{7}$$

where i_{CTR} is the current corresponding to the charge transfer reactions, i.e.

$$O^{2-} + C_2H_4 \rightarrow \text{Products} + 2e^- \tag{8}$$

$$O^{2-} \rightarrow 1/2\ O_2(g) + 2e^- \tag{9}$$

and C_{ad} is the adsorption pseudo capacitance of the oxide which by definition equals (25):

$$C_{ad} = \frac{dq}{dV} = \lambda \cdot F \cdot \frac{d(Sc)}{dV} \tag{10}$$

where q is the charge stored in the oxide and λ is a constant. If one assumes that Sc varies linearly with V, i.e. that the oxide pseudo capacitance is constant one obtains

$$C_{ad} = \lambda \cdot F \frac{\Delta(Sc)}{\Delta V} \tag{11}$$

The capaciatance C_{ad} depends on the gas-electrode-electrolyte interline "area" S' but not on the total electrode surface area S. If the porosity of all the electrode catalysts used is the same, which is a reasonable assumption since they were all prepared by the same calcination procedure, it follows that the interline "area" S' is proportional to the flat electrolyte surface area A, i.e. the constant λ equals $\lambda_o A$, where λ_o is another constant which does not depend on any macroscopic dimension.

$$C_{ad} = \lambda_o \cdot A \cdot F \cdot \frac{\Delta(Sc)}{\Delta V} \qquad (12)$$

Since all reactors used in the present study had the same electrolyte surface area A, it then becomes clear that they all had the same adsorption pseudo capcitance C_{ad}, therefore ΔV is proportional to $\Delta(Sc)$ as previously stated.

Quantitative kinetics: The experimental relations (2) through (5) which express the dependence of Δr_i and $\Delta r_i/r_{io}$ on ΔV and gas phase composition can now be explained in a quantitative manner in terms of a simple model which makes the same assumptions with those made in (17) but also takes into account that the change in the moles of silver oxide (Sc) caused by electrochemical oxygen pumping is directly measurable and proportional to the overvoltage ΔV. Assuming that the changes Δr_i in the rates of ethylene epoxidation r_1 and combustion r_2 are proportional to the change in the moles of AgO_2^* and that both reactions on the AgO_2^* surface are first order in oxygen one obtains

$$\Delta r_i = k_i \cdot P_{O_2} \cdot \Delta(Sc) \qquad (13)$$

Using equation (12) one obtains

$$\Delta r_i = k_i \cdot \lambda_o \cdot A \cdot F \cdot (\Delta V) \cdot P_{O_2} \qquad (14)$$

which coincides with the experimental equation (5) with $k_{io}\alpha_i = k_i \cdot \lambda_o \cdot A \cdot F$. It should be noted that according to (14) Δr_i is proportional to the electrolyte surface area A but does not depend on the electrode surface area. The experimental relation

$$\Delta r_i \propto \Delta V \qquad (2)$$

valid for constant gas phase composition is obviously a special case of (14). Finally to explain the dependence of $\Delta r_i/r_{io}$ on ΔV and gas phase composition one must assume that oxide forms on silver sites which are inactive for reaction before the oxide forms and take into account that at temperatures above 350°C and under open-circuit conditions both r_{10} and r_{20} are first order in ethylene and zero order in oxygen (12).

$$r_{io} = k_{io} \cdot Q \cdot P_{ET} \qquad (4)$$

This last equation is not inconsistent with the hypothesis that the rates on AgO_2^* are first order in oxygen to the extent that the amount of AgO_2^* is small under open circuit conditions.

Combining with equation (14) one obtains the experimental relation

$$\frac{\Delta r_i}{r_{io}} \cdot Q \cdot \frac{P_{ET}}{P_{O_2}} = \alpha_i \Delta V \qquad (3)$$

where

$$\alpha_i = \frac{k_i}{k_{io}} \cdot \lambda_o \cdot A \cdot F \qquad (15)$$

Surface area effect on the relaxation time constant: In a previous communication (17) we have developed a simple dynamic model which allows one to predict the change in the mole number of silver oxide $S \cdot \Delta c$, therefore ΔV, in terms of the imposed current, P_{O_2} and P_{ET}. The dynamic equation of the model was

$$S \cdot \theta_{O_2} \cdot \frac{dc}{dt} = \frac{i}{4F}\left(1-\frac{c}{c_M}\right)+K_1 \cdot S\theta_{O_2} \cdot (c_M - c) - K_2 \cdot S \cdot P_{ET} \cdot c \qquad (16)$$

with $\theta_{O_2} = K_{O_2}P_{O_2}/(1+K_{O_2}P_{O_2})$ (17)

i.e. the model assumed that oxide can form only on sites covered originally with molecular O_2. According to this equation the relaxation time constant of the system $\tau_c = \tau_o$ is given by

$$\frac{1}{\tau_c} = \frac{4FSC_M}{i}\left(1+\frac{1}{K_{O_2}P_{O_2}}\right)+K + \frac{K_2P_{ET}}{K_{O_2}P_{O_2}}\left(1+K_{O_2}P_{O_2}\right) \qquad (18)$$

Equation (18) is in excellent agreement with figure 10 which shows $1/\tau_c$ for 5 different reactors to be a linear increasing function of $4FQ/i$ with a positive intercept. One of the implications is that the amount of surface oxide at full coverage Sc_M is comparable to the reactive oxygen uptake Q of the catalyst.

Temperature effect: There are several ways to account for the observed maximum in Δr_i at constant gas composition and imposed current i (Fig. 12). Although the behavior shown in the figure is quite reproducible, further experimental work is required to examine the effect of gas phase composition and i on the temperature dependence of Δr_i. One possible explanation for the observed maximum can be obtained by closer examination of equation (7). The charge transfer current i can be written as $i_{CTR,A}$ + $i_{CTR,B}$ where the former term corresponds to the charge transfer reaction (8) and the latter to the charge transfer reaction (9). Using the low field law (25) one obtains

$$i_{CTR,A} = i_{O,A} \cdot F(\Delta V)/RT \qquad (19)$$

$$i_{CTR,B} = i_{O,B} \cdot F(\Delta V)/RT \qquad (20)$$

The exchange current densities $i_{0,A}$ and $i_{0,B}$ are temperature dependent and can be expressed as

$$i_{0,A} = \vec{K}_{0,A} \exp\left(-\frac{\Delta G_A^{\ddagger}}{RT}\right) \quad (21)$$

$$i_{0,B} = \vec{K}_{0,B} \exp\left(-\frac{\Delta G_B^{\ddagger}}{RT}\right) \quad (22)$$

where $\vec{K}_{0A}$, $\vec{K}_{0,B}$ are constants and $\Delta G_A^{\ddagger}$, $\Delta G_B^{\ddagger}$ are the standard Gibbs energies of formation of the activated complex for the charge transfer reactions (8) and (9).

Thus equation (7) can be written as:

$$C_{ad}\frac{d(\Delta V)}{dt} = i - \frac{F(\Delta V)}{RT}\left[\vec{K}_{0,A}\exp\left(-\frac{\Delta G_A^{\ddagger}}{RT}\right)+\vec{K}_{0,B}\exp\left(-\frac{\Delta G_B^{\ddagger}}{RT}\right)\right] \quad (23)$$

At steady state equation (23) gives

$$(\Delta V) = \frac{iRT}{F\cdot\vec{K}_{0,A}\cdot\exp\left(-\frac{\Delta G_A^{\ddagger}}{RT}\right)\cdot\left[1+\frac{\vec{K}_{0,B}}{\vec{K}_{0,A}}\exp\left(-\left(\frac{\Delta G_B^{\ddagger}-\Delta G_A^{\ddagger}}{RT}\right)\right)\right]} \quad (24)$$

If the activation energies for the epoxidation and combustion reactions on silver oxide equal E*, then the rate coefficients k_i in equations (14) can be expressed as

$$k_i = k_i^o\exp(-E^*/RT) \quad (25)$$

Combining equations (14),(24) and (25) one obtains

$$\Delta r_i = \frac{k_i^o\cdot\lambda_o\cdot A.P_{O_2}\cdot i\cdot RT\cdot\exp\left(\frac{-E^*+\Delta G_A^{\ddagger}}{RT}\right)}{1+\frac{\vec{K}_{0,B}}{\vec{K}_{0,A}}\exp\left(-\frac{(\Delta G_B^{\ddagger}-\Delta G_A^{\ddagger})}{RT}\right)} \quad (26)$$

Equation (26) predicts a maximum in Δr_i for a large number of combinations of E*, $\Delta G_A^{\ddagger}$,$\Delta G_B^{\ddagger}$. As an example the set E* = -43 Kcal/mol, $\Delta G_A^{\ddagger}$ = 10 Kcal/mol and $\Delta G_B^{\ddagger}$ = 62 Kcal/mole yields the correct experimental values for the phenomenological activiation energies of Δr_i, i.e. +33 Kcal/mol at low T and -19 Kcal/mole at high T. It should be noticed however that these phenomenological activation energies must be gas phase composition dependent since the quantities $\vec{K}_{0,A}$, $\vec{K}_{0,B}$, $\Delta G_A^{\ddagger}$,$\Delta G_B^{\ddagger}$ which appear in equation (26) will depend on the coverages of ethylene and oxygen at the gas-electrode-electrolyte three phase boundary.

Conclusions

The activity and ethylene oxide selectivity of porous polycrystalline silver catalysts can be altered significantly by using

the catalyst also as an electrode of a stabilized zirconia cell and electrochemically pumping oxygen to or from the catalyst. Oxygen pumping to the catalyst increases both activity and ethylene oxide selectivity. The opposite phenomenon is observed upon reversing the voltage polarity. The increase or decrease in the rate of ethylene oxide and CO_2 production can be at least two orders of magnitude higher than the rate of oxygen transport through the electrolyte.

The relative increase $\Delta r_i/r_{io}$ in the rates of epoxidation (i=1) and combustion (i=2) is proportional to A/S, where A is the electrolyte surface area and S is the surface area of the silver catalyst electrode. Thus with a reactor having a low value of S (reactive oxygen uptake Q =.4·10^{-7} mol O_2) a threefold increase in ethylene oxide yield was observed with a corresponding 20% increase in selectivity.

The absolute increase Δr_i in the rates of epoxidation and combustion is directly proportional to P_{O_2} and the cell overvoltage ΔV both at steady state and during galvanostatic transients. The ratio $\Delta r_1/\Delta r_2$ equals 1.7$\pm$ .3 and appears to be rather insensitive to current, overvoltage, gas phase composition and temperature.

The relaxation time constants of the overvoltage (τ_o) and the rates (τ_c) are practically equal and of order 4FQ/i. They increase with increasing P_{O_2}/P_{ET} ratios. The new observations are in reasonably good agreement with a previously proposed model (17).

The phenomenon appears to be due to formation and destruction of some type of surface silver oxide during oxygen pumping to and from the catalyst respectively. The use of in situ surface science techniques should prove very useful for the elucidation of the exact nature of this surface oxide.

The present study was limited to temperatures above 300°C because of the severe increase in the electrolyte resistance with decreasing temperature. Thinner (<100 μm) electrolyte components must be used to study the temperature range of industrial interest, i.e. 220° to 290°C. We note that this is the first known application of electrochemical oxygen pumping through a solid electrolyte to alter the selectivity of a heterogeneous catalyst reaction. The application of external voltages to solid electrolyte cells with appropriate catalytic electrodes may be a powerful technique for influencing the selectivity of other partial catalytic oxidations as well.

List of symbols

a_o = Oxygen activity, bar$^{1/2}$

A = Electrolyte surface area, cm^2

c = Surface concentration, mol/cm^2

c_m = Surface concentration at full coverage, mol/cm^2

C_{ad} = Adsorption pseudo capacitance, Cb/V

E = Open circuit emf, V

E* = Activation energy for reaction on the surface oxide, Kcal/mol

F = Faraday constant, 96500 Cb/mol

i = Current, A

i_{CTR} = Current of charge transfer reactions, A

$i_{0,A}$, $^{o}{}_{0,B}$ = Exchange currents for reactions (8) and (9), A

k_i = Rate constant for ethylene epoxidation (i=1) and deep oxidation (i-2) on the surface oxide, $s^{-1}\cdot bar^{-1}$

k_{io} = Rate constant for ethylene epoxidation (i=1) and deep oxidation (i=2) on reduced silver, $s^{-1}\cdot bar^{-1}$

$\vec{K}_{0,A}$, $\vec{K}_{0,B}$ = Preexponential factors of the exchange current of reactions (8) and (9), A

K_1 = Rate coefficient, s^{-1}

K_2 = Rate coefficient, $s^{-1}\cdot bar^{-1}$

K_{O_2} = Molecular O_2 adsorption coefficient, bar^{-1}

Q = Reactive oxygen uptake, mols O_2; proportional to catalyst-electrode surface area S.

r_i = Rate of ethylene epoxidation (i=1) and deep oxidation (i=2), -mols ethylene/s

r_{io} = intrinsic open circuit rates of ethylene epoxidation (i=1) and deep oxidation (i=2), -mols ethylene/s

R = Gas constant, 8.31 J/mol·K

R_c = Ohmic cell resistance, Ω

S = Catalyst electrode surface area, cm^2

t = time, s

V = Cell voltage, Volts

In Catalysis Under Transient Conditions; Bell, A., et al.;
ACS Symposium Series; American Chemical Society: Washington, DC, 1982.

Greek symbols

α_i = Proportionality constants, mol/V

Δr_i = Change in rate of ethylene epoxidation (i=1) and deep oxidation (i=2) due to oxygen pumping, -mols ethylene/S

ΔV = Overpotential, Volts

θ_{O_2} = Molecular oxygen coverage, dimensionless

λ = Constant, dimensionless

λ_o = Constant, cm^{-2}

τ_c = Rate relaxation time constant, min

τ_o = Voltage relaxation time constant, min

Acknowledgements

This research was supported under NSF Grant CPE-8009436 and under the MIT J.R. Mares career development professorship Grant.

Literature Cited

1. Voge, H.H.; Adams, C.R. Adv. Catal. 1967, 17, 154
2. Kilty, R.A.; Sachtler, W.M.H. Cat. Rev.-Sci. Eng. 1974, 10(1) 1
3. Verykios, X.E.; Stein, F.P.; Coughlin, R.W. Catal. Rev. Sci. Eng. 1980, 22(2), 197
4. Force, E.L.; Bell, A.T. J. Catal. 1975, 38, 440
5. Force, E.L.; Bell, A.T. J. Catal. 1975, 40, 356
6. Wu, J.C.; Harriot, P. J. Catal. 1975, 39, 395
7. Verykios, X.E.; Stein, F.P.; Coughlin, R.W. J. Catal. 1980, 66, 368
8. Cant, N.W.; Hall, W.K. J. Catal. 1978, 52, 81
9. Wachs, I.E.; Keleman, S.R. Proc. 7th Inter. Congr. Catal. 1980, paper A48.
10. Herzog, W. Ber. Bunsen-Gesel. 1970, 74 (3), 216
11. Stoukides, M.; Vayenas, C.G. J. Catal. 1980, 64, 18

12. Stoukides, M.; Vayenas, C.G. J. Catal. 1981, 69, 18

13. Sato, M.; Seo, J. J. Catal. 1972, 24, 224

14. Flank, W.H.; Beachell, H.C. J. Catal. 1967, 8, 316

15. Force, E.L.; Bell, A.T. J. Catal. 1976, 44, 175

16. Carberry, J.J.; Kuczynski, G.C.; Martinez, E. J. Catal. 1972, 26, 247

17. Stoukides, M.; Vayenas, C.G. J. Catal. 1981, in press

18. Pancharatnam, S., Huggins, R.A.; Mason, D.M. J. Electrochem. Soc. 1975, 122, 869.

19. Gur, T.M.; Huggins, R.A. J. Electrochem. Soc. 1979, 126, 1067

20. Vayenas, C.G.; Farr, R.D. Science 1980, 208, 593

21. Farr, R.D.; Vayenas, C.G. J. Electrochem. Soc. 1980, 127, (7), 1478

22. Vayenas, C.G.; Lee, B.; Michaels, J. J. Catal. 1980, 66, 36

23. Vayenas, C.G.; Georgakis, C.; Michaels, J.; Tormo, J. Catal. 1981, 67, 348

24. Holbrook, L.L.; Wise, H. J. Catal. 1975, 38, 294

25. Bockris, J. O'M.; Reddy, A.K.N. "Modern Electrochemistry", New York 1973; P. 1020-1036; 1190-1195

RECEIVED July 28, 1981.

Characterization of the Adsorbed Layer of a Silver Catalyst in the Oxidation of Ethylene from Its Transient Adsorption Behavior

M. KOBAYASHI

Kitami Institute of Technology, Department of Industrial Chemistry,
090 Kitami, Hokkaido, Japan

The adsorbed layer on a silver catalyst surface, during the course of ethylene oxidation at 91°C, was characterized by examining the transient adsorption behavior of CO_2. The analysis of the results obtained by transient response, thermal desorption and pulse techniques suggested the existence of three different adsorbed oxygen species: isolated monoatomic oxygen (O_s^i), adjacent monoatomic oxygen (O_s^a) and diatomic oxygen species (O_s^d), differing in their reactivities. Carbon dioxide and ethylene are competitively adsorbed on these three oxygen species and the strength of CO_2 adsorption on O_s^i is weaker than C_2H_4. CO_2 and C_2H_4 are not adsorbed on the surface reduced by H_2 but adsorbed on the surface reduced by C_2H_4 on which there is O_s^i. The C_2H_4 adsorbed on O_s^i produces no C_2H_4O and CO_2, the C_2H_4 on O_s^a produces an intermediate (In) in the complete oxidation and C_2H_4 on O_s^d produces C_2H_4O.

Desorption of reversibly and irreversibly adsorbed CO_2 is accelerated by the removal of adsorbed oxygen with H_2. The adsorption isotherm for CO_2 obtained on an oxidized surface reaches saturation for P_{CO_2}=0.15 atm. The addition of P_{CO_2}= 0.15 atm into a reaction gas stream retarded the rates of C_2H_4O and CO_2 formation to zero in spite of a presence of adsorbed C_2H_4, indicating the complete blocking of CO_2 to the adsorbed oxygen and no reaction of the adsorbed C_2H_4 with gaseous O_2. The adsorption of CO_2 during reaction obeyed a Langmuir adsorption isotherm. The catalyst surface under steady state reaction is characterized as follows: appreciable parts of the silver surface larger than 0.4 is blocked by (In), irreversibly adsorbed CO_2 and adsorbed C_2H_4. It is sugg-

0097-6156/82/0178-0209$07.25/0
© 1982 American Chemical Society

ested that a very small fractional part of surface oxygen is available for the reaction at higher concentration of ethylene.

A large number of investigators have studied the adsorption behavior of oxygen, carbon dioxide and ethylene on silver catalysts. The chemisorption data using a variety of techniques have suggested the following (1): oxygen is chemisorbed on silver surfaces to form both monoatomic and diatomic oxygen species based on a rough classification, ethylene is chemisorbed on silver ions (2) whereas no its adsorption occurs on reduced silver (3) and carbon dioxide is chemisorbed on previously oxidized surfaces (4,5). Based on these experimental findings it is drawn that adsorbed oxygen species should play an important role to form adsorbed intermediates and adsorption sites for reaction gas components. Therefore, to know the detailed reaction mechanism of ethylene oxidation, it is necessary to clarify a situation of the adsorbed layer formed during the reaction, especially on the adsorbed oxygen species available for the progress of reaction.

Carbon dioxide adsorbs on adsorbed oxygen species, not bare silver surfaces, in competition with other reaction gas components and retards the overall reaction. One can conveniently use this nature to reveal the situation of the adsorbed layer during the reaction. For example, the adsorption isotherm of CO_2 obtained on the surface used for reaction will present an efficient information for the amounts of the adsorbed oxygen species free from adsorbed intermediates, when the intermediates are irreversibly adsorbed and stably retained on the surface. And an examination for the competitive adsorption of CO_2 and C_2H_4 on its surface will propose an information for their adsorption strength and/or for a reactivity of the adsorbed ethylene to react with the adsorbed oxygen or with gaseous oxygen. In the present study, the transient response method (6,7,8) has been efficiently used to follow the competitive adsorption behavior between CO_2 and other reaction gas components in ethylene oxidation, and thereby the adsorbed layer of a silver catalyst was characterized. A low reaction temperature as 90°C and a large amount of catalyst were used to follow more clearly the transient states of adsorption and desorption of reaction components.

Experimental Method

The silver catalyst was prepared by reducing silver oxide. The silver oxide used was prepared by adding a solution of potasium hydroxide to an aqueous solution of silver nitrate. A small amount of 0.3% K_2SO_4 solution was added to the silver oxide powder as a promoter and, after mixing, was dried at 105°C for 24hr in a dark room. This was coated on α-Al_2O_3 of 20-42 mesh in the presence of a small amount of ethanol until the sample reached a size of 12-14 mesh. After the ethanol in the silver oxide powder had been completely vaporized in air at room temperature, the sample was reduced in a reactor with a flow of H_2 for 12 hr at 50°C and successively for 12 hr at 100°C. The composition of the catalyst so prepared was 206.0 g-Ag, 1.13 g-K_2SO_4/53.5 g-Al_2O_3. The BET surface area was 0.3 m^2/g-Ag. The constant activity of this catalyst was obtained by flowing the mixture of 5% C_2H_4, 20% O_2 and 75% He at 91°C for 48 hr.

The reactor used consists of a Pyrex glass tube containing 260.6 g catalyst and was immersed in an oil bath. The temperature of the catalyst bed remained constant within ± 0.1°C of the desired temperature. Oxygen (O_2 99.9%), nitrogen (N_2 99.9%), nitrous oxide (N_2O 99.99%), carbon dioxide (99.9%) and helium (He 99.999%) from commercial cylinders were purified through a dry ice-methanol trap to remove water vapor. For He the further purification to remove oxygen was conducted by passing through molecular sieves 5A which was cooled at the liquid nitrogen temperature. Ethylene (C_2H_4 99.9%) from a commercial cylinder was used without treatment.

The total flow rate of the gas was kept constant at 160(± 2) ml (NTP)/min and the composition of reaction mixture was varied by changing the concentration of helium as a diluent. The transient response to a change in the composition of He-N_2 mixture was completed within 15 sec. The intraparticle diffusion resistance was confirmed to be negligible by examining the rate data for catalysts of different sizes, 12-14 mesh and 20-42 mesh at 91°C. The external mass transport effect was also found to be negligible at 123°C by examining the rate data at constant W/F with various flow rates and catalyst amounts. The reaction conditions were chosen in such a way that the total conversion of ethylene did not exceed 0.08 in all experiments. In this condition, it was confirmed, by analysing the gas at five positions along the reactor length during the reaction, that the concentration of products (C_2H_4O and CO_2) increased linearly from the entrance of the catalyst bed to the exit.

In Catalysis Under Transient Conditions; Bell, A., et al.;
ACS Symposium Series; American Chemical Society: Washington, DC, 1982.

Three gas chromatographes, each kept under different conditions, were simultaneously used to analyse all reaction gas components as continuously as possible. In the special case of a very rapid response with the period shorter than a few minutes, the same response was repeated a few times and the results obtained were superimposed in order to draw a response curve as continuously as possible.

Three flow systems with different gas composition were prepared so that the transient response experiments could be completed for three different gas mixtures within a few minutes. A more detailed description of transient response method used in this study can be found elsewhere (6,7,8).

Experimental Results and Discussion

The response of the component Y in the outlet gas mixture to a step change in the concentration of X in the inlet gas stream is designated as X-Y response. The following symbols will be used:when X is increased, X(inc.,)-Y; when X is decreased, X(dec.,)-Y; when X is increased from nil, X(inc.,0)-Y; when decreased to nil X(dec.,0)-Y; when X is pulsed in the inlet gas stream, X(pulse)-Y response; when the temperature of the catalyst bed is raised linearly with respect to the elapsed time, T(linear)-Y response.

Transient Behavior of Oxygen

In order to analyze the adsorption behavior of carbon dioxide on silver it was necessary to understand the adsorption behavior of O_2 and its reactivity, because the adsorption of CO_2 strongly relatedto the adsorbed oxygen species as will be described later. For this reason, the following transient experiments were purformed.

Total Amount of Adsorbed Oxygen. The amount of adsorbed oxygen can easily be estimated from the graphical integration of the O_2-O_2 response curve. After the catalyst surface had completely been reduced by a pure hydrogen stream for about 5 hrs, the stream was switched over to a pure helium stream and then the O_2(inc.,0)-O_2, the O_2(dec.,0)-O_2 and again the O_2(inc.,0)-O_2 responses were followed successively. This procedure was repeated after changing the concentration of O_2. Fig.1 clearly shows a delay for the O_2(inc.,0)-O_2 response (Run1) at first time and shows an instantaneous response for both the successive O_2(dec.,0)-O_2

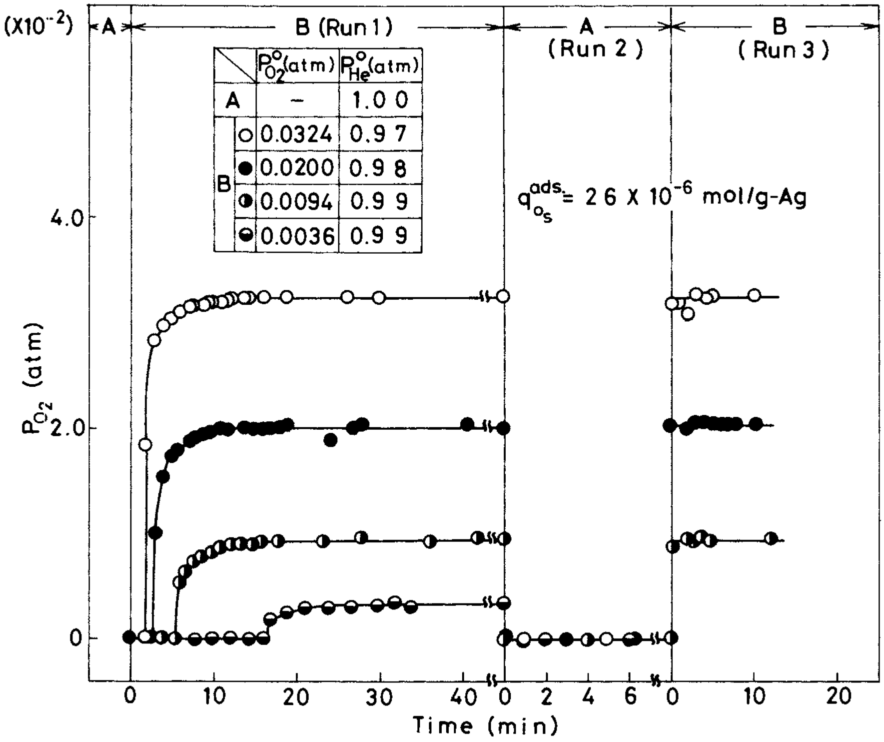

Figure 1. O_2–O_2 response at 91°C.

(Run 2) and O_2(inc.,0)-O_2 (Run 3) responses at second time. These results indicated an irreversible adsorption of O_2 and no appreciable adsorption of oxygen on the oxidized surface. The integrated amount of the oxygen with Run 1 was estimated to be 2.6(±0.1)x10^{-6} mol/g-Ag (1.04(±0.04)x10^{19} atoms/m^2) no dependence on the concentration of O_2.

The adsorption strength of the adsorbed oxygen can be determined by a thermal desorption technique. After the catalyst surface had completely been oxidized in the O_2(20%)-He mixture at 91°C, the reactor was flushed with a pure He stream and temperature of catalyst bed was then raised linearly at a rate of 4.3°C/min from 50 to 280°C. Thus the T(linear)-O_2 response was followed. Fig.2 shows that the desorption spectrum of oxygen has a peak at 250°C. The integrated amount of desorbed oxygen was estimated to be 2.5(±0.1)x10^{-6} mol/g-Ag (1.00(±0.04)x10^{19} atoms/m^2), which is very close to the value estimated from the O_2(inc.,0)-O_2 response. From these results, it was apparent that all the oxygen species adsorbed at 91°C were desorbed at around 250°C. Scholten, Konvalinka and Beekman (9) calculated that the total number of surface silver atoms was 1.31x10^{19} atoms per m^2 based on Sandquist's data (10), and their experiments on oxygen adsorption gave the number of adsorbed oxygen atoms to be about 0.7x10^{19} at 50°C and about 1.2x10^{19} atoms/m^2 at 100°C. Thus the total amount of adsorbed oxygen obtained in this study fell within Scholten et al's range and corresponds to 0.8 of the surface coverage expected for a monoatomic form of adsorbed oxygen.

The surface reduced by H_2 was active for the decomposition of N_2O at 91°C. After the catalyst had been reduced by the H_2 stream for 5 hrs at 91°C, the reactor was flushed by the He stream and then the N_2O(inc.,0)-N_2 response (Run 1) was followed. Run 1 in Fig.3 showed a typical overshoot type response of N_2 with an instantaneous maximum. This instantaneous mode indicated the direct decomposition of gaseous N_2O on active sites: this is also suggested by the N_2O(dec.,0)-N_2O response (Run 2) in Fig.3 which exhibited no delay indicating no adsorption of N_2O. The graphical integration of the N_2O(inc.,0)-N_2 response curve corresponded to the amount of adsorbed oxygen atoms and was estimated to be 2.2x10^{-6} mol/g-Ag (0.90(±0.08)x10^{19} atoms/m^2). This is close to the value 0.80x10^{19} which is roughly estimated from the figure given by Scholten et al. The difference between the amount of adsorbed oxygen found oxygen adsorption and as compared to N_2O decomposition may be attributed to the presence of

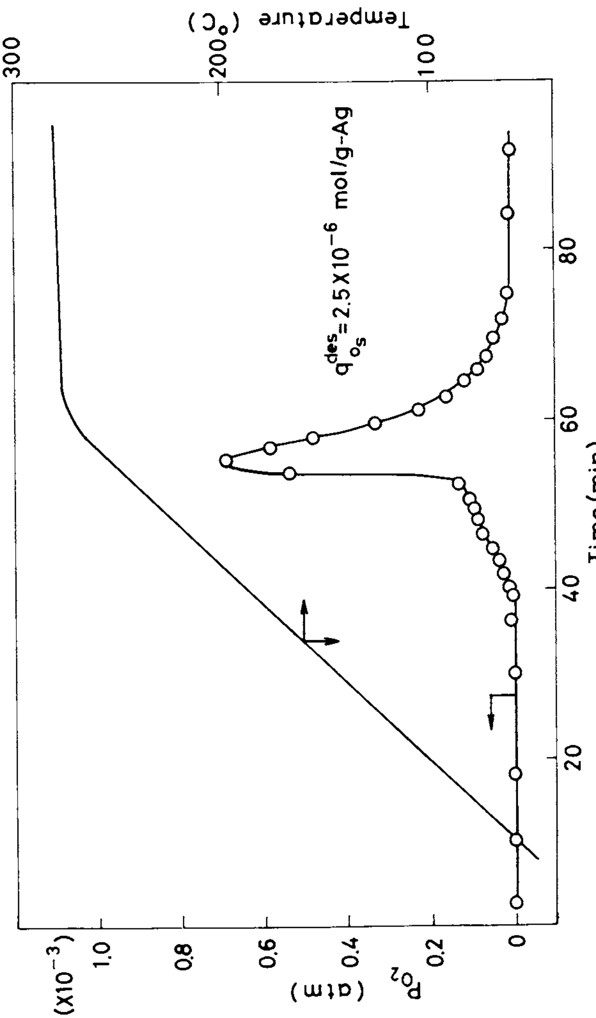

Figure 2. Thermal desorption spectrum for O_2.

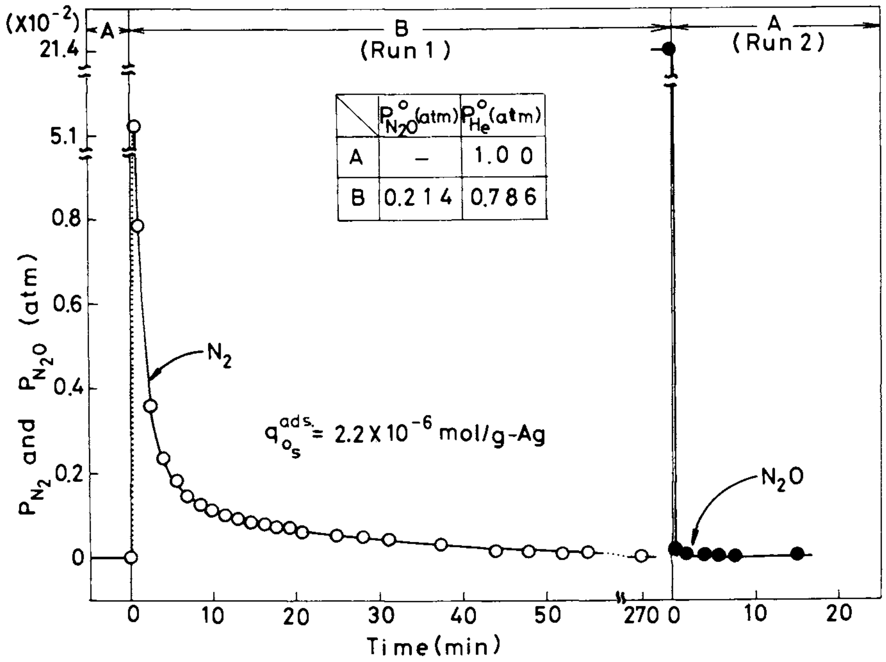

Figure 3. N_2O(inc. O)–N_2 and N_2O(dec. O)–N_2O responses at 91°C.

adsorbed oxygen in a diatomic form. The amount of diatomic oxgen in the case of the O_2 adsorption was estimated to be 0.4×10^{19} molecules/m^2, disregarding the recombination of atomic oxygen formed during the N_2O decomposition.

Reactivity of Adsorbed Oxygen. The existence of two types of adsorbed oxygen on silver, diatomic and monoatomic oxygen, has frequently been claimed (1). In the present study the catalytic activity of the two types of adsorbed oxygen was also investigated again using the pulse technique. Before use the pulse technique one should examine the desorption behavior of ethylene oxide because the pulse spectrum of the ethylene oxide formed by a reaction of ethylene with adsorbed oxygen species is strongly affected by it.

After the catalyst had been oxidized in an O_2-He stream for 5 hrs, the stream was switched over to either a C_2H_4-O_2-He mixture (Run 1) or a C_2H_4-He mixture (Run 2) and the C_2H_4, O_2(inc.,0)-C_2H_4O and -CO_2 and the C_2H_4(inc.,0)-C_2H_4O and -CO_2 responses were followed separately. All the responses in the two Runs were of the overshoot type as shown in Fig.4. During the initial stage of the responses, C_2H_4O and CO_2 in two Runs reached the same maximum points irrespective of whether oxygen existed in the gas phase. This result strongly indicated that adsorbed oxygen not gaseous oxygen was responsible for the production of C_2H_4O and CO_2. Furthermore, the response of C_2H_4O was of the overshoot type with an instantaneous maximum. Such behavior probably resulted from the rapid desorption of the C_2H_4O produced. This idea can also be supported by the following results.

The height at the maximum point of C_2H_4,O_2(inc.,0) -C_2H_4O response in Fig.4 corresponds to the reaction rate ($r^{max}_{C_2H_4O}$) of adsorbed oxygen with C_2H_4. The $r^{max}_{C_2H_4O}$ was plotted as a function of $P_{C_2H_4}$ and a good straight line obtained at temperatures ranging from 80 to 91°C as shown in Fig.5. The Arrhenius plot of the apparent rate constant estimated from these straight lines was 58.6 kJ as shown in Fig.6. These results strongly suggest that C_2H_4O is formed by the reaction between gaseous C_2H_4 and adsorbed oxygen, an Eley-Rideal type mechanism, and that the C_2H_4O formed desorbs rapidly.

In such a case,pulse techniques can be conveniently used to examine the reactivity of the adsorbed species as follows. After the catalyst had been reduced by a pure H_2 stream at 160°C for 2 hrs, the catalyst bed was flushed by He and then the sream changed to an C_2H_4(12.8%)-He stream. O_2 and N_2O gases were separa-

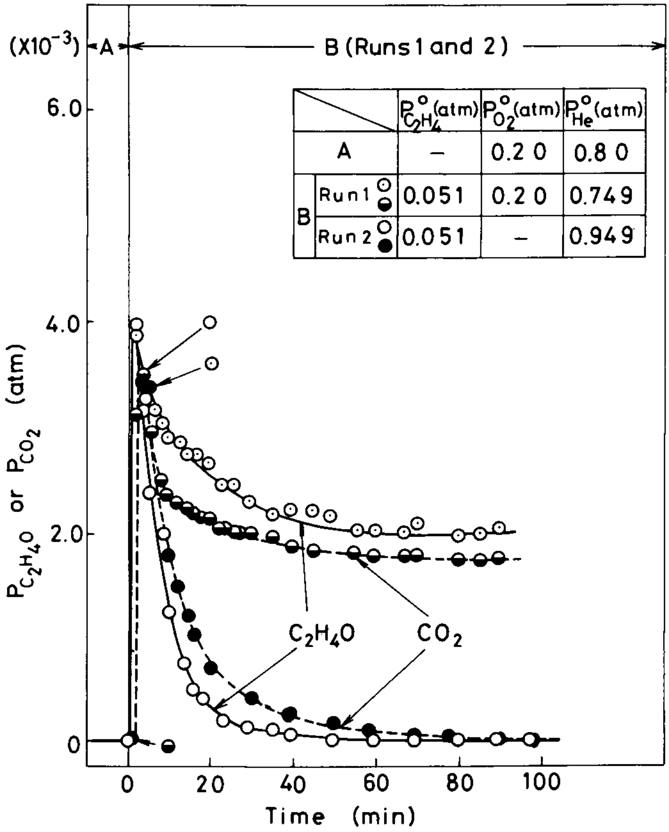

Figure 4. Comparison of Run 1, the C_2H_4(inc. O)–C_2H_4O and –CO_2 responses and Run 2, the C_2H_4(inc. O)– and O_2(dec. O)–C_2H_4O and –CO_2 responses at 91°C.

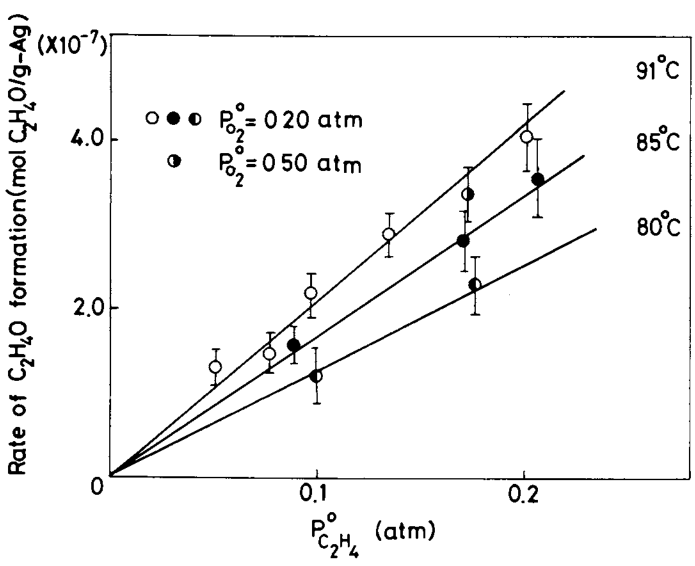

Figure 5. The rate of C_2H_4O formation at the maximum point of the C_2H_4(inc. O)–C_2H_4O response.

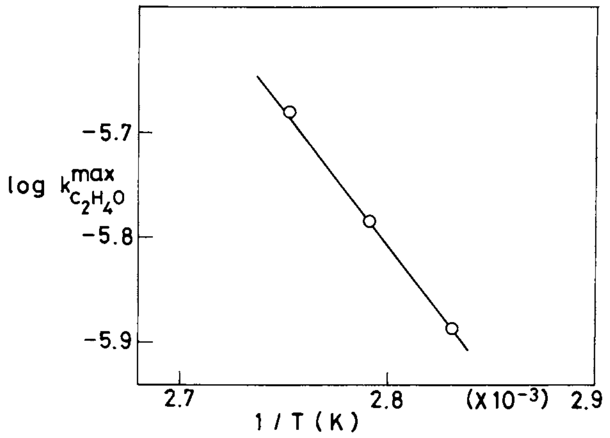

Figure 6. Arrhenius plot for $k_{C_2H_4O}^{max}$ at $P_{O_2}{}^{\circ} = 0.2 - 0.5$ atm.

tely pulsed into the inlet stream of this mixture in various pulse sizes. The O_2(pulse)-C_2H_4O and -CO_2 responses and the N_2O(pulse)-C_2H_4O and -CO_2 responses were separately followed. The same measurements were repeated three times for each pulse and typical data obtained were presented in Figs.7 and 8 by Run 1.

Comparison shows that,in the case of the O_2-pulse, co-production of CO_2 and C_2H_4O was observed whereas with N_2O, CO_2 was mainly formed. One can roughly estimate the total amount of each oxygen species,taken up by the catalyst surface from each pulse, by the application of simple stoichiometry to the amount of the produced CO_2 and C_2H_4O and an intermediate (In) in the complete oxidation. Here the existence of the intermediate (In) was demonstrated in our previous papers (11,12). The amount of (In) is obtained from the amount of CO_2 formed by the decomposition of it in an O_2-He stream (see Run 2 in Figs.7 and 8). In addition it is assumed that (In) keeps the carbon-carbon bond and retains four atomic oxygen (11). Fig. 9 indicates that the adsorbed oxygen species from the O_2 pulses produced C_2H_4O more than hundred times faster than that from N_2O pulse. This is consistent with Herzog's results (13) which demonstrated very low selectivity to C_2H_4O from C_2H_4-N_2O under steady state conditions at temperatures above 210°C. Furthermore, at 91°C, the oxygen species formed with the N_2O pulses produced only (In) with no production of CO_2 or C_2H_4O, and the formed (In) was decomposed to the equal amounts of CO_2 and H_2O in an O_2-He stream whereas no its decomposition occured in a N_2O-He stream (13).

From the above results, one can conclude the existence of the two types of adsorbed oxygen species which may be speculated as monoatomic and diatomic oxygen species. The monoatomic oxygen species can produce (In) and the diatomic oxygen species can produce C_2H_4O and decompose (In).

Adsorption Behavior of C_2H_4

Adsorption behavior of C_2H_4 was examined on three different surfaces: those reduced with H_2, those reduced with C_2H_4 and those previously used in reaction. On the surface reduced by H_2 the C_2H_4-C_2H_4 response simply was an instantaneous response as shown in Fig. 10. This showed that C_2H_4 did not adsorb on bare silver surface. In fact, no production of CO_2 or desorption of C_2H_4 was observed even when the catalyst surface was exposed to the O_2-He mixture following the C_2H_4-C_2H_4 response experiment.

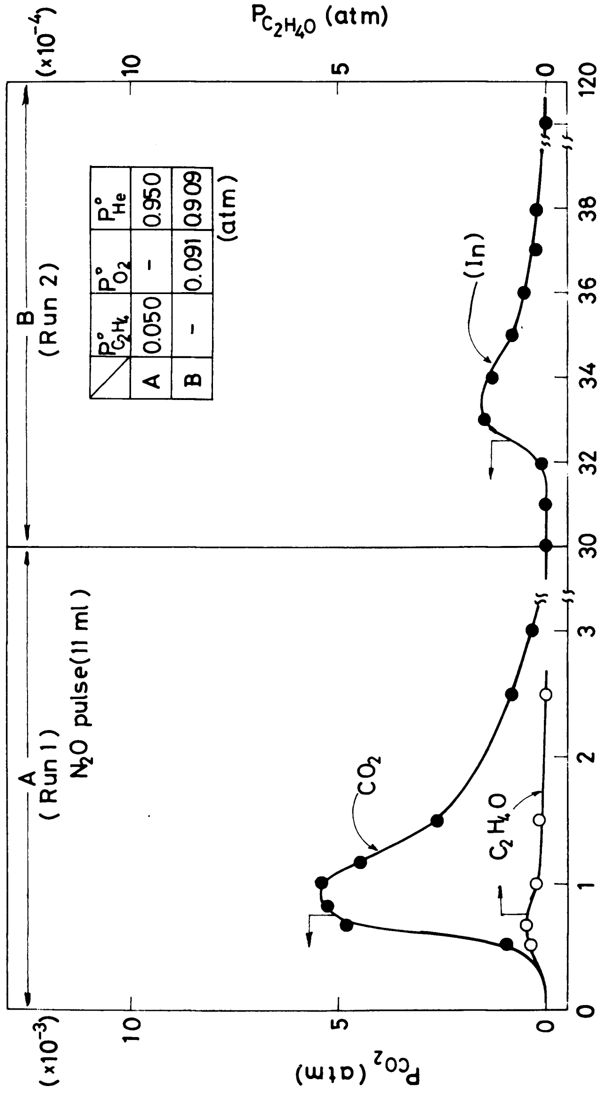

Figure 7. N_2O(pulse)–C_2H_4O and –CO_2 responses and the decomposition of (In) in the O_2–He mixture at 160°C.

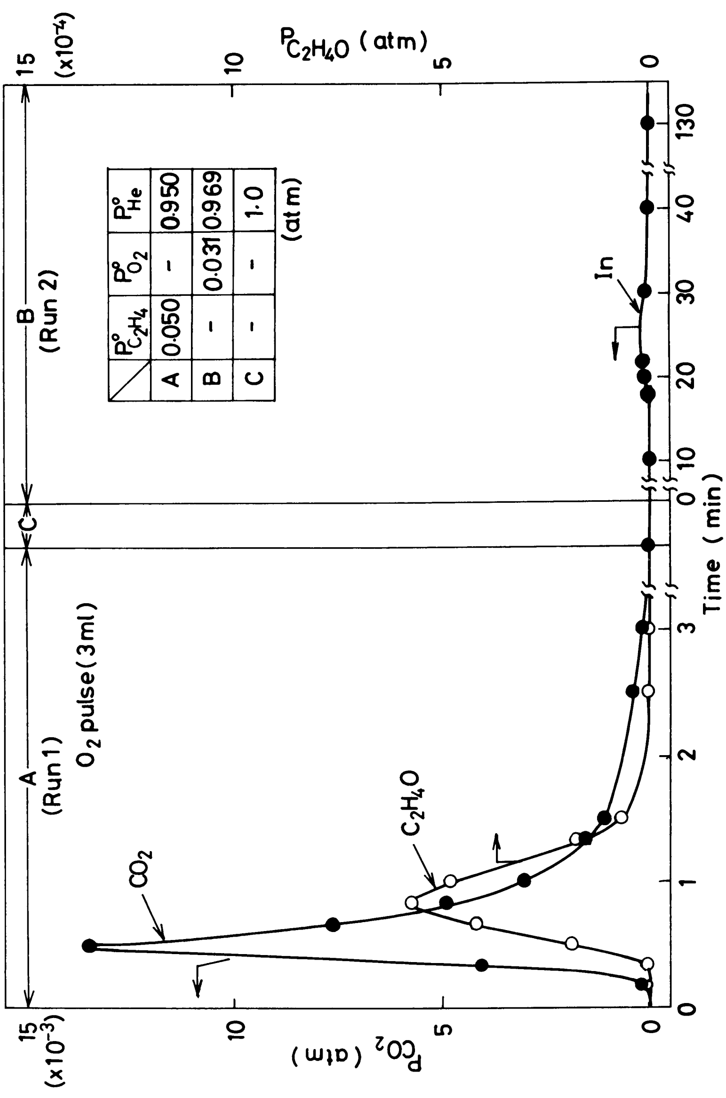

Figure 8. O_2(pulse)–C_2H_4O and –CO_2 responses and the decomposition of (In) in the O_2–He mixture at 160°C.

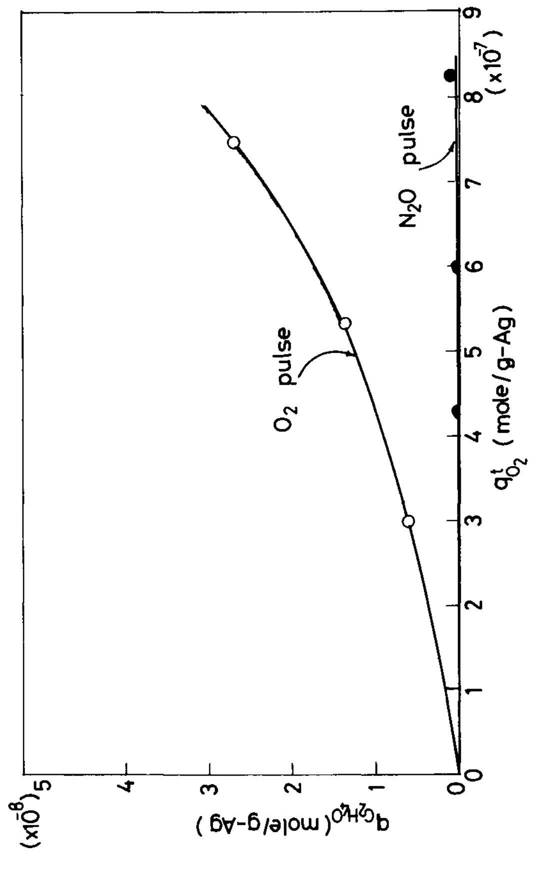

Figure 9. Comparison of the amounts of C_2H_4O formed by the O_2 and N_2O pulses at 160°C.

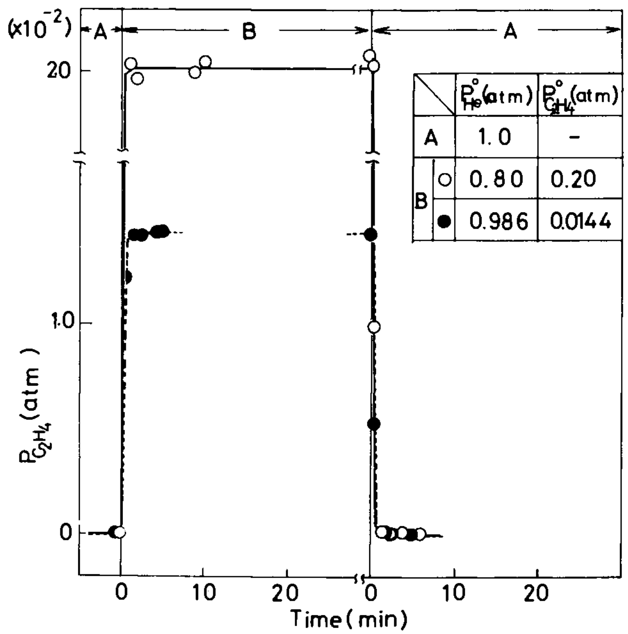

Figure 10. C_2H_4–C_2H_4 response on the reduced surface with H_2 at 91°C.

The adsorption behavior of C_2H_4 on a surface which had been reduced by C_2H_4-He stream for 24 hrs until no CO_2 and C_2H_4O was rather different. The C_2H_4(dec.,0)-C_2H_4 response clearly showed a delay indicating the existene of an appreciable amount of adsorbed C_2H_4 on the surface. The integrated amount of adsorbed C_2H_4 plotted as a function of the pressure of C_2H_4 was as shown in Fig.11 by curve I. This adsorption isotherm gave the amount of C_2H_4 at saturation to be $3.8(\pm 0.4) \times 10^{-7}$ mol/g-Ag ($7.6 \times 10^{17}/m^2$). Since C_2H_4 did not adsorb on bare silver, adsorbed oxygen species must be the active sites for the adsorption of C_2H_4. Furthermore this adsorbed oxygen could produce neither CO_2 nor C_2H_4O,being only active sites for C_2H_4 adsorption. The diatomic oxygen species can not be these active sites, because they form C_2H_4O immediately by the reaction. Thus monoatomic adsorbed oxygen species are believed to be the sites. As described previously, since the monoatomic oxygen species can also form the intermediate (In) in the complete oxidation of ethylene, it may reasonably be considered that monoatomic oxygen species are of two types: one is those consisting of more than two atoms and which can produce (In) and those present as isolated monoatomic oxygen species and which are the active sites for C_2H_4 adsorption. These isolated oxygen species may be able to migrate on surface to make adjacent oxygen species or diatomic oxygen species. It is these isolated monoatomic oxygen which exist on the reduced surface with C_2H_4. Using this idea one can also explain the following experimental results.

The amount of C_2H_4 adsorbed during reaction can easily be estimated from the graphical integration of the C_2H_4,O_2(dec.,0)-C_2H_4 response curves obtained at steady state. The result is presented in Fig.11 by Curve I and shows a linear adsorption isotherm. It was also determined that this isotherm was not affected by the presence of oxygen in the gas phase during the course of the C_2H_4 desorption. This strongly indicates that the isolated monoatomic oxygen species also exist on the surface during reaction and that C_2H_4 adsorbed on these isolated species does not produce any products. i.e. the adsorbed C_2H_4 is inactive for the reaction. Furthermore, when the surface reduced with C_2H_4 was kept in a pure He stream for several hours, and the surface was exposed again to the C_2H_4-He stream, a small amount of C_2H_4O was detected in the effluent gas stream. This suggests that isolated monoatomic oxygen migrates very slowly on surface to form the diatomic oxygen species.

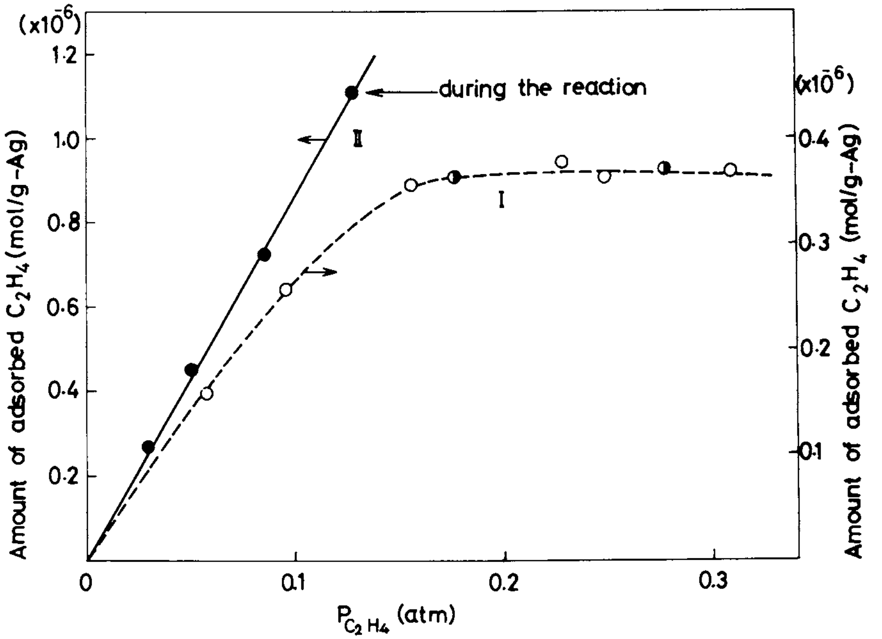

Figure 11. Adsorption isotherms for C_2H_4 on the surface reduced with C_2H_4 and on the surface used for the reaction at 91°C. Key: ○, in He; and ◑, in CO_2–He.

Transient Behavior of CO_2

Adsorption Behavior of CO_2. The adsorption behavior of CO_2 on silver is greatly influenced by whether the surface was reduced or oxidized. In the present study four different surfaces were studied: a surface reduced by H_2, a surface reduced by C_2H_4, an oxidized surface and a surface used for reaction. The CO_2(inc.,0)-CO_2 and CO_2(dec.,0)-CO_2 responses for a surface reduced by H_2 exhibited no delay, indicating no adsorption of CO_2 on the bare silver surface in agreement with the works of Drake and Benton (4) and of Czanderna (5).

When the CO_2(inc.,0)-CO_2 and CO_2(dec.,0)-CO_2 responses were followed in a He stream on a surface reduced by C_2H_4, the response showed a delay indicating a reversible adsorption of CO_2. The integrated amount of the adsorbed CO_2 was estimated to be $4.0x10^{-7}$ mol/g-Ag ($8x10^{17}/m^2$) independent of concentration of CO_2 as shown by its adsorption isotherm (Curve II in Fig. 12). This is close to the saturation amount of adsorbed C_2H_4 on the same surface (compare to Curve I in Fig.11). This good agreement indicates that isolated monoatomic oxygen species are also the active sites for the adsorption of CO_2. In contrast, CO_2-CO_2 responses conducted in a C_2H_4(16%)-He stream instead of in the He stream were instantaneous indicating no adsorption of CO_2 (see Curve IV in Fig.12). This is a consequence of competitive adsorption between C_2H_4 and CO_2 on the same isolated monoatomic oxygen species with adsorption of C_2H_4 being stronger than CO_2.

After the catalyst had completely been oxidized in the O_2(20%)-He stream for 24 hrs, the CO_2-CO_2 response was followed in a He stream. The amount of adsorbed CO_2 estimated from the CO_2(inc.,0)-CO_2 response was in good agreement with the amount of desorbed CO_2 estimated from the CO_2(dec.,0)-CO_2 response, except the amount of adsorbed CO_2 estimated from the first CO_2(inc.,0)-CO_2 response was more than for subsequent responses. The difference was estimated to be $6(\pm1)x10^{-7}$ mol/g-Ag independent on the concentration of CO_2. This disagreement is considered due to the existence of some irreversible adsorption of CO_2. The existence of this irreversible adsorption was confirmed by the following experiment.

After several CO_2(inc.,0)-CO_2 responses had been completed, the CO_2-He mixture was changed to pure H_2 and the CO_2(dec.,0)-CO_2 response was followed. As seen in Fig.13 these was large amount of CO_2 desorption during the initial stage of the response followed by a

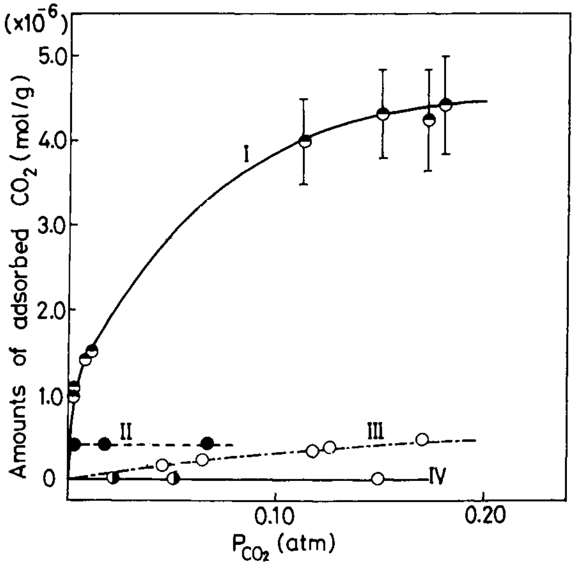

Figure 12. Adsorption isotherms at 91°C for CO_2 on the differently treated catalyst surfaces. Key: I, ◒, in He (oxidized surface); II, ●, in He (surface reduced by C_2H_4); III, ○, in He (surface used for the reaction); and IV, ◑, in C_2H_4–He (surface reduced by C_2H_4) and ○, in He (surface reduced by H_2).

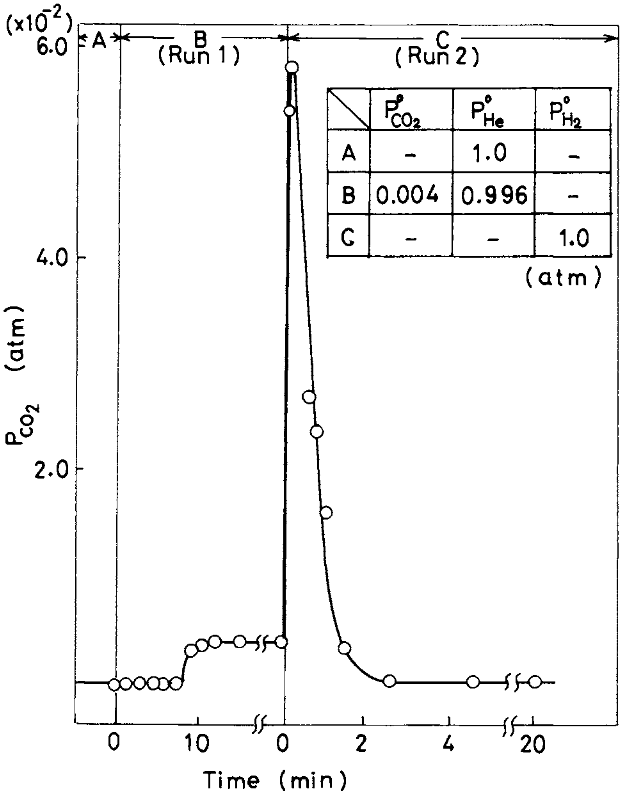

	$P^0_{CO_2}$	P^0_{He}	$P^0_{H_2}$
A	-	1.0	-
B	0.004	0.996	-
C	-	-	1.0

Figure 13. CO_2*(inc. O)–*CO_2 *response and the* CO_2*(dec. O)–*CO_2 *and* H_2*(inc. O)–*CO_2 *response at 91°C.*

steep decline to zero within a few minutes. The mode of the response is typical of false start responses and may be attributed to an acceleration of the desorption rate of CO_2 caused by the rapid removal of adsorbed oxygen by H_2 reduction. The integrated amount of the desorbed CO_2 in Run 2 is larger than that estimated from the CO_2(dec.,0)-CO_2 response in a He stream and the difference is estimated to be 7 ($\pm$1)x10^{-7} mol/g-Ag (1.4x10^{18}/m^2). This corresponds to the amount of the irreversibly adsorbed CO_2 estimated previously. One can conclude that the desorption rates of both reversibly and irreversibly adsorbed CO_2 are greatly accelerated by the reduction of surface with H_2.

The adsorption isotherm for reversibly adsorbed CO_2 estimated from the CO_2-CO_2 response is presented in Fig.12 by Curve I. From Curve I the saturated amount of CO_2 is estimated to be 4.3($\pm$0.5)x10^{-6} mol/g-Ag (8.6x10^{18}/m^2). This amount plus the amount of the irreversibly adsorbed CO_2 is about 5x10^{-6} mol/g-Ag which is very close to the amount of adsorbed oxygen atoms estimated from the adsorption of O_2. This good agreement strongly indicates that all adsorbed oxygen species are blocked by the adsorbed CO_2 at a partial pressure of CO_2 higher than P_{CO_2}= 0.15 atm: probably one carbon dioxide molecule adsorbs on one adsorbed oxygen species in which both diatomic and monatomic oxygen are included.

Since the reaction rate is strongly retarded by the adsorption of CO_2, it is difficult to measure the adsorption behavior of CO_2 during the reaction. However one can roughly estimate the amount of CO_2 adsorbed on the surface which has been employed for reaction, by using the following experiments. After the reaction had reached a steady state, the C_2H_4, O_2(dec.,0)-CO_2 response (Run 1) was followed. Run 1 in Fig.14 shows a very slow out flow of CO_2 for an extraordinarily long period of time: this may be attributed to slow surface migration of adsorbed oxygen to react with (In). In a separate experiment, the same C_2H_4,O_2(dec.,0)-CO_2 response was followed for 120 min and a CO_2-CO_2 response measured. The result obtained is presented in Fig.14 by Run 2. This CO_2-CO_2 response should be considered as the response which was superposed with the pseudo steady state level of the C_2H_4,O_2(dec.,0) -CO_2 response (Run 1). The amount of adsorbed CO_2 (q_{CO_2}) can be estimated from the difference between both the CO_2(dec.,0)-CO_2 and the C_2H_4, O_2(dec.,0)-CO_2 response curves as schematically shown in Run 2 in Fig.14 by the shaded area. The adsorption isotherm for CO_2 thus obtained is presented in Fig.12 by Curve III. This

In Catalysis Under Transient Conditions; Bell, A., et al.;
ACS Symposium Series; American Chemical Society: Washington, DC, 1982.

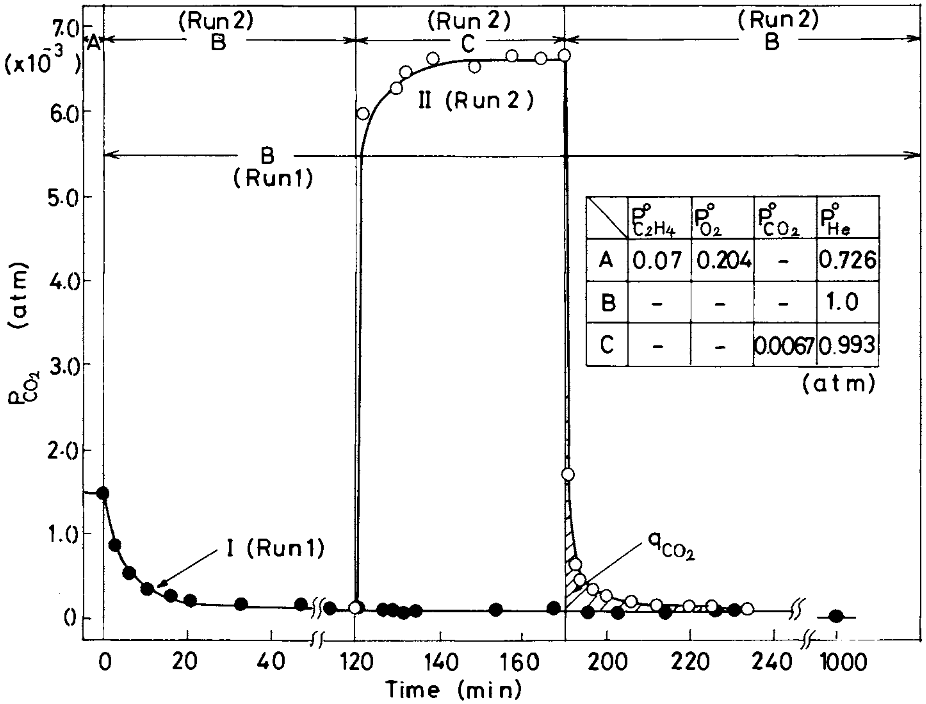

Figure 14. CO_2–CO_2 response at 91 °C on the surface used for the reaction.

curve obeys Langmuir adsorption isotherm with a saturation amount of adsorbed CO_2 of about 0.9×10^{-6} mol/g-Ag ($1.8 \times 10^{18}/m^2$).

Let us consider the composition of the adsorbed layer of catalyst during reaction. The amount of (In) at a steady state is given by the amount of CO_2 during its decomposition in a O_2-He stream and is estimated to range from 1.4×10^{-6} to 2.5×10^{-6} mol CO_2/g-Ag depending on the concentration of ethylene. Assuming that one carbon dioxide molecule formed from (In) arose from one adsorbed atomic oxygen, the above amount exactly corresponded to the amount of the adsorbed atomic oxygen which had been blocked by (In). On the other hand, C_2H_4 and CO_2(rev.) were also reversibly adsorbed on adsorbed oxygen species to block the reaction and the amounts of them, by using each adsorption isotherm (see Cuve II in Fig.11 and Cuve III in Fig. 12), could be estimated to be $0.2\text{-}1.2 \times 10^{-6}$ and $0.5\text{-}3 \times 10^{-7}$ mol/g-Ag, respectively, the ranges being the result of a dependence on the concentration of C_2H_4. In addition, one has to take into account the existence of the adsorbed oxygen blocked by the irreversibly adsorbed CO_2(irr.) which is estimated to be 6×10^{-7} mol/g-Ag. Finally, assuming that one CO_2 or C_2H_4 molecule occupies one adsorbed monoatomic oxygen species, the total amount of adsorbed oxygen blocked by the adsorption of (In), C_2H_4, CO_2(irr.) and CO_2(rev.) are roughly estimated to range from 1×10^{-6} to 2×10^{-6} mol/g-Ag depending on the concentration of ethylene. The upper values are equal to the total amount of adsorbed oxygen estimated from the decomposition of N_2O. This agreement strongly suggests that that appreciable part of the ctalyst surface ($\theta = 0.8$) is oxidized during the reaction and the fractional part of those surface oxygen higher than 0.4 is blocked by the adsorption of (In), C_2H_4 and CO_2(irr.). When the high concentration of C_2H_4 is used, very small fractional part of the surface oxygen is available for the reaction. This is also consistent with the steady state rate data in which the rates of C_2H_4O and CO_2 formation are gradually lowered with increasing the partial pressure of ethylene.

Behavior of CO_2 during the Reaction. The effect of CO_2 on both the rates of C_2H_4 formation and complete oxidation was examined by adding CO_2 into the reaction gas stream at the steady state of reaction. The rate of complete oxidation was measured by the rate of H_2O formation. Fig.15 clearly indicated that both rates were strongly retarded by the addition of CO_2: when

$P^{\circ}_{C_2H_4}$ was 0.13 atm, C_2H_4O formation ceased when P_{CO_2} 0.13 atm and complete oxidation ceased when $P_{CO_2} \geq$ 0.11 atm. with $P^{\circ}_{C_2H_4}$ = 0.27 atm the same was true when $P^{\circ}_{CO_2}$ = 0.18 and 0.12 atm respectively. Thus the degree of the retardation depended on the concentration of C_2H_4. This is probably caused by the effect of adsorbed C_2H_4 which inhibits the adsorption of CO_2 onto the adjacent adsorbed oxygen, taking into account the previous fact that the strength of C_2H_4 adsorption was larger than that of CO_2.

Noting the selectivity to C_2H_4O in Fig.16, it gradually increased with the concentration of CO_2. The selectivity estimates involve much experimental error because of the difficulty of the accurate detection of the small amount of water produced. However the increase may be real and can be accounted for explained in terms of the various adsorbed oxygen species: a fractional part of the adjacent adsorbed oxygen species is decreased with increasing the concentration of CO_2 by the blocking effect of adsorbed CO_2 onto the adjacent oxygen. A fractional part of the isolated adsorbed oxygen is thus increased. The isolated diatomic oxygen can produce C_2H_4O, but the isolated monoatomic oxygen can not produce CO_2. This is the reason why the selectivity to C_2H_4O increased with increasing the adsorption of CO_2. This idea is also available to explain the following competitive adsorption behavior of CO_2 and C_2H_4.

After the oxidized surface had completely been blocked by the adsorption of CO_2 from a stream of CO_2 (18%)-He mixture (Run 1), a C_2H_4O-O_2-CO_2-He stream was introduced into the reactor in a stepwise fashion (Run 2) and C_2H_4,O_2(inc.,0)-C_2H_4O and -H_2O responses were followed. The results are presented in Fig.16. Run 2 in Fig.16 exhibited no production of C_2H_4O and H_2O, indicating complete blocking by CO_2 of both the diatomic and monoatomic oxygen species. Then the C_2H_4-O_2-CO_2-He stream was switched over to either the O_2-He stream (Run 3) or C_2H_4-O_2-He stream (Run 4) and the responses of CO_2, C_2H_4O and C_2H_4 were followed. Run 3 in Fig.16 clearly shows the desorption of C_2H_4 and no production of H_2O (this is not shown in the figure). From these results one can conclude that adsorbed C_2H_4 can not react with either gaseous oxygen or adsorbed oxygen to produce C_2H_4O and (In). This means that the adsorbed C_2H_4 just sits on the adsorbed oxygen species which are isolated from the neighboring adsorbed oxygen by the blocking effect of the adsorbed CO_2.

On the other hand, Run 4 in Fig.16 shows the slow increase for the rate of C_2H_4O formation and the

In Catalysis Under Transient Conditions; Bell, A., et al.;
ACS Symposium Series; American Chemical Society: Washington, DC, 1982.

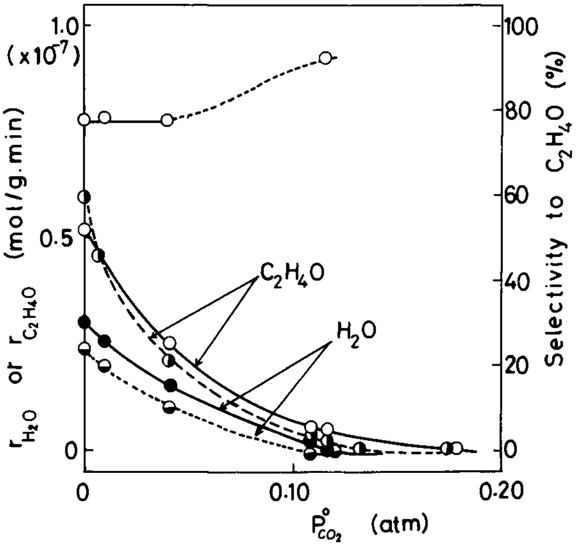

Figure 15. The retardation effect of CO_2 on the rates of C_2H_4O and H_2O formation at 91°C. Key: ○, ●, $P^o_{C_2H_4}$ = 0.27 atm, $P^o_{O_2}$ = 0.21 atm; and ◐, ◒, $P^o_{C_2H_4}$ = 0.13 atm, $P^o_{O_2}$ = 0.21 atm.

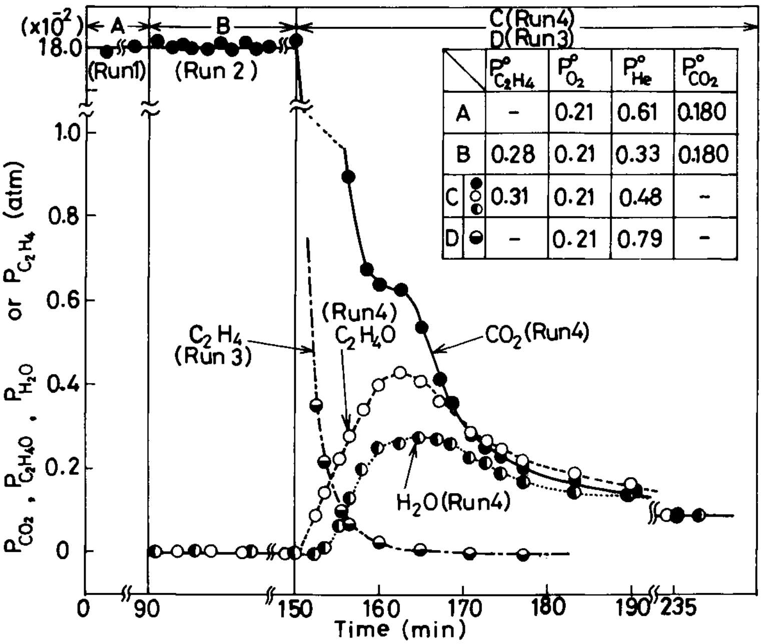

Figure 16. The effect of CO_2 adsorption on the C_2H_4(dec. O)–C_2H_4 response and on the C_2H_4(inc. O)–C_2H_4O and –H_2O responses at 91°C.

induction period for the H_2O formation at the initial stage of the response, in contrast to the C_2H_4(inc.,0)-C_2H_4 and -CO_2 responses in Fig.4. These slow responses are caused by the slow desorption of CO_2 from the adsorbed oxygen species. Here the reason for the induction period of H_2O may reasonably be attributed to the evidence that CO_2 and H_2O are formed via the stable intermediate (In).

The C_2H_4, CO_2(inc.,0)-C_2H_4O and -H_2O responses were followed on the oxidized surface without previously treating the catalyst with the CO_2-O_2-He stream. The results obtained at two different conentrations of CO_2 are presented in Fig.17 as Runs 1($P^{\circ}_{CO_2}$=0.117 atm) and 2 ($P^{\circ}_{CO_2}$=0.18 atm). Appreciable amounts of C_2H_4O and H_2O are produced at the initial stage of the responses in contrast to Run 2 in Fig.16. The both amounts strongly depend on the concentration of CO_2 introduced and decline steeply to near zero within 7 min. This is resulted from the competitive attacking of CO_2 and C_2H_4 onto the same adsorbed oxygen species. The rate of CO_2 adsorption is not fast enough for instantaneously blocking the adsorbed oxygen species, faster than which react with C_2H_4.

After Runs 1 and 2 in Fig.17 had been followed for 2 hrs, the two C_2H_4-O_2-CO_2-He mixtures were separately replaced by the O_2-He mixture (Runs 3 and 4) and the C_2H_4, CO_2(dec.,0)-CO_2 and -H_2O responses were followed. Runs 3 and 4 in fig.17 clearly indicated the production of H_2O with progressive desorption of CO_2 from the adsorbed oxygen species. The total amount of the produced H_2O strongly depends on the concentration of CO_2 in Runs 1 and 2. These results can reasonably be explained as follows: the intermediate (In), which had been formed during the course of Runs 1 and 2 and retained on the surface without reacting with gaseous O_2, is decomposed into H_2O and CO_2 by the reaction with the adjacent adsorbed oxygen species which has been free from the adsorbed CO_2. The higher the concentration of CO_2 in Runs 1 and 2 in Fig.17, the smaller amount of (In) is formed,because the degree of the blocking effect to the adjacent adsorbed monoatomic oxygen depends on the concentration of CO_2.

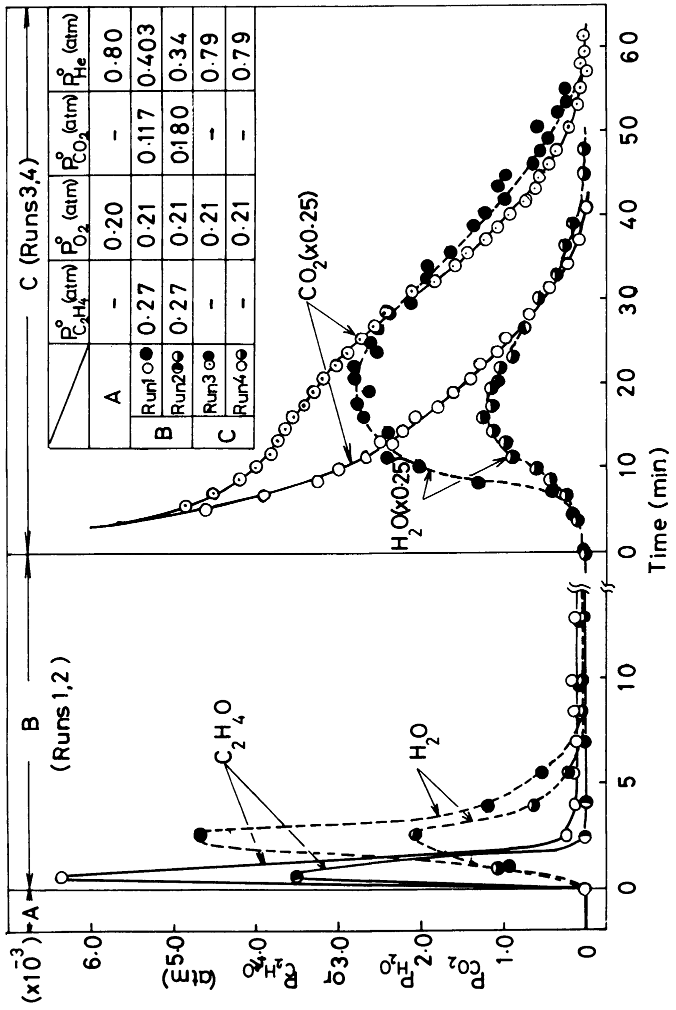

Figure 17. *The effect of CO_2 adsorption on the C_2H_4(inc. O)–C_2H_4O and H_2O responses and on the (In) formation at 91°C.*

Acknowledgment

Thanks are due to Mr.Yamamoto for carrying out some of the experiments.

Literature Cited

1) Kilty,P.A. and Sachtler,W.M., Catalysis Rev.,1974, 10, 1.
2) Force,E.L. and Bell,A.T., J.Catal., 1975, 38, 440.
3) Gerei,S.V., Kalyavenko,K.M., and Rubanik,M.Ya, Ukr.Khim.Zh., 1965, 31(2), 166.
4) Drake,L.C., and Benton,A.F., J.A.C.S.,1934, 56, 506.
5) Czanderna,A.W., J.Colloid.Interface Sci., 1966, 22, 482.
6) Kobayashi,M. and Kobayashi,H., J.Catal., 1972, 27, 100, 108, 114; Catal.Reviews, 1975, 10, 139.
7) Kobayashi,M., Doctral thesis, Hokkaido Univ. 1975.
8) Kobayashi,M., Preprint, 5th Canadian Symposium on Catalysis, 1977, 202.
9) Scholten,J.J.F., Konvalinka,J.A. and Beekman,F.W., J.Catal., 1973, 28, 209.
10) Sundquist,B.E., Acta.Met., 1964, 12, 67.
11) Kobayashi,M., Yamamoto,M. and Kobayashi,H.,Proceeding.6th Intern.Cong.Catal., 1976, A24.
12) Kobayashi,M. and Kobayashi,H., J.C.S.,Chem.Comm., 1976, 103; ibd., 1977, 71.

RECEIVED July 28, 1981.

Development of a Pulse Reactor with On-Line MS Analysis to Study the Oxidation of Methanol

C. J. MACHIELS

E. I. du Pont de Nemours & Co., Inc., Central Research and Development Department, Experimental Station, Wilmington, DE 19898

Whereas steady state kinetic experiments are usually more easy to perform and certainly more easy to analyze, information is normally only obtained pertaining to the rate limiting step in the reaction sequence. Experiments of a dynamic type, such as pulse experiments or other transients, can give additional information about reaction mechanisms that is often difficult to obtain by other techniques. Additional advantages of pulse experiments are that they often take less time and require just small amounts of materials, both catalyst and reactants. The major problems of the pulse and other transient techniques seem to be related to the lack of good and rapid transient analytical methods and the fact that data analysis is not straightforward. Many good reviews are available concerning the theory and applications of pulse and other transient experiments (1,2,3).

In a typical pulse experiment, a pulse of known size, shape and composition is introduced to a reactor, preferably one with a simple flow pattern, either plug flow or well mixed. The response to the perturbation is then measured behind the reactor. A thermal conductivity detector can be used to compare the shape of the peaks before and after the reactor. This is usually done in the case of non-reacting systems, and moment analysis of the response curve can give information on diffusivities, mass transfer coefficients and adsorption constants. The typical pulse experiment in a reacting system traditionally uses GC analysis by leading the effluent from the reactor directly into a gas chromatographic column. This method yields conversions and selectivities for the total pulse, the time coordinate is lost. It is desirable to be able to continuously monitor all the reactants and products so that a time resolved response curve is obtained for the separate components in the pulse. The sequence in which the products appear and the shape of each individual peak can, in principle, give information on the reaction sequence and on adsorption properties that cannot easily be obtained in any other way. Infrared spectroscopy has been used with good results, but the number of systems suitable is limited and at best only a small number of components can be analyzed for, Figure 1. The

0097-6156/82/0178-0239$05.00/0
© 1982 American Chemical Society

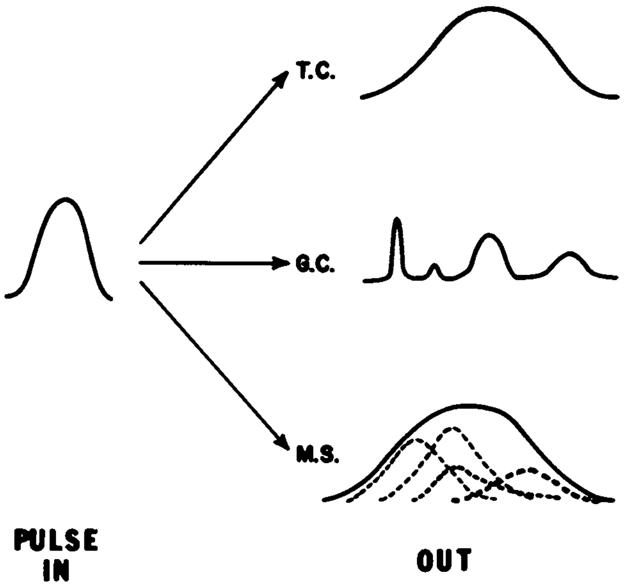

Figure 1. Analytical methods for pulse experiments.

In Catalysis Under Transient Conditions; Bell, A., et al.;
ACS Symposium Series; American Chemical Society: Washington, DC, 1982.

most general method is a mass spectrometer with continuous inlet system, and several reports have appeared recently describing such systems (4-8). Many of these systems lacked sufficient speed for pulse experiments, often an experiment had to be repeated several times, looking at a different component each time.

Methanol Oxidation

Initial tests using the pulse reactor described in this paper have been done on the selective oxidation of methanol to formaldehyde using molybdate catalysts.

A commercial catalyst from Harshaw was used, a 3:1 mixture of molybdenum trioxide and ferric molybdate, as well as the two separate phases. Kinetic experiments were done previously in a differential reactor with external recycle using these same catalysts as well as several other preparations of molybdenum trioxide, including supported samples. The steady state kinetic experiments were done in the temperature range 180-300 C, and besides formaldehyde, the following products were observed, dimethylether, dimethoxymethane, methyl formate, and carbon-monoxide. Usually very little carbon dioxide was obtained, and under certain conditions, hydrogen and methane can be produced. The steady state experiments showed that the two separate phases and the mixture are not very different in activity, give approximately the same product distributions, and have similar kinetic parameters. The reaction is about .5 order in methanol, nearly zero order in oxygen, and has an apparent activation energy of 18-20 kcal/mol. These kinetic parameters are similar to those previously reported (9,10), but often ferric molybdate was regarded to be the major catalytically active phase, with the excess molybdenum trioxide serving for mechanical properties and increased surface area (10,11,12).

At least four different steps have been reported to be the rate determining step in this reaction, ranging from the adsorption of methanol to the desorption of the products and the reoxidation of the surface. Studies in the recycle reactor using deuterium labeled methanol showed that over a limited temperature range, the rate limiting step on the commercial catalyst is the breaking of a carbon-hydrogen bond (13). The ratios of rate constants in Table I show that a deuterium in the hydroxyl group has little effect on activity; selectivities are not affected. A primary kinetic isotope effect is observed, however, when completely deuterated methanol is used, and the product distribution also changes significantly; much more dimethylether is formed and less formaldehyde. For the formation of the ether, no carbon-hydrogen bonds need to be broken.

Table I

Kinetic isotope effect on $Fe_2(MoO_4)_3/MoO_3$

	k_{CH_3OD}/k_{CH_3OH}	k_{CD_3OD}/k_{CH_3OH}
220	0.93	-
230	0.92	0.26
260	0.94	0.37

Experimental

A flow schematic of the pulse reactor is shown in Figure 2. The flexible design allows dynamic experiments of various types. Helium carrier gas flows through the two channels of a Gow-Mac thermal conductivity cell before and after passing through the reactor. Pulses of methanol in argon or an argon-oxygen mixture can be introduced using a six-port Valco valve with a 1 cc sample loop. Pulses of methanol can be alternated with oxygen pulses. A four-port Valco valve allows application of step changes. For this purpose, the helium stream can be replaced by another methanol-containing stream. This set up can also be used for pulses of isotopically labeled species onto a steady state of unlabeled materials. Methanol streams are obtained using a saturator method and concentrations are determined by gas chromatographic analysis. Back pressure regulators in the reactor stream and the sample gas stream maintain an equal pressure of 1-2 psig in both streams. Pulses can be dispersed in a column before the reactor if desired.

The reactor itself Figure 3 is made of Pyrex, using 1mm capillary tubing wherever possible. The catalyst (0.2-0.5 g) is on a fritted disk, 14 mm in diameter. The catalyst bed is several mm high. A continuous sample to the mass spectrometer is taken from just above the catalyst bed. A short section of 1/16" stainless steel tubing is coupled to a 1-m stainless steel capillary, 0.15 mm i.d./2 mm o.d. Part of the reactor effluent is pumped through this capillary and through the inlet valve of the mass spectrometer. If this valve is opened, a small portion of the gas leaks through an orifice directly into the ion formation region of the ion source. The pressure reduction in two stages from atmospheric to approximately 1 mbar in the valve to 10^{-6}-10^{-5} mbar in the spectrometer ensures viscous flow in the capillary and minimizes mass discrimination effects. Good results were also obtained when the stainless capillary was replaced by a section of fused silica capillary.

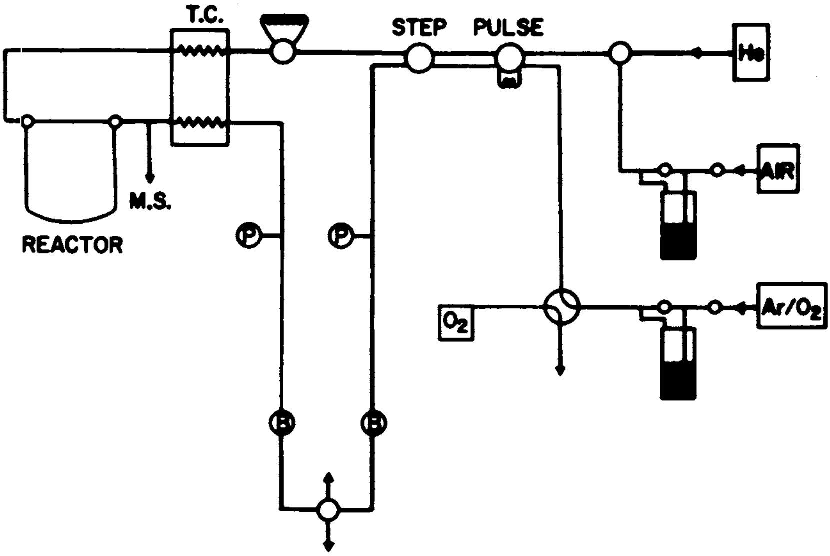

Figure 2. Flow diagram of reactor for transient experiments.

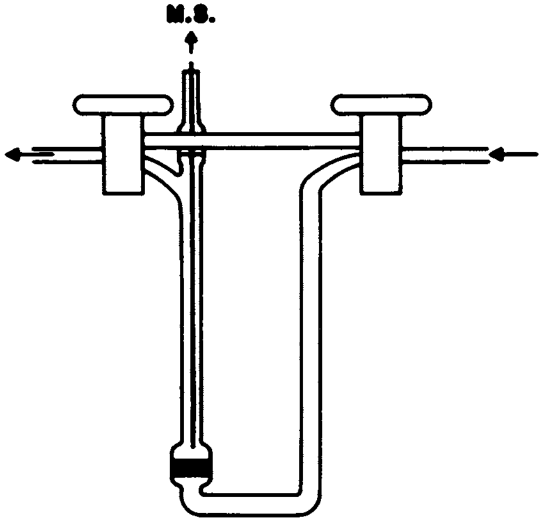

Figure 3. Pyrex pulse reactor.

The quadrupole mass spectrometer used for analysis is a QMG 511 by Balzers. This system comes as a compact, mobile package, uses turbomolecular pumping, and is interfaced to a DEC PDP-11/34 minicomputer. A limited software package allows full computer control of all the spectrometer functions and various methods of data acquisition. A gas tight axial ion source is used for high ionization efficiency, and a 90° off axis electron multiplier improves the signal to noise ratio. A data integrator allows for maximum speed and stability of data acquisition; ion signals are collected at 17 μs/point, and each 64 data points are averaged in hardware in the integrator before transferring to the interface. Peaks are symmetrical and have flattened tops, typically the change of intensity at the top of a peak is not more than 5% over 1/4 of a mass unit. This is an important characteristic, because with the rapid scanning during a pulse, there is no opportunity to scan the complete mass range and determine the exact location of each peak in each scan. Instead, we have to jump from the top of one peak to the next and so on in a cyclical fashion. Flattened tops ensure that slight shifts in peak location do not cause large errors in this process. Figure 4 shows a flow diagram for sample analysis. Raw intensity data are stored in core memory and then transferred to disk after the experiment. They can be used for plotting and further analysis. Before an experiment, the exact location of the peaks of interest is determined and if necessary a background spectrum is obtained. After a pulse is taken, scanning is not started until triggered by mass 40 (argon).

To test the reactor and analysis system, pulses of methanol, singly, and completely deuterated methanol were led over the commercial $Fe_2(MoO_4)_3/MoO_3$ catalyst and the two separate phases. In this way, we can check if a kinetic isotope takes place on the separate phases, and the measurements can be extended to a larger temperature range more readily than under steady state conditions. The pulses contained about 12% methanol in argon and 10% oxygen.

Results and Discussion

Pulses were taken at temperatures between 210 and 450 C at 30° intervals, and in each case the conversion of methanol and the product distribution were determined. Figure 5 shows a typical result of an experiment. The intensity of various mass numbers is plotted as a function of time. In this case 660 mg of the commercial catalyst was in the reactor and twelve masses were scanned at a rate of approximately 200 ms/scan, using the data integrator. In most of the experiments, the scanning rate was faster; 80-100 ms/scan for 8-10 masses.

In Catalysis Under Transient Conditions; Bell, A., et al.;
ACS Symposium Series; American Chemical Society: Washington, DC, 1982.

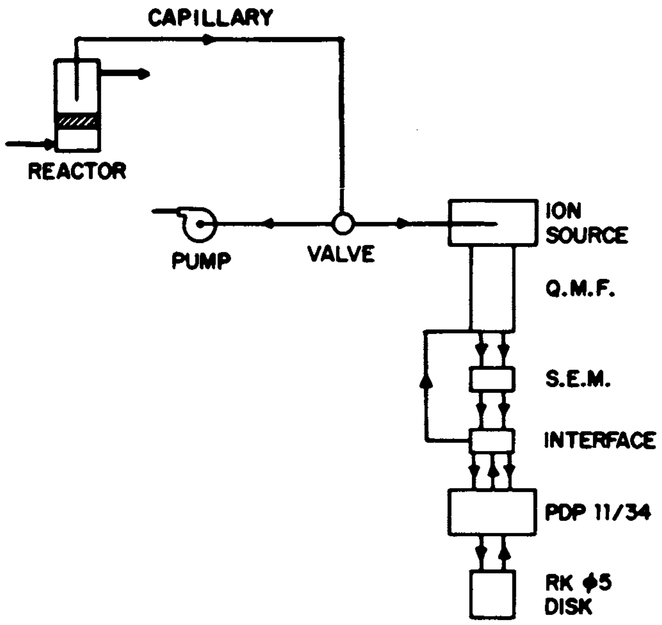

Figure 4. On-line sample analysis.

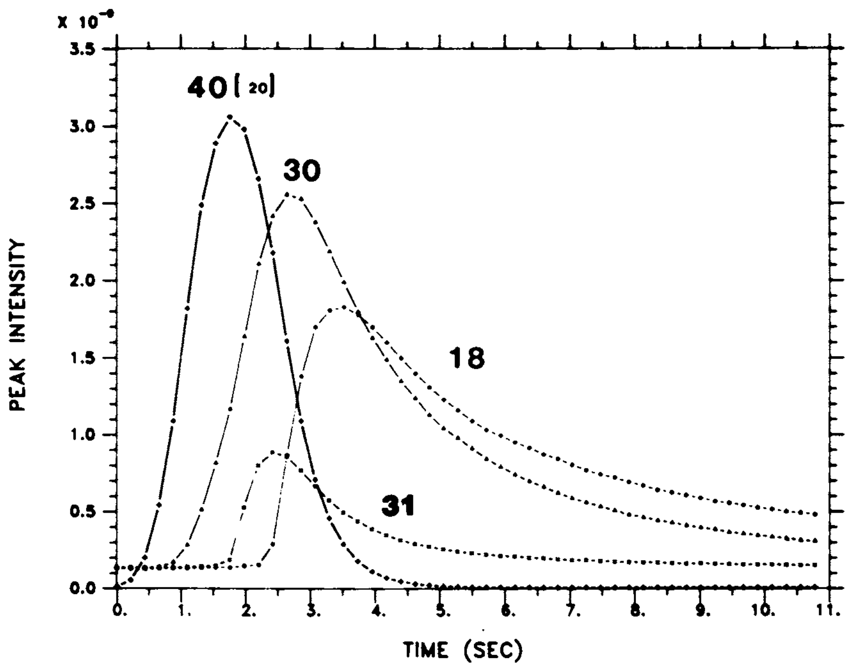

Figure 5. Mass intensities vs. time using $Fe_2(MoO_4)_3/MoO_3$ at 270°. Curve numbers indicate mass. Key: 40, Ar/20; 30, CH_2O; 31, CH_3OH; and 18, H_2O.

The only products observed in the pulse experiments were dimethylether, formaldehyde and water. This is a different product distribution than in the continuous flow experiments and indicates that dimethoxymethane and methylformate are not primary products. In the analysis, peaks 18, 30, 31 and 45 are used for water, formaldehyde, methanol and dimethylether, respectively. Fragmentation patterns were also determined for the deuterated species; they are nearly equal to that of CH_3OH. Small amounts of carbon monoxide cannot be determined with great accuracy. The figure shows clearly that all peaks have been delayed compared to argon by several seconds. The peak for oxygen coincides with that for argon, dimethylether coincides with methanol, and is somewhat faster than formaldehyde. Water is adsorbed most strongly on the catalyst. In blank experiments, the delay between peaks is not more that 0.2 s. Figure 6 shows the delays of the tops of the peaks for methanol, formaldehyde, and water relative to argon as a function of temperature. As expected, there is a decrease with increasing temperature, except for water which shows a minimum in all cases.

Figures 7-9 show the fractional conversion of methanol in the pulse as a function of temperature for the three catalysts and the three methanol feeds. Evidently the kinetic isotope effect is present on all three catalysts and over the complete temperature range, indicating that the rate limiting step is the breaking of a carbon-hydrogen bond under all conditions. From these experiments, the effect cannot be determined quantitatively as in the case of the continuous flow experiments, but to obtain the same conversion of CD_3OD, the temperature needs to be 50-60° higher. This corresponds to a factor of about three in reaction rate. The difference in activity between MoO_3 and $Fe_2(MoO_4)_3$ is larger in the pulse experiments compared to the steady state results.

The conclusions on the rate limiting step are again supported by the differences in product selectivity if completely deuterated methanol is used; the selectivity to dimethylether relative to formaldehyde is much larger. This is shown for the three catalysts in Figures 10-12, in which the ratio of the amounts of dimethylether and formaldehyde formed is plotted as a function of temperature. In the case of CH_3OD, the water observed is a mixture of H_2O, HDO, and D_2O, most of it being HDO.

A suggested reaction mechanism based on kinetic and isotope experiments, product distributions, and the effect on these of addition of water to the feed or leaving oxygen out is shown in Figure 13.

In Catalysis Under Transient Conditions; Bell, A., et al.;
ACS Symposium Series; American Chemical Society: Washington, DC, 1982.

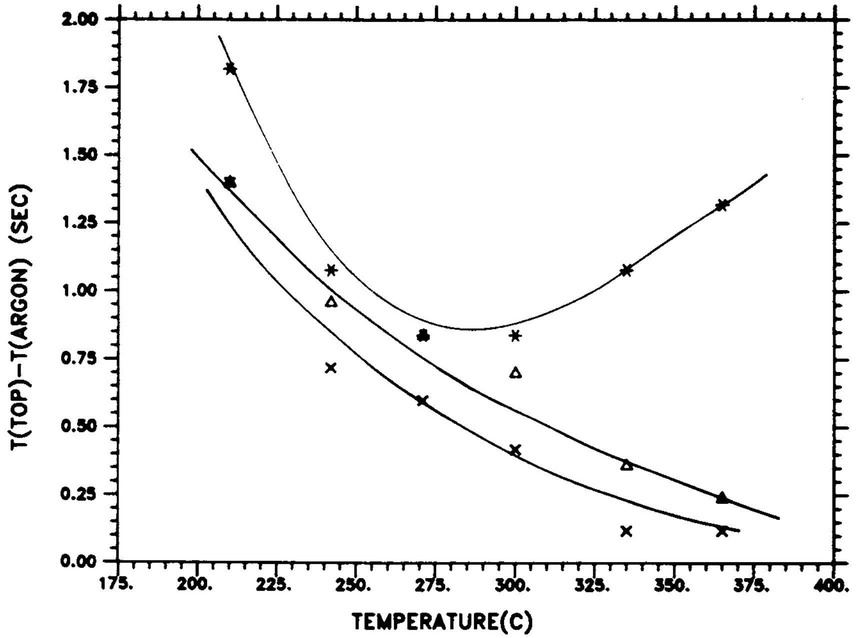

*Figure 6. Delay of top of peaks relative to Ar as a function of temperature. Key: ×, mass 34 (CD_3OD); △, mass 32 (CD_2O); and *, mass 20 (D_2O).*

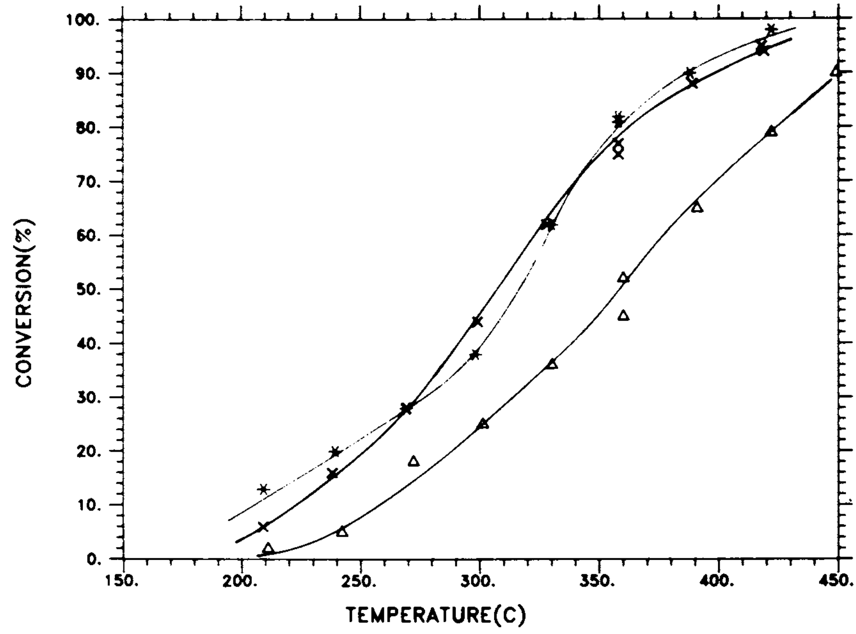

*Figure 7. Conversion vs. temperature on 0.3 g of MoO_3. Key: △, CD_3OD; *, CH_3OD; and ×, CH_3OH.*

American Chemical
Society Library
1155 16th St. N. W.
Washington, D. C. 20036

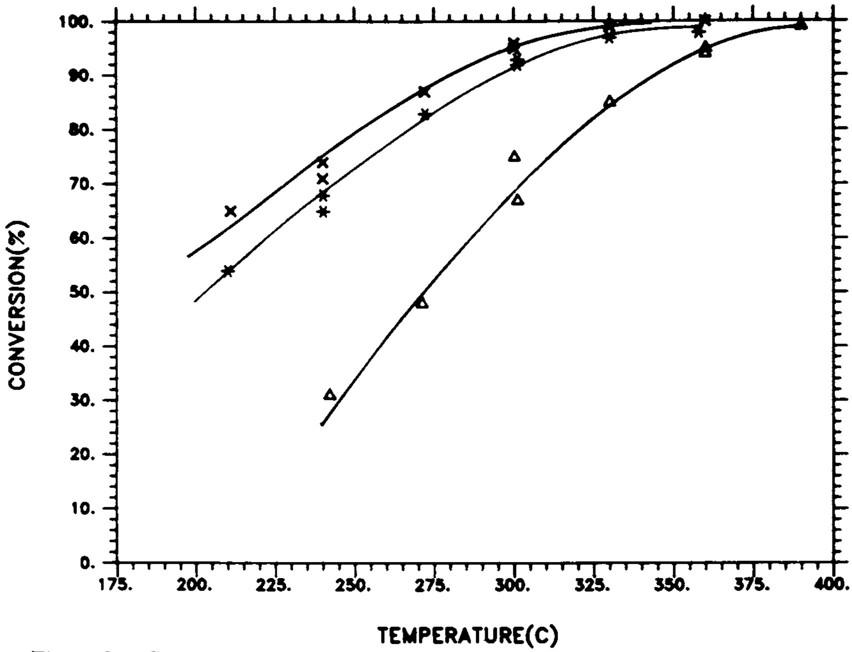

*Figure 8. Conversion vs. temperature on 0.3 g of $Fe_2(MoO_4)_3$. Key: △, CD_3OD; ×, CH_3OD; and *, CH_3OH.*

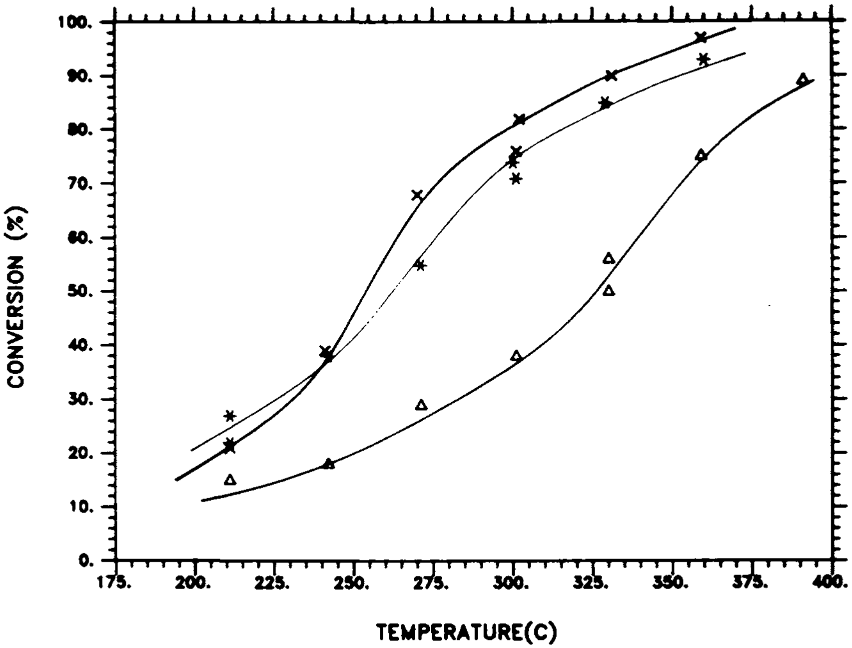

*Figure 9. Conversion vs. temperature on 0.2 g of $Fe_2(MoO_4)_3/MoO_3$. Key: △, CD_3OD; ×, CH_3OD; and *, CH_3OH.*

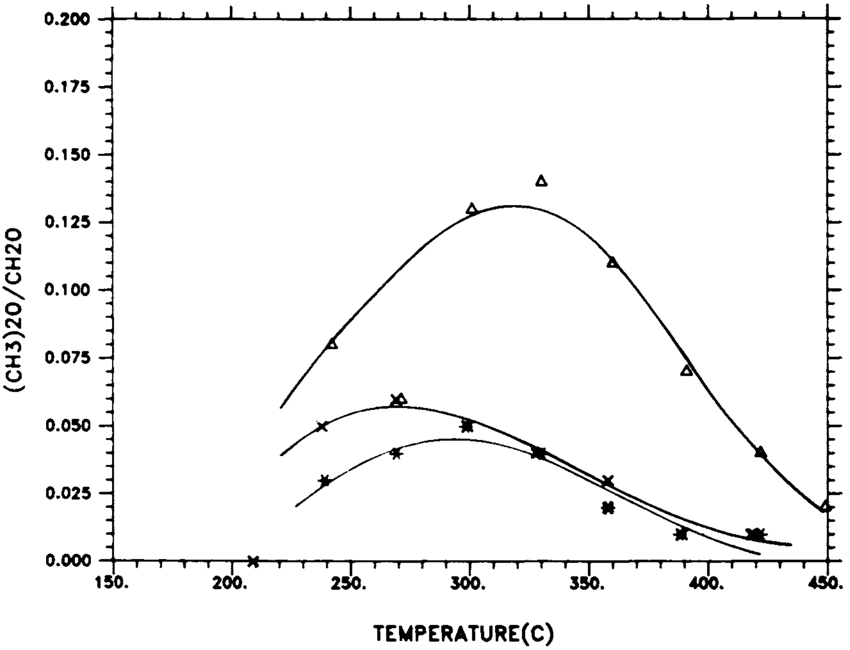

*Figure 10. Ratio of CH_3OCH_3 to CH_2O produced on 0.3 g of MoO_3. Key: △, CD_3OD; *, CH_3OD; and ×, CH_3OH.*

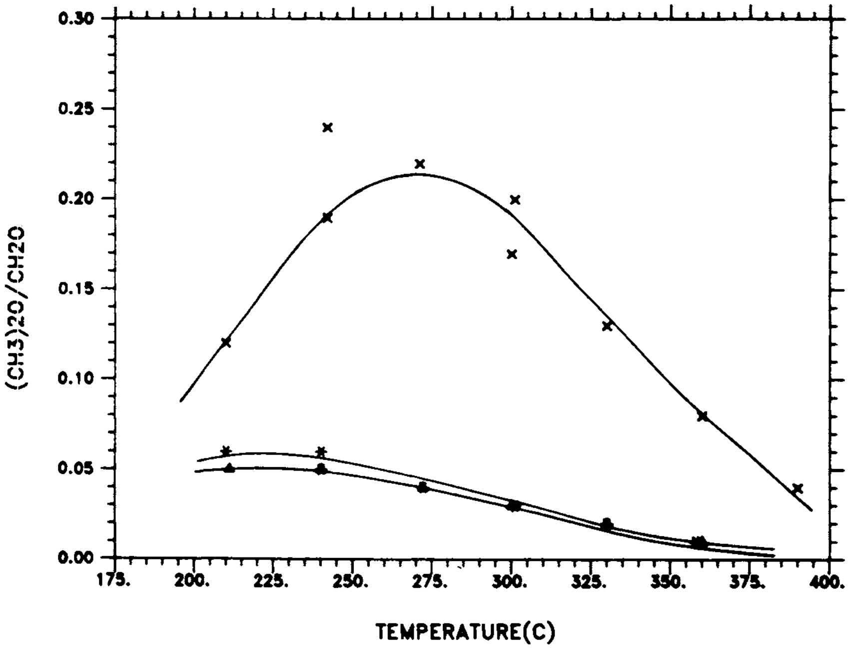

*Figure 11. Ratio of CH_3OCH_3 to CH_2O produced on 0.3 g of $Fe_2(MoO_4)_3$. Key: ×, CD_3OD; △, CH_3OD; and *, CH_3OH.*

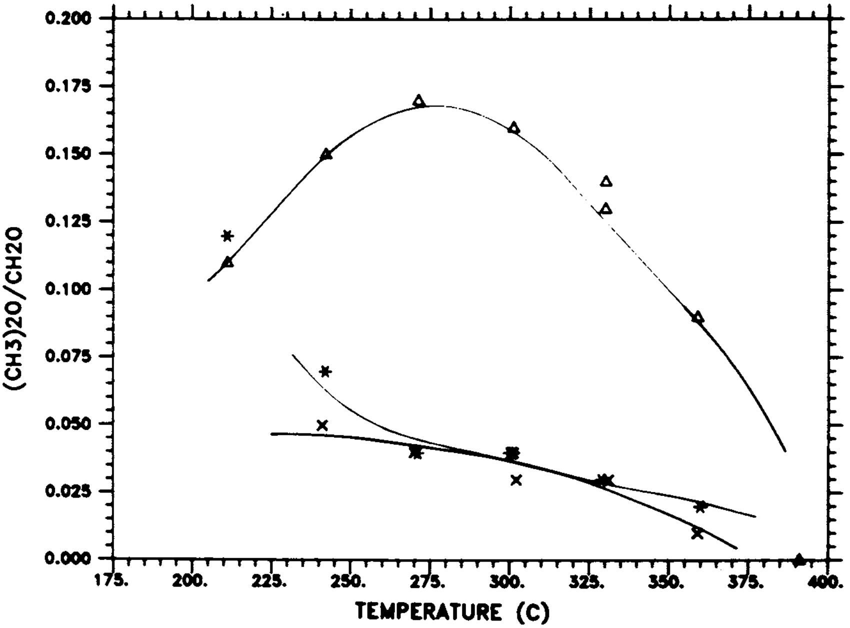

*Figure 12. Ratio of CH_3OCH_3 to CH_2O produced on 0.2 g of $Fe_2(MoO_4)_3/MoO_3$. Key: △, CD_3OD; ×, CH_3OD; and *, CH_3OH.*

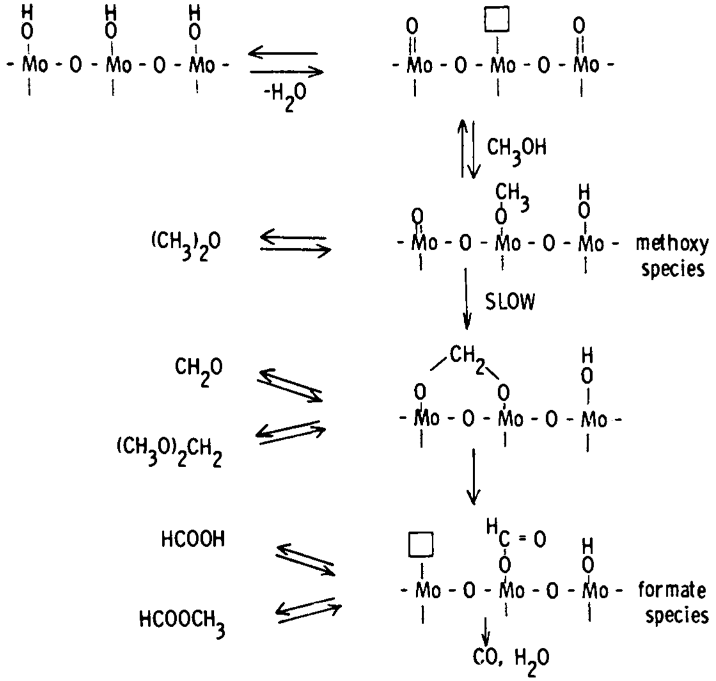

Figure 13. Suggested reaction mechanism for CH_3OH oxidation on MoO_3.

A dissociative adsorption of methanol forming surface methoxy groups is suggested as the initial step. This is followed by the slow step, the formation of some form of adsorbed formaldehyde species. Evidence for the bridged species is not available, experiments with ^{18}O labeled methanol are expected to clarify this. Continued surface oxidation leads to a surface formate group and to carbon monoxide. All the byproducts can be obtained by combination of the appropriate surface species.

These initial experiments show that results can be obtained from this system that are comparable to those from the continuous flow reactor. The analytical system satisfies the requirements for accurate and rapid repetitive analysis. Scanning of 12 masses is possible at rates of approximately 100 ms/scan with good results. Further data manipulations are expected to yield additional results from this type of experiments.

Acknowledgement

The author is thankful to U. Chowdhry for preparing the pure phase ferric molybdate.

Literature Cited

1. Smith, J. M., Suzuki, M., Furusawa, T., Catal. Rev. 1976, 13(1), 43.
2. Bennett, C. O., Catal. Rev. 1976, 13(2), 121.
3. Kobayashi, H., Kobayashi, M., Catal. Rev. 1974, 10(2), 139.
4. Schweich, Villermaux, J., Anal. Chem. 1979, 51(1), 77.
5. Bernasek, S. L. Chadwick, P. A., Chem. Biomed. and Environ. Instrum., 1979, 9(3), 229.
6. Kasemo, B., Rev. Sci. Instrum. 1979, 50(12), 1602.
7. Winters, H. F., Raimondi, D. L., Grant, P. M., Clarke, D. C., IBM J. Res. Dev., July 1971, 307.
8. Latzel, J., React. Kinet. Catal. Lett. 1977, 7(4), 393.
9. Pernicone, N., Lazzerin, F., Liberti, G., Lanzavecchia, G., J. Catal. 1969, 14, 293.
10. Carbucicchio, M., Trifiro, F., J. Catal. 1976, 45, 77.
11. Van Truong, N., Tittarelli, P., Villa, P. L., Proceedings of the Climax Third International Conference on the Chemistry and Uses of Molybdenum, (H. F. Barry and P. C. H. Mitchell - eds.) Climax Molybdenum Company, Ann Arbor, Michigan, 1979, page 161.
12. "Catalyse de contact", ed. LePage, J. F., page 385, Editions Technip, 1978.
13. C. J. Machiels, submitted to J. Catal.

RECEIVED June 26, 1981.

11

Square Concentration Pulses in Oxidation Catalysis over Perovskite-type Oxides of Manganese and Iron

R. J. H. VOORHOEVE[1], L. E. TRIMBLE, and S. NAKAJIMA[2]
Bell Laboratories, Murray Hill, NJ 07974

E. BANKS
Polytechnic Institute of New York, Chemistry Department, Brooklyn, NY 11201

The objective of this work was to provide a technique for measuring catalytic reaction kinetics over oxides in a manner unaffected by hysteresis effects. Hysteresis is commonly introduced by changes in the stoichiometry of the catalyst in response to the reaction conditions (1). We wanted to measure the reaction kinetics in a time sufficiently short that the catalyst stoichiometry would not have changed between the beginning and the end of a series of measurements. To this end, it was necessary to substantially decrease the time on stream per data point, and the use of a pulse technique was therefore attractive.

In the commonly used pulse technique introduced by Kokes et al. (2), a spike of reagents is introduced into a carrier gas flowing over the catalyst and after that over a gas chromatography column which is used to determine the conversion of reagents to products. In this method, the concentrations of reagents in the catalyst bed are not defined, and kinetic measurements relating reaction rates to concentrations are impractical.

Our aim was to use a pulse sufficiently long so that a steady state concentration of reagents would be established (i.e., a flat-topped or "square" pulse), and to measure conversion by sampling a slice from that pulse into the gas chromatograph. Figure 1a shows the square concentration pulse desired, contrasted with the usual unshaped peak in Figure 1b. To enable us to "age" catalysts or to condition them, we also needed to provide a continuous mode corresponding to the traditional steady state rate measurement. Simple "flick of a switch" conversion between continuous and pulse mode operation would enable us to obtain a kinetic snapshot of a catalyst at any point during its life.

[1] Current address: Celanese Research Company, Summit, NJ 07901.
[2] Current address: Polytechnic Institute of New York, Chemistry Department, Brooklyn, NY 11201.

0097-6156/82/0178-0253$05.00/0
© 1982 American Chemical Society

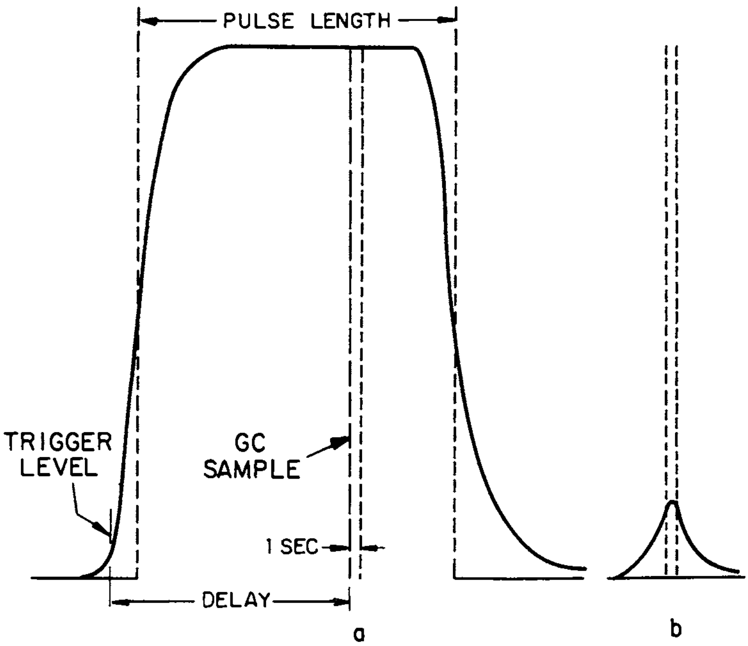

Figure 1. Pulse shapes in the square pulse method (a) and in the conventional pulse method (b). Solid lines give the pulse shape after passage through the catalyst. Trigger level refers to the point at which the pulse detector is triggered by the leading edge of the pulse.

The incentive to modify our existing continuous-flow micro-unit to incorporate the square pulse capability was provided by our work on perovskite-type oxides as oxidation-reduction catalysts. In earlier work, it had been inferred that oxygen vacancies in the perovskite structure played an important role in catalytic activity (3). Pursuing this idea with perovskites of the type $La_{1-x}Sr_xFe_{0.5}Mn_{0.5}O_3$, our experiments were hampered by hysteresis effects which we assumed to be due to the response of the catalyst's oxygen stoichiometry to the reaction conditions. An example of such hysteresis is given in Figure 2 for the oxidation of CO over Sr_2MnFeO_6 and La_2MnFeO_6. Elimination of this hysteresis would enable us to collect a set of data descriptive of a constant state of the catalyst, and hence analyzable in terms of a true reaction order and activation energy.

In this work we attempt to measure kinetics data in a time short compared with the response time of the catalyst stoichiometry. An alternative is to measure kinetics in a true steady state, i.e., to increase the line-out time at each reactor condition until hysteresis is eliminated. The resulting apparent reaction orders and activation energies would be appropriate for an industrial mathematical model of reactor behavior.

Catalysts

The catalysts used in this study were La_2FeMnO_6 and Sr_2FeMnO_6 prepared by repeatedly mixing, ball milling, pressing and firing ceramic solids prepared from the corresponding carbonate raw materials (4). The pellets were fired in air at 1200°C in a Pt boat in a tube furnace. The surface areas of the samples were measured by krypton adsorption in a Micromeritics automatic BET apparatus and were 0.29 m^2/g for Sr_2MnFeO_6 and 0.31 m^2/g for La_2MnFeO_6. Analysis of the samples by X-ray fluorescence showed a small contamination with Pt, presumably due to the firing in a Pt boat. The Pt level was not quantified.

Micro Flow Unit and Square Pulse Unit

The experimental set up (Figure 3) provides for continuous as well as pulse flow operation. Conversion between the two modes is instantaneous, limited only by the ~2 minute flush out time of the reactor. In the continuous flow mode, a mixture of CO, O_2 and He from a flow and ratio controller are fed over the catalyst via valve V_1 (AD) and then through GC sample valve V_4, by way of valves V_2 (EG) and V_3 (LN). The GC sampling is timed at regular intervals. After the sample has been taken, the reactor conditions are changed according to a pre-set pattern and the reactor is allowed to line out before the next sample is taken. In the pulse mode, a constant flow of He flows through valves V_5, V_1 (BD) over the reactor, through a pulse detector PD via valve V_2 (EH) and through the GC sample valve via valve

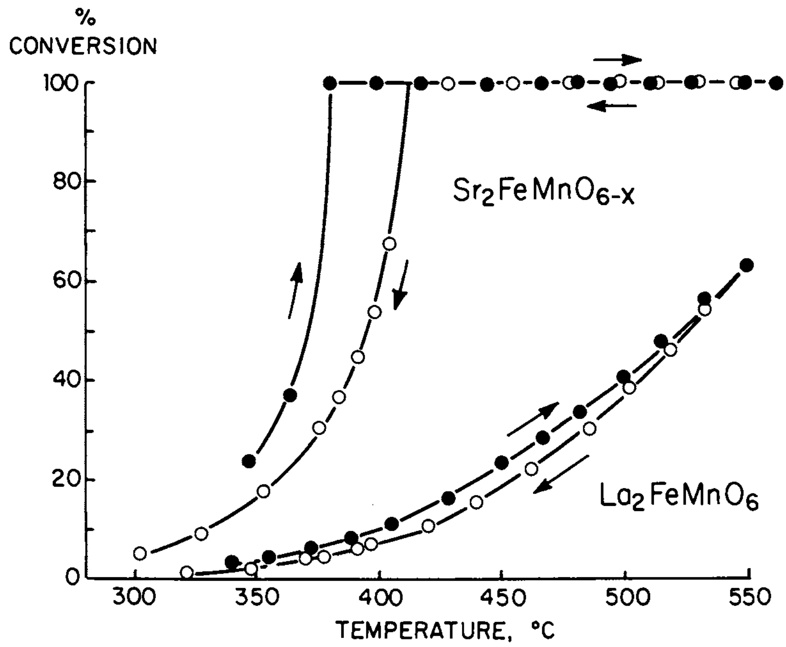

Figure 2. Continuous flow measurements of the conversion of CO over perovskite-type catalysts. The temperature is held constant for ~10 min for each data point. Conditions: 5% CO and 5% O_2 in He at a total flow of 100 mL/60 s (NPT); and catalyst weight 177 mg. Catalysts used as received.

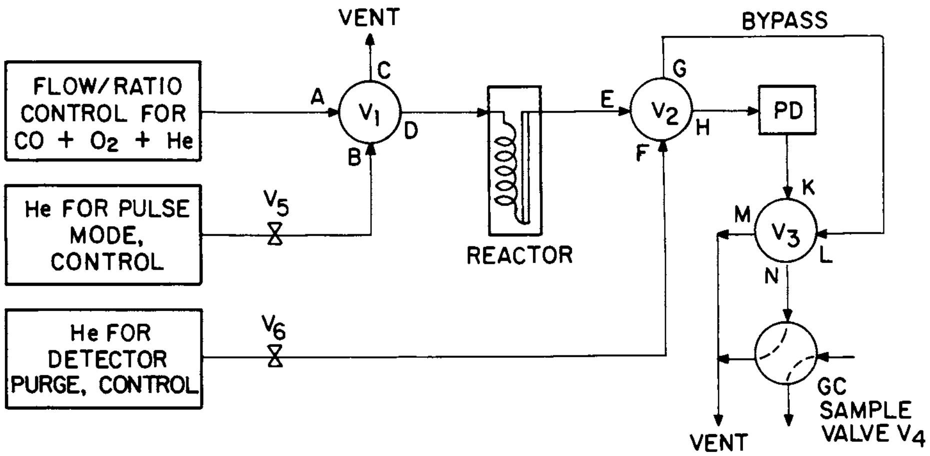

Figure 3. The square pulse method combined with a conventional continuous flow setup.

V_3 (KN). A pulse of the CO, O_2, He mixture is introduced by switching valve V_1 from (AC, BD) to (AD, BC) for a predetermined length of time, generally about 30 sec. After leaving the reactor, the pulse is detected by PD at the trigger level (see Figure 1a). The GC sample valve V_4 is at that time switched into the "sample" position and after a preset delay a sample is injected into the GC carrier flow. The size of the slice taken from the effluent pulse (1 sec in Figure 1a) is determined by the volume of the sample loop in V_4. After the sample has been injected into the GC carrier flow, the conditions in the reactor, e.g. the temperature, are automatically adjusted for the next sample and data point. Figure 4 is a logic diagram of the pulse mode operation. T_1-T_4 are event timers. V_1-V_4 are solenoid valves. The reactor is heated by a fluidized sand bath with internal exposed heating coil, allowing rapid changes of the temperature.

Results

Hysteresis. Application of the pulse method to the measurement of the reaction rate of the oxidation of CO over La_2FeMnO_6 in pre-reduced and pre-oxidized states (top and bottom curves in Figure 5, respectively) shows that hysteresis-free measurements were made with 30 sec pulse length, 18-23 sec delay (see Figure 1a) and 10-minute intervals between data points. Measurements by the continuous flow method in Figure 2 (bottom curve) serve as comparison. The same duty cycle when applied to measurements on Sr_2MnFeO_6 resulted in much reduced hysteresis effects (Figure 6) as compared to the continuous flow measurements (Figure 2, top curves). The residual hysteresis was shown to be due to bulk oxidation of the solid at temperatures of 550°C and higher. It was observed that at 567°C, with a pulse flow of 5% CO and 5% O_2 in He completely converted to CO_2 and O_2, the amount of O_2 absorbed by the catalyst in a single 30 sec pulse was sufficient to increase the bulk oxygen content by 1%. Maintaining the Sr_2MnFeO_6 catalyst below 380°C eliminates hysteresis completely, both in the pulse and in the continuous modes (Figure 7). It was observed that the extent of hysteresis depends also on the oxidation state of the catalyst, suggesting that the rate of oxygen transport in the solid depends on its stoichiometry. All data reported below were obtained after conditioning the catalysts: a) by reduction in 5% CO in He at 600°C for 1 hour, b) lining out in the pulse mode for 1 day at 340°C in 5% CO and 5% O_2 in He.

Elution of CO, O_2, CO_2 from the Catalyst. By varying the delay time in Figure 1a, the elution of CO, O_2 and CO_2 can be followed against argon as an internal non-adsorbing standard. CO and O_2 are delayed by 1 second or less in a flow of 100 ml/min of He over 177 mg of La_2FeMnO_6 at 490°C, while CO_2 is delayed by 2

In Catalysis Under Transient Conditions; Bell, A., et al.;
ACS Symposium Series; American Chemical Society: Washington, DC, 1982.

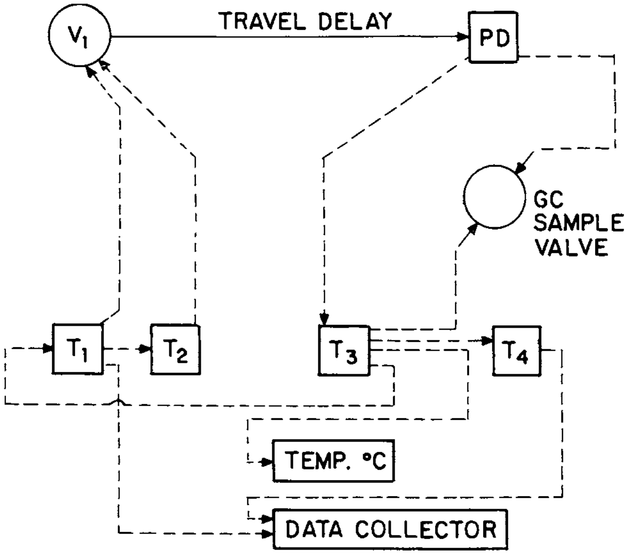

Figure 4. Logic control diagram for the square pulse method as shown in Fig. 3. – – –→ indicates causal directions. Timer T3 sets the "delay" indicated in Fig. 1; T4 prevents injection instabilities from registering in the data collection devices; T1 determines the interval between pulses; and T2 determines pulse length.

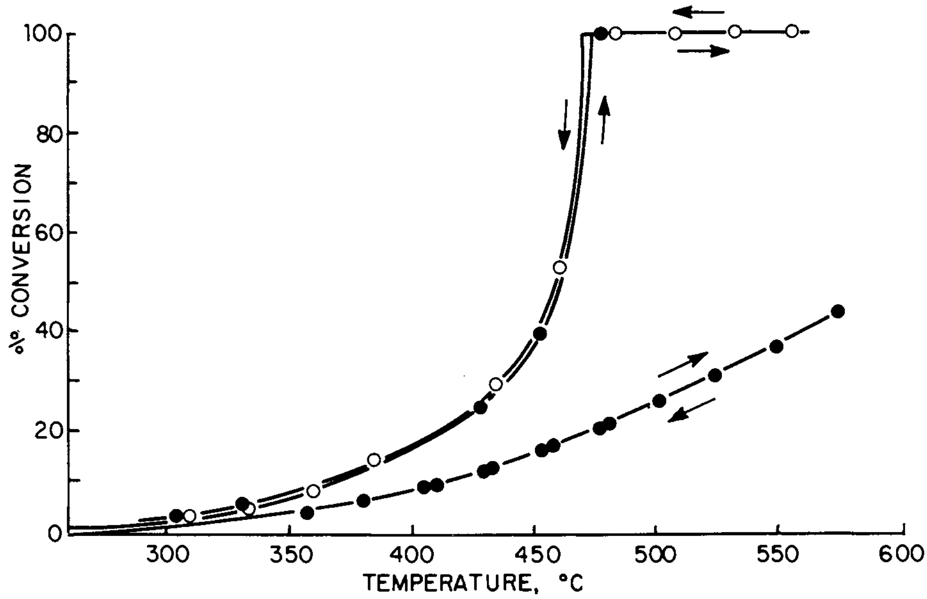

Figure 5. Pulse flow measurement of the conversion of CO over prereduced (top curves; reduction in 5% CO in He at 600°C for 1 h at a flow of 100 mL/60 s.) and as received (bottom curves) La_2FeMnO_6. Duty cycle: 30 s pulse length, 10 min interval, 18–23-s sample delay. Conditions: t, decreased or increased in steps; catalyst weight, 176 mg; and flow, 100 mL/60 s of 5% CO and 5% O_2 in He.

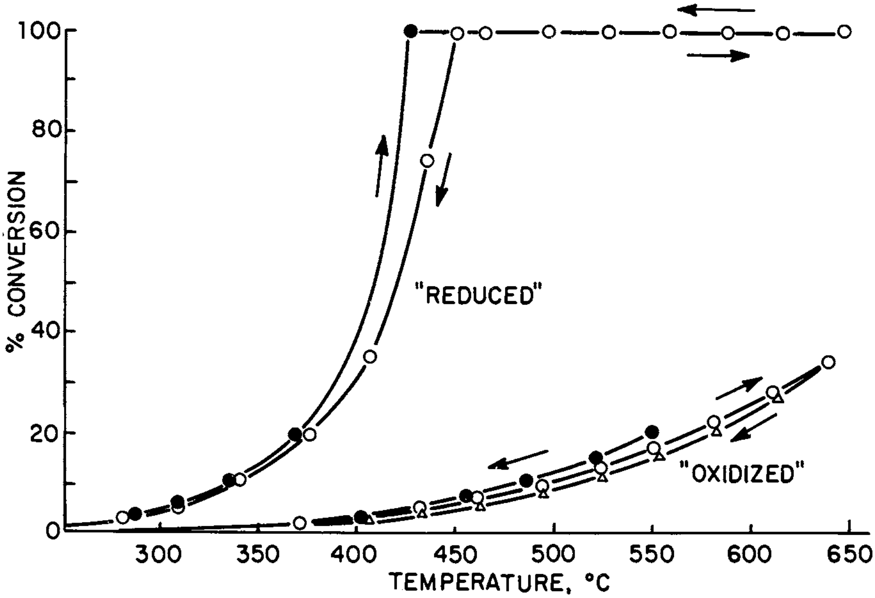

Figure 6. Pulse flow measurement of the conversion of CO over prereduced (top curves; reduction in 5% CO in He at 600°C for 1 h at a flow of 100 mL/60 s) and as received (bottom curves) Sr_2FeMnO_6. Measurement as in Fig. 5. Catalyst weight, 177 mg.

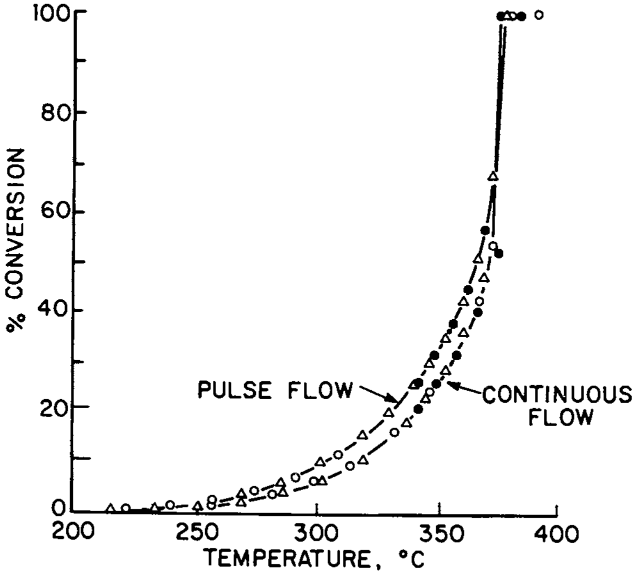

Figure 7. Pulse flow and continuous flow measurements of the conversion of CO over prereduced (see Fig. 6 for conditions) Sr_2FeMnO_6. Flow of 100 mL/60 s of 5% CO and 5% O_2 in He over 177 mg of catalyst. Key: ●, points taken during stepwise decrease of temperature; and ○, △, during stepwise increase.

seconds (Figure 8). Over Sr_2FeMnO_6 at 340°C, CO_2 is delayed 2 seconds under similar flow conditions. This illustrates that a peak-shaped pulse as in Figure 1b would have suffered considerable chromatographic separation over the catalyst bed. It should be noted that transient measurements of this type are much more conveniently made by continuous sampling into a GC-MS interface (5).

Reaction Orders. Employing the same duty cycle of 30-second pulses, delay of 13-23 seconds and 10-minute intervals between pulses, we measured the effect of the partial pressures of O_2 and CO on the reaction rates. The effect of the O_2 pressure is given in Figure 9 for La_2FeMnO_6 and in Figure 10 for Sr_2FeMnO_6. The effects of oxygen pressure are small: a five-fold increase in pressure yields only a 30-50% increase in rate. The formal reaction order at 320-325°C is +0.15 for La_2FeMnO_6 and +0.25 for Sr_2FeMnO_6. The effect of the partial pressure of CO on the rate over La_2FeMnO_6 (Figure 11) reflects a formal order of +0.60 at 308-320°C and an order of +0.4 at 340°C. The effect of the partial pressure of CO on the rate over Sr_2FeMnO_6 (Figure 12) shows a more complicated behavior indicative of two different processes yielding CO_2. At higher pressures of CO ($\gtrsim$0.05 atm) a process with nearly zero order in CO predominates. At partial pressures of CO decreasing below 0.05 atm, rapidly increasing CO conversion rates indicate the existence of a high-rate process which is strongly inhibited by CO.

Discussion

The objective of this work was to make hysteresis-free measurements of oxide catalysts which are changing their oxygen stoichiometry in response to the reaction conditions of the measurement. This can be done if the time used for the measurement is much shorter than the relaxation time of the oxide (stoichiometry is "frozen") or if the oxide stoichiometry equilibrates sufficiently fast that true steady state measurements can be made (6). In the intermediate case, non-equilibrium concentration profiles for oxide ion vacancies, oxide interstitials or other defects are set up across the catalyst particles. These concentration profiles will change with time in response to the boundary conditions imposed by the reacting gas mixture. For the duty cycle employed in the present work (30-second pulse, 10-minute interval), the stoichiometry of La_2FeMnO_6 appears to be "frozen" up to the highest temperature used, i.e., 575°C. In contrast, Sr_2FeMnO_6 relaxes rapidly at that temperature, as shown by changes of its oxygen content by 1% in a 30-second pulse. At much lower temperatures, below 380°C, hysteresis-free measurements could be made on Sr_2FeMnO_6 in either the continuous or pulse modes (Figure 7), suggesting a "frozen" stoichiometry. However, the fact that the activity is different in the two modes

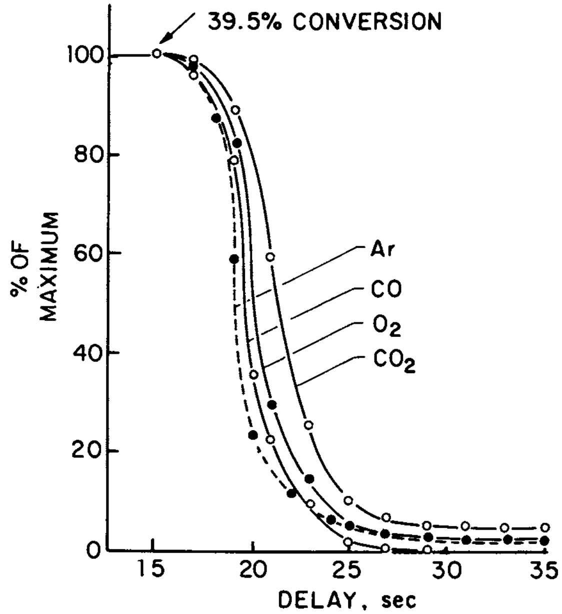

Figure 8. The trailing edge of a square pulse over La_2FeMnO_6 at 490°C. Ar was used as an internal standard. Feed gas was 5% CO and 5% O_2 in He at 100 mL/ 60 s. Data were normalized to 100% for the maximum level of the signal.

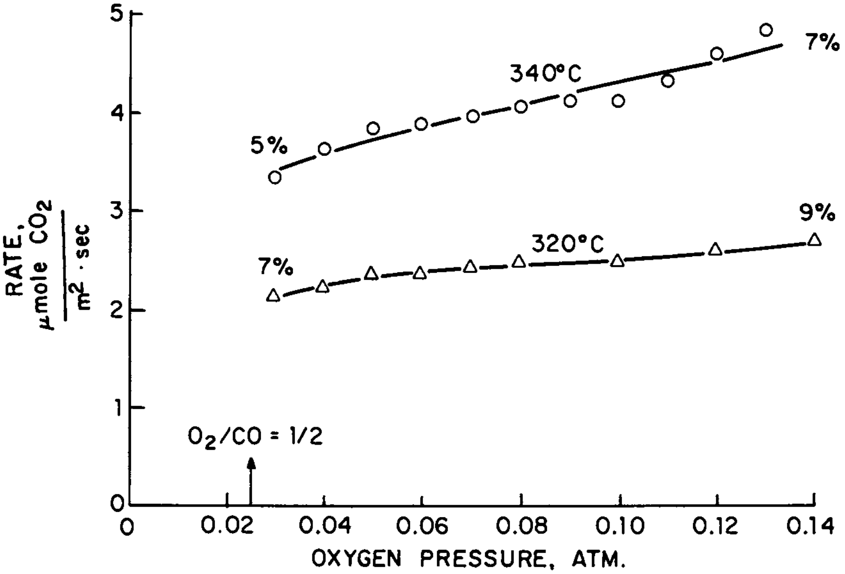

Figure 9. Reaction rate of the oxidation of CO over prereduced La_2FeMnO_6 at 320°C (△) and 340°C (○). See Fig. 5 caption for reduction. Dependence on partial pressure of O_2. CO partial pressure was constant at 0.05 atm. Percentages indicated at the extreme data points are CO conversions.

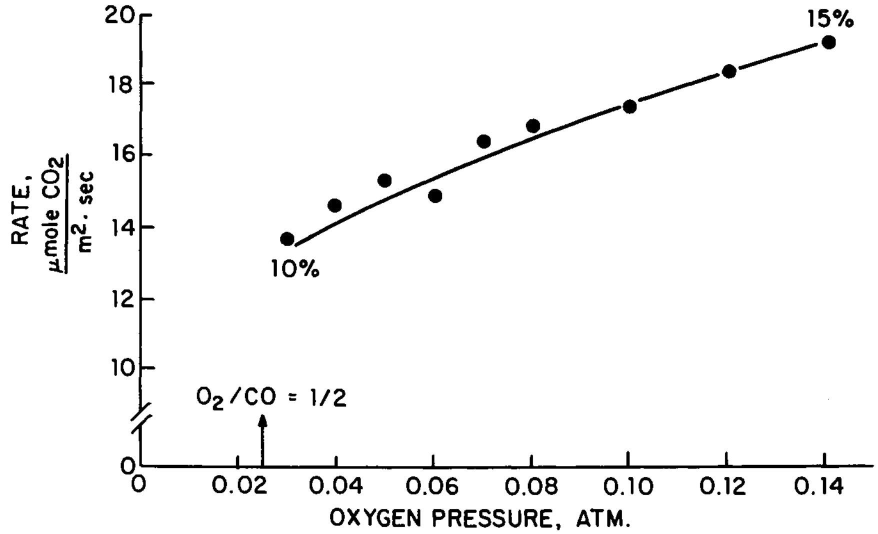

Figure 10. Reaction rate over prereduced Sr_2FeMnO_6 at 325°C. See Fig. 9 caption.

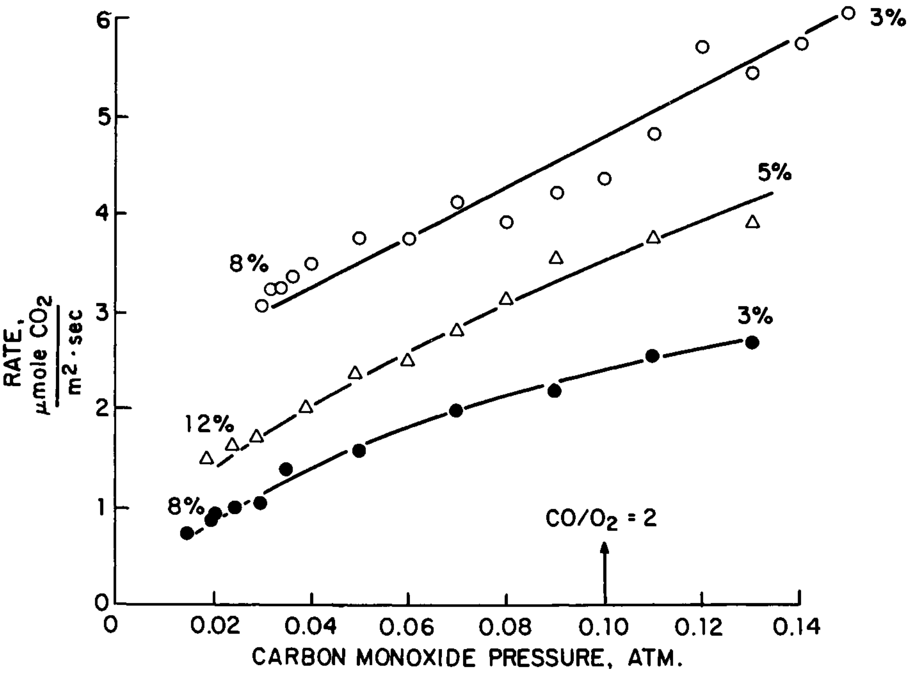

Figure 11. Reaction rate for the oxidation of CO with O_2 over prereduced La_2FeMnO_6 at 308° (●), 320° (△), and 340°C (○). See Fig. 5 caption. Dependence on partial pressure of CO. Oxygen pressure was constant at 0.05 atm. Percentages indicated with extreme data points are CO conversions.

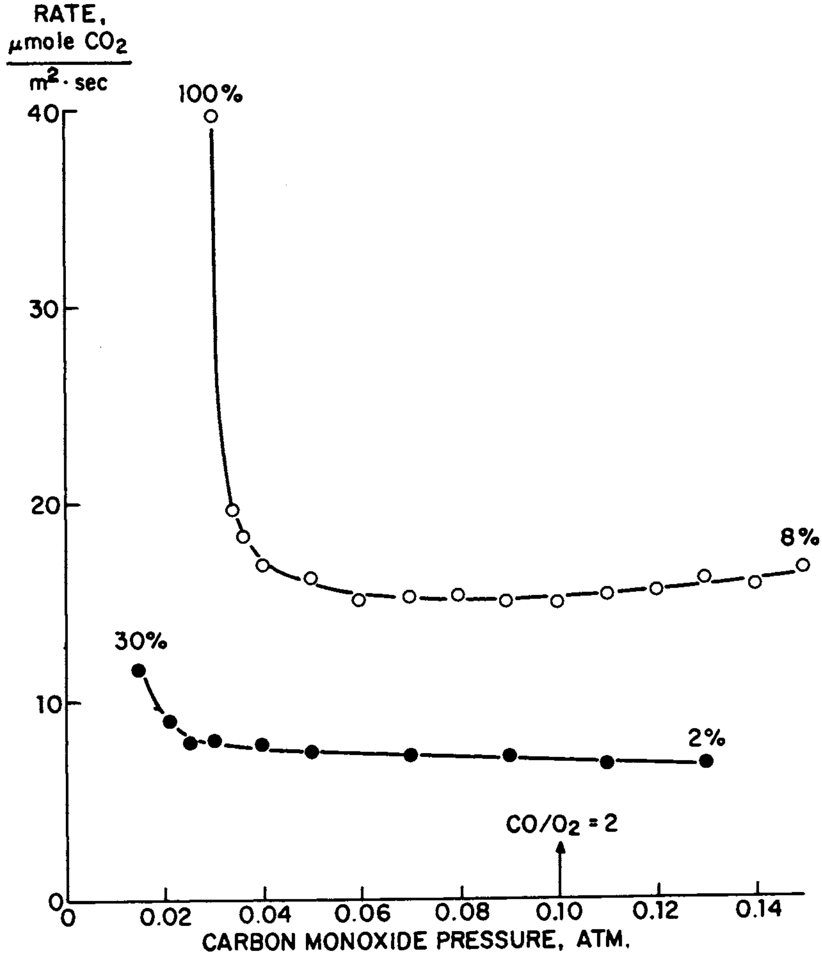

Figure 12. Reaction rate over prereduced Sr_2FeMnO_6 at 312°C (●) and 340°C (○). See Fig. 11 caption.

(i.e. about 30% higher in the pulse flow mode) leaves the possibility that relaxation of the near-surface region of the catalyst affects the measurements of catalytic activity. Further work will be necessary to elucidate this point.

The Sr_2FeMnO_6 and La_2FeMnO_6 perovskites show substantial differences in the temperatures at which solid state relaxation is observed. The data show that relaxation of Sr_2FeMnO_6 is appreciably faster than that of La_2FeMnO_6. The catalytic activities are also quite different, with Sr_2FeMnO_6 more active by about a factor 5. Dependence on the partial pressure of oxygen is small, in accordance with the view that lattice oxygen is used in the oxidation of CO (7, 8). The most striking difference was found in the dependence of the reaction rate on the CO pressure (cf. Figures 11 and 12). On Sr_2FeMnO_6, CO appears to be tightly bound on the active sites (formal order ≤ 0) and we found some preliminary evidence that CO might enter the solid, giving rise to excess CO_2 being formed upon heating the catalyst to 570°C. In contrast, La_2FeMnO_6 behaves more as expected for nearly-stoichiometric oxides on which adsorption of CO is frequently limited, with the formal reaction order (0.4-0.6) being in a range frequently found for oxide catalysts (9).

Significant differences between Sr_2FeMnO_6 and La_2FeMnO_6 were expected on the basis of their solid state properties. Stoichiometric Sr_2FeMnO_6 has formal valence states of Mn^{4+} and Fe^{4+}. The latter is not stable, giving rise to complex defect structures in the "parent" compound $SrFeO_{3-x}$ (10, 11). Sr_2FeMnO_{6-x} is similarly expected to show defect structures including oxygen vacancies at low x and tetrahedral rearrangements of oxygen around Fe at higher values of x. Stoichiometric La_2FeMnO_6 has the stable valence states Fe^{3+} and Mn^{3+}. High temperature (900-1000°C) treatment in oxygen promotes the formation of Mn^{4+} and of La-vacancies in the "parent" compound $LaMnO_{3+x}$ (12), with important effects on its catalytic activity (8). The present preparation (including firing at 1200°C in air) is expected to lead to a more closely stoichiometric composition for La_2FeMnO_6. Solid state studies of these compounds (4) will be related to their catalytic properties in further studies now in progress.

The activities of the perovskite-type oxides are strongly dependent on pretreatment in reducing or oxidizing atmospheres at ∿600°C. This was found for other perovskite catalysts as well (1). Reducing pretreatments lead to more active catalysts (Figures 5 and 6). The reason for this is not known, but better binding of CO to the reduced surface is a possible explanation.

The striking rise of the reaction rate observed over Sr_2FeMnO_6 as the partial pressure of CO decreases (Figure 12) was attributed to an oxidation process inhibited by CO. This is an intriguing result. Since this behavior might be due to contamination by low levels of Pt (from the Pt boat in which the ceramic samples were fired), it will be necessary to study this feature further with catalysts prepared without Pt hardware.

Conclusions

A square concentration pulse flow technique has been developed to study the kinetics of catalytic reactions over catalysts which change their stoichiometry in response to the reaction conditions. The technique makes it possible to obtain hysteresis-free kinetics data while greatly reducing the time during which the catalyst is exposed to the reaction mixture.

The technique has been applied to measurements of the kinetics of the oxidation of carbon monoxide over the perovskite-type catalysts Sr_2FeMnO_6 and La_2FeMnO_6. The pronounced defect nature of Sr_2FeMnO_6 was shown to give rise to higher activity, faster solid state relaxation and different kinetics than found for the more closely stoichiometric La_2FeMnO_6. Zero and negative reaction orders in CO indicate strong binding of CO to the defect catalyst.

Acknowledgements

We thank F. Schrey at Bell Laboratories for the surface area measurements and E. Bowers at Celanese Research Company for the Pt analysis. The work at Polytechnic Institute of New York was supported by the NSF (F. Stafford), Grant DMR-77-24133.

Literature Cited

1. Voorhoeve, R. J. H.; Trimble, L. E.; Khattak, C. P. Materials Res. Bull. 1974, 9, 655.
2. Tobin, H.; Kokes, R. J.; Emmett, P. H. J. Am. Chem. Soc. 1955, 77, 5860.
3. Voorhoeve, R. J. H.; Remeika, J. P.; Trimble, L. E.; in Klimisch, R. L.; Larson, J. G., Editors; "The Catalytic Chemistry of Nitrogen Oxides"; Plenum: New York, 1955; p 215.
4. Banks, E.; Berkooz, O.; Nakagawa, T. NBS Special Publication 364, "Solid State Chemistry," Proceed. Fifth Materials Research Symposium, p. 265, issued July 1972, Washington, D.C.
5. Happel, J.; Suzuki, I.; Kokayeff, P.; Fthenakis, V. J. Catal. 1980, 65, 59.
6. The method of isotopic transient reaction kinetics (see 5), applied in a chemical steady state is an elegant application of the true steady state measurement.
7. Keulks, G. W. J. Catal. 1970, 19, 232.
8. Voorhoeve, R. J. H.; Remeika, J. P.; Trimble, L. E. Ann. N. Y. Acad. Sci. 1976, 272, 3.
9. Yao, Y. F. Y. J. Catal. 1975, 36, 266.
10. MacChesney, J. B.; Sherwood, R. C.; Potter, J. F. J. Chem. Phys. 1965, 43, 1907.

11. Tofield, B. C.; Greaves, C.; Fender, B. E. F. Mater. Res. Bull. 1975, 10, 737.
12. Voorhoeve, R. J. H.; in Burton, J. J.; Garten, R. L., Editors; "Advanced Materials in Catalysis"; Acad. Press: N.Y., 1977, p 129.

RECEIVED July 28, 1981.

12

Reaction Rate Resonance in the Concentration Cycling of the Catalytic Oxidation of Carbon Monoxide

A. K. JAIN, P. L. SILVESTON, and R. R. HUDGINS

University of Waterloo, Department of Chemical Engineering, Waterloo, ON, Canada

Abstract

The effect of forced concentration cycling was investigated on the oxidation of CO over industrial V_2O_5 catalyst. The resulting rate, when time-averaged, exhibited frequency-dependent harmonic behavior, with multiple extrema. Some preliminary interpretation is provided by analogy to an electrical network containing resistance and inductance.

Some experimental studies (1-7) have demonstrated the possibility of improving the performance of a catalytic reactor through cyclic operation. Renken et al. (4) reported an improvement of 70% in conversion of ethylene to ethane under periodic operation. In a later article (2), they concluded that periodic operations can be used to eliminate an excessively high local temperature inside the catalytic reactor for a highly exothermic reaction. In our laboratory, Unni et al. (5) showed that under certain conditions of frequency and amplitude associated with the forced concentration cycling of reactants, the rate of oxidation of SO_2 over V_2O_5 catalyst can be increased by as much as 30%. Recently Cutlip (6) reported a thirty-fold increase in the rate of CO oxidation over Pt/alumina catalyst under forced concentration cycling at high frequencies. Abdul-Kareem et al. (7) observed large effects of the mean composition, period and the amplitude of cycling on the rate of oxidation of CO over V_2O_5. In this study, rate resonance was observed in the low frequency region (10 min $< \tau <$ 60 min). In the present work, the search for such a phenomenon was extended to higher frequencies (1 min $< \tau <$ 10 min), although the low frequency range was also re-examined. Symmetrical square concentration waves were used, as illustrated in Figure 1. The effects of amplitude and cycle period were investigated. Temperature (400°C) and space velocity (80,000 h^{-1}) were held constant. To identify processes which control behavior under cyclic operation, variations in rate during step-changes in gas phase concentration were studied at two temperatures: 390 and 440°C.

0097-6156/82/0178-0267$05.00/0
© 1982 American Chemical Society

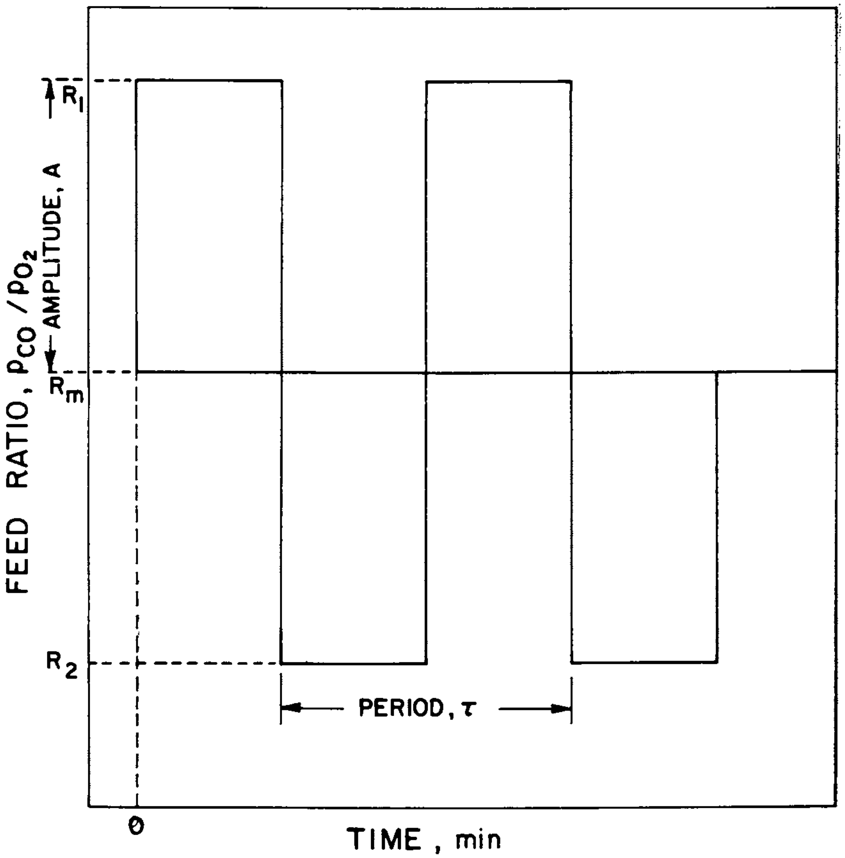

Figure 1. Waveforms of concentration cycles used for forced periodic operation.

Experimental

The reaction was carried out in a differential flow reactor shown in Figure 2. It was packed with commercial vanadium catalyst supplied under the trade name "Aero SA" by Cyanamid of Canada Ltd. The catalyst contained 9.1% by weight vanadium reported as pentoxide, 10.1% potassium reported as oxide and 0.45% iron and was supported on diatomaceous silica. A specific surface are of 1.4 m^2/g and pore volume of 0.56 cm^3/g was measured in our laboratory (5,7). 30/40 U.S. mesh screen size particles were used to eliminate internal mass and heat transfer resistances. A total flow rate of 300 mL/min was used in all experiments to avoid external transport processes. The reactor was held isothermal by diluting the catalyst with an inert packing (glass beads) and immersing the reactor and preheating coil in a sand bath whose temperature was controlled to within 1°C by a proportional controller. All the cycling experiments were carried out at 126 kPa and 440°C.

Square-wave concentration cycling was achieved by means of an automatic timer, three-way solenoid valves and two flow circuits each containing fine-control needle-valves as shown in Figure 2. Thus for one half-period, high CO and low O_2 flow rates for a high CO/O_2 ratio were obtained; for the remaining half-period the flow was diverted by a solenoid valve and an automatic timer through a second flow circuit, to provide low CO and high O_2 flow rates for a low CO/O_2 ratio. The concentration of CO_2 in the product stream (containing O_2, CO, CO_2 and He) was recorded continuously by infra-red spectroscopy tuned to the peak of CO_2 at 2160 cm^{-1}. Mean values of rates shown in Figure 3 were found by integrating the spectrographic records.

Results and Discussion

The feed concentration of reactants was modulated about a mean CO/O_2 concentration ratio of 0.86 with amplitude A of 0.12 and 0.24. The instantaneous product concentration-time profile obtained during periodic operation is shown in Figure 4 for $\tau = 1$ min. During the first few cycles, the time-average rate in one cycle is increased followed by a decrease in the time-average rate until the cycle-invariant condition was achieved after approximately 70 cycles. When $\tau = 10$ min was employed, the maximum time-average rate was achieved in the first cycle and cycle-invariant condition was obtained after about 7-8 cycles. Thus the total time required to achieve the cycle-invariant condition was observed to be practically independent of the period of cycling. The time-average cycle-invariant rate was strongly affected by the period and amplitude as shown in Figure 3. The time-average rate was always higher than the corresponding steady state irrespective of the period of cycling. Resonance peaks appeared at $\tau = 2$ min, 20 min, and 40 min. The corresponding time-average rates were 150%, 100% and 60% higher than the steady-state rate under identi-

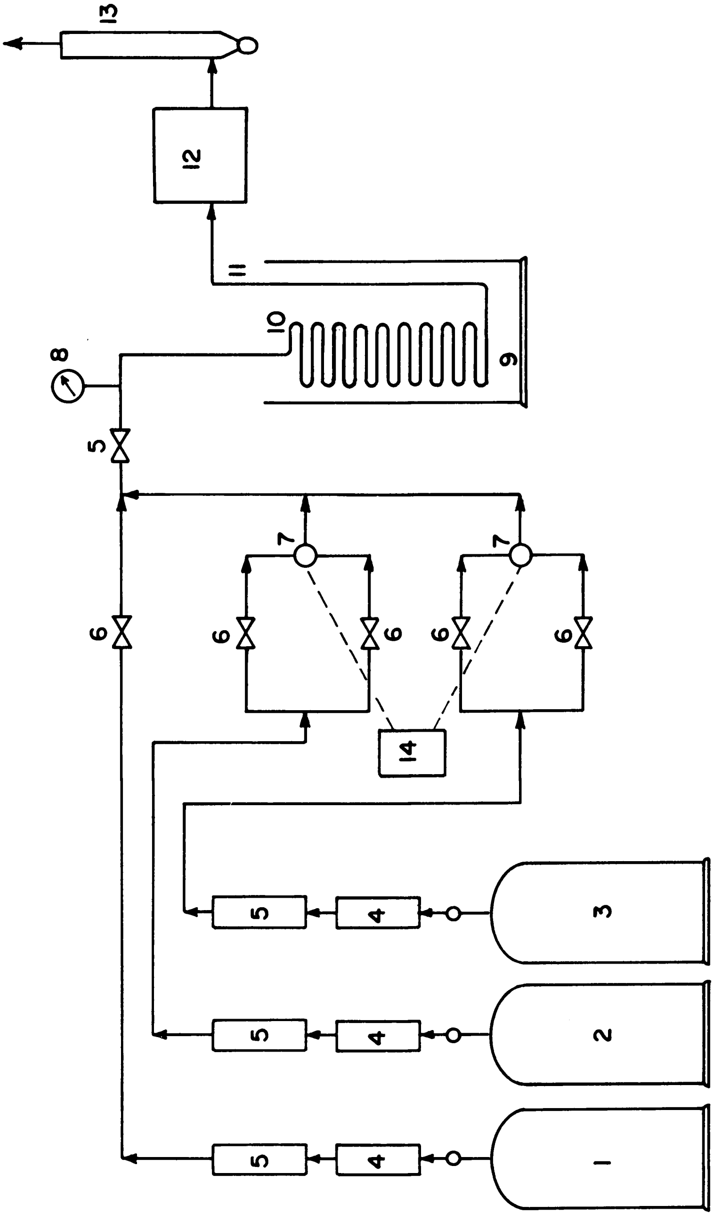

Figure 2. Schematic of the apparatus. Key: 1, He cylinder; 2, O cylinder; 3, CO cylinder; 4, molecular sieve dryer; 5, rotameter; 6, fine-control needle valve; 7, solenoid valve; 8, pressure gauge; 9, sand bath; 10, preheater; 11, reactor; 12, IR spectrometer; 13, gas bubbler; and 14, automatic timer.

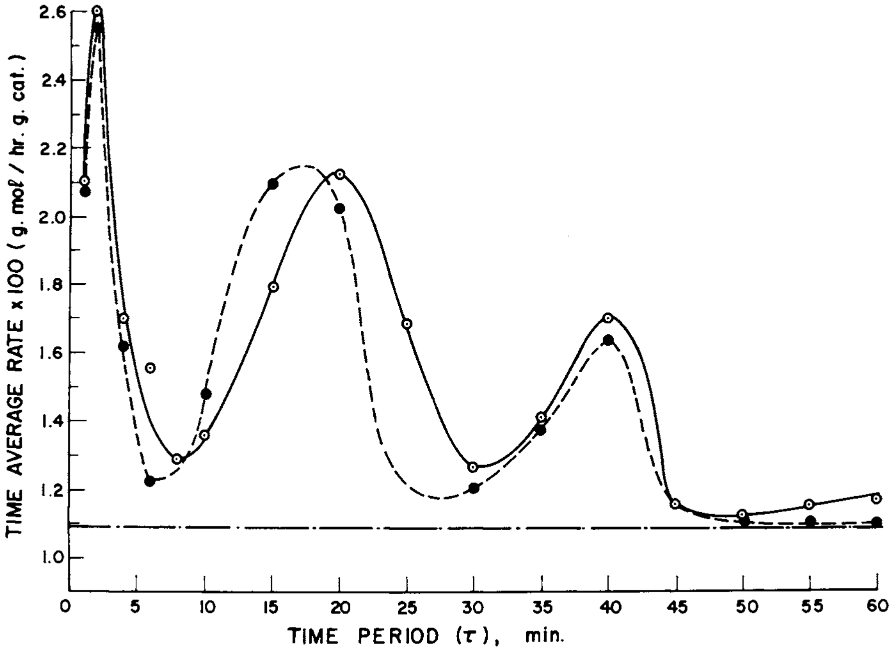

Figure 3. Time-averaged reaction rate as a function of period. Key (concentration wave amplitude): ⊙, 0.24; ●, 0.12; and ———, steady-state rate.

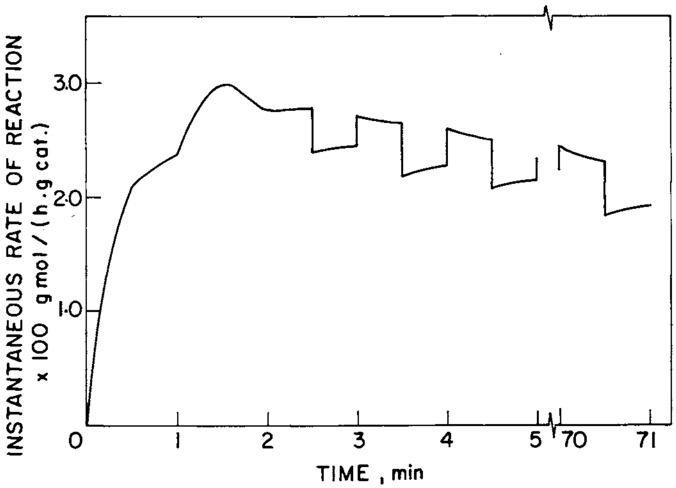

Figure 4. Instantaneous CO_2 production as a function of time during periodic operation for $\tau = 1$ min.

In Catalysis Under Transient Conditions; Bell, A., et al.;
ACS Symposium Series; American Chemical Society: Washington, DC, 1982.

cal conditions of temperature and time-average concentration. The remarkable trend of the maxima with increasing τ resembles a damped harmonic sequence.

Above τ = 60 minutes, changes in the time-average cycling rate at an amplitude of 0.24 were too small to be significant. At the other end of the frequency spectrum, a different timer would have been required to achieve periods less than 1 minute. Periods of less than 1 minute were not investigated furthermore because at shorter periods the square wave becomes increasingly distorted by mixing in the system.

Figure 5 shows the response of the reaction system to the step-change in the gas phase composition from pure oxygen to CO/O_2 = 0.86. This experiment was conducted at two different bed temperature 440°C and 390°C. The figure shows that a transition period occurs between the start of the step-change and the final steady state. It is important to notice that the temperature has practically no effect on the length of the transition period, although the rate of reaction is changed eightfold. If surface relaxation were responsible for the transition period, about an eightfold change in the relaxation time over the fifty degree change in temperature used should have been seen. The change shown in the Figure 5 is very much smaller, implying that the process underlying the transition period has an activation energy of just a few kcal/mol. In contrast the activation energy for oxidation over this catalyst is about 39 kcal/mole. An exact value for the transition process cannot be calculated because the process has not been modelled.

A number of studies (9,10) have demonstrated that the valence of coordination of vanadium in typical vanadia catalysts changed with gas composition in contact with the catalyst. As we discuss below, changes at the surface are partially offset by transport of oxygen from interior strata of the catalyst. We believe it is the diffusion of oxygen, as an ion, which is responsible for the relaxation time observed.

The steady-state mechanism of CO oxidation over V_2O_5 catalyst is believed to involve adsorption of CO, possibly as carbonate ion on the oxidized catalyst site, decomposition of this ion releasing CO_2 and reduction of the co-ordination of vanadium at the site. The original co-ordination is restored by gas-phase oxidation. Apparently, lattice oxygen plays a direct role, while gas-phase oxygen only regenerates the reduced sites. The rate of CO_2 production is proportional to the concentration of CO and oxidized sites. Under cycling conditions, interior catalyst strata act as a reservoir for oxygen diffusing to or from the catalyst surface according to the steepness of the concentration gradient of lattice oxygen. This viewpoint is developed quantitatively in an as yet unpublished article (11). The resonance is attributed to constructive interference of the concentration cycling frequency and the natural frequencies of the system. Resonance in AC circuits requires resistance, conductance, and

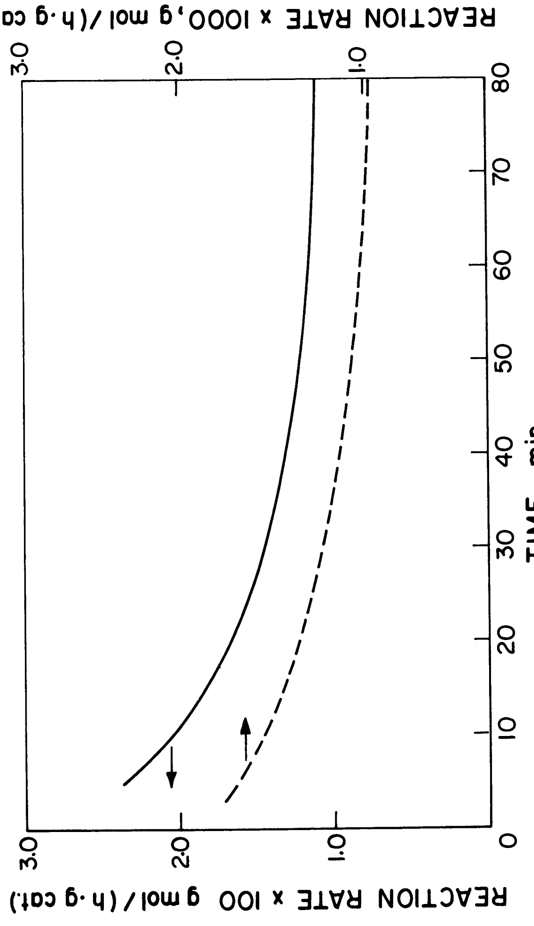

Figure 5. Response of the reaction system to a step change in concentration at 440°C (——) and 390°C (– – –).

inductance. Such circuits are an useful analogy to chemical reactions with forced cyclically varying reactant concentrations. Resistance in the catalytic system occurs, we believe, in the surface processes mentioned above, which are found in the reaction sequence from adsorbed CO to adsorbed CO_2. Capacitance can be assigned to the storage of unreacted adsorbed CO or some other intermediate on the surface, whereas inductance results from the transport of lattice oxygen between the interior of the catalyst and the surface in response to the changing co-ordination of vanadium at the surface. Models proposed by other investigators of cyclic forcing of catalytic reactions (1,12-14) assume that adsorption/desorption and surface reaction steps. These allow, therefore, only for resistance and conductance. They do not predict resonance. Indeed, we show elsewhere (15-17) that they even fail to predict rate improvement by cyclic operation.

Conclusions

Cycling reactant composition has been shown to significantly increase the rate of oxidation of CO over a vanadia catalyst. The time-average rate under cycling condition is strongly influenced by the choice of amplitude and period of cycling. A plot of the time-average rate vs. period exhibits multiple maxima and minima suggesting a damped, harmonic response. The chemical relaxation time of the reaction is shown to be practically independent of the reaction rate and temperature. Diffusion of ionic oxygen between the catalyst surface and the lattice is invoked in the oxidation mechanism because it would provide inductance for the catalytic reaction. Inductance is necessary to explain the resonance observations.

Legend of Symbols

A = amplitude of the change in concentration ratio, dimensionless
R_1 = ratio of partial pressure of CO to O_2 in CO rich half-cycle dimensionless
R_2 = ratio of partial pressure of CO to O_2 in CO poor half-cycle dimensionless
R_m = time-average ratio of partial pressure of CO to O_2, dimensionless
τ = period of the composition cycle, min.

Acknowledgements

Support for the work reported herein was provided through grant A-2099 of the National Research Council (Canada). Catalyst was provided by Cyanamid of Canada Ltd. Financial Support to A.K. Jain through Dean of Engineering Scholarship by University of Waterloo was appreciated.

Literature Cited

1. Denis, G.H. and Kabel, R.L., Chem. Eng. Sci. 1970, 25, 1057.
2. Renken, A., Müller, M., and Wandrey, C., Proc. 4th Int. Conf. Chem. Reac. Eng., 1976, p. 107.
3. Denis, G.H., and Kabel, R.L., AIChEJ, 1970, 16, 972.
4. Renken, A., Helmrich, H., and Schügerl, K., Chem. Ingr. Techn., 1974, 46, 647.
5. Unni, M.P., Hudgins, R.R., and Silveston, P.L., Can. J. Chem. Eng., 1973, 51, 623.
6. Cutlip, M.B., AIChEJ, 1979, 25(3), 502
7. Abdul-Kareem, H.K., Silveston, P.L., and Hudgins, R.R., Chem. Eng. Sci., 1980, 35, 2077.
8. Kadlec, B., Hudgins, R.R., and Silveston, P.L., Chem. Eng. Sci., 1973, 28, 935.
9. Mars, P. and Maessen J.G.H., Proc. Int. Gong. Catal. 3rd, 1965, 1, 264.
10. Boreskov, G.K., Polyakova, G.M., Ivanov, A.J., and Mastikhin, V.M., Dokl. Akad. Nauk SSR, 210 (3), 423 (Engl. transl).
11. Jain, A.K., Hudgins, R.R., and Silveston, P.L. Paper presented at ACS Symposium on Catalysis Under Transient Conditions. Las Vegas, Aug. 1980.
12. Mihail, R. and Paul, R., Chem. Eng. Sci., 34, 1058 (1979).
13. Horn, F.J.M. and Bailey, J.E., J. Optimiz. Theo. and Applic., 1968, 2, 441.
14. Bailey, J.E., "Periodic Phenomena", Chemical Reactor Theory: A Review (Edited by Lapidus, L. and Amundson, N.R.), Chap. 12, p. 785, Prentice-Hall, Englewood Cliffs, New Jersey, 1977.
15. Feimer, J.L., Jain, A.K., Hudgins, R.R. and Silveston, P.L., "A Critique of the Horn-Bailey Model of Forced Periodic Operation of Catalytic Reactors," paper submitted to Chem. Eng. Sci, 1980.
16. Jain, A.K., Hudgins, R.R. and Silveston, P.L., "Adsorption/ Desorption Models: How Useful to Predict Catalyst Behavior under Transient Conditions", paper submitted to Seventh North American Meeting, The Catalysis Society, Boston, 1981.
17. Jain, A.K., Hudgins, R.R. and Silveston, P.L., "Review of Bailey's Work on the Periodic Operations", paper submitted to Chem. Eng. Sci., 1980.

RECEIVED July 28, 1981.

Wavefront Analysis—A Special Transient Technique for Kinetic Investigations in Distributed Catalytic Systems

Application to the Water-Gas Shift Reaction

E. FIOLITAKIS and H. HOFMANN

Institut für Technische Chemie I der Universität Erlangen, Egerlandstr. 3, D-8520 Erlangen, Federal Republic of Germany

Abstract

The wavefront analysis of the reaction kinetics, a specific analysis of transient responses and a specific transient operation of distributed heterogeneous systems, is here shortly presented. The following results, obtained by the application of this technique for investigation of the low temperature watergas shift reaction, seem to be relevant for the transient operation under technical operating conditions of catalytic systems consisted of oxide-type catalysts. The existence of two microkinetic mechanisms of the formal Eley-Rideal type, i.e. having a linear dependence on p_{CO} and p_{H_2O}, has been found, besides a redox type reaction between the ambient fluid and the catalyst which regulates the oxygen activity on the catalyst surface. A systematic investigation with the intension to find the dependence of the microkinetics on definite oxidation states of the catalyst (established by its pretreatment until equilibrium in a defined H_2O, H_2, N_2 mixture) has revealed that for intermediary oxidation states and lower temperatures the redox reaction is slow and the overall shift activity has a logarithmic dependence on the pretreatment ratio p_{H_2O}/p_{H_2}. For extreme oxidation states and higher temperatures, the redox reaction becomes faster and most important than one of the microkinetic reaction steps of the formal E.R. type.

Heterogeneous catalysis under transient conditions encounters relaxation processes of the chemical conversion itself, proceeding by means of some surface intermediates, and relaxation processes of the catalytic surface and/or the catalyst bulk caused by the changes in the composition of the ambient fluid (1, 19) We like to name the first ones, following Temkin (1), the intrinsic or microrelaxations, having usually small relaxation times, the last ones, the extrinsic or macrorelaxations, corresponding in general to large relaxation times. In the case of macrorelaxations, we include here only the changes in the oxidation state of catalyst, i.e. redox reactions between the ambient fluid and the

0097-6156/82/0178-0277$06.25/0
© 1982 American Chemical Society

catalyst. For the oxygen activity distribution on different catalyst surfaces, a logarithmic dependence on the ambient fluid concentration has been found (2, 3, 5). This suggests in a first approximation for the rate law of the macrorelaxations of this kind an Elovich type dependence and in general a low activation energy for low or high oxygen coverage on the catalyst surface and a higher one for intermediary oxidation states. Therefore it can be expected that at extreme oxidation states of the catalyst (highly oxidated or highly reduced) the macrorelaxations proceed equally fast as the microrelaxations, whereas at intermediary oxidation states or/and near equilibrium the relaxation times of the macrorelaxation would be large, maybe in the order of magnitude of one hour.

Kinetic investigations of catalytic processes under transient conditions have to take into account this problem (see e.g. (4), where the macrorelaxation of the redox type reaction has been suppressed by means of a specific periodic operation). Kinetic expressions obtained by dynamic methods in general would give a better understanding of the rate law than those obtained from steady state measurements.

Apart from the above mentioned redox type reactions, we like to consider (in connection with work to be published by us elsewhere) another type of relaxations, due to the possible reorganisations of sorption intermediates on the catalyst surface, as suggested by some investigations in our laboratory. This structuring on the catalyst surface is equivalent to a change in the entropy of the system catalyst surface / adsorbed intermediates and seems to be responsible e.g. for the selectivity change under transient conditions in the oxidation of hydrocarbons. Actually this structural organization of the surface intermediates is also a rate process which can be observed under transient conditions.

Our main motivation to develop the specific transient technique of wavefront analysis, presented in detail in (21, 22, 5), was to make feasible the direct separation and direct measurements of individual relaxation steps. As we will show this objective is feasible, because the elements of this technique correspond to integral (therefore amplified) effects of the initial rate, the initial acceleration and the differential accumulative effect. Unfortunately the implication of the space coordinate makes the general mathematical analysis of the transient responses cumbersome, particularly if one has to take into account the axial dispersion effects. But we will show that the mathematical analysis of the fastest wavefront which only will be considered here, is straight forward, because it is limited to ordinary differential equations; dispersion effects are important only for large residence times of wavefronts in the system, i.e. for slow waves. We naturally recognize that this technique requires an additional experimental and theoretical effort, but we believe that it is an effective technique for the study of catalysis under technical operating conditions, where the micro- as well as the macrorelaxations above mentioned are equally important.

The elements of the wavefront analysis

The transient technique of wavefront analysis is based on one hand on a specific analysis of the transient responses, on the other hand also on a specific transient operation and is applicable only to distributed heterogeneous systems, e.g. a heterogeneous catalytic packed bed reactor (see Figure 1). By wavefront is meant here a disturbance, e.g. a step disturbance in the composition at the inlet of the system which preserves more or less its identity and propagates at a definite speed to the exit of the system. The only mechanism considered here, responsible for the origin and propagation of the wavefront is that of the convective accumulation. By this, we mean that there are at least two phases, one movable and the other one fixed, and we have to deal with the transfer of energy (heat) and material between the phases and simultaneously with the chemical conversion. The wave propagation considered here, is thus connected with the energy (heat) and mass capacitances of the phases; we like therefore to name this "capacitive waves". The propagation speed corresponds to the ratio of the respective total capacity (of heat or mass) to the respective capacity of the movable phase. Dissipation effects like dispersion, heat conduction etc. are not considered here, because they have been suppressed conveniently by means of a specific operation (e.g. choosing relatively large flow rates) in order to have a small influence on the transients around the wavefront.

The specific interpretation of the transient response consists in separating it into two parts.

- the wavefront strictly speaking. For an observer on the wavefront, the change of the amplitude of the disturbance is noticed as the relaxation along the propagation line and is named here the space relaxation.
- The remaining transient response after passage of the wavefront, it is the transient beyond the wavefront, as observed by an observer fixed at a definite position in space, named here time relaxation.

The elements of the wavefront analysis are:

- the propagation speed of the wavefront
- the space relaxation of the wavefront
- the time gradient of the time relaxation at the wavefront.

Basic equations

The following Eqns. are important for the mathematical analysis of the elements of the transient responses around the wavefront (see (5, 6). In these equations y_i stays for the state variables, such as concentration in the ambient fluid, or on the catalyst surface, temperature etc., f_i is the relaxation function (e.g.

In Catalysis Under Transient Conditions; Bell, A., et al.;
ACS Symposium Series; American Chemical Society: Washington, DC, 1982.

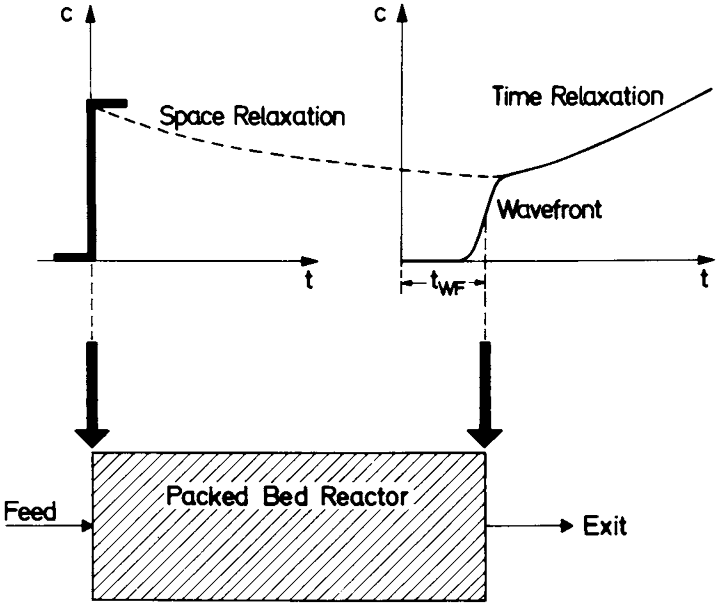

Figure 1. One-dimensional representation of the propagation of a concentration step-disturbance in a packed bed reactor (5).

chemical rate) and f_{ij} is the partial derivative $\partial f_i/\partial y_j$. We assume that a step inlet disturbance in the variable y_1 has been propagated in the system, the propagation line of the wavefront $\alpha_o(t,z) = 0$ separates the undisturbed from the disturbed region in the propagation field. The varible y_1 changes discontinuously on α_o (space relaxation) and other variables are constant on α_o.

Space relaxation

$$(y_1)_{\alpha_o} = \int_0^{\tau_o} (f_1)_{\alpha_o} dt' \tag{1}$$

Time relaxation

$$\left(\frac{\partial y_i}{\partial t}\right)_{\alpha_{o+}} = (f_i)_{\alpha_o} \quad , \; i = 2,\ldots, N \tag{2}$$

$$\left(\frac{\partial y_1}{\partial t}\right)_{\alpha_{o+}} = \left[f_1(\tau_o)\right]_{\alpha_o} \int_0^{\tau_o} \frac{\sum_{i=2}^{N} \left[f_{1i} f_i\right]_{\alpha_o}}{\left[f_1(t')\right]_{\alpha_o}} dt' \tag{3}$$

Propagation speed

$$\left(\frac{dz}{dt}\right)_{\alpha_o} = \frac{1}{\lambda_1} \frac{\partial (uy_1)}{\partial y_1} \tag{4a}$$

for a simple wavefront

$$\left(\frac{dz}{dt}\right)_{\alpha_o} = \frac{[uy_1]}{[\lambda_1 y_1]} \quad \text{for a shock wavefront } (\underline{10}) \tag{4b}$$

where u is the average velocity in the convective direction and λ_1 the capacity parameter, the brackets meaning discontinuities.

For the special case of linear relaxation functions f_i or when the integrand in Eq. (3) is invariant on the wavefront, we have the simplified Equation for the time relaxation of the propagating disturbance:

$$\left(\frac{\partial y_1}{\partial t}\right)_{\alpha_{o+}} = \tau_o \sum_{i=2}^{N} \left[f_{1i} f_i\right]_{\alpha_o} \tag{5}$$

Application principles of wavefront analysis

As for any transient technique, it is essential also for wavefront analysis

a) to ascertain (by preliminary experiments) mechanistic information by means of a qualitative and semi-quantitative analysis

b) to perform systematic experiments in order to obtain accurate numerical values for the kinetic parameters by means of a quantitative analysis.

The qualitative analysis consists e.g. in stimulating pure sorption steps by using a step inlet disturbance in the fluid concentration of the corresponding species. The responses are different depending on whether the step is kinetically controlled or not (see Figure 2, 3).

In the first case, the following equation, derived from (5), is important for a good adjustment of the individual relaxations (see (5)).

$$\frac{\tau_{c,\text{time relx}}}{\tau_{\theta,\text{time relx}}} = \frac{\tau_{c,\text{space relx}}}{\tau_o} \frac{\theta_{eq}}{\theta_{max}} \tag{6}$$

which links the time constant of time and space relaxations with the maximal and equilibrium internal storage.

If the step is only equilibrium controlled, a lumped analysis of both fluid and solid phase is possible and the corresponding nonlinear wavefront analysis is straight forward too. Analysis of propagation speed data yield information about the relevant equilibrium sorption mechanism (7). The different form of the transients when a reaction step has been stimulated, is discussed in the Appendix.

Application of wavefront analysis to watergas shift reaction

We report here about the investigation of the low temperature watergas shift reaction on an industrial catalyst (GIRDLER G 66-B and E with copper and zinc oxides as main components) under transient conditions by means of wavefront analysis. After a qualitative analysis to obtain information about the relevant mechanistic scheme the main effort has been concentrated on the dependence of the microkinetics on different oxidation states of the catalyst. The watergas shift reaction in its overall formulation

$$CO + H_2O \rightleftharpoons H_2 + CO_2 \qquad -\Delta H = 42{,}7 \text{ kJ/mole}$$

is a simple reaction without any selectivity problems. The investigations have been mainly performed under atmospheric pressure and in the temperature interval 180 to 280°C. The order of magnitude of the overall relaxation time of the microkinetics is about 1 second. For the macrorelaxations of the redox type, also included here (9), it is important that for extreme oxidation states of

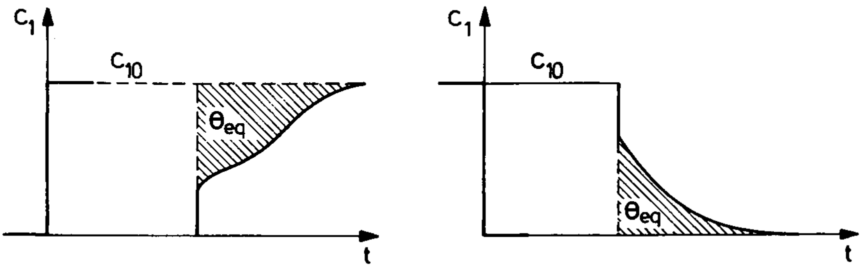

Figure 2. Transient responses when stimulating pure sorption step that is kinetically controlled (5). Key: left, loading; and right, unloading the storage.

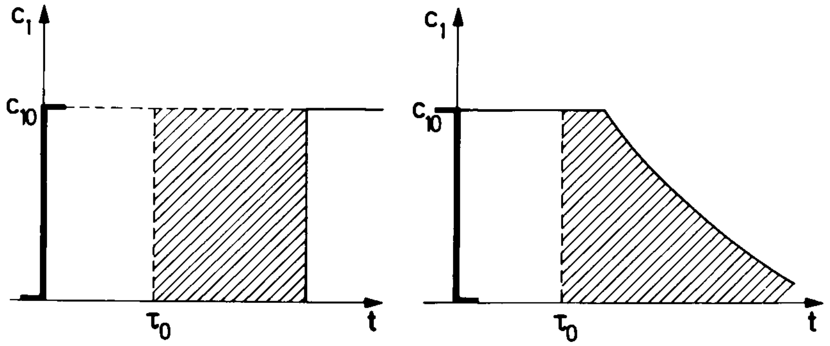

Figure 3. Transient responses when stimulating a pure sorption step that is not kinetically controlled (5).

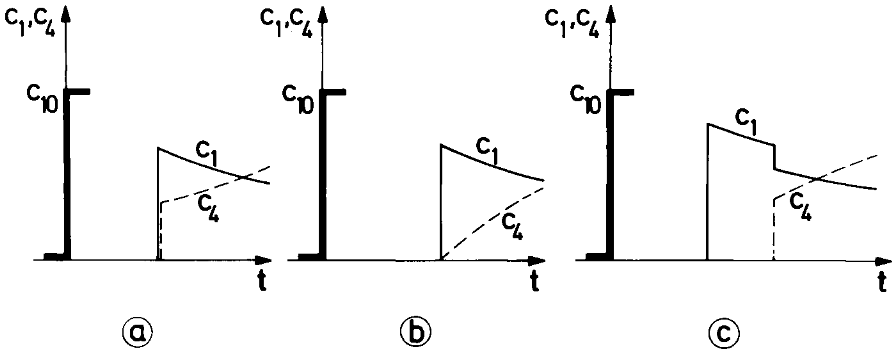

Figure 4. Transient responses when the reaction step $A_1 + \ldots \rightarrow A_4 + \ldots$ has been stimulated (see Appendix) (5).

the catalyst, the conversion at the wavefront (that means the space relaxation) contains significantly both micro- and macrorelaxations. The time relaxation reflects the change of the surface potential with time (i.e. the change of the oxidic active sites with time).

The experimental equipment used in these investigations and the analytic system, are described in detail elsewhere (5, 7).

Qualitative and semiquantitative analysis

Typical transient responses. The transient responses of the four reactants after a simultaneous step change in the inlet concentration of both CO and H_2O for a catalyst being initially in N_2 at 130°C are depicted in Figure 5. The CO response is the fastest one and behaves practically like a step response (the ascending signal has a time constant of about 5/4 seconds which is nearly equal to the time constant of the gas inlet system to achieve a continuous sampling from the normal pressure reactor vessel to the high vacuum chamber for mass spectrometric analysis; the lower operating temperature has been selected here in order to obtain stronger chromatographic separation effects). The same is also valid for the ascending CO_2-signal, but the last one is shifted parallel to the CO-front by a time interval of about 10 seconds, obviously caused by the retention of CO_2 on the solid capacitance. The CO_2 transient exhibits a maximum on the wavefront, whereas the CO transient exhibits a minimum on the wavefront. The H_2O wavefront has a larger retention time of about 30 s compared to the CO wavefront. As independent investigations with faster H_2O-fronts confirmed the H_2O transient as a shockfront, the H_2O transient here observed would represent a "blurred shockfront", because of the longer influence of dispersion effects (10). The maximum in the CO_2 concentration on the wavefront has been obviously caused by the partial reduction of the catalyst surface by CO, that means consumption of a part of the oxygen capacitance of the catalyst, whereas a possible subsequent reoxidation of the catalyst by H_2O seems to proceed slowly. The H_2 response in this experiment is certainly not a step response, it starts ascending from zero at the same time as the CO front appears, suggesting that the CO front and the H_2 front propagate with the same velocity. As during the pretreatment of the catalyst no H_2 and H_2O was present, the H_2 production is generated only by the shift reaction. The fact that CO_2 is not measured at the reactor exit for a certain period of time, for which H_2 has been observed, is caused by the large CO_2 capacitances of the catalyst, giving rise to the CO_2 shockfront. The slowest shockfront, it is this of H_2O represents in this case the moving boundary, behind of which the shift reaction only can take place. Actually the slow H_2O wavefront implies that the H_2 signal is ascending slowly, but in any case the reduction of the catalyst by CO (suggested also by the small stoichiometric deviation of CO_2, H_2 in the intermediary steady state) proceeds immediately behind the CO wavefront, independent

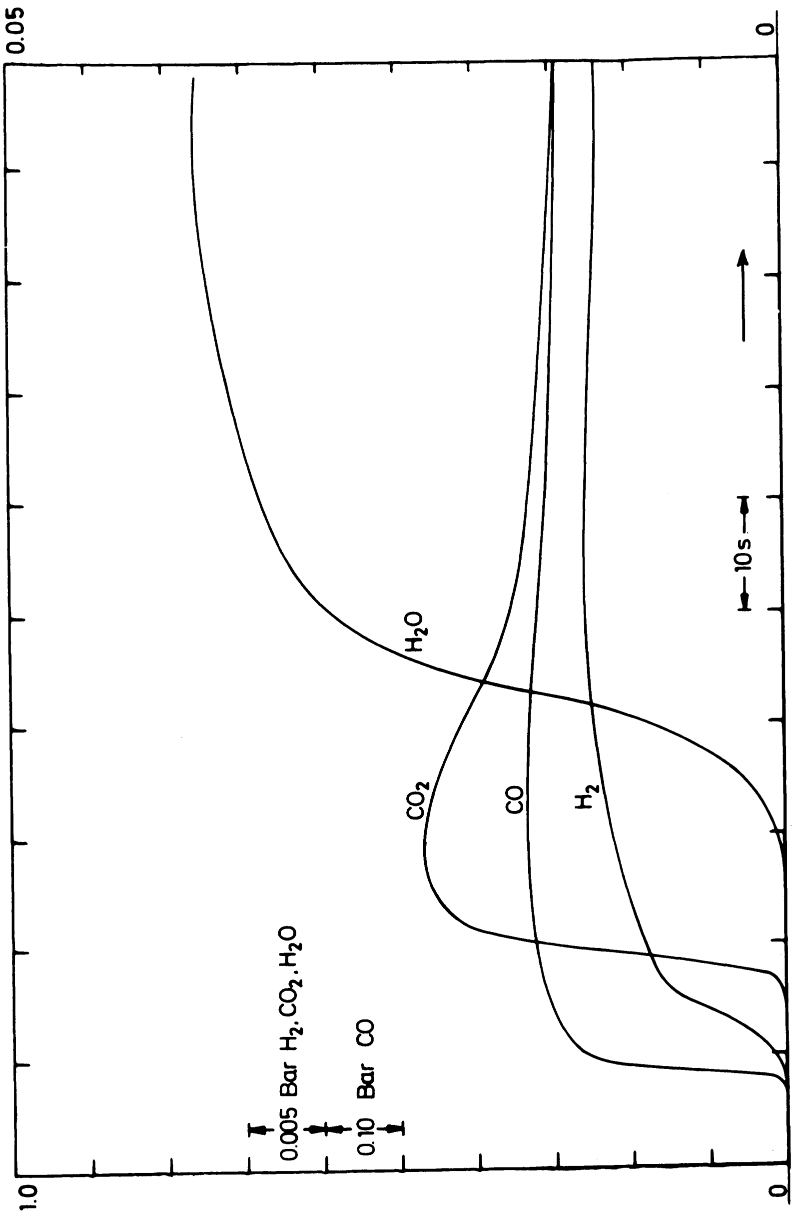

Figure 5. Transient responses after a step in CO (0.333 bar) and H_2O (0.067 bar), Z = 0.115 m, 60 g at 130°C. Catalysator Girdler G-66B, 0.11 Nm^3/h (5).

of the presence of H_2O. Independent investigations have also confirmed that H_2O inhibits the reduction of the catalyst by CO (see (7)). The case handled here, is a typical example, where more quantitative information can be gained only by the nonlinear wavefront analysis. But in the investigations which are reported below the experimental conditions have been always selected so that the effects of the nonlinear wave propagation discussed above (e.g. the slowly ascending H_2-signal) do not complicate the kinetic investigations.

Furthermore for the relevant adsorption steps: CO-adsorption, H_2O-adsorption, CO_2-desorption, H_2-desorption, one concludes from the form of the transients that the first three are not kinetically controlled, as they are shock fronts and that H_2 has no measurable sorption capacitance in presence of CO. The last conclusion has been also confirmed by independent experiments, i.e. stripping-off of adsorbed H_2 by CO, and the transients in this case suggest that also the H_2 desorption, at least under the selected experimental conditions, is not kinetically controlled. Independent transient experiments showing that the CO_2 sorption transients can have the form of shock wavefronts or simple wavefronts (see (7)) support the conclusion that CO_2 sorption is not kinetically controlled; it could be also shown that H_2O can strip off CO_2.

Sorption of H_2O. A systematic investigation of the H_2O sorption by analysing the wave propagation data has implied that H_2O sorption proceeds by two mechanisms, one of which follows a Langmuir isotherm ($-\Delta H$ = 33,5 kJ/mole) and the other one, probably chemisorption or capillary condensation in the micropores of the catalyst, has a capacitance which is saturated even at low partial pressures of H_2O (see (7)).

Sorption intermediates of CO and H_2O in the shift reaction. Additional information regarding the participation of the sorption intermediates of CO and H_2O in the shift reaction have been established by the following experiments:
The catalyst has been pretreated for several hours with a CO/N_2 mixture to attain a uniform and, as shown, low shift activity. Thereafter a periodic operation has been established as follows: testing time 1 min with a H_2O/N_2 mixture, recuperation time of 30 min with the same CO/N_2 mixture as before.

The transients shown in Figure 6 (see (9)) suggest that in the H_2O/N_2 phase, H_2O reacts with adsorbed CO to produce CO_2 and H_2 and that the H_2 wavefront concentration is two-fold of the CO_2 wavefront concentration. The overproduction of H_2 on the wavefront seems to have been caused by the reoxidation of the catalyst by H_2O. The reoxidation rate is therefore on the wavefront equal to the rate of the shift reaction, it is namely the limiting step in the global relaxation process. Furthermore, the fact that $H_2:CO_2$ is 2:1 on the wavefront suggests that presumably the shift con-

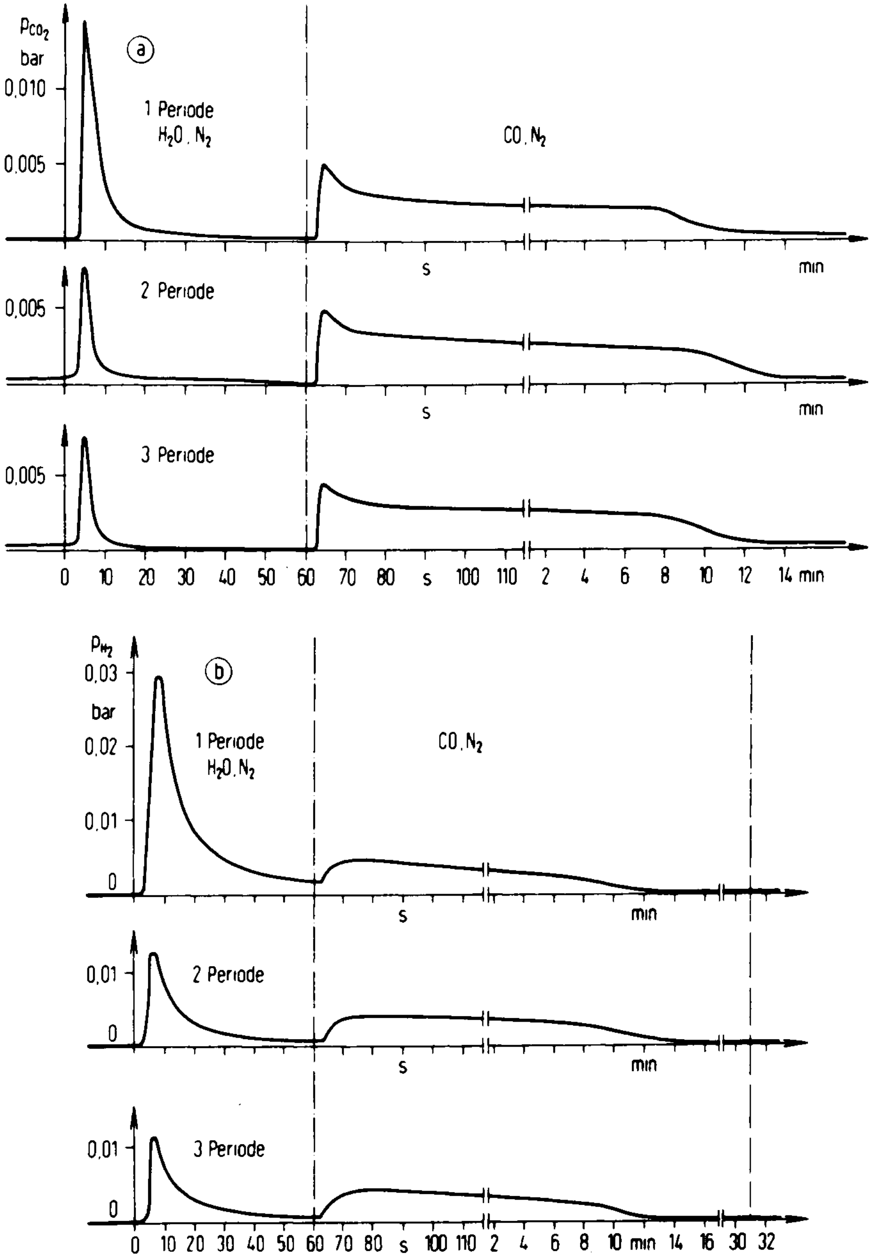

Chemie Ingenieur Technik

Figure 6. CO_2, H_2 transients for a periodic operation at 220°C for a catalyst initially intensively reduced about 18 h in CO/N_2 (9).

version is not possible for a catalyst surface at low oxidation state (intensively reduced catalyst). It is only possible after some structures of oxygen on the surface have been built up, e.g. some oxide forms of copper. In the subsequent 2nd period, the shift activity on the wavefront is lowered by the factor of about 2, that means a time constant for CO-recuperation of the initial activity of about 43 min (time constant = 30 min/ln2).

During the CO/N_2 phase, one obtains a long ranging low production of both CO_2 and H_2 in stoichiometric ration and at practically constant rate. This kind of responses suggest that the stimulated H_2O sorption capacitance is much larger than the CO capacitance and that this part of H_2O sorption must take place on surface sites different from the shift reaction sites, from where H_2O is probably transported by a slow mechanism to the shift reaction sites. The limiting step during this period is obviously the transfer of H_2O.

In order to clear up whether the sorption intermediates of CO and H_2O participating in the shift reaction are reversibly or irreversibly adsorbed a similar experiment has been accomplished with an additional stripping period of 30 min with purified N_2, enclosed between the testing periods. As it could be shown, this stripping phase was sufficient to remove the adsorbed H_2O but not the CO (see (9)), therefore we like to regard the H_2O sorption as reversible and the CO sorption as irreversible.

Transient behavior of the catalyst at high oxidation state. The significance of the redox type reactions between reaction medium and catalyst is depicted in Figure 7, where the conversion of CO to CO_2 has been stimulated under shift conditions. After a long range pretreatment of the catalyst in a mixture of H_2O/N_2 (0,30 bar H_2O) a periodic operation has been established consisting of a testing phase of 1 min with a mixture of CO, H_2O, N_2 (0,30 bar CO, 0,30 bar H_2O) at 160°C followed by a recuperation phase with the same H_2O/N_2 mixture of 12 min. The transients of both H_2 and CO_2 show in the concentration phase plan a hysteresis loop, caused obviously by the redox reaction between the reaction medium, mainly CO, and the catalyst. In the consecutive periods, the hysteresis loop becomes smaller and smaller and vanishes practically after the fourth period. Furthermore, the intermediate steady state of the shift conversion decreases from the first to the fifth period, suggesting its dependence on the oxidation state of the catalyst, as it changes from period to period. Also in this case, one can expect that the recuperation time constant is in the order of magnitude of several minutes, as the 12 min exposure of the catalyst to H_2O is not sufficient to retain the initial redox and shift activity.

Transient behavior of the catalyst at low oxidation state. After a reduction of the catalyst in a CO/N_2 mixture, the transient shift operation, depicted in Figure 8 (see also (7)), re-

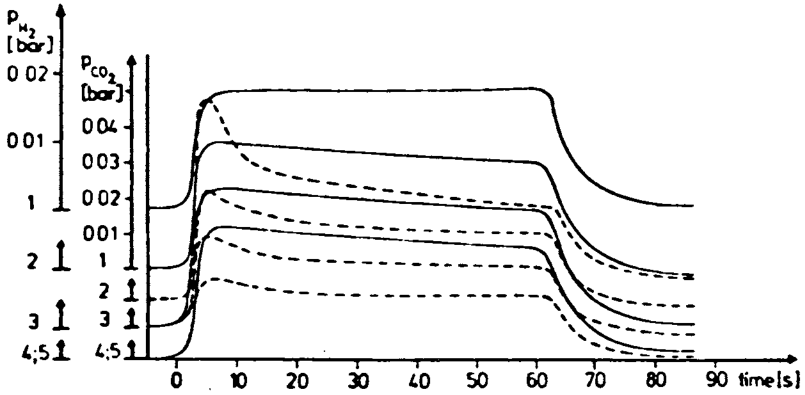

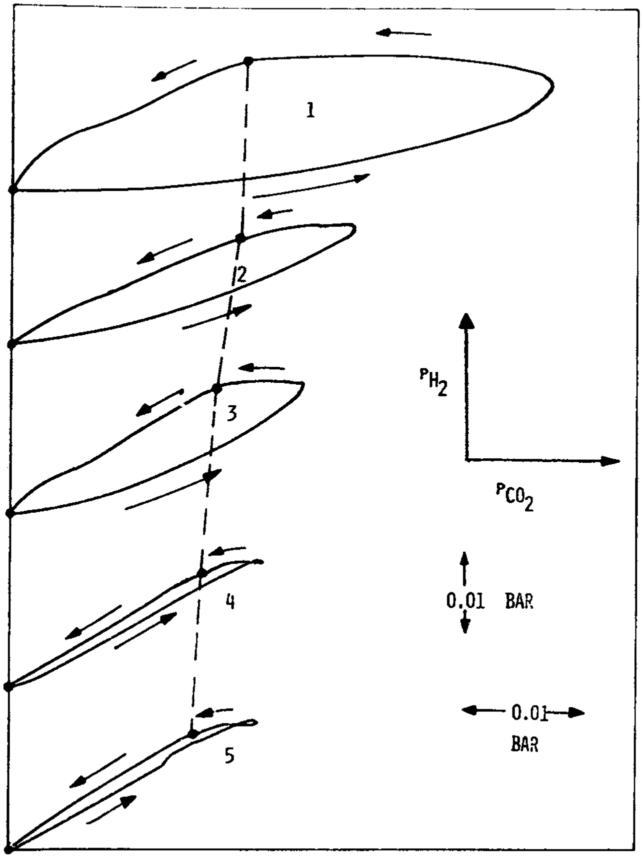

Chemical Engineering Science

Figure 7. CO_2, H_2 transients (top) and reaction trajectories (bottom) for a periodic operation with the catalyst initially at high oxidation level (7). Key: ——, P_{H_2}; and – – –, P_{CO_2}.

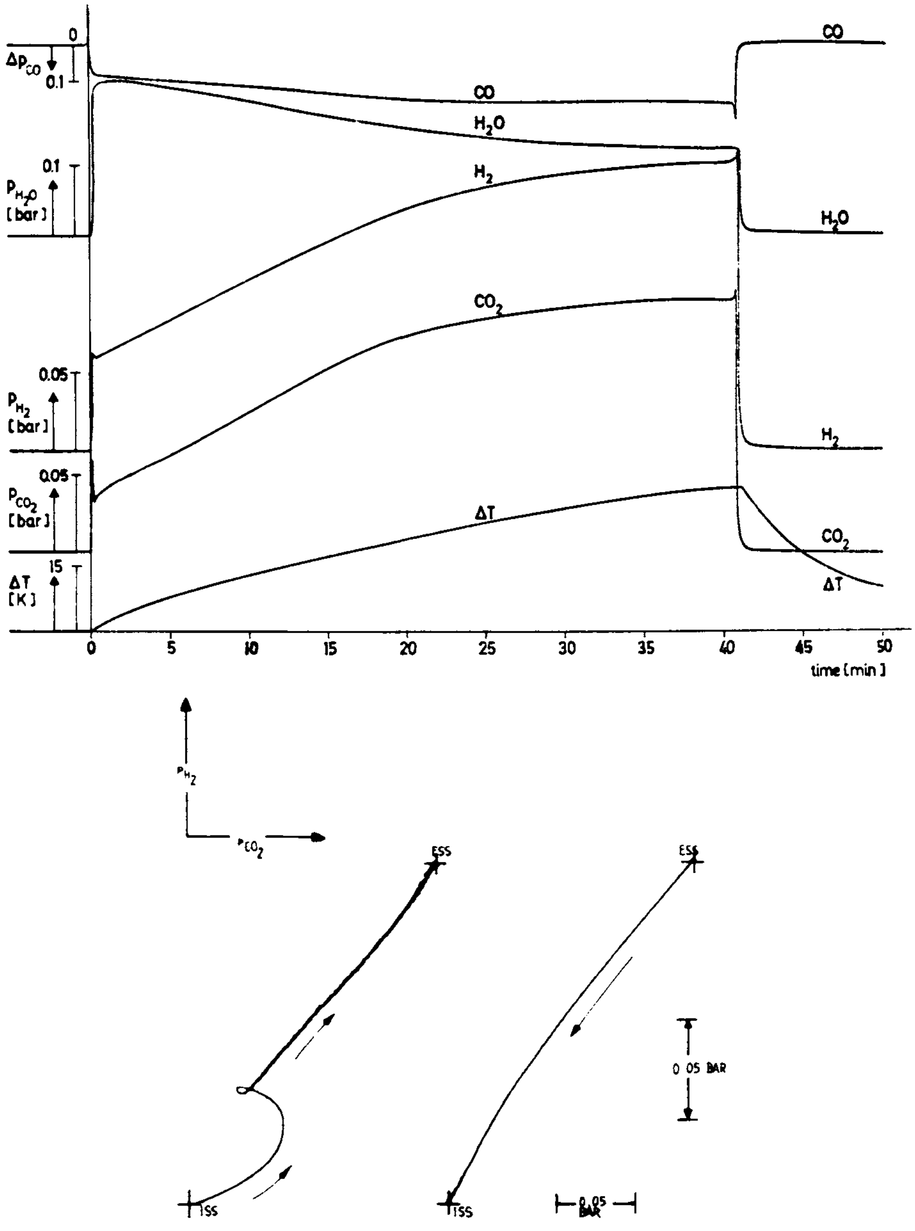

Chemical Engineering Science

Figure 8. Transient responses (top) and reaction trajectories (bottom) with the catalyst initially at low oxidation level (7). Key: ISS, initial steady state; and ESS, end.

sulted in an increase of the overall activity. This has been established by a subsequent testing with the same CO, H_2O, N_2 mixture after cooling of the reactor in a N_2 stream, where the wavefront concentration of CO_2, H_2 was higher than the corresponding one in Figure 8. This different behavior (compared to Figure 6) has presumably its cause to the fact that there the catalyst, because of the intensive reduction, has been presumably deactivated through brass formation (see (11)). But also in this case, the wavefront concentrations of H_2 and CO_2 behave like 2:1 and the reaction trajectory in the phase plane approaches only asymptotically the stoichiometric line 1:1 (as the concentration transients become stationary after 30 min, the time constant of this relaxation process amounts 30/4 ≈ 7,5 min).

Semiquantitative analysis. In a preliminary investigation, the analysis using Eq. (1) of space relaxation data, obtained by testing under shift conditions the catalyst at high oxidation state by a CO, H_2O, N_2 mixture at constant p_{H_2O} = 0,40 bar and various p_{CO} and at different temperature levels between 180°C and 260°C, resulted in the following kinetic parameters for the power law rate $r = k \cdot p_{CO}^n$:

$$n = 0{,}625 \pm 0{,}007, \quad E = 46{,}270 \pm 0{,}147 \text{ kJ/mole} \quad \text{(see (7))}$$

The nonlinear dependence of the reaction rate on the partial pressure of CO suggests that there are stimulated either a single reaction step with the established nonlinearity or at least two steps, one of which has a linear and the other one a nonlinear ($n < 1$) dependence on p_{CO}. To clear up this question, a periodic operation of the reactor at the 180°C level and at a middle oxidation state (pretreatment at p_{H_2O}/p_{H_2} = 5,0) has been accomplished (see Figure 9) with a H_2O/N_2 testing mixture followed by a CO/N_2 recuperation mixture. After an intermediate activity of the catalyst has been attained by this periodic operation, CO has been added in the testing mixture.
The transients of Figure 9 suggest that the wavefront conversion, when both CO and H_2O are present in the gas phase, is approximately equal to the sum of the wavefront conversions in the CO/N_2 and H_2O/N_2 phase. (At the established pretreatment T = 180°C, p_{H_2O}/p_{H_2} = 5,0 are relevant sorption effects of CO_2 but not of H_2; thus only the H_2 wavefronts represent rather the shift conversion). Therefore it seems conceivable that there are two different mechanisms which participate in the CO shift conversion which is also in agreement with the established two different sorption mechanisms for H_2O and with the transient behavior, depicted on Figure 6.

Quantitative Analysis. A systematic kinetic investigation has been performed therafter as follows: The catalyst has been pretreated for several hours with a mixture of $H_2O/H_2/N_2$ at defi-

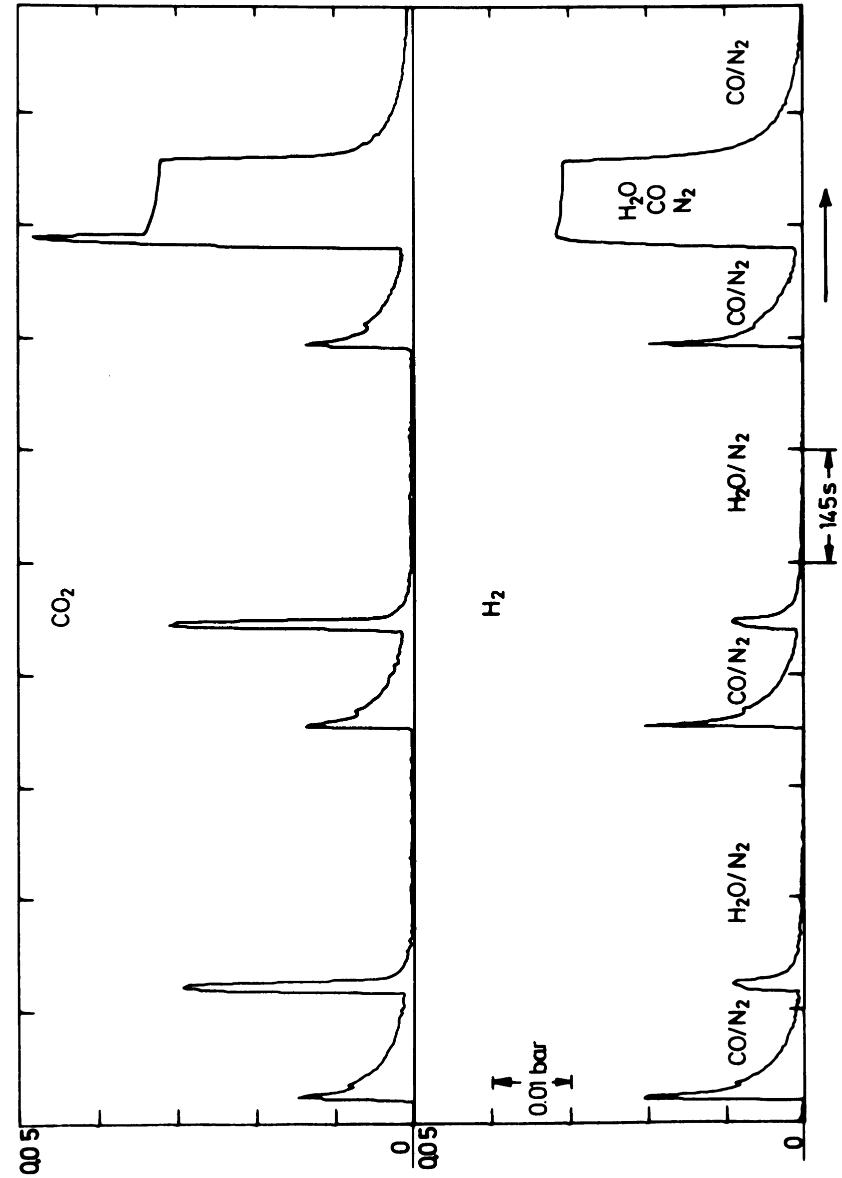

Figure 9. CO_2, H_2 transients for a periodic operation at 180°C, pretreatment at $\Psi = 5.0$, feed of 0.25 bar H_2O and 0.33 bar CO. Other conditions as Fig. 5.

nite levels of the ratio $\psi = p_{H2O}/p_{H2}$, until equilibrium has been established. The ψ has been variied over three decades, from 0,01 to 10,0. The shift activity of the catalyst has been tested thereafter by a mixture of CO, H_2O, N_2 with the inlet step disturbance of CO and H_2O being variied between 0,062 to 0,333 and 0,134 to 0,667 bar at the temperature levels 230, 250, 280°C. A series of experiments at the 230°C level has been performed earlier and in the meantime the reactor was shut down for about three months and stood in contact with air at room-temperature. This "resting" period resulted obviously in a higher overall activity of the catalyst as established by the conversion on the wavefront (see (12)).

In both cases the fitting of the space relaxation data with a single Langmuir-Hinshelwood kinetics as well as with a single stationary redox kinetics (i.e. assuming that on the wavefront the microkinetics are in quasi steady state) has failed (see (3, 12)). On the other hand, the attempt to fit the data has given the hint that there must exist a practically linear dependence of the rate on both, p_{CO} and p_{H2O}. If one takes into consideration the results of the qualitative analysis, in particular the fact that there are two microkinetic mechanisms, by which the shift reaction proceeds under the participation of sorption intermediates, it seems plausible that these mechanisms are of the formal type of the Eley-Rideal mechanism; whether the linear dependence on the p_{CO}, p_{H2O} has its origin in the reaction of gas phase CO and H_2O, or of linearly adsorbed CO and H_2O with chemisorbed H_2O and CO, respectively, is still an open question (it can exist for example a "linear" weak adsorption accompanied by a second stronger adsorption after Wicke (18). Therefore the following mechanistic scheme seems to describe the low temperature watergas shift reaction under transient conditions (neglecting the reverse reaction, as here $K_p \approx 100$)

(i) $H_2O+(CO)^* \longrightarrow H_2O+CO_2$, where $(CO)^*$ is CO chemisorbed

(ii) $CO+(H_2O)^* \longrightarrow H_2+CO_2$, where $(H_2O)^*$ is H_2O chemisorbed

(iii) Redox mechanism regulating the surface oxygen activity

(a) $CO+(O) \longrightarrow CO_2+(\ )$, where (O) is reducible surface oxygen

(b) $H_2O+(\ ) \longrightarrow H_2+(O)$

The fitting of space relaxation data using Eq. (1) to this mechanistic scheme (space relaxation data are always isothermal, because transient temperature effects are not relevant for the amplitude change of a concentration disturbance; this is just an advantage of wavefront analysis of reaction kinetics), reported in (3, 5, 12), supposing a Langmuir type chemisorption for (CO) and (H_2O) has confirmed that (see Figure 10, 11):

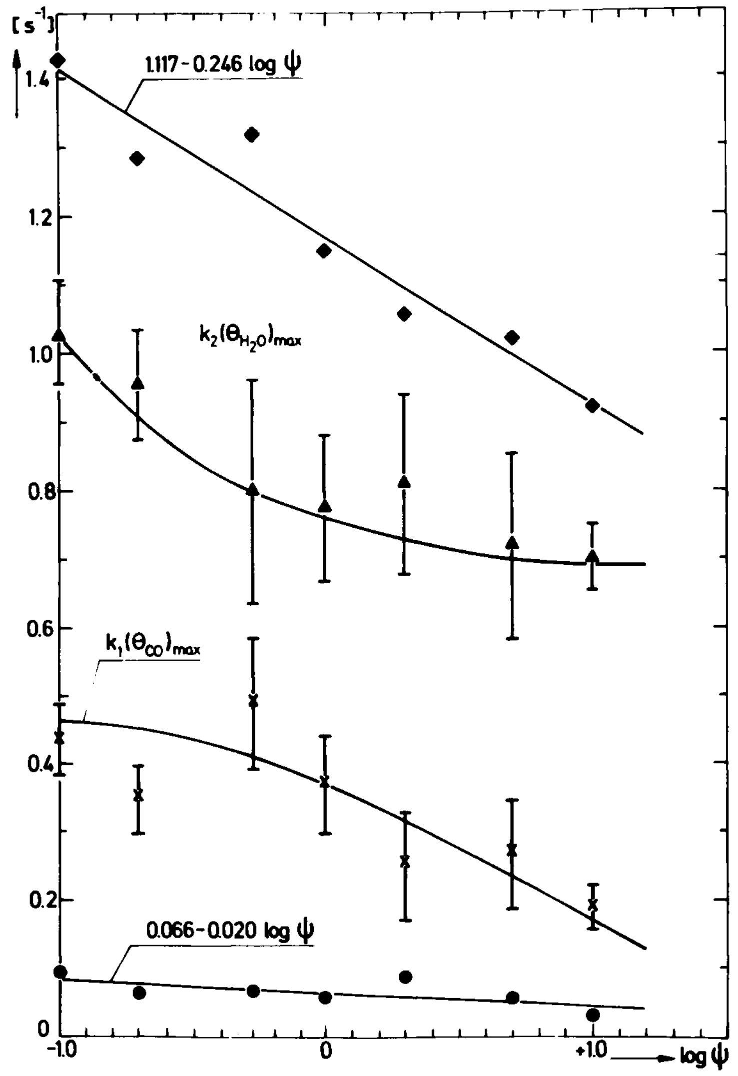

Figure 10. Dependence of the effective microkinetic parameters $k_i\,\theta_i$ and of the eigenvalues of the space relaxation on log Ψ for 230°C, first investigation (3). Key: × ≙ k_1', Eley-Rideal, CO adsorbed; ▲ ≙ k_2', Eley-Rideal, H_2O adsorbed; ● ≙ m_1; and ◆ ≙ m_2. Conditions: $\Psi = P_{H_2O}/P_{H_2}$ in pretreatment phase at 230°C.

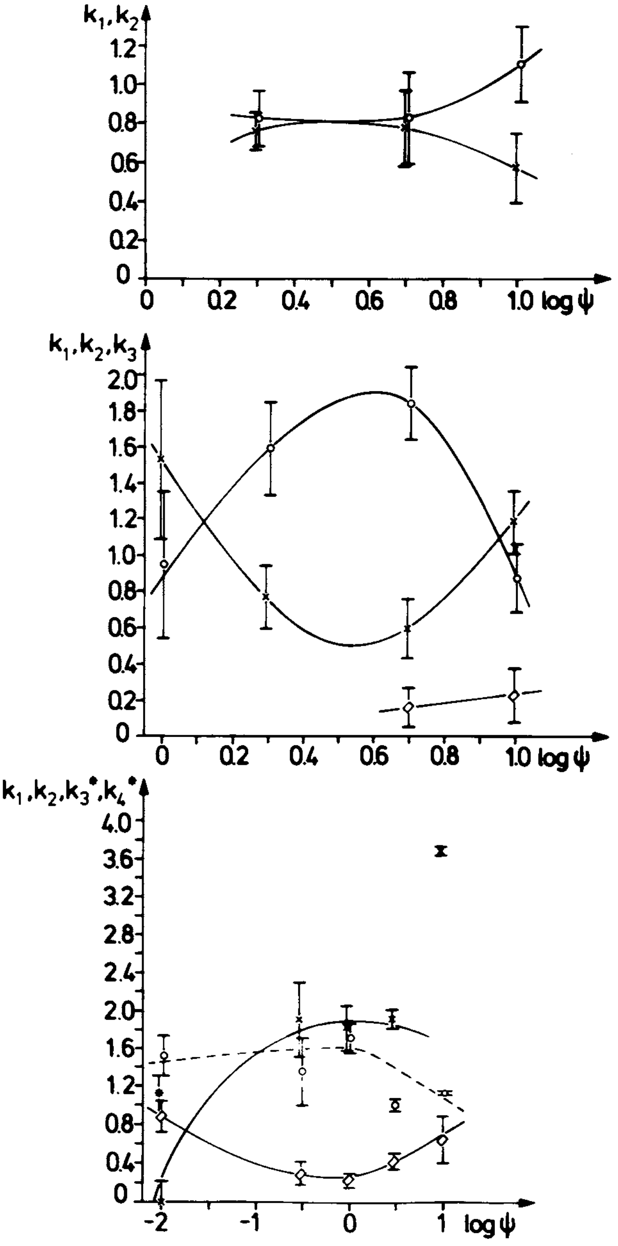

Chemie Ingenieur Technik

Figure 11. Dependence of the microkinetic parameters on log Ψ, second investigation (12). Key: ○, k_1; ×, k_2; □, k_3; *, k_4*; top, 230°C; middle, 250°C; and bottom, 280°C.*

a) there is a significant dependence of the kinetic parameters on the oxidation level of the catalyst
b) for intermediary oxidation states the redox parameters are not significant and highly correlated; for low oxidation states, a shift in the mechanistic scheme occurs that means one of the Eley-Rideal mechanisms vanishes completely in favour of the redox mechanism (Figure 11, 280°C)
c) the linear dependence of the largest eigenvalue (corresponding here to the overall shift activity (from the space relaxation data) on log ψ depicted in Figure 10 (see (3, 5)) suggests that for the oxygen distribution on the catalyst surface (oxygen activity) a logarithmic dependence on the gas phase partial pressure exists, i.e. a chemisorption isotherm of Temkin type. This suggests on the other hand in a first approximation an Elovich type kinetics for the redox reactions (iii).

Conclusions

General Remarks. The wavefront analysis as presented here, is limited only to the chemical relaxations and excludes any dissipation effects. The space relaxation, manifested as the change of the propagating primary wavefront itself, is met with and corresponds to the initial steady state or an equilibrium state of the system. On the other hand, the time relaxation manifests the changes in the system, caused by the primary wavefront.

From a thermodynamic standpoint, the space relaxation corresponds to the initial entropy of the system, i.e. to the initial entropy state on the catalyst surface, attained by establishing equilibrium between the ambient fluid and the catalyst surface.

The time relaxation corresponds to the change in the initial entropy state. As it has been established by one of the present authors (6), it is possible to derive generalized thermodynamic forces and fluxes in the sense of Onsager's theory and to study e.g. stability problems of tubular reactors.

All the elements of wavefront analysis have the common characteristic that they depend only and in a straight forward way on the initial steady state (for a nonlinear relaxation and/or nonlinear wave propagation also on the amplitude of the disturbance). That means, they are directly accessible for kinetic analysis. It is also possible to achieve a splitting of the initial information content of the transient response and make feasible a direct measurement of the initial rate of the entropy change. The space relaxation is the integral effect of the initial rate of the chemical conversion, the initial time gradient of the time relaxation is the integral effect of the initial acceleration of the chemical conversion. The residence time of the wavefront (dead time of the system) is the integral effect of the convective accumulative terms. For a lumped system all three effects have been implicated in the initial time gradient of transient

In Catalysis Under Transient Conditions; Bell, A., et al.;
ACS Symposium Series; American Chemical Society: Washington, DC, 1982.

response (see Table I). It seems therefore that the additional degree of freedom, introduced by the propagating wavefront, makes the new technique an extension to conventional dynamic techniques.

Specific Remarks. The established dependence of the microkinetics on the oxidation state of the catalyst make clear that a) results of kinetic investigations at lower temperatures are different in respect to the mechanistic scheme from those obtained at higher temperatures, b) in a distributed catalytic system in the steady state a distribution of the catalytic steps is possible as a direct consequence of the ambient gas concentration profile and the axial temperature distribution; in an extreme situation it is conceivable that at the reactor inlet, another mechanism dominates as at the reactor exit. These two facts can perhaps explain some contradictory results about the same reaction scheme which have been reported in the past by different authors. As stated recently by Boreskov (19) in a review paper, this conclusion holds true for the most catalytic systems under the technical operating conditions.

It is also clear that for a complete description of a catalytic system, as investigated here, one needs the complete functional describing the microkinetics in dependence on the energetic states of the catalyst surface.

The conclusions, established here, regarding the dependence of the overall activity as well as of the individual microkinetic parameters on the energetic states of the catalyst surface are in agreement with the fact that only the coexistance of oxides of Zn, Cu and Cr make it possible to have a good catalyst. That means a catalyst at intermediate oxidation state is an active one, whereas the oxides by themselves are not good catalysts (see the review paper (20)). Investigations on the dependence of the rate constants and activation energy on the chemical composition of the catalyst (see (20)) are similar to the reported ones here, where the change in the chemical composition is implied by the exposure of the catalyst on different ambient gas mixtures.

Especially for the low temperature water gas shift reaction the mechanistic scheme, proposed here, seems to correspond to the three different adsorbed oxygen species, proposed by Kobayashi (13) for the ethylene oxidation on silver, whereas the importance of some surface complexes of CO - H_2O type has been revealed (14) by analysing steady state data.

The significance of the coupling of micro- and macrorelaxations for resonance phenomena observed in catalytic systems under forced periodic operation (cycling) (15) implies that the wavefront analysis of transients of this kind can eventually suggest a more effective strategy in seeking the optimal conversion and selectivity. Finally the existence of certain surface structures and complexes could be established, if the transients of the surface intermediates will be followed e.g. by infrared spectroscopy (see e.g. (16, 17)).

Table I

Elements of response	Wavefront analysis	Conventional transient response techniques
Propagation speed	$\hat{=}$ Convective accumulative effects	———
Time relaxation	$\hat{=}$ Entropy change of the system in Onsager's sense	$\hat{=}$ Convective accumulative effects and initial entropy of the system and entropy change of the system
Space relaxation	$\hat{=}$ Initial entropy of the system	———

Appendix

We regard here a catalytic reaction with the following stoichiometric formulation:

$$A_1 + A_2 \rightleftarrows A_3 + A_4$$

If one stimulates an individual reaction step, in order to perform a qualitative or quantitative analysis, one uses a step inlet disturbance in one of the species keeping all other constant. It is obviously that the ideal situation exists, when the time constant of the measuring device, of the step signal itself (i.e. the signal has to be "sufficiently ideal") and the residence time of the wavefront in the system τ_o stand in a reasonable relationship to the space and time relaxation. The transients of the disturbed species consist then of clearly separated space and time relaxation and those of the undisturbed species depend on whether there exists for these species a measurable internal storage or not. If not, the transients of the undisturbed species consist of the step disturbance part (space relaxation) and of the time relaxation part, otherwise they consist only of the time relaxation part. When e.g. under transient conditions, a product desorption step is kinetically controlling, its transient caused by a step change in the reactant concentrations consists only of the time relaxation part (see Figure 4b). If the same step is not kinetically controlling the situation of Figure 4a is obtained. The time relaxation in Figure 4b, i.e. in a simple situation, is directly connected to the internal storage and the interchange rate between the phases. When a measurable internal storage exists but the interchange is not kinetically controlled, the transients have the characteristic form of Figure 4c, where the overshooting type effects and the shift in the transient responses is caused by the equilibrium between the fluid and solid phase, being typical for chromatographic reactors (8).
For the nonideal situation which does not fulfill the above mentioned requirements, the wavefront analysis fails to give a detailed information about the mechanistic scheme. But in any case, the relaxations, measured at the wavefront, correspond at least to the stimulated limiting step.

List of Symbols

E	activation energy
f_i	relaxation functions like chemical rate, heat generation etc.
f_{ij}	$\partial f_i/\partial y_j$
k_i	kinetic constants
m_i	eigenvalues equal to the inverse time constants of the space relaxation caused by the reaction system (i)—— (iii)

n	reaction order
p_i	partial pressure of the component i in the fluid phase time
t	time
u	average fluid velocity in the convective direction
y_i	state variables like concentration in fluid and solid phase, temperature etc.
y_l	state variable with the largest propagation speed
Z,z	length of the catalyst bed, space coordinate
α_o	propagation line of the wavefront
θ_i	solid phase concentration
λ_l	accumulation parameter
τ_i	Time constants
τ_o	residence time of the wavefront in the system (hydrodynamic time constant)
Ψ	p_{H_2O}/p_{H_2} in the pretreatment period

Indices

eq	equilibrium
max	maximum
c	referred to fluid concentration
θ	referred to solid concentration
time relx	referred to time relaxation
space relx	referred to space relaxation

Literature Cited

1 Temkin, M.I. Kinet. Catal. 1976, 17, 945
2 Temkin, M.I.; Nakhmanovich, M.L.; Morozov, N.M. Kinet. Catal. 1961, 2 650
3 Fiolitakis, E.; Hofmann, H. Dependence of the Kinetics of the Low Temperature Watergas Shift Reaction on the Catalyst Oxygen Activity, to be published in Journal of Catalysis
4 Voorhoeve, R.J.H. ACS Meeting, Catalysis under Transient Conditions, Las Vegas, Nov. Aug. 25-29, 1980
5 Fiolitakis, E.; Hofmann, H. Lecture Notes of "Summer School on Modeling of Dynamic Systems Based on Experimental Data with Chemical Engineering Applications", Bad Honeff, W.Germany, Aug. 1980, Ed. A. Pethö - submitted for publication in Catal.Rev.-Sci.Eng.

6 Fiolitakis, E., Some Aspects on the Entropy Change in Onsager's Sense for Irreversible Chemical Processes, to be published

7 Fiolitakis, E.; Hoffmann, U.; Hofmann, H. Chem.Engng.Sci. 1980, 35, 1021

8 Schweich, D.; Villermaux, J; Sardin, M. AIChE J. 1980, 26, 477

9 Fiolitakis, E.; Hofmann, H. Chem.Ing.Techn. 1979, 51, 800

10 Aris, R.; Amundson, N. "First order partial differential equations with applications", Prentice Hall, Englewood Cliffs 1973

11 Van Herwijnen, T; de Jong, W.A. Jl. Catal. 1974, 34, 209

12 Kaleńczuk, R.J.; Fiolitakis, E.; Hofmann, H. Chem.Ing.Techn. 1980, 52, 966

13 Kobayashi, M. ACS Meeting, Catalysis under Transient Conditions, Las Vegas, Nev. Aug. 25-29, 1980

14 Van Herwijnen, T.; de Jong, W.A. Jl. Catal. 1980, 63, 83

15 Jain, A.K. ACS Meeting, Catalysis under Transient Conditions, Las Vegas, Nev. Aug. 25-29, 1980

16 Hegedus, L.L. ACS Meeting, Catalysis under Transient Conditions, Las Vegas, Nev. Aug. 29-29, 1980

17 Bell, A.T. ACS Meeting, Catalysis under Transient Conditions, Las Vegas, Nev. Aug. 25-29, 1980

18 Keil, W.; Wicke, E. Preprints of Meeting on "Kinetics of physicochemical oscillations", Aachen Sept. 19-22, 1979, vol. I, 172

19 Boreskov, G.K. Kinet. Catal. 1980, 21, 1

20 Newsome, D.S. Catal. Rev.-Sci. Eng. 1980, 21, 275

21 Fiolitakis, E.; Hoffmann, U.; Hofmann, H. Chem.Engng.Sci. 1979, 34, 677

22 Fiolitakis, E; Hoffmann, U.; Hofmann, H. Chem.Engng.Sci. 1979, 34, 685

RECEIVED July 28, 1981.

INDEX

A

Adsorbed layer of Ag catalyst in oxidation of C_2H_4, characterization ... 209–236
Adsorption
- behavior of C_2H_4 ... 220, 224–226
- CO over Pt–alumina ... 80
- isotherms
  - C_2H_4 ... 226*f*
  - CO_2 ... 228*f*
  - CO–Pt system ... 88, 90*f*

Adsorption–desorption of CO on Ni ... 10*f*
Adsorptive capacity of catalyst ... 1
Air–fuel ratio, CO concentration effect ... 70, 71*f*
Air–fuel ratio, three-way catalyst, content, effect ... 72, 73*f*
Ammonia formation with automotive three-way catalysts ... 146, 147*f*
Ammonia formation in NO reduction ... 109–139
Auger electron spectroscopy ... 8, 20*f*
Automobile exhaust, function of three-way catalysts ... 60
Automotive pollutants: NO, CO, and and hydrocarbons (HC) ... 143
Automotive three-way catalyst(s)
- ammonia formation ... 146, 147*f*
- IR study ... 146
- Mo in ... 143–161
  - Mo–Pd ... 147*f*, 148
  - Mo–Pt ... 146, 147*f*, 148, 149
  - Mo–Rh ... 147*f*, 148
- NO, CO, and HC conversions ... 146, 147*f*
- selectivity ... 146–148
- temperature programmed reduction ... 146, 152, 154*f*

C

Carbon-13, CO oxidation on Pt ... 53, 55*f*
Carbon dioxide
- adsorption isotherms ... 228*f*
- adsorption on adsorbed O species ... 210
- formation on Pt, rate ... 23*f*
- pressure, variation during flash of Pd ... 35*f*, 37
- production on Pt ... 41, 43*f*, 51, 52*f*
- production on Rh surface ... 38, 39*f*, 40*t*
- transient adsorption behavior ... 209–236

Carbon monoxide
- adsorption, integral-averaged CO coverage ... 91, 92*f*
  - intrapellet concentration ... 93, 94*f*
  - O_2 pretreatment effect ... 97, 98*f*
  - transport resistances, step-response effects ... 93, 95*f*
- air–fuel ratio effect on concentration ... 70, 71*f*
- catalytic oxidation, transient low-pressure studies ... 33–56
- chemisorption on Pt–alumina ... 79–101
- chemisorption on Pt–Mo/γ-Al_2O_3, IR spectra ... 157, 158*f*
- concentrations at inlet and outlet of three-way catalytic converter ... 67, 69*f*
- concentrations over pelleted Pt/Pd/Rh/Ce/Al_2O_3 catalyst ... 70, 71*f*
- conversion(s), automotive three-way catalysts ... 146, 147*f*
  - steady and cycled conditions ... 62, 65*f*
  - time-averaged ... 62, 64*f*
  - transient enhancement ... 66
- desorption, integral-averaged CO ... 91, 92*f*
  - intrapellet concentration ... 93, 94*f*
  - Pt/SiO_2 ... 21*f*, 22*f*
  - transport resistances, step-response effects ... 93, 95*f*
- Ni, adsorption–desorption ... 10*f*
- Ni interaction ... 8
- Pt, oxidation ... 15*f*, 18–19
  - preadsorbed O_2 reaction between ... 20*f*, 21*f*, 22*f*
  - system, adsorption isotherm ... 88, 90*f*
- reaction over Fe, H ... 24
- reaction rate resonance in concentration cycling ... 267–274
- removal, O_2 effect ... 97, 98*f*

Carbon, surface, over reduced catalyst, hydrogenation ... 26*f*
Catalysis
- heterogeneous, electron spectroscopy study ... 8
  - gas–phase kinetics ... 2–4
  - IR measurements ... 5–8
  - transient method of study ... 1–29

Catalyst(s)
- adsorptive capacity ... 1
- automotive three-way, dynamic behavior ... 59–76

In Catalysis Under Transient Conditions; Bell, A., et al.;
ACS Symposium Series; American Chemical Society: Washington, DC, 1982.

Catalyst(s) (*continued*)
automotive three-way, Mo 143–161
Ce, cycled performance of Rh/Al_2O_3 effect 17*f*
C_2H_4 epoxidation, Ag 181
CH_3OH oxidation, pulse reactor effect 246–250
monolithic, flow reactor use 144, 145*t*
O_2 content measurement 72–74
O_2 content of pelleted Pt/Pd/Rh/Ce/Al_2O_3 ....74, 75*f*, 76*f*
performance under cycled conditions 62, 63*f*
pulse technique 225
reduced, C_2H_4 and H reaction 27*f*
reduced, surface C hydrogenation .. 26*f*
temperature programmed reduction study 144, 145*t*
three-way, content, air–fuel ratio effect 72, 73*f*
transition metals in CO oxidation ..33–56
Catalytic
CO oxidation, reaction rate resonance in concentration cycling 267–274
CO oxidation, transient low-pressure studies 33–56
three-way, converter, CO concentrations at inlet and outlet 67, 69*f*
Cerium, cycled performance of Rh–Al_2O_3 catalyst effect 17*f*
Chemisorption, on Pt–alumina, CO ..79, 101
Concentration step-disturbance in packed bed reactor 280*f*
Conversion measurements, time-averaged 60, 62
Cupric oxide catalyst, N_2O decomposition 163–179
Current effect on rates of epoxidation and deep oxidation 192, 193*f*
Cycled feed as forcing function 12–14
Cycled performance of Rh–Al_2O_3 catalyst, Ce effect 17*f*
Cyclic operation, improving performance of catalytic reactor 267

D

Decay of reactive O on Pt 42, 43*f*
Decomposition of N_2O 163–179
with CuO catalyst 165–171
over metal oxides catalysts reaction 163
over NiO 11*f*
O_2 effect on CuO 165, 168*f*
Desorption
CO over Pt–alumina 80
CO from Pt–SiO_2 ....21*f*, 22*f*
O from catalyst surface 169, 170*f*
Diffusion-coupled CO chemisorption, transient 84
Dynamic behavior of three-way automotive catalysts 59–76
Dynamic behavior of three-way catalysts in engine exhaust, apparatus 67, 68*f*
Dynamic gas–phase measurements 62–71

E

Electrocatalytic C_2H_4 epoxidation, vapor phase 181–207
Electrochemical O pumping, C_2H_4 epoxidation rates effect 187, 188*f*
Electrode surface area, C_2H_4 epoxidation effect 181
Electron spectroscopy, procedure for detecting surface species 41–55
Electron spectroscopy, heterogeneous catalysis study 8
Emission control system 61*f*
Epoxidation, vapor phase electrocatalytic C_2H_4 181–207
Ethylene, adsorption behavior 220, 224–226
adsorption isotherms 226*f*
characterization of adsorbed layer of Ag catalyst in oxidation 209–236
epoxidation, vapor phase electrocatalytic 131–207
and H on reduced catalyst 27*f*
Exhaust, automobile, three-way catalysts function 60
composition controlled by feedback control system 60, 61*f*
O sensor signal showing oscillation 60, 61*f*
oscillations, transients 60
Experimental methods, transient, heterogeneous catalysis study 1–29
External diffusion on kinetics of N_2O decomposition, effect 164

F

Feed system, fast-response IR spectrophotometer 81, 83*f*
Ferric molybdate, MoO_3 catalyst 241
Fischer–Tropsch reaction 4
Forced periodic operation, waveforms of concentration cycles 268*f*
Forcing function 9, 12–14

G

Galvanostatic response, oxidation and deep oxidation rates 195, 198*f*, 199
Galvanostatic transients, C_2H_4 deep oxidation rate 187, 190*f*

Gas–phase
composition, C_2H_4 epoxidation effects 192, 195*t*
fast-phase IR spectrophotometer, response 84, 85*f*
heterogeneous catalysis, kinetics 2–4
measurements, dynamic 62–71

H

Heterogeneous catalysis,
electron spectroscopy study 8
gas–phase kinetics 2–4
IR measurements 5–8
transient conditions 277
transient method of study 1–29
Hydrocarbon conversions by automotive three-way catalysts 146, 147*f*
partial pressure effects on reduction of adsorbed NO 111, 113*f*, 114*f*, 115*f*
pressure, NO reductions effect 132, 133*f*, 134*f*
reaction with CO over Fe 24
reaction with C_2H_4 over reduced catalyst 27*f*
temperature effect 152, 154*f*
Hydrogenation of surface C over reduced catalyst 26*f*
Hysteresis-free measurements in CO oxidation 257

I

Integral-averaged CO coverage during CO adsorption–desorption 91, 92*f*
Intrapellet concentration during CO adsorption–desorption 93, 94*f*
IR
automotive three-way catalysts 146
CO chemisorbed on Pt–Mo–γ–Al_2O_3 ....157, 158*f*
cell reactor 7*f*
diode laser, HC and CO concentrations in exhaust 66–67
fast-response 81
fast-response, CO chemisorption dynamics of Pt–alumina ..79–101
heterogeneous catalysis measurements 5–8
NO reduction 106, 107*f*
optical system 6*f*
Iridium catalyst in titration of chemisorbed O 44, 47*f*, 48, 49*f*
Iron, catalyst in H–CO reaction 24
Isothermal limit cycles 18
Isotope
experiments, ^{13}CO preadsorbed on Pt 53, 55*f*

Isotope (*continued*)
kinetic, $Fe_2(MoO_4)_3/MoO_3$, effect 242
NO reduction study 111, 116, 117*f*, 118*f*, 132, 135*f*, 136*f*, 137*f*, 138*f*

K

Kinetic(s)
CO_2 production of Rh 40*t*
CuO and MgO catalysts in N_2O decomposition studies 164
distributed catalytic systems 277–300
gas–phase, heterogeneous catalysis 2–4
isotope effect on $Fe_2(MoO_4)_3/MoO_3$ 242*t*
NO adsorption and reduction 121
N_2O decomposition, external diffusion effect 164

M

Magnesium oxide catalyst,
N_2O decomposition 171, 173–177
CuO comparison 163–179
CuO kinetic studies 164
Mass
external, transfer coefficient of CO in fast-response IR system 88, 89*f*
intensities, time effect 244, 245*f*
steady-state, balance equation for reactor cell of fast-response IR system 88
Metal components, three-way catalysts 143
Metal oxides, catalysts in N_2O decomposition 163
Metals, noble, Pt–alumina catalyst in CO chemisorption 79–101
Metals, transition, substrates in CO oxidation 33–56
Methanol oxidation, pulse reactor, catalyst effect 246–250
on-line MS study 239–251
reaction mechanism 246, 250*f*
temperature effect 246, 247*f*
Mixing characteristics, fast-response IR spectrophotometer 84, 85*f*
Molybdenum
automotive three-way catalysts ..143–161
–Pd 147*f*, 148
–Pt 147*f*, 148, 149
–Rh 147*f*, 148
–Pt ratio, selectivity effect 149, 150*f*
trioxide $Fe_2(MoO_4)_3$ catalyst 241
trioxide, vapor pressure 161*t*
MS NO reduction study 106, 108*f*

N

Nickel, CO adsorption–desorption 10*f*
Nickel, CO interaction 8

Nickel oxide, decomposition of N_2O .. 11*f*
Nitric oxide
adsorption and reduction kinetics .. 121
conversion automative three-way catalysts, temperature effect 146, 147*f*, 149, 151*t*
conversions, time-averaged CO 62, 64*f*
exposure time effect on H_2O and NH_3 production 111, 112*f*
exposure time effects on IR band absorbance 111, 112*f*
reduction,
H pressure effect 132, 133*f*, 134*f*
H over Rh 105–139
NO exposure time effect 128, 130*f*, 131*f*, 132, 133*f*
Nitrogen, formation in NO reduction 109–139
Nitrous oxide
decomposition 163–179
CuO catalyst 164, 165–171, 168*f*
external diffusion effect on kinetics 164
metal oxides catalysts 163
MgO catalyst 164, 171, 173–177
NiO_2 catalyst 11*f*
rate equations 171, 172*f*
NO reduction, formation 109–139

O

Oscillations, self-sustained 18
Oscillations, transients in exhaust composition 60
Overvoltage effect on C_2H_4 epoxidation rate ..187, 191*f*, 192, 194*f*
Oxidation
catalysis over Perovskite-type Mn and Fe oxides, pulse reactor 253–265
CH_3OH, pulse reactor with on-line MS analysis 239–251
C_2H_4, characterization adsorbed layer of a Ag catalyst 209–236
CO
on Pt 15*f*, 18–19
reaction rate resonance in concentration cycling 267–274
transient low-pressure studies 33–56
SO_2, C_3H_8 ....149, 152, 153*t*
Oxygen
adsorbed, reactivity 217–220, 222, 223
adsorbed, with H on Ru, titration 48, 50*f*
catalyst, content measurement 72–74, 73*f*
chemisorption,
on Ag 48, 50*f*, 210
on Ir 44, 47*f*, 48, 49*f*
on Pt 42, 43*f*, 44, 45*f*
Oxygen (*continued*)
catalyst surface, desorption 169, 170*f*
CO removal rate, effect 97, 98*f*
CO over Pt, surface reaction 20*f*
content of pelleted catalyst 74, 75*f*, 76*f*
electrochemical, pumping on rates of C_2H_4 epoxidation, effect 187, 188*f*
N_2O decomposition on CuO, effect 165, 168*f*
preadsorbed,
on Pd 53, 54*f*
on Pt reaction with CO 20*f*
on Pt/SiO_2 reaction with CO ..21*f*, 22*f*
pressure, variation during flash of Pd 36*f*, 37
pretreatment effect on CO adsorption rate 97, 98*f*
pulse on steam-reforming activity, effect 152, 155*t*, 156*t*
reactive, on Pt, decay 42, 43*f*
sensor in automobile exhaust 60, 61*f*
transient behavior 212–217

P

Palladium catalyst in titration of preadsorbed O 53, 54*f*
Palladium, automotive three-way catalysts 147*f*, 148
Perovskite-type oxides of Mn and Fe, pulse reactor in oxidation catalysis 253–265
Perturbing function (*see* Forcing function)
Platinum–alumina catalyst disc, properties 82*t*
Platinum–alumina catalyst in CO chemisorption, noble metals 79–101
Platinum
automotive three-way catalyst 146, 147*f*, 148, 149
catalyst
CO oxidation 18–19
^{13}CO oxidation 53, 55*f*
CO_2 production 41, 43*f*, 51, 52*f*
decay of reactive O 42, 43*f*
titration of chemisorbed O 42, 43*f*, 44, 45*f*, 46*f*
CO and preadsorbed O reaction 20*f*
CO_2 formation rate 23*f*
CO oxidation 15*f*
Platinum silica, CO desorption 21*f*, 22*f*
Platinum silica, CO and surface O reaction 21*f*, 22*f*
Pollutants, automotive: NO, CO, and hydrocarbons (HC) 143
Pressure changes, transients induced by 41–55

Propagation speed in wavefront analysis ... 281
Propane oxidation ... 149, 152, 153*t*
Pulse reactor ... 242, 243*f*
  on-line MS analysis to study oxidation of CH_3OH ... 239–251
  oxidation catalysis over Perovskite-type Mn and Fe oxides ... 253–265

R

Rate
  adsorption of CO ... 86
  coefficients to simulate transient response experiments ... 122, 123*t*
  desorption of adsorbed species from a surface ... 87
  equations for N_2O decomposition ... 171, 172*f*
Reaction
  decomposition of N_2O over metal oxides catalysts ... 163
  mechanism for CH_3OH oxidation in pulse reactor ... 246, 250*f*
  mechanism proposed for transient response experiments on NO reduction ... 119, 120*f*
  rate resonance in concentration cycling catalytic CO oxidation ... 267–274
Reactivity of adsorbed O ... 217–220, 222, 223
Reactor
  automotive three-way catalysts ... 144
  cell in fast-response IR system ... 80
  C_2H_4 epoxidation ... 182, 183*f*
  transient experiments, flow diagram ... 242, 243*f*
  transient response study of NO reduction ... 106, 107*f*, 108*f*
Rhodium
  Al_2O_3 catalyst, effect on cycled performance ... 17*f*
  automotive three-way catalysts 147*f*, 148
  catalyst in CO_2 production ... 38, 39*f*, 40*t*
  catalyst in NO reduction ... 105–139
Ruthenium catalyst in titration of adsorbed O with H ... 48, 50*f*

S

Selectivity
  automotive three-way catalysts 146–148, 151*t*
  Mo–Pt ratio effect ... 149, 150*f*
Selectivity surface O activity of freshly calcined Ag catalyst ... 185, 186*f*
Silver catalyst(s)
  C_2H_4 epoxidation ... 181
Silver catalyst(s) (*continued*)
  C_2H_4 oxidation, adsorbed layer characterization ... 209–236
  selectivity, freshly calcined ... 185, 186*f*
  surface O activity, freshly calcined ... 185, 186*f*
  titration of chemisorbed O ... 48, 50*f*
Sorption intermediates of CO and H_2O in shift reaction ... 286
Space relaxation equation in wavefront analysis ... 281
Steam-reforming activity, O pulse effect ... 152, 155*t*, 156*t*
Sulfur dioxide oxidations ... 149, 152, 153*t*
Surface
  area,
    Ag catalyst ... 184, 185*t*
    Ag catalyst-electrode, effect on cell relaxation time 195, 197*f*, 203
    Ag catalyst-electrode, effect on rates of epoxidation r_1 and deep oxidation ... 195, 196*f*
  O activity of freshly calcined Ag catalyst ... 185, 186*f*
  species, electron spectroscopy ... 41–55
  transients over Pt–alumina ... 97, 98*f*

T

Temperature
  automotive three-way catalysts
    NO conversion, effect ... 149, 151*t*
    programmed reduction ... 146, 152, 154*f*
    selectivity effect ... 151*t*
  changes, transients induced ... 34–41
  CH_3OH oxidation in pulse reactor, effect ... 246, 247*f*
  C_2H_4 epoxidation, effect ... 181, 199, 200*f*, 203
  H_2 uptake, effect ... 152, 154*f*
Thermal desorption spectroscopy ... 34
Three-way catalysts, automobile exhaust, function ... 60
Time-averaged
  conversion measurements ... 60, 62
  conversions, CO and NO ... 62, 64*f*
  reaction rate as function of period ... 269, 271*f*
Time relaxation equation in wavefront analysis ... 281
Titration
  adsorbed O with H on Ru ... 48, 50*f*
  O chemisorbed
    on Ag ... 48, 50*f*
    on Ir ... 44, 47*f*, 48, 49*f*
    on Pt ... 42, 43*f*, 44, 45*f*
  preadsorbed O on Pd ... 53, 54*f*
Transient
  behavior of catalyst ... 288

Transient (*continued*)
of CO_2 ... 209–236
of O ... 212–217
diffusion-coupled CO chemisorption 84
enhancement in CO conversion 66
experiments, flow sheet ... 3*f*
inducing method ... 33
pressure changes ... 41–55
temperature changes ... 34–41
low-pressure studies of catalytic CO oxidation ... 33–56
method of study, heterogeneous catalysis ... 1–29
oscillations in exhaust composition 60
response
experiments, rate coefficients used to simulate ... 122, 123*t*
N_2, N_2O, H_2O, and NH_3, during reduction of preadsorbed NO ... 109, 110*f*
techniques to study NO_2 reduction ... 105–139
Transition metal substrates in CO oxidation ... 33–56
Transport resistances ... 1
Transport resistances, effects on step-response of CO adsorption–desorption 93, 95*f*

V

Vapor phase electrocatalytic C_2H_4 epoxidation ... 181–207
Vapor pressure of MoO_3 ... 161*t*
Voltage, C_2H_4 epoxidation, effect ... 181
Voltage, C_2H_4 epoxidation, response to constant current ... 187, 189*f*

W

Water, formation in NO reduction .. 109–139
Water–gas shift reaction ... 277–300
Wavefront analysis ... 277–300

X

X-ray photoelectron spectroscopy 8

Z

Zirconia cells in electrocatalytic C_2H_4 epoxidation ... 184–207

In Catalysis Under Transient Conditions; Bell, A., et al.;
ACS Symposium Series; American Chemical Society: Washington, DC, 1982.